Response-Based Synchrophasor Controls for Power Systems

Ryan D. Quint

Dissertation submitted to the faculty of the Virginia Polytechnic Institute and State University in partial fulfillment of the requirements for the degree of

Doctor of Philosophy
in
Electrical Engineering

James S. Thorp (Co-Chair)
Virgilio A. Centeno (Co-Chair)
Jaime De La Ree
Sandeep K. Shukla
Eileen M. Van Aken

March 29, 2013
Blacksburg, VA

Keywords: phasor measurement unit, power system security, power system stability, reactive power, remedial action scheme, synchrophasor

Response-Based Synchrophasor Controls for Power Systems

Ryan D. Quint

ABSTRACT

The electric power grid is operated with exceptionally high levels of reliability, yet recent large-scale outages have highlighted areas for improvement in operation, control, and planning of power systems. Synchrophasor technology may be able to address these concerns, and Phasor Measurement Units (PMUs) are actively being deployed across the Western Interconnection and North America. Initiatives such as the Western Interconnection Synchrophasor Program (WISP) are making significant investments PMUs with the expectation that wide-area, synchronized, high-resolution measurements will improve operator situational awareness, enable advanced control strategies, and aid in planning the grid.

This research is multifaceted in that it focuses on improved operator awareness and alarming as well as innovative remedial controls utilizing synchrophasors. It integrates existing tools, controls, and infrastructure with new technology to propose applications and schemes that can be implemented for any utility. This work presents solutions to problems relevant to the industry today, emphasizing utility design and implementation. The Bonneville Power Administration (BPA) and Western Electricity Coordinating Council (WECC) transmission systems are used as the testing environment, and the work performed here is being explored for implementation at BPA. However, this work is general in nature such that it can be implemented in myriad networks and control centers.

A Phase Angle Alarming methodology is proposed for improving operator situational awareness. The methodology is used for setting phase angle limits for a two-tiered angle alarming application. PMUs are clustered using an adapted disturbance-based probabilistic rms-coherency analysis. While the lower tier angle limits are determined using static security assessment between the PMU clusters, the higher tier limits are based on pre-contingency operating conditions that signify poorly damped post-

contingency oscillation ringdown. Data mining tools, specifically decision trees, are employed to determine critical indicators and their respective thresholds. An application is presented as a prototype; however, the methodology may be implemented in online tools as well as offline studies.

System response to disturbances is not only dependent on pre-contingency conditions but also highly dependent on post-contingency controls. Pre-defined controls such as Special Protection Schemes (SPSs) or Remedial Action Schemes (RAS) have a substantial impact on the stability of the system. However, existing RAS controls are generally event-driven, meaning they respond to predetermined events on the system. This research expands an existing event-driven voltage stability RAS to a response-based scheme using synchrophasor measurements. A rate-of-change algorithm is used to detect substantial events that may put the WECC system at risk of instability. Pickup of this algorithm triggers a RAS that provides high-speed wide-area reactive support in the BPA area. The controls have proved effective for varying system conditions and topologies, and maintain stability for low probability, high consequence contingencies generally dismissed in today's deterministic planning studies.

With investments being made in synchrophasor technology, the path of innovation has been laid; it's a matter of where it goes. The goal of this research is to present simple, yet highly effective solutions to problems. Doing so, the momentum behind synchrophasors can continue to build upon itself as it matures industry-wide.

To my fiancée Scotti Rose, and our girls Tesla & Faraday

Acknowledgements

I would like to express my deepest gratitude to my advisors, mentors, and employing organization. Throughout my research endeavors thus far, they have provided a comprehensive insight on what keeps the lights on each and every day.

Dr. James Thorp and Dr. Virgilio Centeno have provided me with the academic skills to approach problems and find innovative solutions. Discussions with them have driven my research to areas previously unanticipated. It is that drive that keeps an eager student intrigued and motivated not only to solve problems but find new ones.

I want to thank committee members for their continued support and recommendations along this journey. Dr. Jaime De La Ree does not teach; he enlightens students to find the solution through deeper understanding of the topics at hand. Dr. Eileen Van Aken has provided an external viewpoint to power systems problems and taught me to always pursue improvement. I have had the honor of learning side by side with Dr. Sandeep Shukla, and his questions have helped me better understand the material at hand.

The continuing support from the Bonneville Power Administration has accelerated my learning and motivation exponentially. Dr. Dmitry Kosterev has proved to be one of the best mentors a student and young mind could ask for. A coffee break can turn into an enlightening discussion on the back of a napkin, an idea can turn into a realization, and motivation can turn into achievement. For the numerous and generous hours spent teaching and inspiring, I thank you deeply. Also, the time and energy spent answering an endless number of questions and providing useful system information by Eric Heredia, Tony Faris, and Greg Stults has been extremely valuable to my ongoing education. Lastly, John Haner and the BPA Student Board have provided ongoing support and guidance for a mind that likes to explore the limits.

Most importantly I would like to thank my fiancée Scotti Rose, who inspired me to pursue a higher degree, continually motivated me towards my goals, and supported me throughout this journey. I look forward to spending the rest of my life with you, pursuing our dreams.

Table of Contents

List of Figures

List of Tables

List of Acronyms

ACE	Area Control Error
ALIS	All Lines In Service
APS	Arizona Public Service
AVC	Automatic Voltage Control
BA	Balancing Authority
BAA	Balancing Authority Area
BES	Bulk Electric System
BPA	Bonneville Power Administration
BPS	Bulk Power System
COI	California-Oregon Intertie
DOE	US Department of Energy
DSA	Dynamic Security Assessment
DSO	Dispatcher Standing Order
EHV	Extra-High Voltage
EMS	Energy Management System
EO	External Outage
ERCOT	Electric Reliability Council of Texas
FACRI	Fast AC Reactive Insert
FACTS	Flexible AC Transmission System
FERC	Federal Energy Regulatory Commission
FIDVR	Fault-Induced Delayed Voltage Recovery
FR	Frequency Response
GPS	Global Positioning System
IID	Imperial Irrigation District
JSIS	Joint Synchronized Information Subcommittee (under WECC)
LC	Lower Columbia
LDC	Line Drop Compensation
LLL	Line Loss Logic
LPM	Linear Prediction Model
LVO	Lower Voltage Outage

MOD	Mechanically-Operated Disconnect
MOV	Metal-Oxide Varistor
NASPI	North American Synchrophasor Initiative (under NERC)
NERC	North American Electric Reliability Corporation
NI	Northern Intertie
PDC	Phasor Data Concentrator
PDCI	Pacific DC Intertie
PDX	Portland Area
PMU	Phasor Measurement Unit
PTDF	Power Transfer Distribution Factor
RAS	Remedial Action Scheme
RC	Reliability Coordinator
RTCA	Real-Time Contingency Analysis
RTU	Remote Terminal Unit
SCADA	Supervisory Control and Data Acquisition
SCE	Southern California Edison
SEA	Seattle Area
SIL	Surge Impedance Limit
SLG	Single Line to Ground Fault
SOL	System Operating Limit
SONGS	San Onofre Nuclear Generating Station
SP RAS	Synchrophasor Remedial Action Scheme
SPS	Special Protection Scheme
SSA	Static Security Assessment
SSS	Small Signal Stability
SVC	Static Var Compensator
TCR	Thyristor-Controlled Reactors
TCSC	Thyristor-Controlled Series Capacitors
TOS	Top-of-Second
TPL	Transmission Planning (NERC Reliability Standards)
TS	Transient Stability

UC	Upper Columbia
ULTC	Under-Load Tap Changing Transformer
UVLS	Under-Voltage Load Shedding
VSRI	Voltage Stability Reactive Insert
WACS	Wide-Area Control System
WAMCS	Wide-Area Measurement and Control System
WAMPAC	Wide-Area Measurement, Protection, and Control
WAMS	Wide-Area Measurement System
WAN	Wide-Area Network
WASA	Wide-Area Situational Awareness
WCA	Worst Case Contingency Analysis
WECC	Western Electricity Coordinating Council
WISP	Western Interconnection Synchrophasor Program

Chapter 1. Introduction

Since its inception in the 1880s, the electric power industry has striven for very high levels of reliability through economical design and operation. Today's power systems have revolutionized all aspects of life, from business to transportation to entertainment. Because of the power system's impact on society, reliability is of paramount importance. To ensure such high levels of reliability, grid operators follow standards and operating procedures to keep the system in a safe and secure state. However, electric power systems are dynamic in nature, changing from one operating condition to another. If not carefully monitored and controlled, these conditions can lead towards unsafe operation. Recent large-scale outages such as the 2003 Northeast United States–Canada and 2011 Southern California–Arizona blackouts have highlighted the need for improved operation and planning of the power system [1, 2]. Fortunately, the North American Electric Reliability Corporation (NERC) and its Reliability Coordinators (RCs) are taking proactive measures to mitigate these reliability concerns in the future [3].

A common recommendation between these two outages is the need for improved situational awareness of the grid. One significant response to this has been widespread deployment of synchronized phasor measurement devices, called synchrophasors. This technology was developed in the late 1970s and 1980s; however, the industry has been relatively slow in adopting the technology but is currently making extraordinary efforts to improve reliability through advanced technologies [4, 5, 6]. Synchronized phasor measurement can aid in real-time power system operations as well as offline planning tools. The Bonneville Power Administration (BPA) was an early adopter of synchrophasor technology, using the data mainly for offline applications such as post-mortem event analysis, baselining power system dynamic performance, and generator model validation [7, 8, 9]. In addition, BPA also explored several methods and applications using synchronized phasor measurements for response-based controls, known as the WACS [10, 11, 12]. WACS was BPA's first step towards real-time response-based controls using synchrophasor measurements. However, this system was based on the initial installation of synchrophasors from the 1980s and 1990s, and the infrastructure was not reliable or secure for real-time system controls or alarming.

In 2009, BPA started a project to build a production-grade synchrophasor infrastructure. This project is coordinated with a wide Western Electricity Coordinating Council (WECC) initiative called the Western Interconnection Synchrophasor Program (WISP) [13, 14, 15]. WISP is a joint investment effort between the US Department of Energy (US DOE) and eleven operating entities in the Western Interconnection, aimed at developing a WECC-wide synchrophasor network. This investment in synchrophasor technology is expected to improve grid reliability, unlock previously unavailable transmission capacity, aid in congestion management, and enable reliable integration and operation of renewable energy. Utilities across WECC are installing PMUs to capture higher resolution data, improve situational awareness, and innovative control and operation strategies [16, 17, 18, 19]. BPA is currently exploring myriad applications for the upcoming synchrophasor data, including but not limited to a synchrophasor-based remedial action scheme (RAS) controller and phase angle alarming application.

This research is focused on application of synchrophasors, centered around innovative applications utilizing this technology, with an emphasis on real-world power system implementation and design. An actual full-scale WECC model of the power system is used to test applications for improving reliability of the Bonneville Power Administration (BPA) and the larger WECC. The concepts and methodologies presented can be generalized and applied to other transmission systems and Balancing Authorities for improved grid reliability and operator situational awareness.

This chapter establishes a foundation for the research presented in this paper. Past disturbances in the WECC and rest of North America highlight a number of critical areas for improvement for situational awareness in real-time operation and advanced control schemes to detect abnormal system conditions. Power system reliability, security, and stability are at the forefront of this work. Chapter 2 reviews the literature and concepts applicable to this research, and provides a high-level overview on a number of relevant topics discussed in this paper. In Chapter 3, a methodology for determining steady state phase angle limits on a bulk electric system is presented and applied to the BPA transmission network. The goal of this component of the research is to explore the behavior of the grid in terms of phase angle and devise a tool for alarming and visualizing

system stress based on angles. Chapter 4 proposes a response-based synchrophasor remedial action scheme (RAS) for detecting large disturbances that would otherwise be undetectable with existing tools and measurements. The detection algorithm is applied to a RAS action for providing reactive support through a controllable shunt reactive switching scheme. Chapter 5 presents the conclusions drawn from this work and recommendations for future work.

1.1. Power System Reliability and Operating State

Power system reliability in a bulk electric system has been defined by the North American Electricity Reliability Council (NERC) as "*the degree to which the performance of the elements of that system results in power being delivered to consumers within accepted standards and in the amount desired*." Additionally, "*the degree of reliability may be measured by the frequency, duration, and magnitude of adverse effects on consumer service* [20]." This definition consists of two concepts: adequacy and operating reliability. These concepts are defined as [21]:

- Adequacy: *The ability of the electric system to supply the aggregate electric power and energy requirements of the electricity consumers at all times, taking into account scheduled and reasonably expected unscheduled outages of system components.*
- Operating reliability: *The ability of the electric system to withstand sudden disturbances such as electric short circuits or unanticipated loss of system components.*

Until September 2001, NERC used the term "security", but replaced this ubiquitous term with a more detailed description of "operating reliability [22]." However, much of the literature has continued using the term "security" and this term is adopted throughout this research.

NERC has redefined reliability to include six general characteristics for maintaining an "adequate level of reliability," in which the Bulk Power System (BPS) can be operated with an acceptable certainty of reliability [22].

1. The power system is "operated within acceptable limits during normal operation," which may include voltage, frequency and System Operating Limits (SOLs) that specify operationally safe and studied conditions.
2. The system "performs acceptably after credible contingencies," which requires that the current operating conditions have been studied ahead of time such that inevitable contingencies occurring do not adversely impact reliability.
3. "The impact and scope of instability and cascading outages" has been assessed through thorough investigation of planned and forced outages. Cascading events can lead to instability, catastrophic failure, and system blackouts.
4. System "facilities are protected from unacceptable damage by operating them within facility ratings."
5. Restoration procedures are in place such that the "integrity [of the system] can be restored promptly if it is lost."
6. The power system is planned such that it "has the ability to supply the aggregate electric power and energy requirements of the electricity consumers at all times, taking into account scheduled and reasonably unscheduled outages of system components." The system is planned such that possible outage conditions do not reduce adequacy of generation and transmission resources.

This comprehensive description of adequate levels of reliability establishes a set of criteria that must be adhered to for planning and operating the electric power grid reliably and economically. To help illustrate reliable operation of the electric power grid, the operating state is generally classified into five conditions: *normal*, *alert*, *emergency*, *in extremis*, and *restorative* [23, 24]. Figure 1 illustrates these operating states and their connectivity.

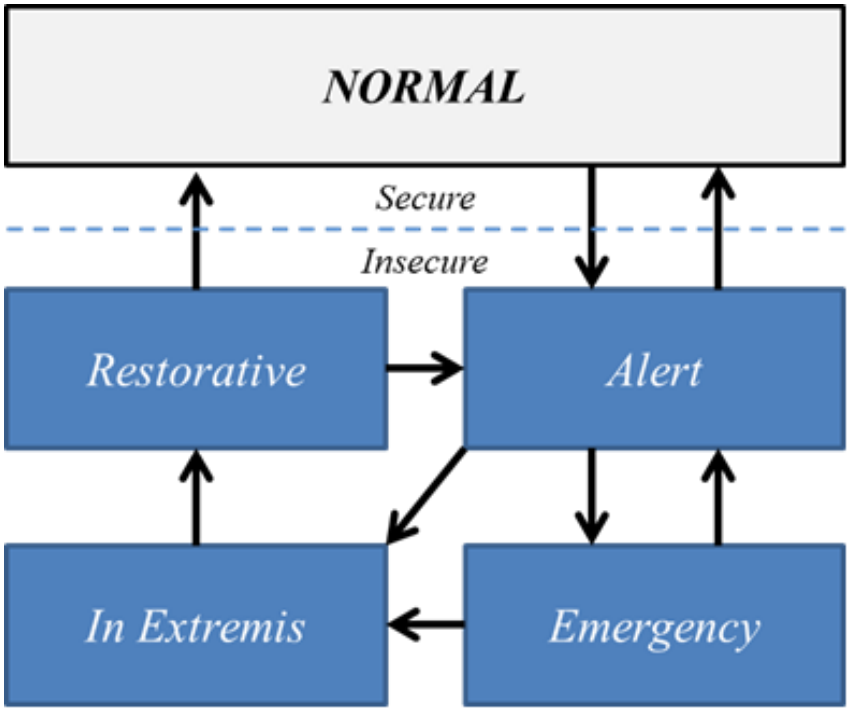

Figure 1. Power System Operating States, adapted from [23]

System operators aim at operating in the *normal* state where load is supplied, operating constraints are met, and the system is able to withstand credible disturbances without consequent violations. The operating point may fall to the *alert* state where all constraints are still met and load is being served, but an outage would result in violation of constraints; this is an insecure operating condition. Operators can take corrective action such as generation redispatch or schedule curtailment to bring the system back to *normal* state. However, the system may enter an *emergency* state if a contingency results in severe violations such as low voltage or thermal overloading above emergency ratings. Control actions such as generation dropping, dynamic brake insertion, DC fast ramping, generator fast valving, and load shedding may be initiated to maintain the integrity of most of the system [24]. If these actions are insufficient, the system moves to the *in extremis* state; cascading outages may disconnect large parts of the system and loss of load occurs. The operating state moves from *in extremis* to *restorative*, where the operators are taking action to reconnect parts of the system and restore load. At this point, the goal is returning the power system to *normal* state as quickly as possible.

This description of power system operating state its transitions illustrates the importance of maintaining a high degree of reliability through secure operation of the grid. While disturbances are inevitable, the goal is to minimize their impacts on system performance by designing, operating, and controlling the power system efficiently and effectively. With sufficient tools and resources, operators can identify problematic situations and take preventive actions. In addition, degraded system conditions can be returned within acceptable limits by utilizing appropriate controls.

1.2. Synchrophasors and Wide Area Measurement and Control Systems

The operating state of a power system, which is continually changing, is based on the instantaneous conditions for that given time. Estimation of system state requires measurement of currents and voltages across the grid. Traditionally, these measurements have been collected synchronously through Supervisory Control and Data Acquisition (SCADA) systems, which collect measurements from remote terminal units (RTUs) [16]. However, the drawback of this tool is the synchronicity of its measurement. The system quantities measured at the RTUs are scanned by the SCADA system, with rates ranging from 2 seconds to 10 seconds [25]. The measurements do not have a time measurement associated with them, and therefore are assumed to have been collected at the same time. Due to the state of technology at the time, this was the best assumption that could be made. The power industry has been operated in this manner for many years and SCADA is the most common wide-area measurement and control system in production today [25]. Yet, there has always been an understanding that there is room for improvement either through faster data rates or time-referenced measurement.

Introduction of synchronized phasor measurement has revolutionized the concept of operating the power grid. Rather than synchronously query remote devices for measurements and the estimate the state of the system, measurements are gathered asynchronously and time aligned based on their accompanying time stamp such that the state can be measured [26]. A synchrophasor is defined as "*a phasor calculated from data samples using a standard time signal as the reference for the measurement* [27]." A phasor is a representation of a sinusoidal waveform.

A pure sinusoid

$$x(t) = X_m \cos(\omega t + \phi) \tag{1.1}$$

can be represented using a phasor as

$$\overline{\mathrm{X}} = \frac{X_m}{\sqrt{2}} e^{j\phi} \tag{1.2}$$

$$\overline{\mathrm{X}} = \frac{X_m}{\sqrt{2}} (\cos\phi + j\sin\phi) \tag{1.3}$$

$$\overline{\mathrm{X}} = X_r + jX_i \tag{1.4}$$

where

$$X_r = \mathrm{Re}\left(\frac{X_m}{\sqrt{2}} e^{j\phi} \right) = \frac{X_m}{\sqrt{2}} (\cos\phi) \tag{1.5}$$

$$X_i = \mathrm{Im}\left(\frac{X_m}{\sqrt{2}} e^{j\phi} \right) = \frac{X_m}{\sqrt{2}} (\sin\phi) \tag{1.6}$$

$X_m/\sqrt{2}$ is the magnitude of the waveform as a root-mean-square (rms) quantity, ω is angular frequency, ϕ is the phase angle referenced to a time source, and r and i denote the real and imaginary components of the phasor representation, respectively [27]. Based on this definition, a phasor is represented with a magnitude $X_m/\sqrt{2}$ and phase angle ϕ, either in polar or rectangular format.

Synchrophasor measurements are made at devices called phasor measurement units (PMUs) that measure analog and digital quantities and provide a time synchronized time stamp with the measurements. The PMUs derive the phasor representation of complex voltages and currents, and then calculate frequency and its rate-of-change from them. In addition, analog quantities such as real and reactive power can be calculated from the voltage and current phasors. The time reference generally comes from satellite precise timing networks such as Global Position System (GPS) [27]. PMUs measurements are referenced to the Top-of-Second (TOS) such that their phase angle calculation is based on

synchronized time. All PMUs are therefore referenced to the same time, within accuracy of microseconds, regardless of their location or distance from the central measurement location. Figure 2 illustrates the convention for synchrophasor representation of a sinusoidal waveform.

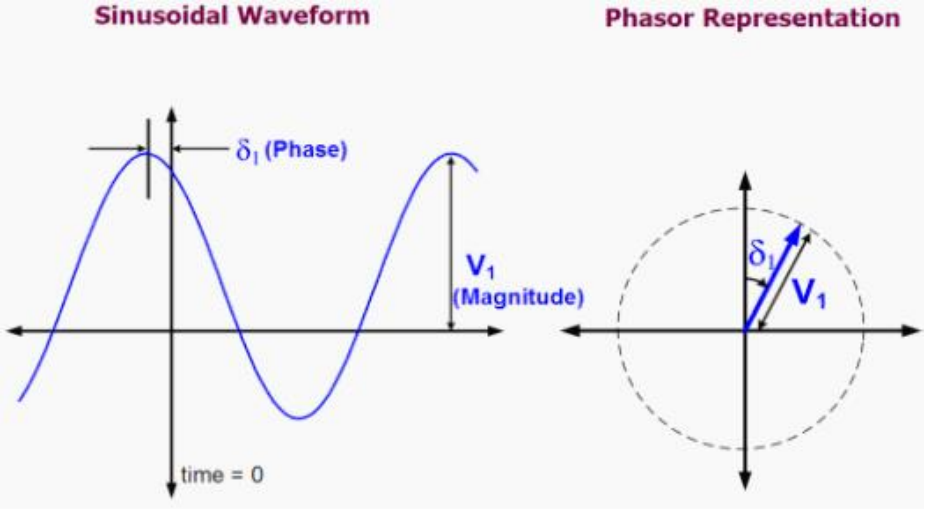

Figure 2. Synchrophasor Representation of Sinusoid [28], public domain

Data from PMUs are sent from remote locations across the system at rates of up to 60 samples per second (sps) per the standard's requirement, although some PMUs may report up to 120sps. This is significantly faster than traditional SCADA reporting rates of 2 to 10 seconds per new measurement. The PMU data is sent using C37.118 synchrophasor protocol over a wide area network (WAN) to a central location such as a control center [29]. At this location, the incoming PMU data is aggregated and time aligned at a phasor data concentrator (PDC). Once the measurements have been time aligned, they are passed to applications that can utilize not only the increased reporting rate, but also the time alignment of the measurements. This comprehensive system of synchronized phasor measurement, communication, and application is commonly referred to as a wide area measurement system (WAMS). Similarly, utilizing these synchrophasors for advanced applications may be referred to as wide area measurement, protection, and control (WAMPAC) [18].

Bonneville Power Administration (BPA) has been a pioneer in synchrophasor technology, testing and deploying the first prototype PMUs from Virginia Tech in 1988,

and later installing the first commercial devices in 1994 [30]. This legacy PMU system has provided valuable information for research and development of new applications and technologies. However, the technology has come a long way since its inception, and US Department of Energy (DOE) stimulus money is funding aggressive implementation of newer devices. In particular, the US DOE is partnering with WECC participant including eleven operating entities in a collaborative effort to deploy synchrophasor devices and develop new applications for real time operations and planning. BPA is currently installing over 150 PMUs at critical high voltage substations across its system. Figure 3 shows WECC deployment of synchrophasors, released mid-October 2012 [15].

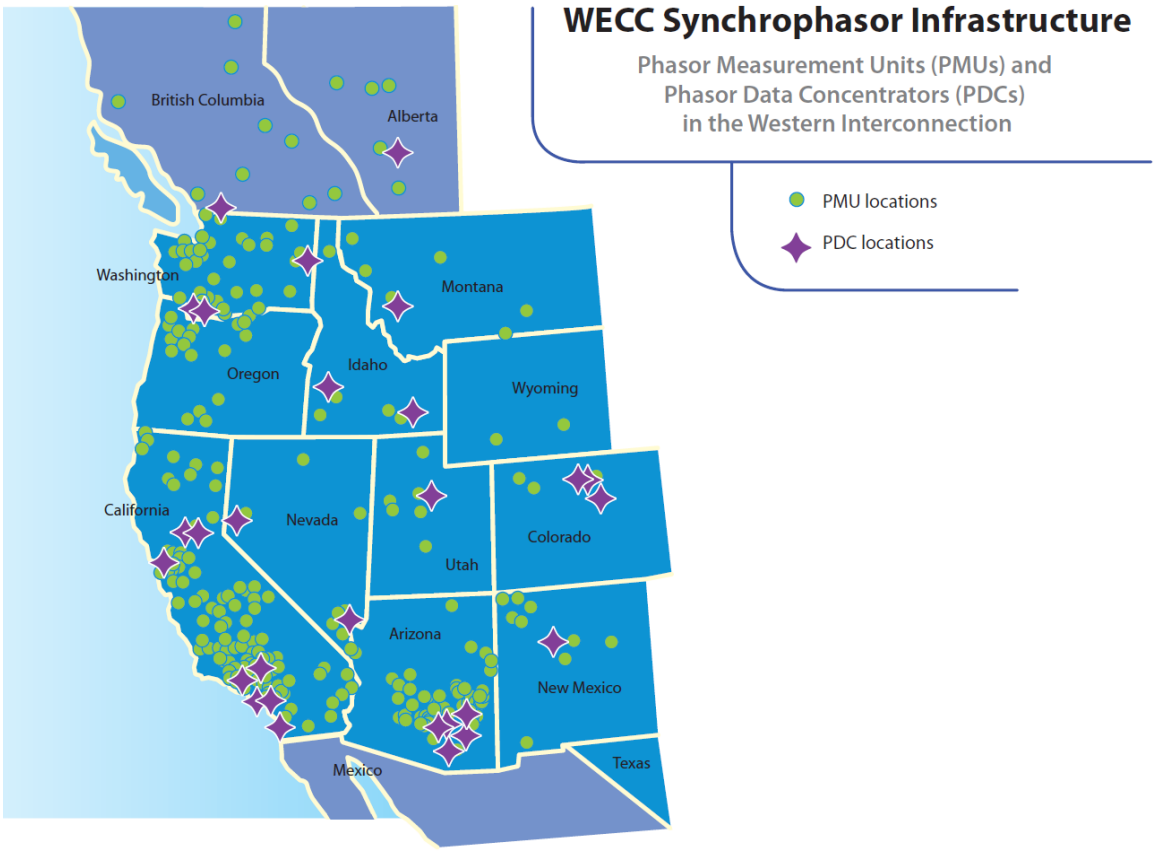

Figure 3. WECC WISP Synchrophasor Deployment [15], public domain

Deployment and sharing of synchrophasor data across an entire network, internally for a utility or more widespread for the entire Interconnection, provides new insight. Current work in the industry is involved primarily in finding applications and processes that best utilize the data in both offline planning and real-time operational timeframes.

BPA is currently installing PMUs for two major functions. A wide-area situational awareness (WASA) suite of applications will aggregate, time align, and store the incoming data for various applications within the control center. Also, a synchrophasor-based remedial action scheme (SP RAS) controller is being developed that will utilize a subset of the WASA measurements for specific synchrophasor-based controls. Both wide area measurement and control systems (WAMCS) are being designed and implemented to ensure adequate levels of measurement reliability, minimized data latency, and application redundancy and accuracy [27, 29]. Figure 4 shows the BPA Synchrophasor RAS (SP RAS) and Synchrophasor WASA architectures as an illustrative example.

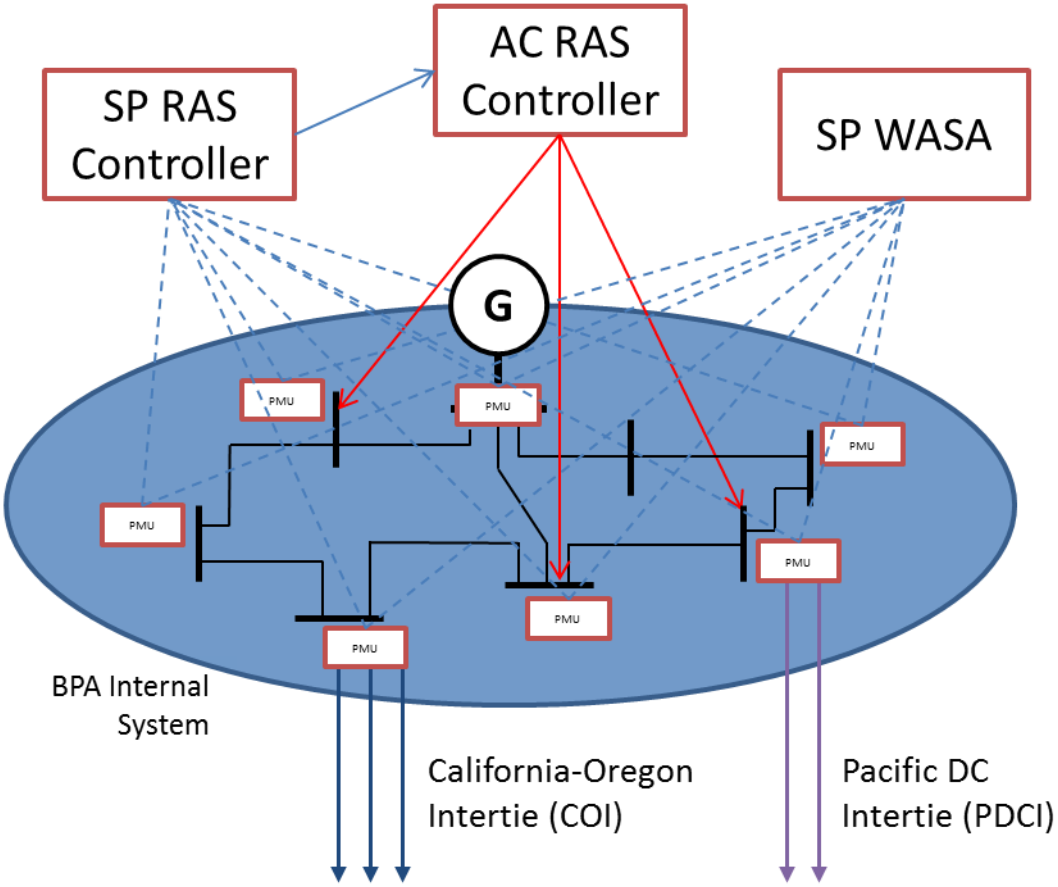

Figure 4. BPA Synchrophasor RAS (SP RAS) Architecture

PMUs are being deployed across the BPA high voltage transmission system at location including major substations, generation interconnections, and interties with other Control Areas. The synchrophasor measurements are sent over the WAN at 60 samples per second (sps) using C37.118 protocol to centralized PDCs or controllers. In parallel to the BPA

WASA PDCs, control-grade PMU data is also available to a new Synchrophasor RAS (SP RAS) controller. Currently being designed and constructed, this controller will include alignment and synchronization logic, data quality logic, and algorithms for RAS action based on the incoming synchrophasor data. Output of the SP RAS controller is expected to integrate with the existing RAS controllers for simple and timely actuation of control signals. As an additional input, the existing RAS schemes can be configured to include SP RAS controls if deemed effective. Control signals are sent to the field devices, generators, interties, etc. using the existing RAS architecture and communications systems. This architecture provides new opportunities for measurement but also constraints on available control actions. The goal is to utilize the existing measurement structures while minimizing the necessary changes or updates to the control systems for implementing new logic and control strategies.

1.3. Overview of BPA and the WECC System

The North American electric power grid is regulated by the Federal Energy Regulatory Commission (FERC), who "*promote[s] the development of safe, reliable and efficient energy infrastructure that serves the public interest* [31]". The North American Electric Reliability Corporation (NERC) is the electric reliability organization certified by FERC to enforce reliability standards along with other ancillary services to its members [3]. There are three synchronously-connected Interconnections (Western, Eastern, and ERCOT) under FERC and NERC regulation, which are connected to one another through asynchronous links. NERC consists of eight regional entities that oversee and enforce reliability of the Bulk Electric System (BES). The Regional Entities have the responsibility of working with the various Balancing Authorities (BAs) to coordinate operation and planning activities of each of its members. Each BA "integrates resource plans ahead of time, maintains load-interchange-generation balance within a Balancing Authority Area, and supports Interconnection frequency in real time [21]." Figure 5 shows a map of the NERC Regional Entities and Balancing Authorities [3].

WECC is the geographically largest of the eight Regional Entities under NERC jurisdiction, with its footprint extending from Alberta and British Columbia in Canada to the northern parts of Baja California in Mexico. The latest facts released by WECC show a

service territory of over 1.8 million square miles, with 126,285 miles of transmission and a population of 78 million people [32]. Due to the geographic diversity and composition of the western United States, WECC faces substantial electrical challenges unlike other systems. While Canada can experience severely cold winter conditions, southern states such as California and Arizona may have severely hot summers. While California is primarily an energy importer, Canada and the Pacific Northwest can experience over-generation conditions from their hydroelectric generation systems due to heavy river runoff and high wind penetration. These are just a few examples of the diversity of WECC, that can contribute to reliability concerns from the BAs and WECC as the Regional Entity.

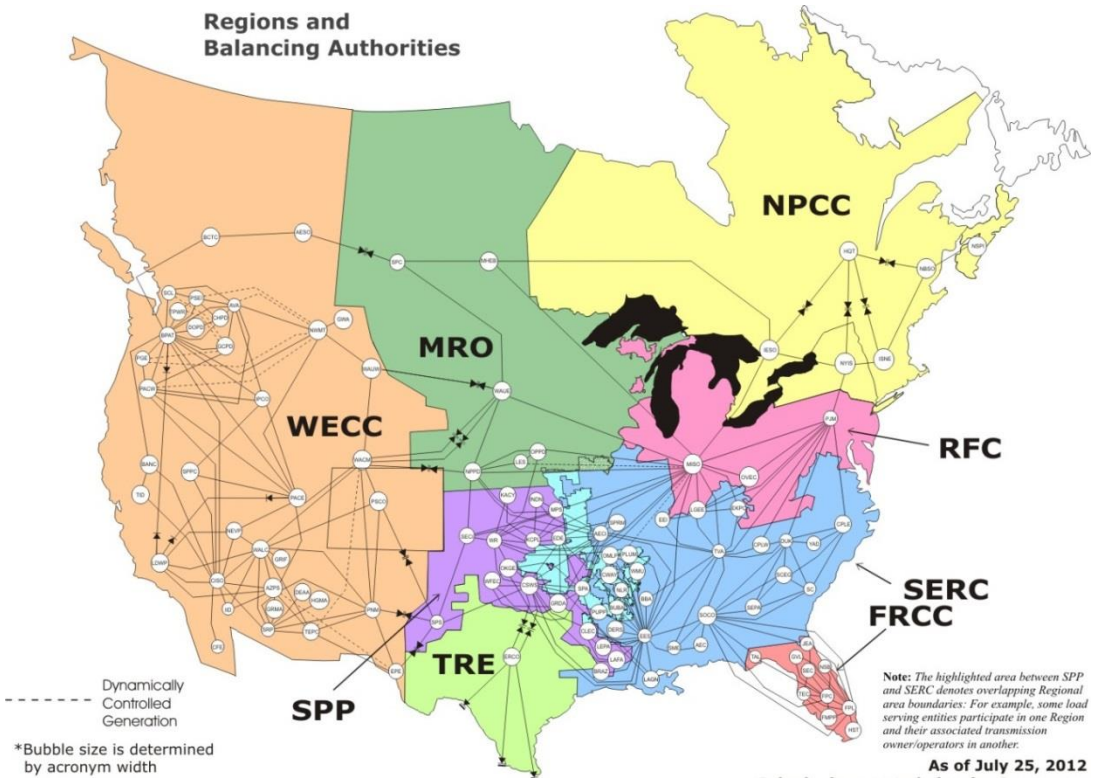

Figure 5. NERC Regional Entities and Balancing Authorities [3], public domain

The Bonneville Power Administration (BPA) is a federal nonprofit organization in the Pacific Northwest, established in 1937 to market electric power from the hydroelectric dams to the load centers. BPA markets wholesale electric energy from 31 federal hydroelectric generation projects throughout the Columbia River Basin, one nuclear generation facility, and several smaller generating plants. With over 15,000 circuit-miles of high voltage transmission, BPA operates and maintains approximately three-fourths of

the high voltage transmission in its service territory. With about 45% of the energy produced from relatively cheap hydroelectric generation facilities, BPA is a large exporter of power to California through the California-Oregon Intertie (COI) and the Pacific DC Intertie (PDCI). In addition, large hydro projects in Canada also sell power to California, wheeling through the BPA system, over the Northern Intertie (NI). With the Cascade Mountains running down the states of Washington and Oregon, the geographic topology and landscape drives the electrical characteristics of the power grid. Figure 6 shows a map of the BPA high voltage transmission system [13].

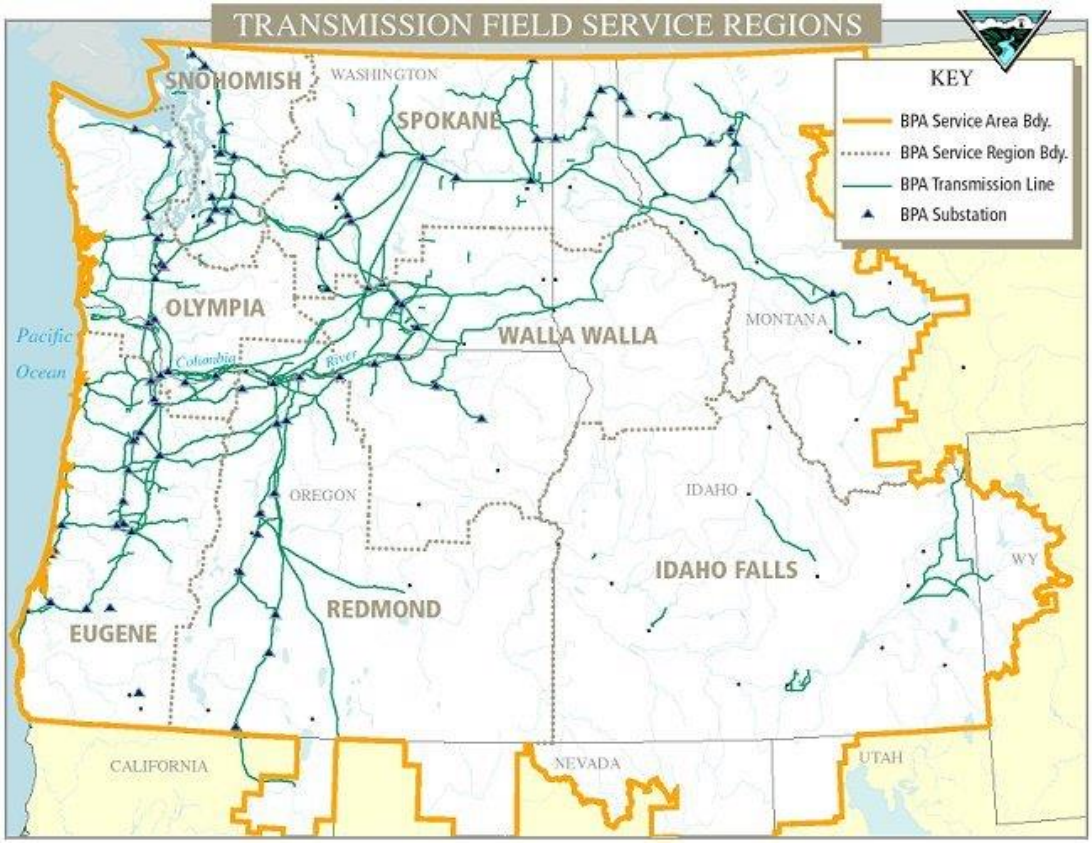

Figure 6. Bonneville Power Administration Transmission System [13], public domain

1.4. Synopsis of the September 8, 2011 Outage

San Diego and the surrounding areas experienced a large outage on September 8, 2011. The staffs of FERC and NERC convened to provide insight regarding the causes of the outage and recommendations on improving reliability of the electric grid. 2.7 million customers were out of power following an 11 minute cascading disturbance initiated by

improper switching of a series capacitor bank on a major 500kV line. Figure 7 illustrates a graphic of the affected region of WECC [2].

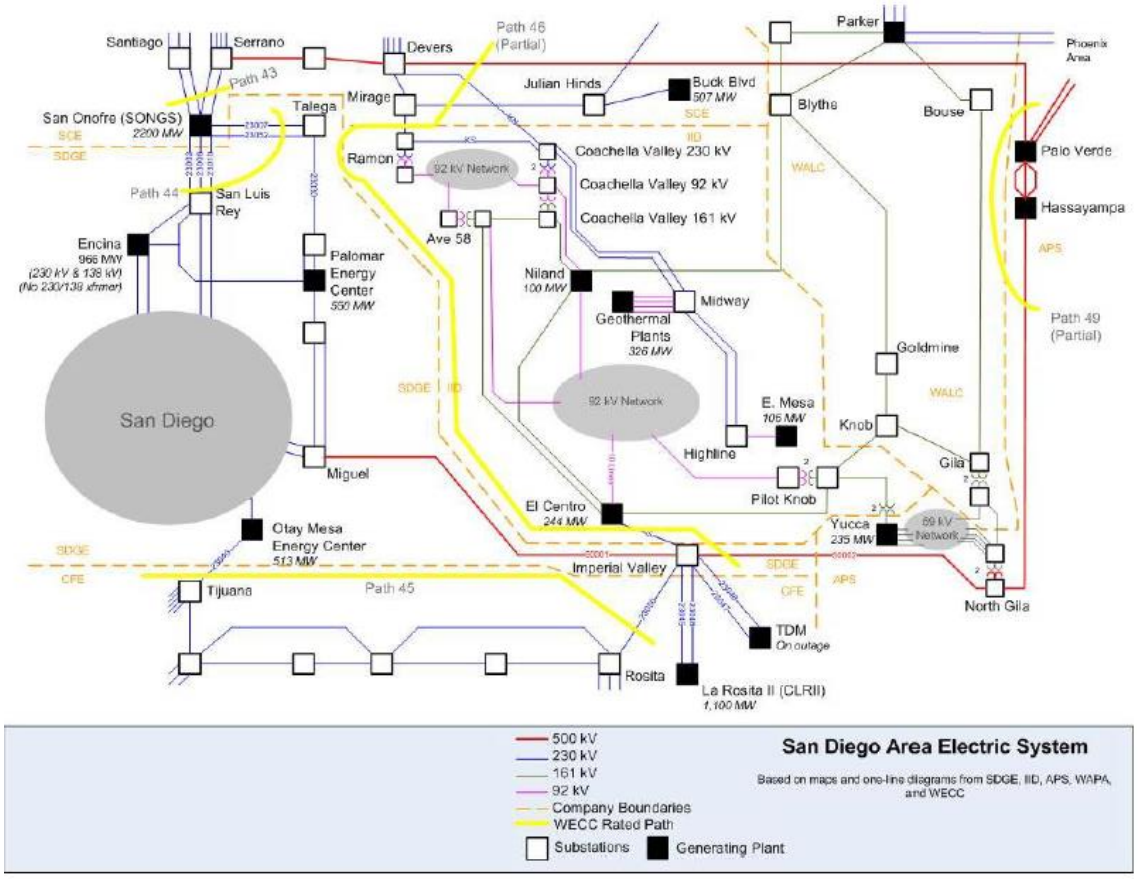

Figure 7. Southern US-Baja California Affected Outage Area [2], public domain

Although improper switching caused a line-line fault on the Hassyampa-North Gila 500kV transmission line, the cause of the outage is much more complex due to the nature of reliable and secure operation of the power system. Approximately 44 minutes prior to the initiating disturbance, the Imperial Irrigation District Real-Time Contingency Analysis (RTCA) tool identified that the system was being operated in an insecure condition but was not noticed by the system operators because the screen was not visible and audible alarms were disabled. Following the outage of 500kV line, Arizona Public Service (APS) believed that the line could be returned to service very quickly, unaware that the phase angle difference between the two ends of the line had exceeded the synch-check limit of 60°. Consequent tripping due to overloading conditions caused increasing stress on the surviving system. Eventually, a responsive remedial action scheme (RAS) tripped

generation at the Imperial Valley substation when generation should not have been tripped. This caused Path 44, a path consisting of five transmission lines south of the San Onofre Nuclear Generation Station (SONGS), to exceed their overload limit of 8000A. The SONGS Separation Scheme severed the connection of these five lines, cutting off Southern California and parts of Arizona and northern Baja California from the rest of WECC. Unable to balance generation and load during the underfrequency load shedding and generator tripping following the separation, these areas went completely black [2].

The outage highlights a number of critical concepts of reliable operation and planning of the Bulk Power System (BPS). The following causes and recommendations, taken from the full list of causes and recommendations from the blackout, formulate a basis and necessity for the research performed here [33]:

1. *Lack of situational awareness, significant phase angle difference*: Firstly, the IID RTCA was not utilized properly with the visual screen hidden and the audible alarms disabled. In addition, visualization of phase angles across the system would have identified the inability of immediately returning the Hassyampa-North Gila 500kV line to service.
2. *Lack of coordination of RAS, and lack of 'safety nets' for providing backup protection*: The S Line RAS scheme and the SONGS Separation Scheme tripped due to response-based overloading conditions. RAS schemes must be studied and coordinated such that they impact the condition of the system positively. No 'safety net' schemes were in place that could mitigate the prevailing blackout conditions.

This research utilized synchrophasor technology to focuses on incorporating phase angle limits into the control center through an alarming application and a response-based RAS scheme to detect large disturbances to apply reactive support. With the blackout recommendations in mind, visualization of phase angle and alarming of excessive or unacceptable phase angle is a major goal. In addition, study and application of a response-based RAS scheme should incorporate a focus of the implications and negative impacts it could have on the system.

Chapter 2. Review of Concepts and Literature

The electric power grid is composed of a large number of electric power producers and consumers. Energy is produced at generating facilities that convert potential and kinetic energy into electromechanical torque. The rotating shaft of an electric machine generates a rotating magnetic and electric field which is transformed to high voltage electric power. At these high voltages, electric power can be transported through transmission networks over vast distances with minimal losses before again transforming the voltage to a lower distribution level. At distribution voltages, electric power is delivered to a variety of customers. These customers can range from large industrials such as manufacturing facilities to small single-family residential homes.

Today's power grid is a highly complex and sophisticated machine that remains in equilibrium to "keep the lights on." It is important to understand the fundamental relationships behind this equilibrium in order to apply effective protection and controls to improve system reliability. This chapter illustrates some of the core concepts behind the innovative applications and methodologies presented in this research.

2.1. Power and Angle Relationship

System stress can be described effectively using the simple equations of power flow through a transmission line. Let us assume a lossless transmission line between two buses, as shown in Figure 8.

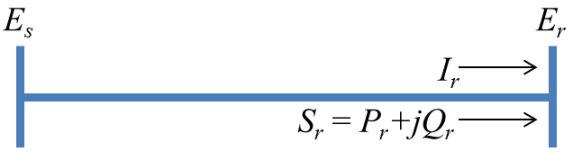

Figure 8. Basic Representation of Lossless Transmission Line

This voltage equation for this line can be represented as

$$\overline{E_s} = \overline{E_r}\cos\theta + jZ_c\overline{I_r}\sin\theta \qquad (2.1)$$

where E_s and E_r represent the sending and receiving end voltages, I_r is the receiving end current flow on the line, and Z_C is the characteristic impedance of the line. $\theta = \beta l$ is the

electrical length ("line angle") of the transmission line where β is the phase constant, which is the imaginary component of the propagation constant of the line, and l is the length of the line [24]. Expressing (2.1) in terms of the real and reactive power quantities, we get

$$\overline{E_s} = \overline{E_r}\cos\theta + jZ_c \sin\theta \left(\frac{P_r - jQ_r}{\overline{E_r}^*} \right) \tag{2.2}$$

where P_r and Q_r are the receiving end real and reactive power flow, respectively. Now assume the line is loaded such that E_s leads E_r in phase by δ, where δ is the phase angle difference between the bus voltage phasors, as shown in Figure 9.

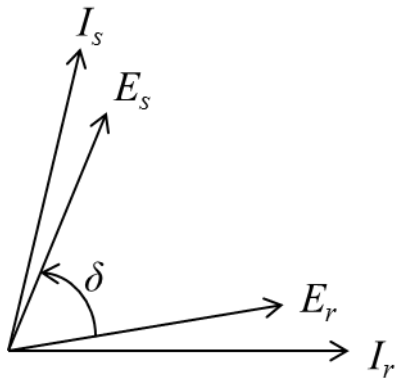

Figure 9. Phasor Diagram of Lossless Line

Expressing the sending end voltage in terms of this angle difference, and equating the real and imaginary components of (2.2) with (2.1), we obtain

$$\overline{E_s} = E_s e^{j\delta} = E_s(\cos\delta + j\sin\delta) \tag{2.3}$$

$$E_s \cos\delta = E_r \cos\theta + Z_c \left(\frac{Q_r}{E_r} \right) \sin\theta \tag{2.4}$$

$$E_s \sin\delta = Z_c \left(\frac{P_r}{E_r} \right) \sin\theta \tag{2.5}$$

Rearranging (2.5), we obtain a relationship between the real power flow, sending and receiving end voltages, the electrical length of the line, and the phase angle difference between the bus voltages, as shown in (2.6).

$$P_r = \left(\frac{E_s E_r}{Z_c \sin\theta} \right) \sin\delta \tag{2.6}$$

For the case of a short line approximation, $\sin(\theta) \approx \theta$ because θ is relatively small. So,

$$Z_c \sin\theta = Z_C \theta = \omega L l = X_L \tag{2.7}$$

where L is the per phase inductance of the line, ω is system frequency, and X_L is the series reactance of the line. This gives the conventional description of power transfer across a transmission line assuming a short, lossless line. Additionally, the phase angle can be represented in terms of the same variables, as shown in (2.8) and (2.9).

$$P_r \approx \left(\frac{E_s E_r}{X_L} \right) \sin\delta \tag{2.8}$$

$$\delta = \sin^{-1}\left(\frac{P_r X_L}{E_s E_r} \right) \tag{2.9}$$

Although this is an approximation, it provides a foundational expression between critical system variables. The sending and receiving ends of the line are generally kept near the scheduled voltage; let us assume 1.0pu. Accordingly, the angular difference between the ends of the line is dependent on the power transfer across the line and the impedance of the line. This concept can be generalized to describe larger paths or corridors on a full transmission system. The "stress" of a path or corridor depends on the total power being transferred across the path and the impedance between the sending and receiving ends. Power transfer primarily depends on generation dispatch and transmission schedules while impedance is based on the integrity of system elements. Outages will affect the impedance of the corridor, and impact the phase angle difference. The overall phase angle difference between two buses on a large power grid is dependent on the overall impedance between the two locations and the total transferred power.

2.2. Power System Security

Operating and planning analyses aim at ensuring that the system can withstand the worst expected and plausible conditions pre- and post-contingency. The approach to analyzing a system operating point and its response to a disturbance is broadly referred to as security assessment. Power system security is defined by NERC as "*the ability of the bulk power system to withstand sudden, unexpected disturbances such as short circuits, or unanticipated loss of system elements due to natural or man-made causes* [3]." A power system's security can also be defined as "*the degree of risk in its ability to survive imminent disturbances (contingencies) without interruption of customer service* [20]." Both definitions highlight a dependence on operating condition and unexpected disturbances upon the system. These two dependencies form the foundation of power system security and its impacts on reliable planning and operation of the bulk power system. During the operational horizon, security assessment is performed to ensure that current or expected system conditions are within acceptable limits. In the planning timeframe, security assessment is used as a tool for assessing system performance for changing system conditions such as load growth, system additions, or system retirements.

Security is analyzed on the basis of three timeframes: pre-contingency steady state, post-contingency transient condition, and post-contingency steady state [34]. The power system is planned and operated such that it stays within studied security limits, prior to and after a contingency occurs. In addition, the transient timeframe also has performance criteria, used to monitor system response for acceptable performance. Based on this approach, power system security is generally characterized into two forms of analysis: steady-state (static) security assessment (SSA) and dynamic security assessment (DSA). Static security assessment checks the pre- and post-contingency operating conditions for thermal and voltage violations, assuming that the system can find a new steady state after the contingency. Dynamic security assessment analyzes the response of the system during the transient timeframe of the contingency to ensure that angular, frequency, and voltage stability are maintained [20]. The relationship between these analyses is shown in Figure 10.

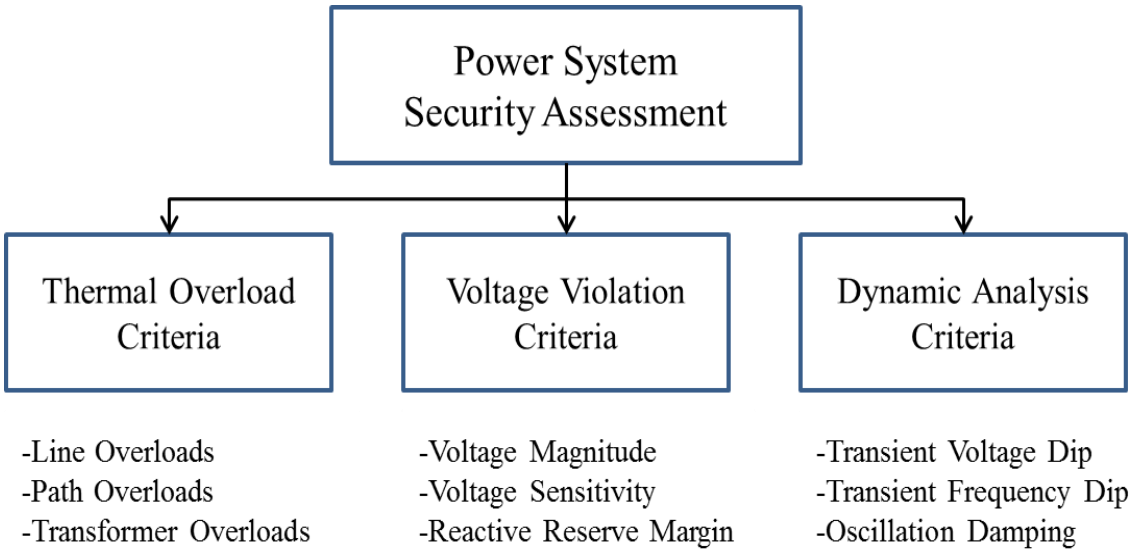

Figure 10. Power System Security Assessment

Security assessment of power systems can be classified into three major categories: thermal violations, voltage violations, and dynamic performance violations. Contingency analysis generally refers to analyzing the pre- and post-contingency operating points using either a Full AC Power Flow or Linearized DC power flow [35]. The full or linearized power flow simulations do not consider the transient timeframe immediate after the perturbing event but do consider the major outages and subsequent switching of automated controls. These controls may include Special Protection Schemes (SPSs), transformer tap changing, reactive device switching, and other dynamic elements. Positive sequence transient simulation tools such as PSS/E or PSLF are commonly used to assess the dynamic performance of the system response to contingencies [36, 37]. Currently, the disconnect between effective power flow tools and transient simulation tools makes integrated static and dynamic security assessment a significantly labor-intensive process. The cases must be converted between different formats and validated to ensure conversion is successful. Contingency definitions in the power flow contingency analysis tools are not easily transported over to the transient timeframe and must be reconstructed in time domain simulations. It is expected that the next few years will bring a more integrated and collaborative effort between these tools to make this process more streamlined.

Each subcategory of security assessment has its own analysis and tools to determine if the criteria is met. Static security assessment can be performed using power flow and

contingency analysis tools embedded in the software platforms. The thermal overload limits are related directly to the current (and/or real power) flowing through the conductors. These limits relate to the increased temperature of the conductors and/or the line sag of the transmission lines approaching minimum clearance. The overload criteria can be defined by

$$I_l < I_R, \ l \in \Lambda \tag{2.10}$$

$$MVA_t < MVA_R, \ t \in \mathrm{T} \tag{2.11}$$

where l is the line number, t is the transformer number, and Λ and T are the subset of studied transmission lines and transformers, respectively. Λ and T are simply the total number of elements in the Interconnection if the entire system is under consideration. I_R and MVA_R are the line and transformer ratings, respectively. Line rating is based on the maximum current flow [Amps] and transformer ratings are based on total complex power [MVA]. These ratings can change pre- and post-contingency from normal rating to short-term emergency rating. Additionally, the ratings may change based on season such as heavy summer and heavy winter operating cases. This is based on lower ambient temperature and therefore higher carrying capacity of the line during colder weather conditions.

Voltage violation criterion is also a component of static security assessment since it is based on power flow and contingency analysis results. Pre-contingency voltage levels in the base case must fall within expected levels. BPA uses operating voltage schedules for its major EHV buses, and these schedules are maintained within a small window of operation (e.g. 540±3kV). The scheduled voltages are reflected in the BPA planning base cases, but data for most the rest of the system is unavailable. Therefore, generic voltage criterion is used for the remainder of the system as a simplification. Voltage magnitude thresholds are defined as

$$V_{L1} < V_b < V_{H1}, \ b \in \mathrm{B} \tag{2.12}$$

where B is the subset of studied buses, V_{L1} and V_{H1} are the base case voltage low and high thresholds. Post-contingency voltage deviation shall not fall below predefined levels for different types of contingencies, defined as

$$V_{b,post} \geq \chi \cdot V_{b,pre} \tag{2.13}$$

where χ is the voltage deviation definition for the given contingency category (described below). In addition, voltage swings caused by shunt capacitor or reactor switching should be minimized. Strong sensitivity of voltage to changes in reactive power, dV/dQ, may be indication of voltage instability because the operating point may be near the trough of the Q-V curve [24]. Therefore, a simplification but effective solution to this problem is to require adequate levels of reactive reserve margin through dynamic reactive support (discussed in detail in Section 2.6). In the Pacific Northwest, reactive reserve margin is generally not a concern for operating or planning purposes because of the presence of hydro generation operating in the bucking position (consuming VARs, allowing for ample reactive support if necessary). Regardless, the reactive reserve margin requirement can be defined as

$$Q_{res} = \sum_{i=1}^{n_g} \left(Q_{cap,i} - Q_{out,i} \right) \tag{2.14}$$

$$Q_{res} \geq Q_{RRM} \tag{2.15}$$

where $Q_{out,i}$ is the reactive power output of dynamic reactive element i, $Q_{cap,i}$ is the reactive power capability of element i, Q_{res} is the reactive reserve available, and $Q_{RRM}$is the reactive reserve margin requirement. n_g is the number of generators or dynamic reactive elements considered in the reserve calculation. For example, the Pacific Northwest uses two major generation hubs for calculating reactive reserve margins. These two calculations are used by the system operators for reliable operation and sufficient voltage support for major flowgates and Paths on the system.

While the static security assessment checks the steady-state operating conditions pre- and post-contingency, dynamic security assessment focuses on the transient response of the

system following the disturbance to ensure that a new steady-state operating point is reached. Any disturbance will perturb the power system to some degree, and severe contingencies may cause stability concerns such as undamped power swings or voltage deviations. Instability may occur if the generators begin to lose synchronism with the rest of the system. Planning studies analyze the system response to ensure that foreseen operating points do not lead to unstable conditions. Similarly, real-time online dynamic security tools scan possible contingencies for unstable response because the power system is never operated as planned for. The hope is that the planning cases are the worst-case scenario in terms of system stress and operating state, but this may not be the case as has been shown in major blackouts such as the 2003 US-Canada blackout [1]. The problem with real-time dynamic security tools is the computational burden and time requirement. Time domain transient simulations require massive amounts of time for large databases of contingencies. For online studies, the computation must be relatively fast, making online DSA a significant challenge.

The planning standards (described below) use a voltage dip criteria that encompasses both magnitude and duration. If a given bus voltage, $V_{b,i}$, is

$$V_{b,i} < V_{\min}, \ i = 0,...,n_b \tag{2.16}$$

where V_{min} is the minimum voltage dip threshold and n_b is the number of buses observed, then the voltage magnitude criteria is violated. V_{min} is generally a percentage of the pre-contingency voltage, and may be more strict for load buses than non-load buses in an attempt to protect against motor load stalling. A voltage deviation with duration requirement is also invoked to protect against delayed voltage recovery such as Fault-Induced Delayed Voltage Recovery (FIDVR) which has been observed in various parts of the US. Utilities such as BPA and Sothern California Edison (SCE) are exploring real-time tools to mitigate the possibility of FIDVR and eventual voltage instability [38]. The voltage deviation-duration requirement can be defined as

$$V_{b,i-d} < V_{\min-d}, \ i = 0,...,n_b \tag{2.17}$$

where $V_{min-d} > V_{min}$, and $-d$ refers to the time duration associated with low voltage threshold. The V_{min-d} limit can be exceeded so long as the voltage recovers within a predefined time limit.

Similar to the voltage dip, a minimum frequency deviation requirement is set to mitigate the potential for frequency instability. As will be discussed later, frequency excursions are a result of real power imbalance, so the frequency criterion seeks to limit the deviation following large losses of generation. Analogous with the voltage duration criteria,

$$f_{b,i-d} < f_{\min-d}, \ i = 0,...,n_b \tag{2.18}$$

where f_{min-d} is a minimum frequency limit that can be exceeded so long as frequency recovers within a predefined time limit.

The security assessment described above is inherently based on predefined study requirements that must be met. In the planning timeframe, these standards are defined by the Transmission Planning (TPL) Reliability Standards TPL-001 to TPL-004 set by NERC [39]. Transmission operators are required to ensure reliable operation of the bulk electric system under normal conditions as well as outages consisting of one or more system elements. TABLE I is adapted from the TPL standards and defines the criteria for contingency definition [39].

TABLE I. TRANSMISSION PLANNING STANDARDS, ADAPTED FROM [39]

Category	Contingency	System Limits or Impacts		
	Initiating Event(s) and Contingency Elements(s)	**System Stable, Thermal and Voltage Limits within Ratings**	**Loss of Demand or Curtailed Firm Transfers**	**Cascading Outages**
A No Contingency	All Facilities in Service	Yes	No	No
B Event resulting in the loss of a single element	Single Line to Ground (SLG) or 3-Phase (3φ) Fault, Normal Clearing - Generator - Transmission Circuit - Transformer Loss of an Element without Fault	Yes	No	No
	Single Pole DC Line Fault, Normal Clearing	Yes	No	No
C Event(s) resulting in loss of two or more	SLG Fault, Normal Clearing - Bus Section - Breaker failure or internal fault	Yes	Planned or Controlled	No
	SLG or 3φ Fault, Normal Clearing, Manual	Yes	Planned or	No

(multiple) elements	System Adjustment, Followed by Another SLG or 3φ Fault, with Normal Clearing		Controlled	
	Bipole DC Line Fault, Normal Clearing Any two circuits of multiple circuit tower	Yes	Planned or Controlled	No
	SLG Fault, Delayed Clearing (stuck breaker or protection system failure) - Generator - Transformer - Transmission Circuit - Bus Section	Yes	Planned or Controlled	No
D Extreme event resulting in two or more (multiple) elements removed or cascading out of service	3φ Fault, Delayed Clearing (stuck breaker or protection system failure) - Generator - Transformer - Transmission Circuit - Bus Section	Evaluate for risks and consequences - May involve substantial loss of demand and generation is widespread areas - Portions or all of interconnected system may or may not achieve new, stable operating point - Evaluation may require joint studies with neighboring entities		
	3φ Fault, Normal Clearing - Breaker (faulre or internal fault)			
	- Loss of towerline with 3+ circuits - Loss of all lines in common right-of-way - Loss of substation or switching station (one voltage level plus transformers) - Loss of all generating units at station - Loss of large load or major load center - Failure of fully redundant Special Protection System (Remedial Action Scheme) to operate when required - Operation or misoperation of fully redundant RAS in response to event or abnormal system condition for which it is not intended to operate - Impact of severe power swings or oscillations from disturbance in another Regional Reliability Organization			

Category A defines the normal operating point prior to any disturbance on the system. A Category B event is a single element "N-1" outage on the system; generally the 3-phase fault is studied first because it is more severe and easily modeled in the positive sequence load flow programs. Category C contingencies are the most severe contingency in which load cannot be unexpectedly lost and the entire system must maintain stability. These include "N-2" or greater outages of generating units, transformers, double circuit lines, and bus sections. In addition, delayed clearing from stuck breaker, breaker failure, other protection system failures, or breaker faults is considered. This requires understanding of the breaker configuration or each substation to determine where hidden failures may result in failed protection. Lastly, Category D contingencies are those credible contingencies that have a high risk of cascading failure and widespread blackout conditions. Examples are listed in TABLE I and are generally too severe to credibly study all scenarios. Therefore

operational and planning experience and engineering judgment are used to define these contingencies.

In addition to the definitions above defined by NERC reliability standards, WECC also requires that reliability criteria is met to ensure compliance with NERC policies and standards. The WECC Planning Standards provide more quantitative guidance for the operating entities for performing security and stability assessment for the bulk electric grid. TABLE II provides the WECC criteria used to assess system performance for various disturbance classifications [34]. This performance criterion holds for effects not only on the planning entity's system but for other systems as well.

TABLE II. WECC CONTINGENCY PERFORMANCE CRITERIA, ADAPTED FROM [34]

NERC/WECC Category	Outage Frequency (outages/yr)	Transient Voltage Dip Requirement	Minimum Transient Frequency Requirement	Post-Transient Voltage Deviation Requirement
A	N/A	Nothing in addition to NERC		
B	≥ 0.33	Not to exceed 25% at load buses or 30% at non-load buses Not to exceed 20% for more than 20 cycles at load buses	Not below 59.6Hz for 6 cycles or more at load buses	Not to exceed 5% at any bus
C	0.033 – 0.33	Not to exceed 30% at any bus Not to exceed 20% for more than 40 cycles at load buses	Not below 59.0Hz for 6 cycles or more at a load bus	Not to exceed 10% at any bus
D	< 0.033	Nothing in addition to NERC		

As the criteria explain, Category B and C contingencies (the bulk of planning study contingency analysis) are held to criteria based on time duration and % deviation from pre-contingency operating point. Post-transient conditions are also considered in the criteria to ensure sufficient voltage recovery after the fault. Worst Case Contingency Analysis (WCA) tools are used by system planners to determine system variables experiencing the worst or violating response in terms of the defined criteria. Figure 11 is taken from the WECC Planning Standards and is used to portray the transient requirement in terms of voltage [34]. The figure gives an illustrative example of how to calculate the various parameters and determine whether responses are in violation of the standard.

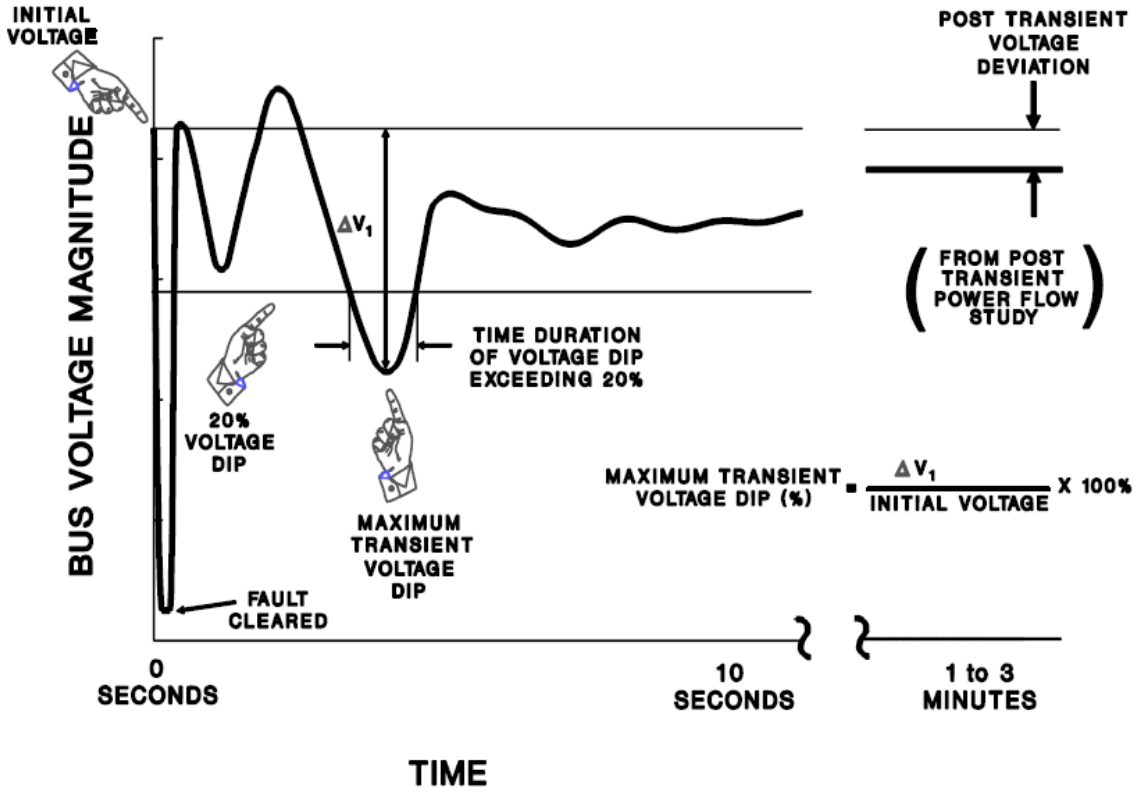

Figure 11. WECC Transient Performance Requirements [34], public domain

These tools and analysis techniques are used across the board, from real-time tools to operations planning to transmission planning. This research utilizes both static and dynamic security assessment for performing offline studies to create real-time tools and applications.

2.3. Real Power Balance and Frequency Response

An interconnected power system is a complex machine that must maintain equilibrium through power balance of generation and load. In North America, an imbalance between input and output powers is directly reflected in deviation from the 60Hz nominal frequency of the power grid. Because the grid is such a dynamic machine, frequency is always moving around this scheduled value. These small changes are expected since loads are constantly changing and generation is accommodating to these changes as quickly as possible. However, large disturbances such as loss of generation or load can cause more severe deviations in frequency.

The equations of motion provide a fundamental background behind power balance and its effect on frequency. Let us explore the swing equation and its principles. A difference in torque between the mechanical input torque, T_m, and the electromagnetic output torque, T_e, of a generator creates an accelerating torque, T_a, on the shaft of the machine

$$T_a = T_m - T_e \quad [N \cdot m] \tag{2.19}$$

This same concept holds for machines as well, except reversed sign for the input and output torques; the driving input torque is the electrical torque and the output torque is the mechanical torque. The total inertia behind the generator and the prime mover supplying the mechanical input torque is represented by the simple equation of motion

$$J \frac{d\omega_m}{dt} = T_m - T_e \tag{2.20}$$

where J is the moment of inertia of the machine and ω_m is the angular velocity of the machine [24]. This explains that a change in the velocity of the machine is due to a difference between input and output torque, proportional to the amount of inertia on the system.

The moment of inertia can be expressed in terms of normalized inertia constant *H*. This constant represents the kinetic energy at rated speed divided by the volt-ampere base of the machine. The moment of inertia and inertia constant can be expressed as

$$H = \frac{1}{2} \frac{J\omega_0^2}{BASE_{VA}} \tag{2.21}$$

$$J = \frac{2H}{J\omega_0^2} BASE_{VA} \tag{2.22}$$

where ω_0 is the rated speed and $BASE_{VA}$ is the machine base value in volt-amperes. We can now introduce the angular position of the machine rotor with respect to a synchronously rotating reference frame as

$$\delta = \omega_r t - \omega_0 t + \delta_0 \tag{2.23}$$

where t is time, and δ_0 and ω_0 are the initial position and speed of the rotor at $t = 0$, respectively. Substituting these expressions into the equation of motion and simplifying will give

$$\frac{2H}{\omega_0}\frac{d^2\delta}{dt^2} = T_m - T_e - K_D\Delta\omega_r \tag{2.24}$$

The term K_D is often included to describe a proportional damping constant related to the change in rotating speed of the machine. (2.24) is most commonly referred to as the *swing equation*.

The swing equation represents a machine's rotor position, or rotor angle, with respect to a synchronous reference. This concept can be expanded for power system analysis using two nonlinear first order differential equations, as in (2.25) and (2.26) [24].

$$\frac{d\Delta\overline{\omega_r}}{dt} = \frac{1}{2H}\left(\overline{T_m} - \overline{T_e} - K_D\Delta\overline{\omega_r}\right) \tag{2.25}$$

$$\frac{d\delta}{dt} = \omega_0\Delta\overline{\omega_r} \tag{2.26}$$

Note that $\overline{T}_m$, $\overline{T}_e$, and $\overline{\omega}_r$ are all normalized to a per unit system, and

$$\overline{\omega_r} = \frac{\omega_r}{\omega_0}. \tag{2.27}$$

In (2.25), the mechanical and electrical torque can be considered as the generator input power and load output power, respectively, because power equals torque multiplied by speed

$$P = \omega_r T. \tag{2.28}$$

These two equations represent a number of fundamental concepts of power system stability and analysis:

1. A change in either mechanical or electromechanical torque will cause a change in the position of rotor angles with respect to a synchronous reference.
2. As the rotor angles change, a resultant change in system frequency will occur.
3. The rate of change of frequency depends upon inertia and applied torques of generation and load, as well as system damping.
4. The resistance of a machine to change in frequency is proportional to the size, or inertia, of that machine.

These concepts are foundational for describing an Interconnection or Control Area's response to system frequency. It has been proposed by many that both the Eastern and Western Interconnections are experiencing a decrease in Frequency Response [40]. Let us explore a power system's FR and the impacts this can have on system conditions.

A power system's ability to respond to deviations from nominal frequency can significantly affect post-contingency operating conditions. Each Balancing Authority Area (BAA) should contribute to support of frequency through its generators and loads. Frequency Response (FR) is defined as "*an automatic and sustained change in the power consumption or output of a device that occurs within 5-30 seconds of and is in a direction to oppose a change in the Interconnection frequency* [41]." Essentially, FR can be used as a measure of an interconnected power system's ability to "*arrest and then stabilize rapid changes in frequency* [40]." Frequency Response can be measured as

$$Frequency\ \mathrm{Re}sponse = -\frac{\Delta MW}{10\Delta f} \quad \left[\frac{MW}{0.1Hz}\right] \tag{2.29}$$

where ΔMW is the sudden difference in real power balance between generation and load, and Δf is the settled frequency after the disturbance. It is important to include the (-) term since stable operation of the power system requires a positive response in generation output for a negative change in system frequency. FR is therefore generally referred to as a positive value for discussion.

There are four fundamental types of frequency control in a power system: inertial, primary, secondary, and tertiary control [42, 43]. These types of frequency control and their timeframes are visualized in Figure 12. They can be defined as:

- Inertial Response: Initial "arresting" response prior to control actions taken, driven by the inertia behind rotating masses that deters significant acceleration of the units. This is a natural response to change in torques, and occurs before any automated controls take action.
- Primary Frequency Control: Actions provided by the Interconnection as a whole in response to frequency deviations from nominal to arrest large excursions. These controls include generator governor response, motor load response, and other automated fast-acting device-level controls.
- Secondary Frequency Control: Actions provided by individual Balancing Authorities or other entities to mitigate real power imbalance created from the initial disturbance. These types of controls occur after the primary response, and involve manual or automated adjustment.
- Tertiary Frequency Control: Actions by Balancing Authorities that have "net zero effect" on Area Control Error (ACE). These actions may include economic dispatch of generation, dispatching for native load requirements or intertie flows, and other controls that affect reserve requirements. Examples include utilizing spinning reserves between BAs and initiating reserve sharing agreement to replace lost power [42].

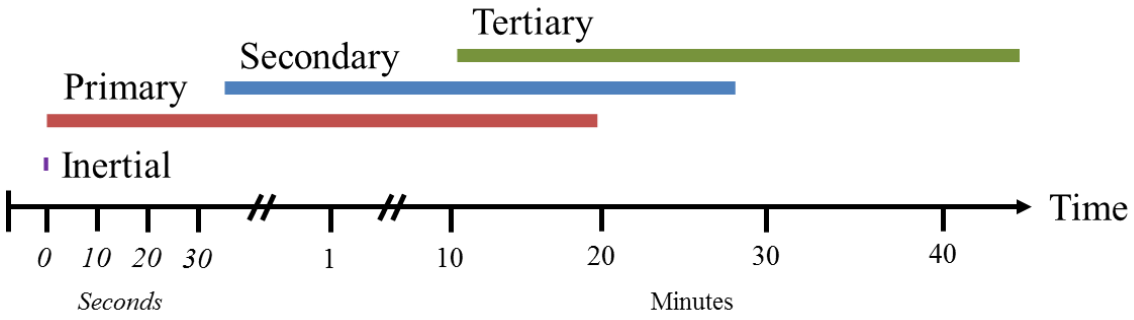

Figure 12. Frequency Control Timeframes

Let us use an illustrative example to describe system response to change in frequency. The data in Figure 13 is from PMU data sampled at 30 samples per second from the BPA synchrophasor network for a large loss of generation in the southern part of WECC. The time axis is referenced to the start of sampling time prior to the event occurrence.

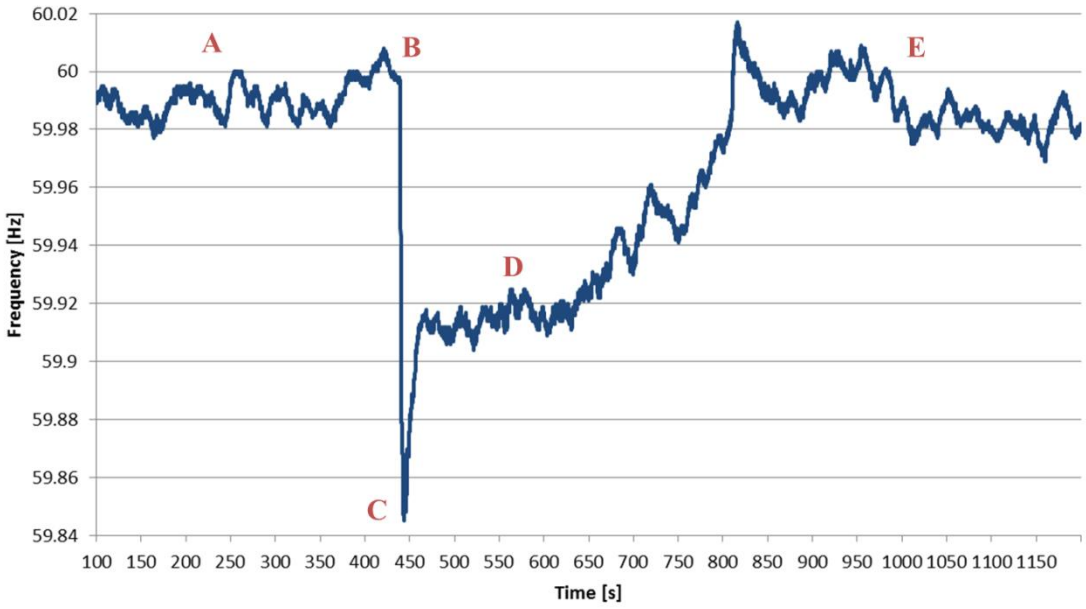

Figure 13. Frequency Response Illustration

Point *A* represents the system frequency prior to the disturbance, with system frequency measured at slightly less than nominal 60Hz for most of the time. Point *B* represents the instant at which the generation is lost and the system frequency declines rapidly. Point *C* is the nadir of the response, in which the inertial and primary frequency controls have arrested the decline to its minimum. Following this point, frequency returns rapidly to approximately 59.91Hz and the generator governors respond to degraded frequency, moving through Point *D*. Generators with frequency response capability slowly bring more generation online by opening steam valves, wicket gates, etc., to balance real power. At approximately 800 seconds after the recording time, there is a steep increase in system frequency, which may be caused by secondary controls such as operator action or loss of load. Following this increase, system frequency begins to settle back to pre-contingency conditions, represented by Point *E*.

Lastly, let us explore simulated system-wide frequency deviation due to a large loss of generation in the southwest part of the WECC (Figure 14). A simultaneous loss of 2 Palo Verde units is used to demonstrate the frequency dip phenomena over time. Frequency does not drop immediately across the WECC since this problem is electromechanical rather than electromagnetic. The inertia behind the machines on the system creates a time-

differential drop in frequency, as shown in Figure 15. After the contingency occurs at $t = 1s$, frequency begins to deviate rapidly, however there is a substantial time difference between when the Palo Verde 500kV bus begins responding compared to the 500kV bus in northern Alberta. However, frequency deviation is greatest in the northernmost part of the system, where the electrical distance to the disturbance is greatest.

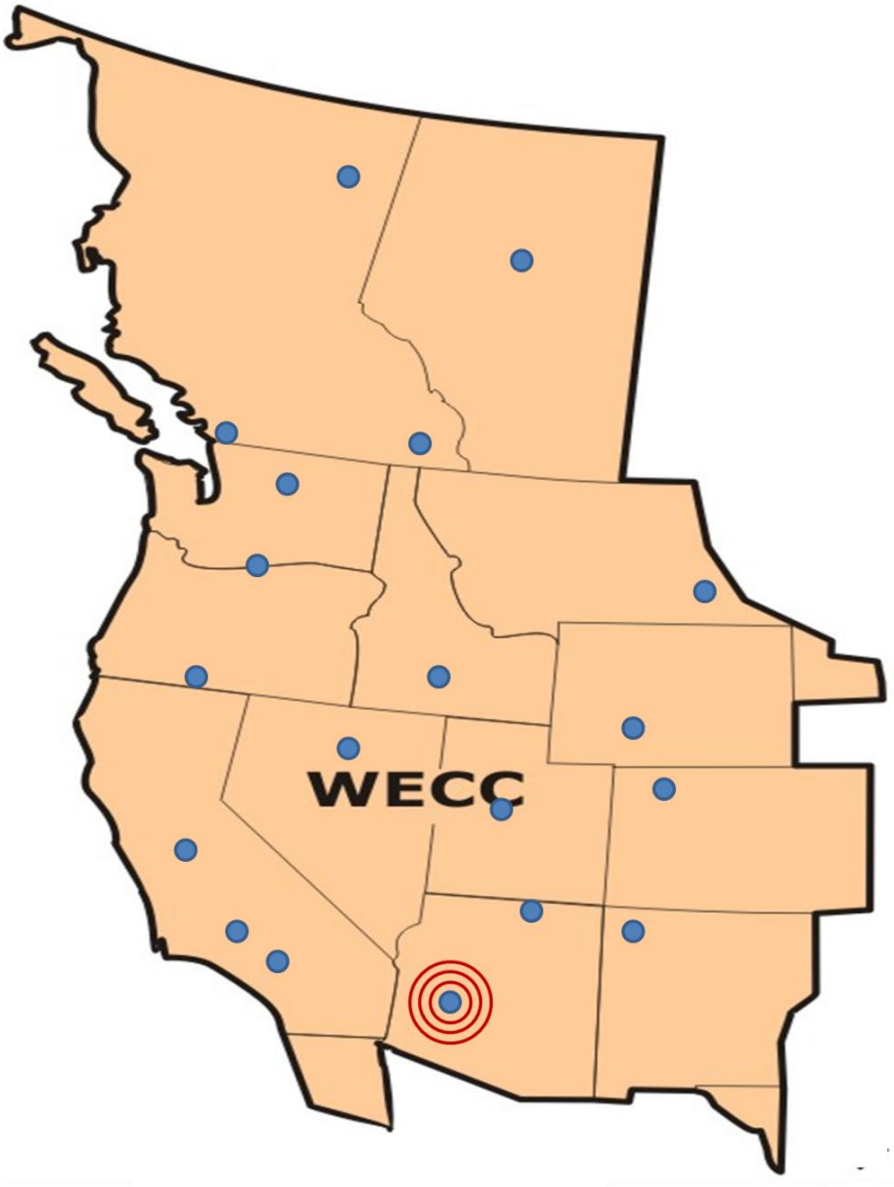

Figure 14. WECC 500kV Simulated Frequency Measurement Points

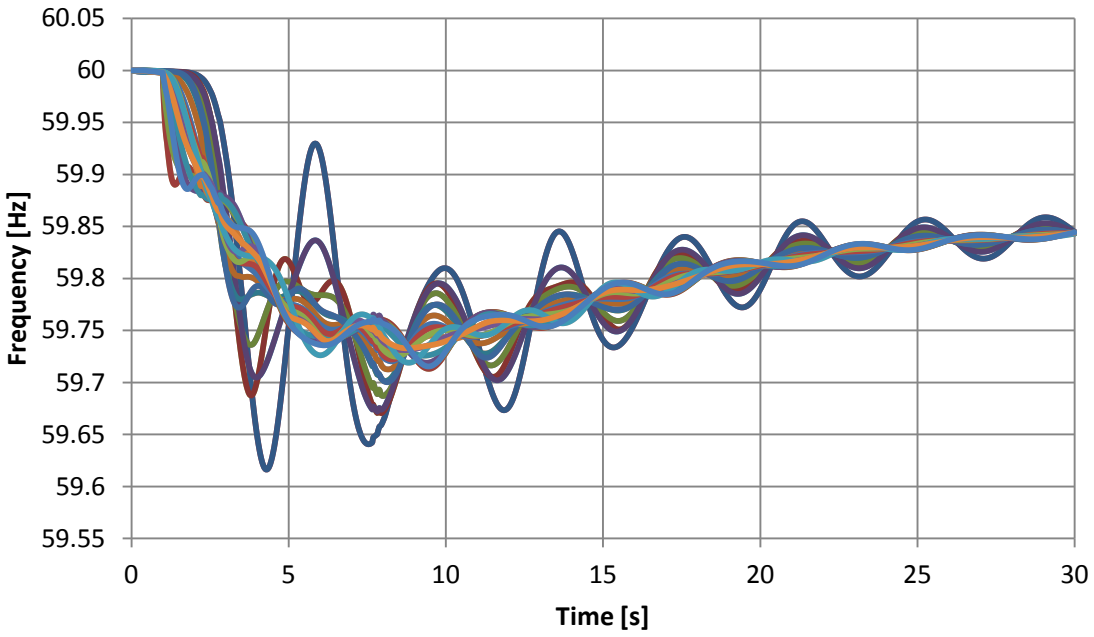

Figure 15. WECC Simulated Frequency Deviation - Loss of 2 Palo Verde

The concept of frequency response and its effect on system condition post-contingency are the driving force behind this research. In particular, the Primary Frequency Response is unbalanced between the north and south parts of WECC, resulting in major power swings following large disturbances. This research takes advantage of these characteristics by detecting these power surges and taking responsive actions.

2.4. Oscillations and Damping

As described in the previous sections, power system stability is dependent on forces acting with and against one another throughout the system. When synchronous machines are perturbed by an acting force, there must exist sufficient opposing force to return the system to an equilibrium operating point. Perturbing the input or output torque on the machines causes an acceleration or deceleration of the rotor. This is directly related to the angular position of the rotating reference frame (60Hz reference frame in North America, 50Hz in most of Europe). However, at some point, a change in rotor angle will result in an unstable operation where increase in angle reduces the real power output, further leading to instability and collapse. Therefore, power system stability is highly dependent on whether the system can provide sufficient restoring torque to the machines in order to maintain

stable operation. The rotor angle stability problem is generally classified into two generalized categories for analysis and discussion [24]:

1. **Small Signal Stability (SSS)** is "*the ability of the power system to maintain synchronism when subjected to small disturbances*", where disturbances are considered small if the equations governing the system response can be linearized for analysis. This type of instability can occur due to either increasing rotor angle due to insufficient synchronizing torque or poorly damped, growing oscillations due to insufficient damping torque.
2. **Transient Stability (TS)** is "*the ability of the power system to maintain synchronism when subjected to a severe transient disturbance*" resulting in large deviations in generator rotor angles. This type of analysis is highly non-linear and is generally studied through time domain simulation by integrating the non-linear differential equations governing system response. Stability is highly dependent on pre-contingency operating condition, contingency severity, and remedial post-contingency control actions.

The SSS analysis focuses on eigenvalues and associated eigenvectors of the linearized state space model of the system [24]

$$\Delta\dot{\mathbf{x}} = \mathbf{A}\Delta\mathbf{x} + \mathbf{B}\Delta\mathbf{u} \tag{2.30}$$

Therefore, the linear assumption of system response is used during the steady state to determine the eigenvalues of the system matrix ***A***. The eigenvalues of ***A*** are determined by finding the roots of the characteristic equation

$$\det(\mathbf{A} - \lambda\mathbf{I}) = (a_{11} - \lambda)(a_{22} - \lambda)\ldots(a_{nm} - \lambda) = 0\,. \tag{2.31}$$

where ***A*** is the system matrix and ***I*** is an (*nxn*) identity matrix. Further analysis of the system eigenvalues and subsequent left and right eigenvectors determines the oscillatory modes of the system, characterized in time by $e^{\lambda_i t}$. The eigenvalues can be either entirely real or complex conjugates. Real eigenvalues correspond to non-oscillatory modes while the complex eigenvalues relate to the oscillatory modes.

The sinusoidal behavior of power systems makes these modes significant. A damped sinusoid can take the form

$$e^{\sigma t}\sin(\omega t+\theta), \tag{2.32}$$

which can be expanded to

$$(a+jb)e^{(\sigma-j\omega)t}+(a-jb)e^{(\sigma+j\omega)t} \tag{2.33}$$

where $\lambda_i = \sigma_i \pm j\omega_i$ is the complex eigenvalue. The real and imaginary components of this complex eigenvalue are used to extract relevant information regarding the stability of the signal. Frequency of oscillation [Hz] can be defined as

$$f = \frac{\omega}{2\pi} \tag{2.34}$$

and the damping ratio is defined as

$$\zeta = \frac{-\omega}{\sqrt{\sigma^2+\omega^2}}. \tag{2.35}$$

The frequency of oscillation and damping ratio of each mode of oscillation are used to determine if the system is sufficiently stable for a given operating condition.

This research focuses primarily on the transient stability problem, analyzing system response to severely large disturbances rather than the static small signal stability problem. A high-level description of small signal stability and pseudo-steady state damping is provided because the analysis methods are very similar. Chiefly, it is important to quantify the level of damping associated with the post-transient response of system variables. The WECC and NERC reliability standards define criteria for transient response to disturbances; however, no level of acceptable damping is provided [34, 39]. Therefore, separate "damping studies" are often conducted to assess an Interconnection's risk to low damping oscillations due to unexpected contingencies.

Calculating the frequency and damping ratio of oscillation modes from time domain simulations requires complex analytical tools. In particular, it is useful to quantify the system variables' response ringdown to quantify whether sufficient damping exists. Various mathematical tools exist for extracting the oscillation characteristics exist; however, this research utilizes a research- and transmission planning-oriented tool that employs the use of advanced Prony methods [44].

2.4.1. Prony Analysis

Prony analysis is a fairly effective method for "*estimating the frequency, damping, strength, and relative phase of modal components present in a given signal* [45]." These are the essential measures required by a Transmission Planner for analyzing high-risk contingencies for low lamping conditions. Prony methods have been used since the mid-1900s and effectively implemented on digital computers since the 1980s [46, 47]. A brief overview of Prony analysis and the implementation used herein is discussed below for reference [48, 49, 50].

Suppose we have a linear, time-invariant system at an initial condition $x(t_0) = x_0$ at time t_0. If the input to this system is removed and no further perturbation occurs, the system will "ring down" according to the form

$$\dot{x} = Ax \,. \tag{2.36}$$

where *x* is system state and *n* is the order of the system (number of components). If λ_i, q_i, p_i are the i^{th} eigenvalue and corresponding left and right eigenvector of the *nxn* system matrix *A*, respectively, then the solution to (2.36) can be expressed as

$$x(t) = \sum_{i=1}^{n} \left(q_i^T x_0\right) p_i e^{\lambda_i t} \tag{2.37}$$

$$= \sum_{i=1}^{n} R_i x_0 e^{\lambda_i t} \,. \tag{2.38}$$

where $R_i = p_i q_i^T$ is the *nxn* residue matrix. Note that $q_i^T x_0$ is a scalar value, implying that the initial state x_0 impacts the stimulus to a given mode λ_i. However, the distribution of

modal content is entirely determined by the right eigenvector p_i. Therefore, relevant information regarding p_i must be extracted via modal decomposition of $x(t)$.

For a signal $y(t)$ consisting of N number of equidistant samples spaced by Δt, Prony method fits a function $\hat{y}(t)$ of complex exponentials

$$\hat{y}(t) = \sum_{i=1}^{N} A_i e^{\sigma_i t} \cos(2\pi f_i t + \phi_i) \tag{2.39}$$

$$= \sum_{i=1}^{N} \frac{1}{2} A_i e^{\pm j\phi_i} e^{\lambda_i t} \tag{2.40}$$

to the observed input $y(t)$. Since the system has a sinusoidal ringdown, the fit will have pairs of complex exponentials such that

$$A_i e^{\sigma_i t} \cos(\omega_i t + \phi_i) = \frac{1}{2} A_i e^{j\phi_i} e^{(\sigma_i + j\omega_i)t} + \frac{1}{2} A_i e^{-j\phi_i} e^{(\sigma_i - j\omega_i)t} \tag{2.41}$$

$$= B_a e^{\lambda_a t} + B_b e^{\lambda_b t} \tag{2.42}$$

where

$$B_a = \frac{1}{2} A_i e^{j\phi_i} \tag{2.43}$$

$$B_a = \frac{1}{2} A_i e^{-j\phi_i} \tag{2.44}$$

$$\lambda_a, \lambda_b = \sigma_i \pm j\omega_i . \tag{2.45}$$

Prony analysis is often summarized into a three step process [45]:

1. Construct a discrete linear prediction model (LPM) to fit the record.
2. Find the roots of the characteristic equation associated with the LPM.
3. Use the roots as complex modal frequencies for the signal to calculate the amplitude and phase of each mode.

(2.40) can be simplified to

$$\hat{y}(t) = \sum_{i=1}^{n} B_i e^{\lambda_i t} = \sum_{i=1}^{n} B_i z_i^k \tag{2.46}$$

for sample time t_k such that $z_i = e^{\lambda_i \Delta t}$. The goal is to solve the linear prediction model (LPM) for B_i and z_i that produce $\hat{y}(k) = y(k)$ for all *k*. Expanding (2.46), we have

$$\begin{bmatrix} B_1 z_1^0 + \ldots + B_n z_n^0 \\ B_1 z_1^1 + \ldots + B_n z_n^1 \\ \vdots \\ B_1 z_1^{N-1} + \ldots + B_n z_n^{N-1} \end{bmatrix} = \begin{bmatrix} z_1^0 & z_2^0 & \ldots & z_n^0 \\ z_1^1 & z_2^1 & \ldots & z_n^1 \\ \vdots & \vdots & \ddots & \vdots \\ z_1^{N-1} & z_2^{N-1} & \ldots & z_1^{N-1} \end{bmatrix} \begin{bmatrix} B_1 \\ B_2 \\ \vdots \\ B_n \end{bmatrix} = \begin{bmatrix} y(0) \\ y(1) \\ \vdots \\ y(N-1) \end{bmatrix} \tag{2.47}$$

which can be expressed as

$$ZB = Y\,. \tag{2.48}$$

z_i are the roots to the n[th] order polynomial, which can be found by solving (2.47) for all z_i. Eigenvalues λ_i can then be calculated from (2.46). The n[th] order polynomial fit with unknown coefficients a_i can be expressed as

$$z^n - \left(a_1 z^{n-1} + a_2 z^{n-2} + \ldots + a_n z^0\right) = 0 \tag{2.49}$$

Prony attempts to fit the next measurement using a linear combination of previous measurements with unknown coefficients. This forms a set of linear equations

$$\begin{bmatrix} y(n-1) & y(n-2) & \ldots & y(0) \\ y(n) & y(n-1) & \ldots & y(1) \\ \vdots & \vdots & \ddots & \vdots \\ y(N-2) & y(n-3) & \ldots & y(N-n-1) \end{bmatrix} \begin{bmatrix} a_1 \\ a_2 \\ \vdots \\ a_n \end{bmatrix} = \begin{bmatrix} y(n) \\ y(n+1) \\ \vdots \\ y(N-1) \end{bmatrix} \tag{2.50}$$

which is be solved for the unknown a_i values.

If the left-hand side (LHS) is a square matrix of full rank, then the inverse exists and can be found simply by $\mathrm{x} = \mathrm{A}^{-1}\mathrm{b}$. However, this may not be the case and alternative options for solving the linear set of equations must be used. One method is the pseudo-inverse method which is a generalization of the matrix inverse when the matrix may not be

invertible. For an *mxn* matrix where $m > n$ and A is full rank, then the pseudo inverse $A^{\dagger}$ can be found by

$$A^{\dagger} = \left(A' A\right)^{-1} A' \tag{2.51}$$

and the solution to $Ax = b$ is simply $x = A^{\dagger} b$. This solution is not exact, but gives the closest solution in the least-squares sense [51]. Another observation is that the A matrix is a Vandermonde matrix of the form [50]

$$V = \begin{bmatrix} 1 & \alpha_1 & \alpha_1^2 & \dots & \alpha_1^{n-1} \\ 1 & \alpha_2 & \alpha_2^2 & \dots & \alpha_2^{n-1} \\ 1 & \alpha_3 & \alpha_3^2 & \dots & \alpha_3^{n-1} \\ \vdots & \vdots & \vdots & \ddots & \vdots \\ 1 & \alpha_m & \alpha_m^2 & \dots & \alpha_m^{n-1} \end{bmatrix}. \tag{2.52}$$

Methods and solution techniques for the Vandermonde problem in addition to Prony analysis on noisy data have been proposed [52]. However, this research uses a Prony application on transient simulated data with no injected noise. In addition, the number of modes of concern has been reduced to the primary N-S WECC-wide modes so the order of the matrix is relatively small, making it numerically simpler to solve.

With the a_i coefficients determined, the roots of the characteristic polynomial can be found in the z-domain. With the roots known, the eigenvalues can be calculated by

$$z_i = e^{\lambda_i \Delta t}. \tag{2.53}$$

For determining the oscillation frequency and percentage damping of the various modes, the z-domain poles can be converted to s-domain by

$$z_i = e^{s_i T_s} \tag{2.54}$$

$$s_i = \frac{\ln\left(z_i\right)}{T_s} \tag{2.55}$$

where z_i, s_i, and T_s are the z-domain pole, s-domain pole, and sampling period, respectively. With the roots z_i calculated, the residue coefficients can be determined by solving (2.48) and the estimated signal $\hat{y}(t)$ can be reconstructed from (2.46). The reconstructed signal is not expected to fit the input signal exactly, and a measure of the fit is the signal to noise ratio (SNR)

$$SNR^{-1} = 20\log\frac{\|\hat{y} - y\|}{\|y\|}. \tag{2.56}$$

Lastly, the energies of each mode can be computed to sort the oscillatory modes based on their energy. Those modes with the highest energy that fall within the oscillation frequency range of interest are exported for results analysis.

The description above provides the basics of Prony method; Chapter 3 uses a tool created by Dr. Dan Trudnowski that performs multi-signal Prony analysis [50]. The tool is tuned to the N-S modes of the Western Interconnection, and provides both the dominant modes' oscillation frequency and % damping. If the fit is characterized as insufficient, then the Prony parameters are adjusted and the fit is recomputed. For each simulated contingency, these parameters are used to determine the oscillatory stability of the system, as will be discussed in Chapter 3 as well.

2.5. Reactive Power Support

Control of reactive power on a transmission system is as critical as the control of frequency and active power flow. Reliable operation of the electric power system includes control of voltage and consequently reactive power. In terms of design and operation of power systems, reactive power is generally discussed hand-in-hand with voltage profile. For varying operating conditions, voltages can be held at pseudo-constant levels if sufficient reactive power is available. Design of reactive power and voltage controls may consider [24, 53]:

- Maintaining a flat voltage profile across the system to maintain acceptable voltage levels for all expected operating conditions.
- Minimizing reactive power flow to reduce real I^2R and reactive I^2X losses.

- Minimizing reactive power flow to alleviate transmission capacity to allow more real power flow and increase revenue.
- All operating conditions to allow for varying reactive power requirements throughout the day, season, or year.
- Compensating long lines to reduce the impedance and therefore voltage drop across the line, and also balance real power transfer across parallel lines.
- Available dynamic reactive support elements and the impact passive or static devices can have on their operation.
- Optimal location of reactive power and voltage control devices.
- System effects due to additional reactive devices.

A number of elements throughout the power system produce or consume reactive power. Some elements constantly draw reactive power from the system while others are meant to provide reactive power. Many change their performance based on system conditions, while some are implemented for control actions. The following list is not comprehensive, but provides an oversight of the major players in reactive power control.

- Transmission Lines and Cables
- Shunt Capacitors and Reactors
- Series Capacitors and
- Under-Load Tap Changing (ULTC) Transformers
- Synchronous Machines
- Synchronous Condensers
- Thyristor-Controlled Reactors (TCRs)
- Thyristor-Controlled Series Capacitors (TCSCs)
- Static Var Compensators (SVCs)

Equipment that produces or consumes reactive power can generally be classified as either a dynamic or static resource. Dynamic reactive support devices are those devices that can control voltage dynamically using some form of self-excitation [54]. These devices can include generators, SVCs, synchronous condensers, and other flexible AC transmission system (FACTS) devices. Static devices are not self-exciting and may change

their output based on the prevailing conditions. These devices may operate automatically based on local or supervisory controls or be operated manually through operator intervention. For example, shunt capacitors change their output based on local voltage magnitude, but may be configured to switch in based on predefined low voltage thresholds. Similarly, high voltage transmission lines produce or consume reactive power based on loading conditions and voltage, and must be dealt with accordingly.

Either lack of real-time reactive power availability or inadequate planning of reactive power demand has been a major component of past power system blackouts. Voltage collapse led to blackout conditions in the July 2, 1996 and August 10, 1996 outages in the WECC [55, 56, 57]. In addition, other international outages involving voltage collapse have included December 19, 1978 in France; July 23, 2987 in Tokyo; March 13, 1989 in Quebec; August 28, 2003 in London; and others [58]. The Northeast United States and Canada blackout of 2003 was not caused by voltage collapse initially; however, "*insufficient reactive power was an issue in the blackout*" due to incorrect and overestimation of the dynamic reactive capability of the generating units in the load pockets around the Great Lakes area [1].

The remaining sections of this chapter describe the characteristics and operation of some of the elements utilized in this research. Although all types have an impact on reactive power control and voltage stability, this research focuses on the effects of static reactive support to alleviate dynamic reactive support following large perturbations to the power system. In the Pacific Northwest, with its usual abundance of hydro capability, the dynamic reactive support mostly takes the form of synchronous generators.

2.5.1. Transmission Lines and Cables

Rewriting (2.2) in terms of reactive power at the receiving end of a line, we get

$$Q_r = \frac{E_r}{Z_c \sin\theta}\left(E_s \cos\delta - E_r \cos\theta\right). \tag{2.57}$$

From this equation, we see that reactive power is related to terminal voltages at both ends of the line, the characteristic impedance of the line, the line angle δ, and the phase

angle difference (or real power) across the line. At the natural loading, there is no reactive power absorption or generation at either end and voltages are equal at both ends (discussed below). Reference [24] provides a figure and description of the relationship between reactive power and active power. When the receiving end active power is greater than the natural load of the line, the line consumes and the terminals supply reactive power; when receiving end active power is less than the natural load, the line produces and the terminals consume reactive power. The natural load, or surge impedance load (SIL), is defined as "*the power transfer on the line when it is terminated by its surge impedance* [24]". For high voltage lossless lines, the surge impedance is equal to the characteristic impedance, $Z_c = \sqrt{L/C}$. The SIL can be represented as

$$SIL = P_0 = \frac{V_{nom,LL}^2}{Z_c} \tag{2.58}$$

where $V_{nom,LL}$ is the rated nominal line-line voltage and the SIL is given as a three-phase quantity [59]. The characteristic impedance, or surge impedance, Z_c, is a real quantity and therefore there is no overall reactive power demand from the line. The reactive power demand of the line inductance equals the reactive power supply of the shunt capacitance of the line. Therefore $X_L = X_c$ and

$$I_l^2 \omega L = V^2 \omega C, \tag{2.59}$$

where L is the line inductance, C is the shunt capacitance, V is the voltage magnitude, and I_l is the line current magnitude.

When a line is loaded below its SIL, there is lower line current and less reactive power requirement from the inductive component of the line. The shunt capacitance produces more reactive power than the line inductance consumes, so the line has a net production in reactive power. The overall effect is production in real power from the line to the terminals of the line. Operation above its SIL results in the inverse effect, where the line current is high and reactive power demand of the inductive element is greater than that of the shunt capacitance. The line nets a consumption of reactive power. Therefore, during heavy

loading conditions reactive power must be supplied at the terminals while light loading conditions require reactive power consumption at the terminals.

At loading levels drastically below the natural load such as shoulder seasons or off-peak hours, shunt reactors may be required to mitigate high voltage conditions. Since an offloaded line acts as a capacitive element, lines may be removed from service during these conditions to handle high voltages. Conversely, heavy loading conditions may require shunt capacitors to combat higher voltage drop across the line. This relationship of loading and reactive power demand of transmission lines is not optimal since high path flow conditions are those conditions where voltages are depressed to begin with.

Underground cables generally have a low characteristic impedance because of a substantially higher capacitance due to the proximity of conductors in a cable, high levels of insulation, and possible shielding (against radio frequencies, for example) [60, 61]. The low characteristic impedance results in a much higher surge impedance loading. Often times, the SIL exceeds the thermal limit of the line and therefore the cable will always produce reactive power [62].

2.5.2. Shunt Capacitors and Reactors

Shunt reactive compensation is one of the most economic and effective reactive power control mechanisms. As mentioned above, voltage profile across the system is operated at a scheduled voltage with margin. However, as system conditions change, voltages cannot be maintained at their schedules solely by generation and transmission elements; there is a need for additional support spread across the system. In addition, controlling voltage profile consequently reduces the reactive power flow on the transmission system. This alleviates congestion, increases capacity for real power flow, and minimizes reactive I^2X losses. Figure 16 illustrates the effects of reactive compensation on power demand [63].

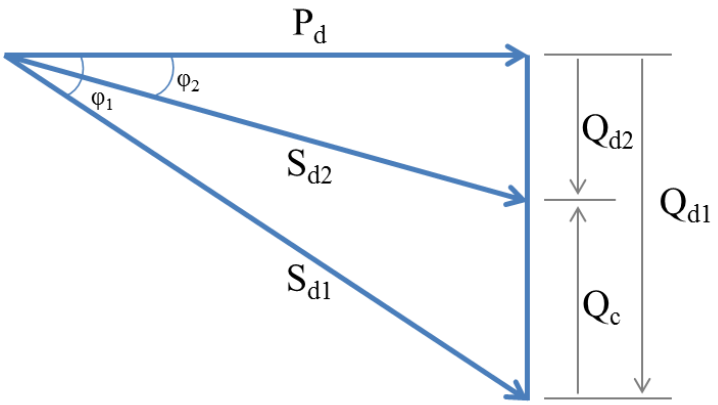

Figure 16. Reactive Power Compensation

Assume that the power system is operating with lagging power factor, ϕ_1, due to the inductive nature of the loads and transmission and distribution equipment. Real power demand, P_d, is needed to supply the load plus losses. The lagging power factor means that the loads require or consume reactive power, Q_{d1}, resulting in total power demand of S_{d1}. If a capacitive element is inserted to provide reactive power support and boost voltages, the reactive power requirement is reduced to Q_{d2}. This reduces the angle between real and reactive power, ϕ_2, subsequent power factor, and total power requirement to S_{d2}. If the real power is constrained due to total or reactive power demands, this constraint is alleviated and P_d can be increased further, improving system capacity. This illustration also shows how the capacitor insertion reduces the reactive power demand and consequent losses. If voltages are higher than natural loading levels and the power factor is leading, the same holds for an inductive insertion such as a shunt reactor, which reduces reactive current production of loads and elements on the system.

Shunt capacitor bank reactive power output can be expressed as

$$Q_r = 2\,fCV_r^2 \tag{2.60}$$

where Q_r is the rated reactive power output of the capacitor bank [MVA], V_r is the nominal system voltage [V], f is the system frequency [Hz], and C is the capacitor bank capacitance [F] [63]. Shunt capacitor reactive power output is dependent on the square of the system voltage. When the system voltage changes, the reactive power output will change by the square of the ratio of system voltage to rated voltage,

$$Q_c = Q_r \left(\frac{V_s}{V_r} \right)^2 . \tag{2.61}$$

The major disadvantage of switched shunt devices is highlighted in (2.60) and (2.61). When system voltages are low, the reactive capability from static shunt capacitors is reduced; this is the time when reactive power production from these devices is required the most. Conversely, high voltage conditions will cause shunt capacitors to generate more VARs on the system when they are not necessarily needed. These same concepts hold for shunt reactors with regard to consumption of reactive power.

"Switched shunts" generally refer to controllable shunt devices either from operator or automatic controls. Switched shunts provide voltage control and flexibility for operational efficiency. The simplest form of shunt reactive support is operator switching either from the local SCADA at the substation or the SCADA Master from the control center. Operator intervention for voltage control is primarily caused by heavy or light loading conditions on localized portions of the system. These conditions are long-duration situations, where sufficient time is available to take preventative actions to maintain voltage schedules. Automated controls sense a need for faster voltage improvement and take corrective actions. Shunt capacitors and reactors can be automatically switched based on low or high voltages. These voltages are usually set substantially lower and/or higher than acceptable steady state operating voltages such that automated action is taken as a last resort. Switching may be delayed by a predetermined amount of time to allow for system conditions to improve, in an attempt to reduce the number of unnecessary switching events [64, 65].

Shunt capacitors have also been used in applications such as reducing harmonics, surge protection, and power factor improvement for large motor loads [63]. However, minimal research and industry application has been performed regarding dynamic use of shunt capacitors for improving power system response to disturbances. Dynamic in this situation refers to fast-responding controlled reactive support through static compensation techniques to improve system response and post-transient conditions. Reference [66] provides a thorough discussion of reactive power support for the Twin Cities bulk power

system. Power flow analysis and post-transient analysis are commonly performed to ensure adequate reactive support during steady-state conditions pre- and post-contingency. The analysis showed that 9 new capacitor banks were the cost effective solution over Static Var Compensation (SVC) and uneconomical operation of metro peaking units. Stability analysis showed sustained voltage depression in South Dakota during the first swing following the disturbance. Fast-switched shunt capacitor insertion in the Twin Cities area provided reactive support to boost voltages within acceptable limits. Three 80 MVAR capacitor banks are enabled for fast-switching within 9 cycles of critical Twin Cities 345kV disturbances (1.5 cycle undervoltage timer, 6 cycle breaker operation, and 1 cycle margin) [66].

Previous research at the Bonneville Power Administration has shown that shunt switching of reactors and capacitors raises voltage and decreases transfer reactance, similar to series capacitor insertion. Results for a simplified analysis show that the required MVAR rating of shunt capacitors at the optimal location is approximately 3-6 times greater than the equivalent series capacitor requirement [67]. However, the results show that an attempt at conceptualizing switched shunt controls for improved stability was considered in the early 1960s. The Bonneville Power Administration also utilizes fast controls on its Fast AC Reactive Insert series and shunt capacitors, which provide responsive voltage support for the California-Oregon Intertie for large disturbances that cause sufficiently low voltages. This scheme is discussed in greater detail in Chapter 4.

2.5.3. Series Capacitors

Series compensation through series capacitors is another effective method of reactive support for efficient power system operation. Series capacitors are connected in series with the transmission line to offset the inductive reactance of the line. The complex line impedance, ignoring the shunt susceptance component of the line, is

$$Z_l = R_l + j\left(X_c - X_l\right) \tag{2.62}$$

Where R_l is the line resistance, and X_c and X_l are the capacitive and inductive components of the line reactance, respectively. The transmission line is inherently inductive by nature,

so $X_c<X_l$. By adding a series capacitor element to the overall line impedance, then the line impedance Z_l is reduced.

Since the capacitance cannot be distributed evenly across the transmission line, banks of capacitors are connected along the length of the line. Each bank is installed in parallel to a segment of transmission line, as shown in Figure 17 [68]. The series capacitors are installed on a platform insulated from ground since they are operated at line potential. Mechanically-operated disconnect (MOD) switches are used to isolate the series capacitor bank from the transmission line once the bypass MOD is closed and the potentials are the same. The spark gap, "triggered gap", is used to bypass the capacitors for severely high voltage. If current is detected in the spark gap circuit, the bypass breaker is closed and the spark gap current is offloaded to the parallel short circuit. When the capacitor is bypassed, the capacitor discharges through the discharge reactor, which limits the instantaneous rate of change of current. The damping circuit limits the magnitude of discharge current and expels the capacitor energy. The metal-oxide varistor (MOV) is used to protect the series capacitor bank from excessive transient voltages such as faults. From a system level perspective, the series capacitor installations along a line can be modeled as lumped capacitive elements that result in stepped voltage profile along the line when inserted.

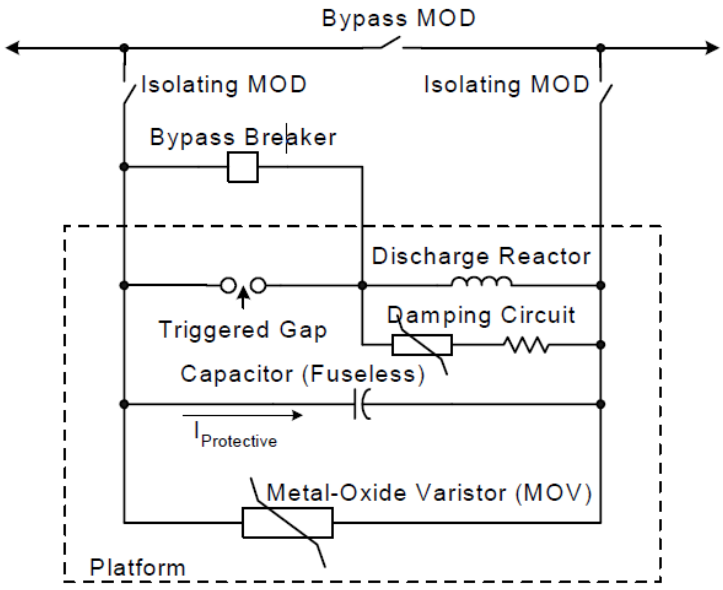

Figure 17. Series Capacitor Installation Example [68], public domain

Reducing the reactance of the line will decrease the reactive current consumption and reduce the reactive power (I^2X) losses. As discussed previously, power transfer is dependent on the impedance between the sending and receiving ends of the line. Decreasing the impedance between the two ends increases the active power transfer capability of the line, making series capacitors an economical means of increasing transfer capability for long EHV transmission lines. Also, compensation is often used to balance the loading between parallel lines of different impedances [24].

The reactive power rating of a series capacitor bank is defined as

$$Q_R = 3I_R^2 X_c \tag{2.63}$$

where Q_R is the total reactive power rating in MVAR, I_R is the per phase rated current in kA, and X_C is the per phase rated reactance of the line in ohms [69]. The reactive power supplied by the series capacitor bank is proportional to the square of the line current and independent of bus voltage, and can be referred to as "self-regulating" for this reason [24]. When loading is high and voltages are depressed, series capacitor compensation produces relatively more reactive support while shunt compensation produces relatively less since it is dependent on bus voltage magnitude.

Series capacitors have been utilized in dynamic controls such as increasing transfer capability and improving damping following disturbances. Especially in the WECC, with long interties connecting the north and south parts of the system, any means of increasing transfer capability results in higher revenues and improved economic dispatch. Reference [67] describes switched series capacitors for improved transient stability limits on major intertie lines, considering outages on the intertie, adjacent systems, and parallel DC tie line. The results show significantly improved stability limits when series capacitors are used on the intertie. The rapid insertion of series capacitors increases the flow on the AC intertie such that an outage does not significantly degrade the post-contingency limit. In addition, the first swing phase angle is reduced due to the rapid change in intertie impedance. Reference [70] further explores switching of series capacitors on test systems using dead-beat posicast switching, which can switch reactive elements in and out at optimal times to attain equilibrium with no further oscillation. However, this method is theoretical and has

major physical implementation issues for real power systems. Local control of capacitor switching is also explored, and is shown to effectively dampen oscillations following disturbances. Further work in the 1990s on a "bang-bang" control of series capacitors for improving transient stability utilizes offline studies of generator rotor angles and their rates-of-change to determine a region boundary for rotor excursions [71]. Major excursions outside the acceptable boundaries on the phase plane result in fast switching of intertie series capacitors to reduce the angular swing and improve damping. These examples form the basis of the Fast AC Reactive Insert (FACRI) now in service on the BPA power system and more advanced controls of series compensation for interties.

2.5.4. Synchronous Machines

The synchronous machine is the most widely used machine for electric power generation, constituting 97% of all electric power generated worldwide [72]. The simplicity and effectiveness in controlling electrical output, frequency, and voltage make it a superb electric generating unit. In addition, salient-pole construction is conducive with the multi-pole, lower speed machines such as hydroelectric generators that have a sufficiently large inertia due to the water flow [73]. A synchronous machine is characterized as an AC machine whose speed is proportional to the frequency of the AC voltage in the armature of the machine under steady state conditions. The machine itself is essentially a transformer, with a rotating magnetic field (rotor) inducing a flux and voltage onto the stationary windings (stator) of the machine. When supplying electric power to the grid, the flux in the stator windings operates near nominal frequency. As the prime mover provides more or less mechanical input torque, the machine will deviate is speed and an opposing torque is applied. The difference in torques causes the angular position, ϕ_r, of the rotor to deviate from the synchronous reference frame. This is the mechanism by which energy is converted from mechanical input to electrical output [73]. A conceptual representation of a synchronous machine and the corresponding equivalent circuit for a classical round rotor machine operating as a generator is shown in Figure 18.

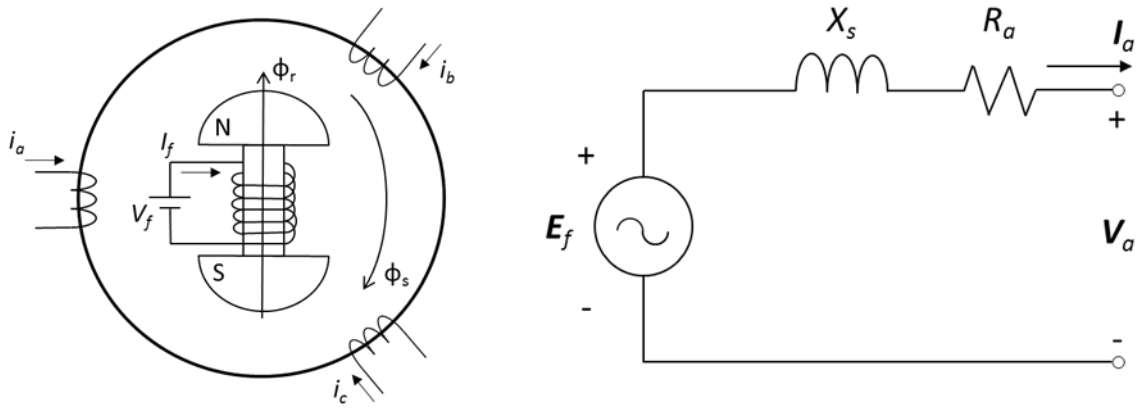

Figure 18. Representation of Synchronous Machine

If resistance is neglected, the governing voltage equation for this circuit can be expressed as

$$E_{af} = V_t + jI_a X_s \tag{2.64}$$

$$V_t = E_{af} - jI_a X_s \tag{2.65}$$

where V_t is the phase-ground terminal voltage of the machine, E_f is the field voltage in the rotor, I_a is the line current on the a-phase, and X_s is the equivalent series reactance of the machine. To best describe operation and transfer of real and reactive power from and to the machine, a phasor diagram is often used. Figure 19 shows the machine under-excited (a), over-excited (b), and at unity power factor (c) [73].

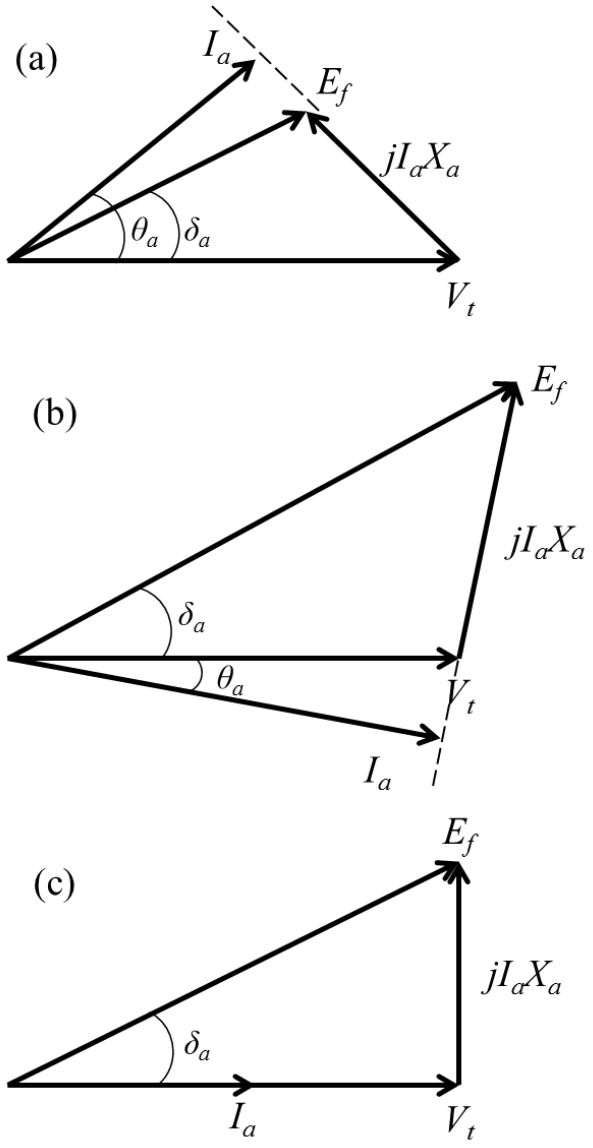

Figure 19. Synchronous Machine Phasor Diagrams

In all scenarios shown above, the terminal voltage of the machine is held constant. A rule of thumb is that "real power runs downhill on voltage angle and reactive power runs downhill on voltage magnitude". Shown in (a), field voltage leads terminal voltage by angle δ_a, meaning real power flows out of the generator (producing). On the other hand, $|E_f| < |V_t|$ so reactive power flows from the bus into the generator (consuming). Shown in (b), field voltage still leads terminal voltage so the generator is still supplying real power to the system; however, $|E_f| > |V_t|$ so current is moving towards the terminals and the generator supplies reactive power. Lastly, (c) shows the generator operating at unity power

factor, where terminal voltage V_t is in phase with the line current I_a. This scenario results in minimum current flow I_a. Assuming the terminal voltage is not directly controlled, the independent variable E_f is used to control reactive power output. Applications such as Line Drop Compensation are used to maintain voltage set point at an location inside the step-up transformer of a generating unit [74]. This creates a coordinated voltage control for multiple units connected at the high-side of their step-up transformers. The ability of AC synchronous machines to easily manipulate their reactive power output by changing their excitation voltage makes them an ideal source of dynamic reactive support. Let us explore operation of a synchronous machine as a synchronous condenser.

2.5.5. Synchronous Condensers

A synchronous condenser is simply a synchronous machine operating with no mechanical input torque, i.e. the shaft has been "de-clutched" from the prime mover supplying the mechanical power. The machine requires a small amount of real power to operate, but can perform as a reactive power source or sink, rotating at synchronous speed from the rotating magnetic field of the armature. Controllable excitation of the field current enables the machine to produce reactive power when over-excited and consume reactive power when under-excited.

Synchronous condensers were popular in the earlier years of power systems; however, their popularity waned upon introduction of static power electronic solutions. Regardless, synchronous condensers offer a number of advantages over static compensation techniques. As with synchronous machines, synchronous condensers provide dynamic reactive support and are not dependent on system voltage magnitude. These machines regulate a location such as their terminals to a controllable set point, and have the capability of low voltage ride-through. Due to their rotating mass, synchronous condensers also contribute to system inertia [53].

To explain operation of synchronous condensers, let us revert to the phasor diagrams shown in Figure 20 [75]. The input mechanical torque is removed, therefore the phase angle difference between V_t and E_f is 0°. Reactive power flow to and from the generator is controlled by the excitation system by changing the field voltage magnitude E_f relative to

the terminal voltage V_t. In (a), $|V_t| < |E_f|$ so the synchronous condenser is supplying reactive power while in (b), $|V_t| > |E_f|$ so the condenser is consuming reactive power.

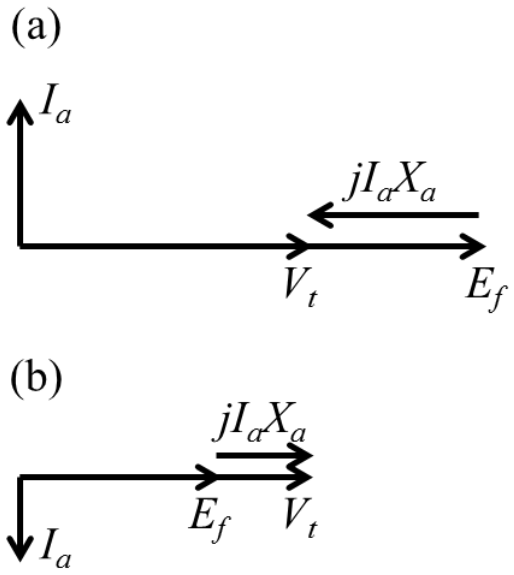

Figure 20. Synchronous Condenser Phasor Diagrams

A number of Columbia River hydroelectric synchronous machines within the BPA Balancing Authority Area (BAA) have been retrofitted for operation as synchronous condensers. "De-watering" controls have been implemented on select generating units that can rapidly eliminate the water moving through the penstock down to the turbine. Assuming no additional constraints such as fish or reservoir coordination, these units provide operators with additional reactive capability during concerns of voltage instability [53].

Chapter 3. Phase Angle Alarming Methodology and Application

Maintaining secure and reliable operation of the power system in real-time requires online tools and controls schemes but also requires detailed and well-informed study of impending system conditions such that a region of operation can be classified as acceptable. Generally, this region is based on a set of reliability criteria that operations engineers will study to determine what the acceptable path limits can be for the upcoming timeframe. The system is constantly changing and it is not uncommon for operations engineers to run new studies when unexpected events occur that were not studied for the current operating point. Advanced applications such as a State Estimator or Real Time Contingency Analysis (RTCA) tool can provide estimates of system security, most commonly on the time scale of every five minutes. These tools are highly valuable for real-time operation of the power system; however, there is no requirement to utilize these tools in the control center. Operators generally follow interchange set points, maintain system frequency, and abide by internal System Operating Limits (SOL) to prevent unwanted conditions [76]. A list of Dispatcher Standing Orders (DSOs) are thoroughly understood and closely followed such that situations needing corrective action have measures in place to effectively mitigate problems when they occur.

The phenomenon of intuition plays a crucial role in expert operations of power systems. In addition to the comprehensive studies and real-time tools providing the operator with large amounts of data, many operators simply have a "feel" for acceptable conditions and stress patterns [76]. This intuition is based on years of experience and understanding of each individual system characteristics. This research seeks to provide the operator with a tool for assessing stress on the system by utilizing the information one can extract from synchronized phase angle measurements. The primary goal is to provide the operators with a tool that can help visualize stress patterns on the system by highlighting areas nearing their respective limits. A secondary goal is to highlight specific areas that may need corrective action by alarming the operator when limits are exceeded.

PMUs enable the synchronized measurement of phase angle and its difference between locations on the system. This measurement has generally been unavailable to engineers and operators in real-time due to the lack of synchronicity between measurements.

Therefore, angle alarming and visualization is a relatively "new" technology in terms of its deployment. Due to the criticality of reliable electric power delivery, "new" technologies require time and effort before they are fully adopted for real-time control. This fact affects this research drastically for a number of reasons. First, the goal is simply to get phase angle measurements in the control center so the operators can begin to familiarize themselves with them. Rather than attempt to require the operators to abide by this unfamiliar measurement, it is best to present the measurements for increased awareness. Second, any tool given to an operator should be *information-heavy* and *data-light*, meaning that the operator should see as little *data* as necessary but be able to extract as much *information* from the data given as possible. For example, this may mean that the operator wants to see intertie flows alongside an angle plot for increased "intuition capability". Third, the tool should be multi-layered such that an operator has multiple layers of detail based on the type of information needed. For example, a wide area angle plot of the system may only be able to display angle difference between locations across the system. On the other hand, specific regions or areas in the system should be capable of detailed visualization if deemed appropriate, and the operator should be able to select those areas quickly. These detailed plots may have the opportunity to provide other information in conjunction to angle such as real power flows on key lines, voltage levels, frequency, etc. Lastly, and of utmost importance, is angle limit setting for *useful* alarming of impending conditions. Limits set too conservatively will alarm the operator for conditions that do not require corrective action. At these same levels, it may be more beneficial for the operator to visually be aware of high stress areas. Limits set too leniently could fail to alarm except for conditions where it is too late to take corrective action.

This research is generic in its sense of application. The study method could be implemented in a State Estimator module or RTCA tool, but could also be performed in the day-ahead studies and uploaded to a tool for alarming purposes. The emphasis of this research is on the study methodology and relevant information applicable to angle alarming, using the BPA power system as a test bed for results.

3.1. PMU Measurement Clustering Through Coherency

Large power systems are one of the most highly complex and diverse machines on earth. Geography, policy, weather, and economics are only a few factors that impact operation and utilization of energy systems. For example, climate conditions such as geography and weather play a major role in determining where major load centers are. These same drivers, as well as political policies, may dictate a region's generation composition and where those generating units are located. The utility industry must accommodate all these factors while designing, maintaining, and operating the power system with sufficient adequacy and reliability to deliver large amounts of energy to its customers.

Expanding this concept to high-level power generation, transmission, and distribution, it is common to find areas rich in generation that are remotely located from load centers, connected through high voltage transmission systems. If one were to try to measure every phase angle difference across a large power system, the amount of data would become burdensome and unintelligible. In addition, most utilities are actively installing PMUs at major high voltage buses, so a comprehensive measurement of phase angle is unavailable and will be for the foreseeable future due to the cost of investment. Therefore, a methodology must exist that utilizes the PMU measurements available and extracts sufficient information from the data to provide to the operator.

Coherency has been used for many years to describe the degree that generators "swing" with respect to each other following an external event or disturbance [77]. One of the most common applications in the literature includes equivalencing complex power systems into simplified networks while maintaining the dynamics of the system by grouping coherent generators [78, 79]. Model reduction was necessary due to limited computational power available at the time; today, this is not as much of a concern due to the processing power of modern computers and advanced techniques such as parallel processing. More recently, some work has been done in applying the concepts of coherency to synchronized phasor measurement technology; the original concepts, and the adaptation and expansion to angle alarming are described in this section.

3.1.1. Disturbance-Based Probabilistic RMS-Coherency for PMUs

Coherency is primarily used for determining which elements (generators, buses, etc.) can be aggregated without the loss of dynamic information, and can be expanded to include phasor measurement technology [80]. The work in [81] and [80] apply a coherency index for PMU measurement placement and dynamic vulnerability assessment. The goal is to minimize the correlation between measurements by minimizing the amount of redundant information from the measurements to minimize cost of observability. A sequential placement algorithm presented as an optimization problem is used for determining the optimal placement under a given set of constraints [81]. This work is expanded in [80] by including a fuzzy c-means algorithm to organize the coherent buses into clusters or groups. The clustered PMU voltage phasor measurements are used for assessing the dynamic vulnerability based on center of inertia concept [82].

In regard to the coherency element of the works discussed, time-domain simulations are run to extract signal responses to disturbances. These responses are used to assess each PMU measurement's coherency with respect to the other measurements. A probabilistic framework is devised such that the coherency indices are generalized to an array of operating conditions. This methodology is discussed in detail below. First, let us elaborate on the fundamental differences and similarities between the literature and this work, as shown in TABLE III.

TABLE III. CLUSTERING METHODOLOGY COMPARISON

	Literature [28, 29]	This Work
Analysis	Disturbance-Based	Disturbance-Based
Study Process	Transient Stability	Transient Stability
Bus Inclusion	Encompassing	Selective
# Simulations	Probabilistic	Probabilistic
Application	DVA/PMU Placement	Phase Angle Alarming
Clustering	Fuzzy c-Means Algorithm	Index Classification

Two buses k and l are said to be coherent for a given disturbance d if the RMS-coherency criterion, as in (1), falls below a given threshold.

$$\alpha_{kl}^{d} = \sqrt{\frac{1}{T}\left(\int_0^T \left[\theta_{kl,d}(t)\right]^2 + \left[\omega_{kl,d}(t)\right]^2 dt\right)} \tag{3.1}$$

where $\theta_{kl,d}(t) = \theta_{k,d}(t) - \theta_{l,d}(t)$ is the phase angle difference and $\omega_{kl,d}(t) = \omega_{k,d}(t) - \omega_{l,d}(t)$ is the frequency difference between buses k and l at time t. For an n bus measured system, the coherency matrix X_d for disturbance d can be expressed as

$$X_d = \begin{bmatrix} \alpha_{11} & \alpha_{12} & \dots & \alpha_{1n} \\ \alpha_{21} & \alpha_{22} & \dots & \alpha_{2n} \\ \vdots & \vdots & \ddots & \vdots \\ \alpha_{n1} & \alpha_{n2} & \dots & \alpha_{nn} \end{bmatrix} \tag{3.2}$$

The elements of X_d provide insight as to the coherency of a given bus with respect to another bus. The diagonal elements of X_d are zero, meaning that a bus is exactly coherent with itself. More generally, the coherency between buses k and l increases as α_{kl} decreases to zero [81].

The coherency assessment thus far has been focused on a single deterministic disturbance d, but can be expanded to a probabilistic framework over a range of operating conditions and a set of possible disturbances. The coherency matrices X_d become random variables because the signal responses are random variables, and a random variable ζ can be defined to capture uncertainty in variations such as season, load patterns, transmission outages, and other case derivatives. Each operating point is given a probability of occurrence, p_r, where $r \in \Omega$, and Ω is the set of all operating conditions defined. Each operating point is subjected to a common set of N_d disturbances [80]. Thus, (1) can be written as

$$A := \sum_{r \in \Omega} p_r \left[\underset{d=1,\dots,N_d}{E} \{X(d,s)\} \right], \ \sum_{r \in \Omega} p_r = 1 \tag{3.3}$$

With this framework in place, the coherency of all PMU measurement locations can be analyzed using a diverse set of operating conditions and a range of possible disturbances.

The population of n candidate PMU measurements in the BPA system was subjected to coherency analysis as described above. Each operating condition was given the same weight, so the coherency measure defined is the expectation of all operating conditions subjected to N_d disturbances. The A matrix defined by the probabilistic framework is an

nxn matrix of statistical coherency measures, and describes the coherency of each PMU location with respect to all other PMU locations. The goal is to determine which measurements can be grouped together while maintaining a relatively full coverage of critical areas on the BPA system.

The coherency assessment above can be subjective; therefore, a range of coherency measures are used rather than a single threshold.

1. $\alpha_{kl} \leq 0.25$: Buses *k* and *l* are strongly coherent. These buses have highly correlated phase angle and frequency trajectories.
2. $0.25 < \alpha_{kl} \leq 0.50$: Buses *k* and *l* are moderately coherent, and may be considered as part of a group.
3. $0.50 < \alpha_{kl} \leq 1.00$: Buses *k* and *l* are weakly coherent, and are unlikely to be considered as part of a group.
4. $\alpha_{kl} \geq 1.00$: Buses *k* and *l* are not considered coherent.

Figure 21 shows the coherency matrix results, reordered with strongly coherent elements near the diagonals. The raw coherency matrix results require engineering judgment. PMUs remote from other PMUs will not be strongly coherent, which is often the case for intertie locations. Significant overlap may exist in locations that are geographically diverse but follow similar stress patterns (Lower Columbia hydro and Portland load center). Conversely, significant diversity may exist in locations that are geographically close due to the characteristics and composition of system elements at those locations (large BPA wind hubs and Lower Columbia hydro). Coherent groups of PMUs that are geographically and electrically diverse from one another are included as regions for the phase angle alarming application (circled in red in Figure 21).

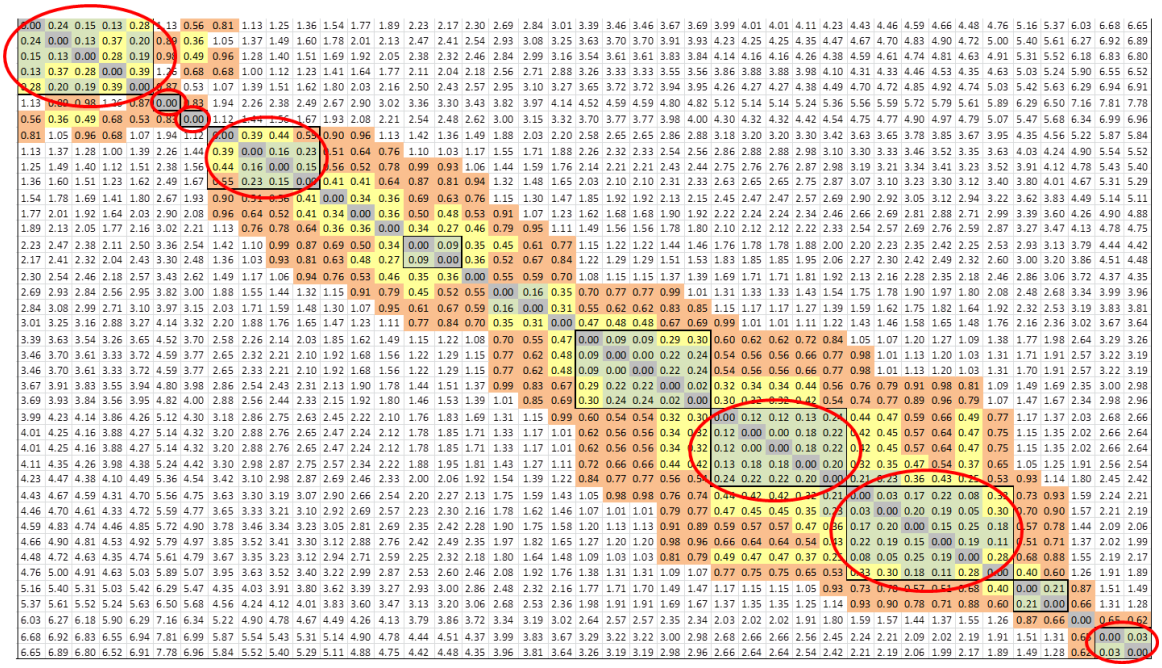

Figure 21. BPA PMU Coherency Matrix

The regions defined by the coherency analysis include all expected critical locations. Major load centers are captured by the Portland and Seattle regions. Large generation hubs include the Upper Columbia and Lower Columbia regions with their abundance of hydroelectric dams. Key interties connecting BPA with the rest of WECC include the Northern Intertie (NI), Montana-Northwest Intertie (MT), and the California-Oregon Intertie (COI). The regions are connected by internally defined flowgates and external WECC rated paths. The results concur with preexisting ideas of PMU clustering and the results are visually simple to display, as shown in Figure 22.

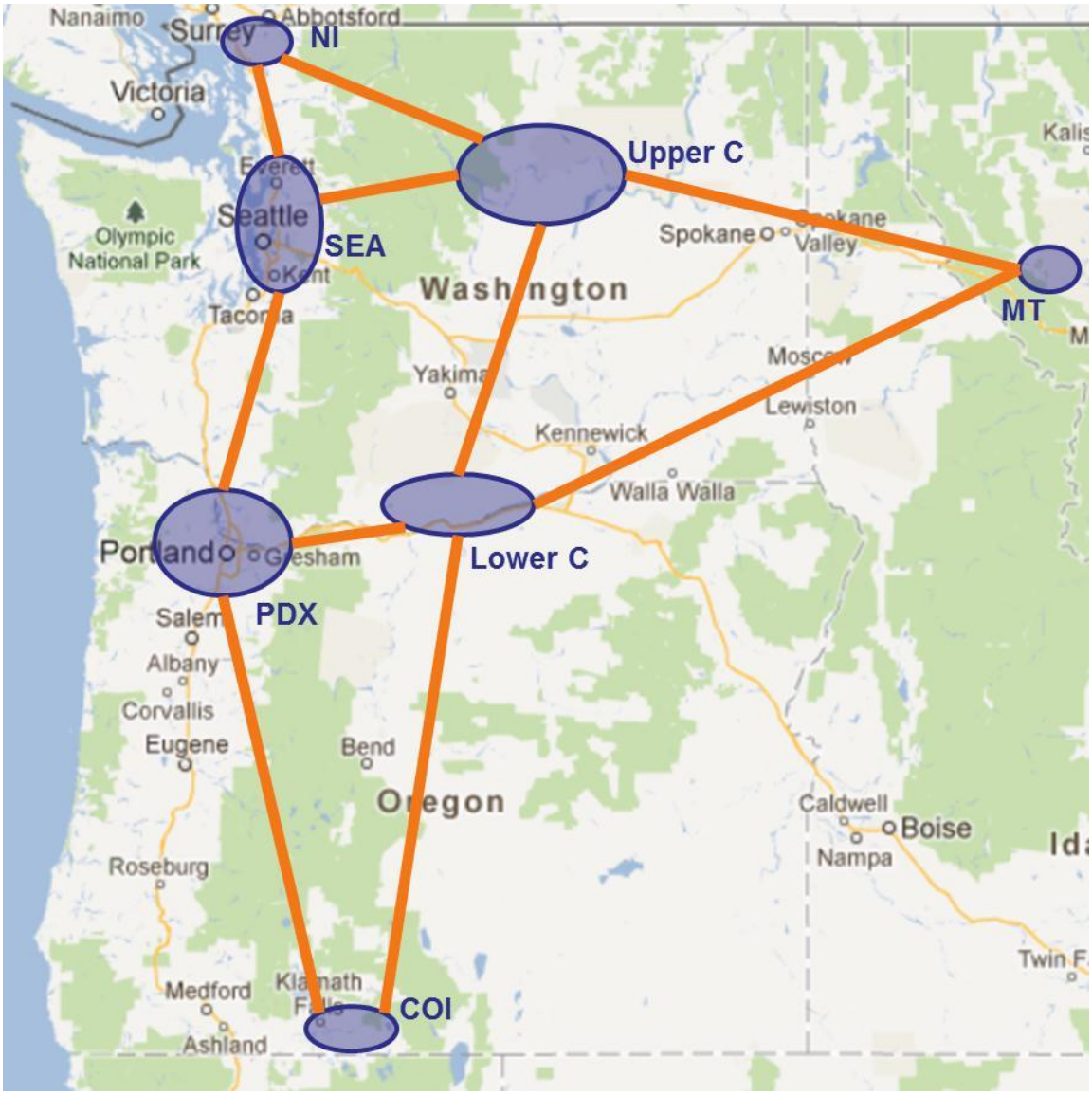

Figure 22. Regional PMU Clustering for Alarm Application [83], public domain

3.2. Benefits and Concerns Using a Representative Angle

A representative angle for each cluster provides measurement reliability by detecting bad or skewed data, and surrogate measurement for lost data packets. For example, a PMU data packet may not arrive at the PDC. More importantly, a potential or current transformer contact could go bad and provide bad data. Using multiple PMUs in a cluster allows for higher measurement availability and capability to select or calculate a representative angle. While the mean filter is prone to bad data skew, a median filter can be used in a number of different configurations. Figure 23 shows an example with two

PMUs in each cluster or area, each with a single measurement of bus voltage angle. This provides four distinct angle difference measurements to choose from. However, bad data for a single measurement, and therefore single PMU, results in bad data for half the measurements. Therefore, a median filter would also provide bad data.

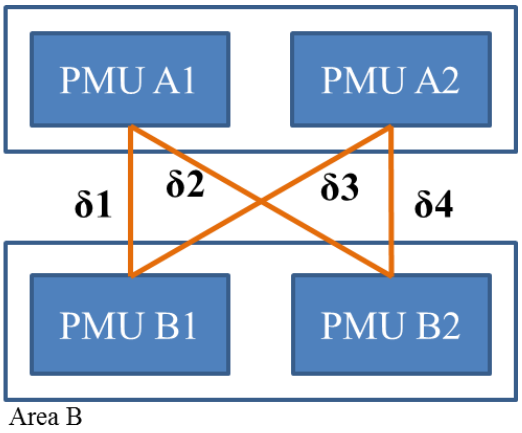

Figure 23. Single Voltage Angle Measurement Median Filter

Figure 24 shows the same PMU configuration where each PMU can provide two independent voltage phase angle measurements. The number of unique phase angle measurements has increased to sixteen, increasing the number of distinct data points drastically. Bad data in one measurement only results in one-quarter of the phase angle difference calculations being invalid while bad data in one PMU still results in half the calculation in error.

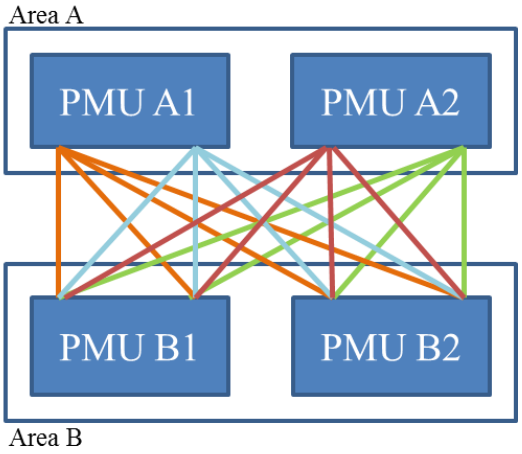

Figure 24. Dual Voltage Angle Measurement Median Filter

A third example is shown in Figure 25 of a median filter configuration that minimizes calculations and data management. Each PMU provides one or more phase angle measurements and a median is calculated for each area. A single representative inter-area angle difference can then be calculated. Let us assume that each PMU provides more than one phase angle measurement, so bad data in a single measurement is discarded.

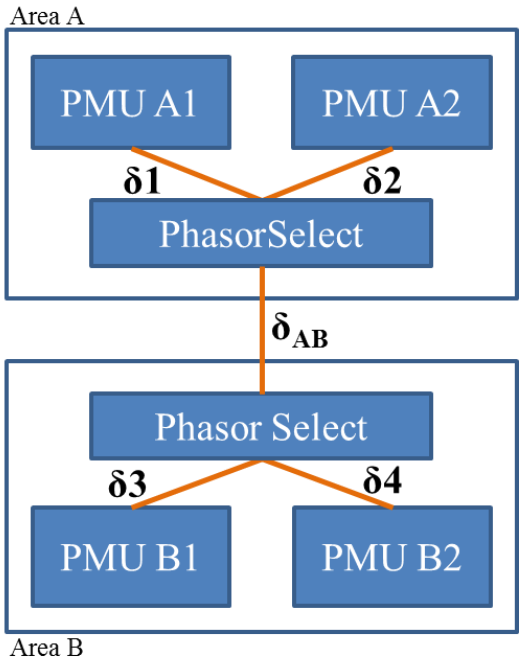

Figure 25. Inter-Area Voltage Angle Median Filter

The initial hypothesis was to use a representative angle from each region and use these angle differences between the regions as indications of system stress and a need for corrective action. A single corridor was selected for analysis of representative angle difference limits as a pilot for the test methodology. Let us explore this concept using a simple DC model that accounts only for real power flow through a hypothetical corridor, as shown in Figure 26. This corridor is composed of major transmission paths connected in series with each other.

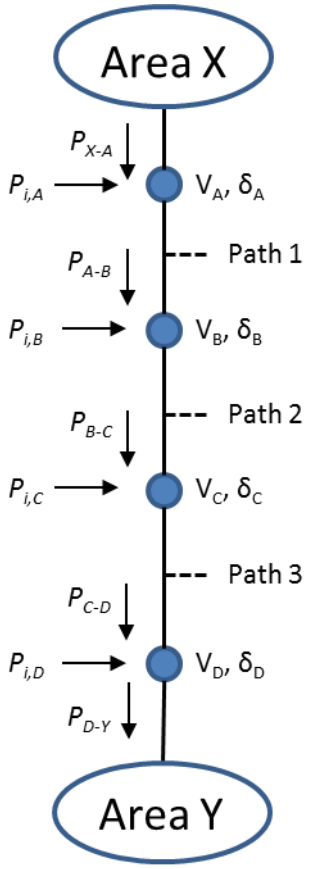

Figure 26. Corridor Stressing Example

Area *X* and Area *Y* represent two PMU clusters selected from the coherency analysis, separated by a corridor of transmission connected through four major transmission nodes or substations. Nodes *A* and *B* are the connecting hubs into the two PMU clusters, and represent the boundary buses between clusters. Therefore, nodes *B* and *C* are connected through three major transmission lines or paths, defined by Path 1, Path 2, and Path 3. Each node connecting the two clusters has an aggregated real power injection P_i, which can be defined by

$$P_i = \sum_{j=1}^{N_g} P_j - \sum_{k=1}^{N_l} P_k \tag{3.4}$$

where N_g and N_l represent the total number of generators and loads at the aggregate node, respectively. Deterministic transmission planning studies generally apply some form of peak or trough load conditions with varying generation patterns. Therefore, load changes are assumed relatively small compared to total generation changes in the area; significant

real power injection changes are from generation dispatch patterns. Assuming all lines in service,

$$Path1 = P_{A-B} = P_{i,A} + P_{X-A} \tag{3.5}$$

$$Path2 = P_{B-C} = P_{i,B} + P_{A-B} \tag{3.6}$$

and so on, which describes the real power flow across the corridor. If the real power injection at a node is removed (a reasonable operating condition due to forced or planned outages), the power must be produced from another location. Keeping all other generation and load constant, that power deficit is supplied by Area *X* or beyond. If Path 2 real power, $P_{B\text{-}C}$, is kept constant, then removal of part or all of the injection at node *B*, $P_{i,B}$, results in increased loading of $P_{A\text{-}B}$, by $P_{i,B}$.

As an analytical example, assume the corridor configuration from above, with all transmission impedances of X_l = 1.0pu. Also assume that there is no underlying lower voltage system for parallel flows to transfer to. TABLE IV provides two drastically different generation and transmission patterns. Scenario 1 is a fairly lightly loaded situation, with a large amount of generation at Node *C*. This could be, for example, all natural gas units offline and a single large coal plant near full output at Node *C*. Although this is a drastic example, it provides a useful illustration. Scenario 1 is classified as *Insecure* because outage of the generating unit at Node *C* would result in increased flows by 1200MW on Paths 1 and 2. This would cause overloading on Path 1, exceeding its limit by 200MW. Scenario 2 is a completely different situation where path flows are increased and there is more diversity in the power injections. Loss of any one injection of real power would not cause overloading on this corridor, so this operating point is classified as *Secure*. It is assumed that loss of transmission would be accommodated by another corridor delivering power to Area *Y*. While the overall stress level of Scenario 1 is lower than Scenario 2, with an overall angle of 4.2 compared with 5.6, it is classified as *Insecure* due to the generation dispatch and Path limits. This is just one example derivative case of a base case and can be generated for a wide range of dispatches to provide varying degrees of corridor stress.

TABLE IV. REPRESENTATIVE ANGLE SCENARIOS

	Scenario 1 Insecure	Scenario 2 Secure	Limit
Path 1 Flow	1000	1500	2000
Path 2 Flow	1000	1900	3000
Path 3 Flow	2200	2200	4000
Node A Injection	0	0	
Node B Injection	0	400	
Node C Injection	1200	300	
Node D Injection	0	0	
Path 1 Angle	1.0	1.5	
Path 2 Angle	1.0	1.9	
Path 3 Angle	2.2	2.2	
Total Angle	4.2	5.6	

To test this claim using an actual system model, static security assessment as discussed in Chapter 2 is used for classifying an array of operating states for a corridor on the BPA system. Myriad operating conditions are created to thoroughly test varying system conditions for all lines in service (ALIS). Generation dispatch is changed by rearranging unit status and output to stress varying parts of the study corridor. As Figure 27 shows, misclassification by using a linear relationship between phase angles and operating state is extremely high. Generation dispatch can be configured such that individual lines or paths can be overloaded while the overall corridor stress is relatively low. Conversely, each individual corridor can be within static secure operating limits while the overall corridor stress and respective wide area angle is high.

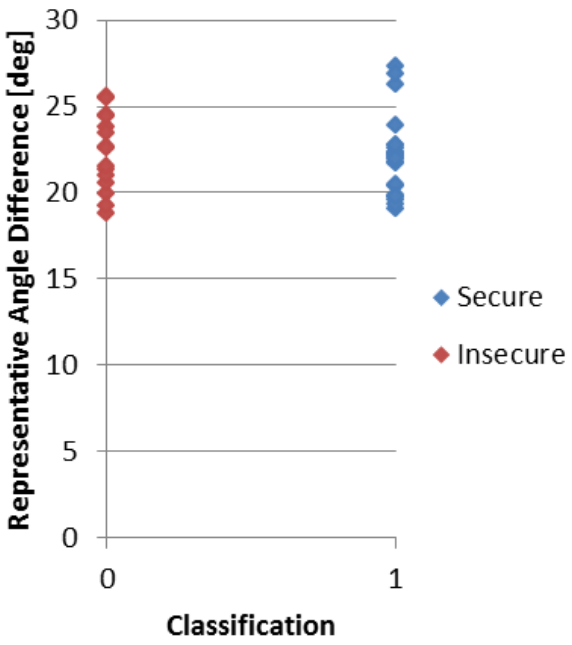

Figure 27. Wide Area Angle Classification Issue

In terms of wide area angles, varying system operating conditions can provide almost identical phase angle measurements for a given corridor. Based on these observations, it is concluded that a wide area angle is not a valuable measure of security or indication of unacceptable operating conditions. Although phase angle is an indicator of stress across a system, correlating a wide area angle to known operating limits such as static security criteria presents a challenge. The initial hypothesis was replaced with a more detailed study methodology that provides highly classifiable phase angle limits across a transmission corridor. This is discussed in the next section, followed by example scenarios on the BPA transmission system to illustrate the methodology for different system topologies and configurations.

3.3. Inter-Cluster Security Assessment Angle Limit Methodology

With candidate PMUs clustered using disturbance-based probabilistic rms-coherency assessment, the WAMS network can be represented using a subset of representative phasor measurements. Although representative angle measurements between the clusters provide a measurement robust to bad data, the management of that data and more importantly the misclassification of that data make it refutable for setting operator alarming limits. This section builds off the PMU clustering, and presents a novel methodology for calculating

phase angle limits for each corridor identified by the algorithm. The methodology can be applied to an array of topology configurations, accounts for generation dispatch patterns, and is readily implementable with System Operating Limit studies or other online tools. The angle limit classification methodology is described below:

0. Perform disturbance-based probabilistic rms-coherency assessment. Determine coherent groups of PMUs and interconnecting transmission corridors.
1. Define full contingency list. This list may consist of all or most major 'N-1' disturbances, credible 'N-2' disturbances such as breaker failure or common tower or common right of way outages, and some 'N-k' outages of less probability but high consequence. The contingency list may be refined based on operational experience and knowledge of the system to consist of those contingencies most pertinent to performance violations.
2. Select a study corridor.
3. Define contingency list for study corridor. This list may be a subset of the full contingency list based on experience of outage impacts, or may simply be the full list.
4. Develop 'Case Information' file within power flow solution engine, to effectively extract relevant case information of the pre-contingency operating point. This can be used for the root case and all sensitivities. Useful information may include generator power output, major line flows, Path flows, and bus phase angles.
5. Develop power flow root base case for study corridor corresponding to specific stress patterns of interest.
    a. Selection may be based on historic analysis of season, year, scenarios and sensitivities, etc.
    b. Generation pattern can be constructed using historic data, unit commitment, and/or economic dispatch of generators.
    c. Topology is generally an all lines in service scenario, with the exception of expected long-term outages or normally open lines.
6. Solve power flow and run contingency analysis. The root case should be a 'secure' operating point as a baseline for the study corridor analysis.

7. Classify the operating point as ‘secure’ or ‘insecure’ based on the classification criteria used.
    a. Note the location of violation, as this is used to classify the operating points based on angle.
    b. Extract the ‘Case Information’ and record in a database.
8. Perform sensitivity analysis around this operating point to generate a range of possible conditions. Perform contingency analysis on these sensitivity cases to classify the operating point and record ‘Case Information’.
9. Increase or decrease stress on the corridor by creating scenario cases. This may require generation redispatch both inside and outside the study corridor.
    a. Examples include high or low hydro conditions, thermal generation vs. green energy, or high interchange flows.
10. Continue Steps 6-9 for various scenario and sensitivity cases, continuing to increase stress (and angle differences) across the corridor. Identify the boundary where operating conditions continue to become ‘insecure’.
11. Ensure that enough operating points have been generated to get a clear picture of each of the angle violations within the corridor.
12. Generate $\Delta\delta$ vs. P plots for each of the angle differences within the corridor. These plots are used to visualize the security boundary in terms of angle difference.
13. Repeat Steps 5-12 for line outage conditions. Repeat the analysis, with the root cases in an ‘N-1’ operating condition. These conditions reflect planned outages or forced outages where the system has been reconfigured. This analysis will determine if the line outage significantly affects the angle limits for the corridor, and whether that outage must be included in adaptive limits.

This methodology is applied to the clusters defined within the BPA power system using the full WECC model. Application of this methodology is used to explore the effectiveness of angle alarming and produce guidelines for future work in terms of implementing production-grade applications.

3.4. Test Scenario: Seattle-Portland Corridor Study

The Seattle-Portland transmission corridor consists of a series combination of EHV 500kV transmission paths, connected by significant generation and load injection nodes. Figure 28 provides a high-level visualization of the transmission corridor. This corridor is selected as the initial test scenario due to its geographic simplicity, yet its electrical complexity.

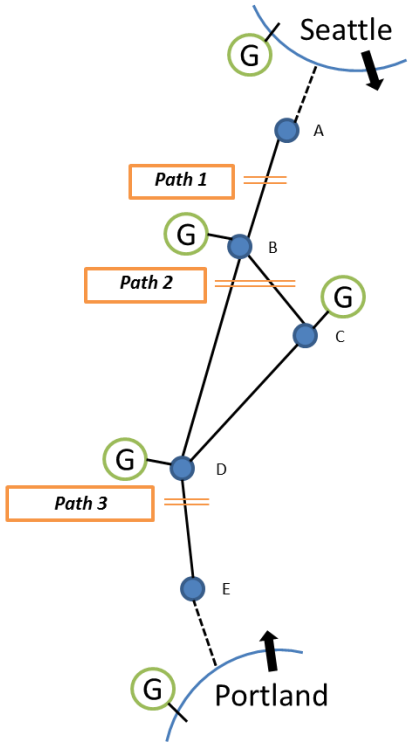

Figure 28. Seattle-Portland Transmission Corridor

3.4.1. SEA-PDX All Lines in Service Condition

A total of 27 cases spanning a wide range of operating conditions are created with varying levels of stress on each of the three Paths. Each path is stressed by altering the generation pattern by incrementing or decrementing specific generating units or removing units or plants from service. For example, a coal-fired unit may be down for maintenance, taking it offline. Similarly, a poor water year may cause significantly reduced river runoff resulting in low hydro generation outputs. Each operating point is classified as 'Secure' or 'Insecure' based on the classification methodology and criteria provided in Section 3.3.

Figure 29 shows the classification results for the three series Paths between the Seattle and Portland areas.

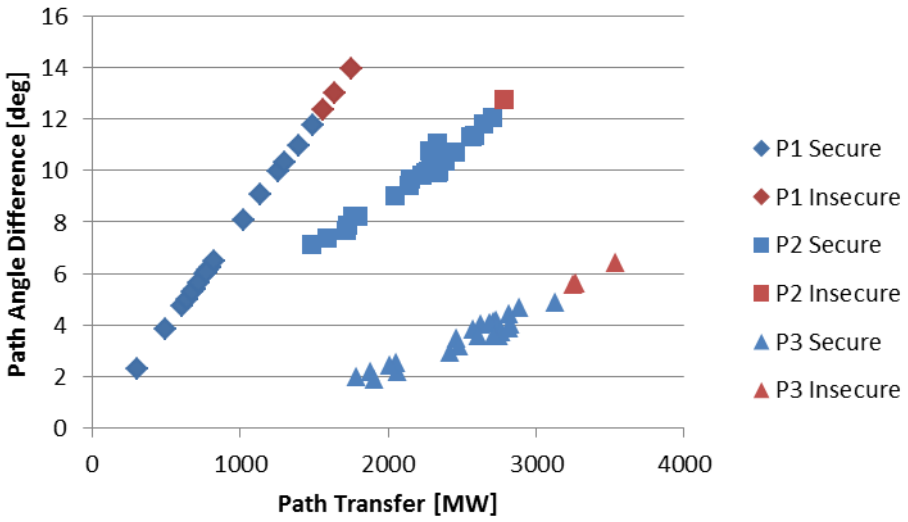

Figure 29. Seattle-Portland Corridor Classification

As expected, the phase angle difference with respect to real power transfer across the Path follows a trajectory defined by the real power transfer equation. It is noted that the slope of this trajectory follows a relatively linear relationship due to the fact that

$$P_{12} = \frac{V_1 V_2}{X_l} \sin(\delta_{12}) \tag{3.7}$$

and for small δ_{12},

$$P_{12} = \frac{V_1 V_2}{X_l} \sin(\delta_{12}) \approx \frac{V_1 V_2}{X_l} \delta_{12}. \tag{3.8}$$

Therefore,

$$\frac{dP_{12}}{d\delta_{12}} = \frac{V_1 V_2}{X_l} \tag{3.9}$$

for smaller values of δ_{12}. Insecurity occurs near a 12 degree angle difference, which is within an acceptable range for the linearization assumption.

Classification of insecurity is based on the location of the outaged element causing the violation with respect to the different Paths identified. If the outage of one or more elements falls on or adjacent to the Path, then that Path is identified as insecure. Appendix A shows the study results for this particular transmission corridor. Notice that the linearity and low degree of variance cause the misclassification rate of the measurements to be very low. Similar to the methodology for setting System Operating Limits, using a $\{P, \delta\}$ plot allows both the real power Path limits as well as the Path phase angle difference limits to be set. Based on the results collected for the Seattle-Portland transmission corridor thus far, the following limits can be set.

TABLE V. SEA-PDX ANGLE LIMITS

Path	Node 1	Node 2	Limit [deg]
Path 1	A	B	12.0
Path 2	B	C/D	12.1
Path 3	D	E	5.2

3.4.2. SEA-PDX Path Outage Condition

Thus far, the analysis has assumed All Lines in Service (ALIS) conditions. However, system topology is continuously changing due to planned or forced outages and system operating limits must be adjusted. It is expected that the requirement of new SOLs would also require updated angle difference threshold values. To test this hypothesis, a major 500kV transmission line is taken out of service, such that Path 1 transfers are equal to 0 for all operating conditions. Path 1 consists of a single 500kV transmission line; however, power can still flow through the lower voltage lines adjacent and parallel to the Path definition. The same operating points created for the ALIS condition are again utilized for the Path 1 outage condition. Additional operating conditions are used to stress specific lines or Paths for increased resolution. Figure 30 shows the results for this study, with only Path 1 and Path 2 shown because these paths were the only ones to violate with reasonable operating conditions. As the figure shows, the real power for Path 1 is always 0 MW while the angle difference changes significantly.

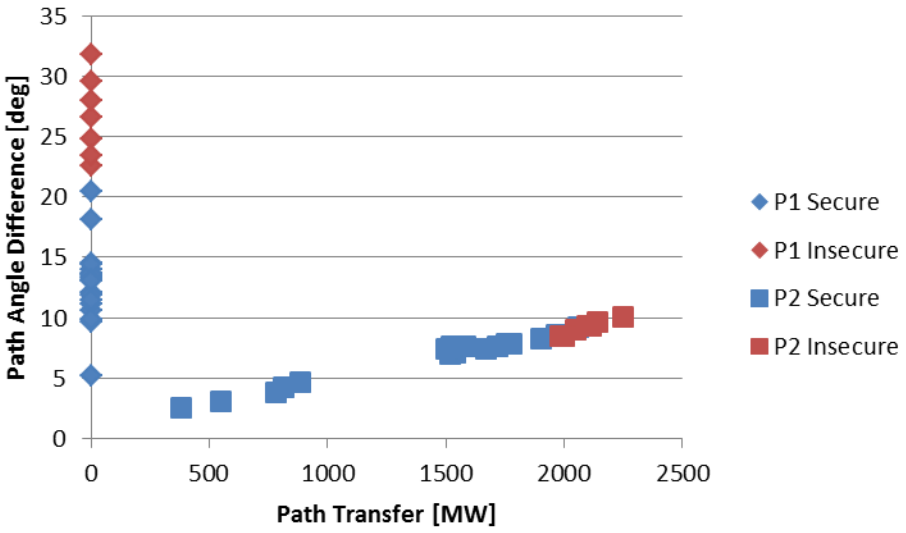

Figure 30. Seattle-Portland Outage Comparison

The results in Figure 30 vary from the limits determined in TABLE V, and are shown below in TABLE VI. Outage of a major Path 500kV transmission line results in substantially increased phase angle difference across the Path due to the increased impedance. Conversely, Path 2 cannot be loaded to its ALIS levels due to heavy loading on the underlying 230kV system.

TABLE VI. SEA-PDX ANGLE LIMIT ALIS AND OUTAGE COMPARISON

Path	Node 1	Node 2	ALIS Limit [deg]	Path 1 Out Limit [deg]
Path 1	A	B	12.0	22.5
Path 2	B	C/D	12.1	8.5
Path 3	D	E	5.2	N/A

Based on this data, it is concluded that phase angle limits must adapt based on system topology within the transmission corridor. Impedance changes, especially due to major 500kV transmission lines, can have a significant effect on phase angle difference across a given Path. Algorithms must have capabilities to adjust to changing system conditions by integrating SCADA or WAMS data, utilizing breaker status information, or estimating line status from measurement data. Adaptability of this nature allows for more precise classification of system stress based on the current operating conditions.

3.4.3. SEA-PDX External Line Outage Condition

The Seattle-Portland transmission corridor is again used as an example for determining the impacts of external outages to the internal transmission corridor. The ALIS conditions from Section 3.4.1 are altered by taking a major 500kV transmission line feeding into the Portland area from the Lower Columbia region out of service. This redistributes flows throughout the system, but primarily increases stress through the Seattle-Portland transmission corridor. Contingency analysis and security assessment are performed on the same set of altered cases to determine if this major outage has any noticeable effect on transfer limits. Figure 31 shows the results of this study; there is no noticeable effect on angle limits due to outages outside the studied corridor. With either the ALIS or external outage (EO) conditions, the Path limit is approximately 12 degrees. The figure gives an excellent portrayal of the fact that the stress on the corridor changes. The operating points do not line up directly, but rather fall in different locations along the angle-real power relationship. However, the point at which the operating points move from secure to insecure does not change.

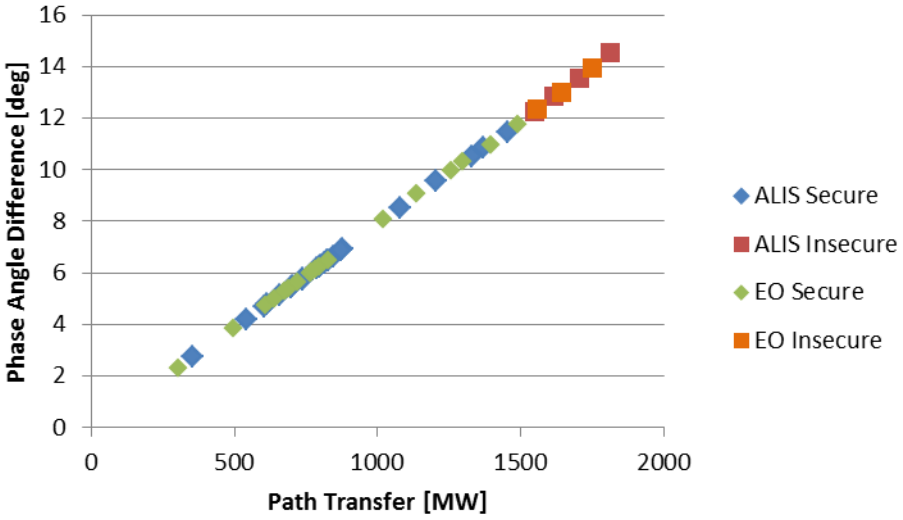

Figure 31. Seattle-Portland External Outage (EO) Comparison

3.4.4. SEA-PDX Lower Voltage Outage Condition

If major 500kV transmission lines drastically affect phase angle limits, then it can be hypothesized that lower voltage transmission facilities can also affect these limits. This is similar to System Operating Limit (SOL) studies and results that create large databases of nomograms based on the status and availability of facilities, including critical lower voltage elements. To test this hypothesis, a 230kV transmission line parallel to Path 1 and Path 2 is taken out of service pre-contingency. Again the operating points from the ALIS conditions are used with the lower voltage facility removed from service. Each operation point is classified based on static security assessment and the results are plotted in terms of path flow and phase angle difference, as shown in Figure 32.

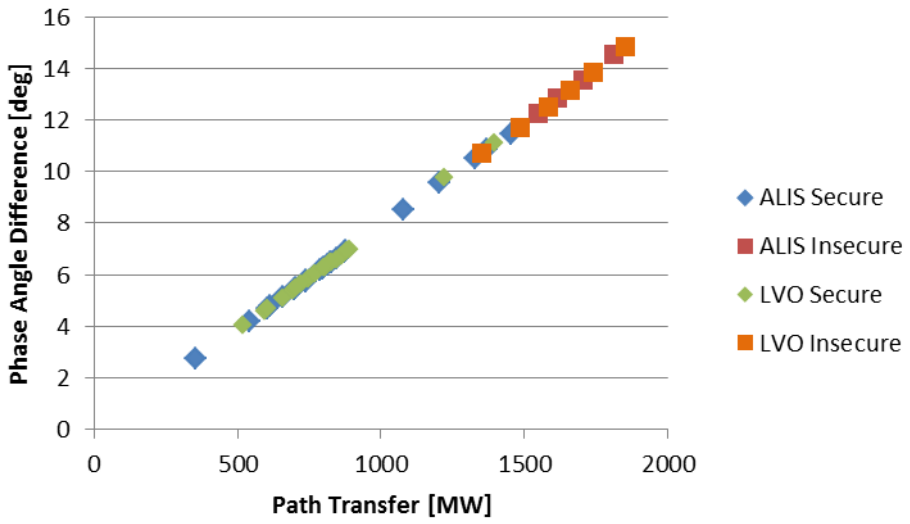

Figure 32. Seattle-Portland Lower Voltage Outage (LVO) Comparison

As the figure shows, the lower voltage outage (LVO) conditions experience insecurity at a lower phase angle difference than the ALIS conditions. At approximately 10.7 degrees for the LVO situation, the operating point has potential for insecurity; for the ALIS situation, this occurs at about 12 degrees. This indicates that outages on the lower voltage 230kV system and possibly the 115kV system may require specific updates to limits based on their statuses. The list of outages that require acknowledgement in the adaptable implementation can be determined offline in the SOL studies or online in a state estimator application.

3.5. Test Scenario: Upper Columbia-Seattle Corridor Study

The same methodology is employed for setting the phase angle limits between the Upper Columbia generation hub and the Seattle area load center. Unlike the Seattle-Portland corridor, this corridor consists of a single Path defined by multiple transmission lines in parallel. Figure 33 shows an illustration of the Upper Columbia-Seattle transmission corridor major transmission lines.

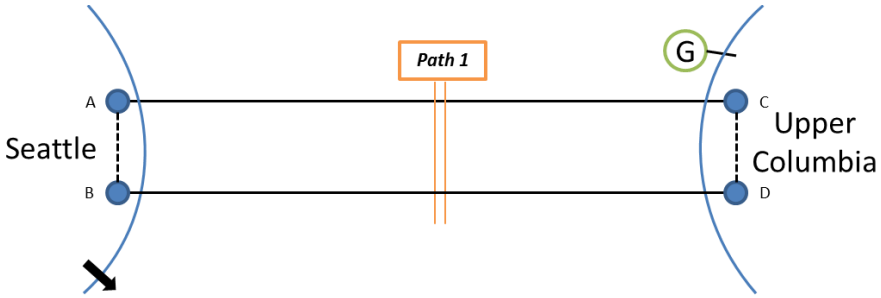

Figure 33. Upper Columbia-Seattle Transmission Corridor

A number of these lines are at lower voltages, and therefore measurement of the actual Path flows from available PMU data is not possible. However, the PMUs are measuring major 500kV line flows across the path and the voltage angles on each side of the Path at substations $\{A, B, C, D\}$. Therefore, these measurements can be used to determine angle limits and plot $\{P, \delta\}$. Based on Figure 33, two angle differences, δ_{AC} and δ_{BD}, can be made for security classification. 500kV transmission lines also connect substations *A* and *B*, and *C* and *D*, but these lines do not cross the corridor or the identified interconnecting path, Path 1, and therefore are not included in the angle difference calculations.

3.5.1. Upper C-Seattle All Lines in Service Condition

Similar to the Seattle-Portland transmission corridor, a number of cases are created by varying generation dispatch and intertie schedules throughout the region. This Path is primarily affected by scheduled flows from Canada, generation in the Seattle and Upper Columbia regions, load in the Seattle area, and transmission topology. Flows may also be affected by the amount and location of generation across the BPA footprint as well as flows to California. Figure 34 shows the two angle difference calculations with respect to the total real power flows of the transmission lines that compose Path 1.

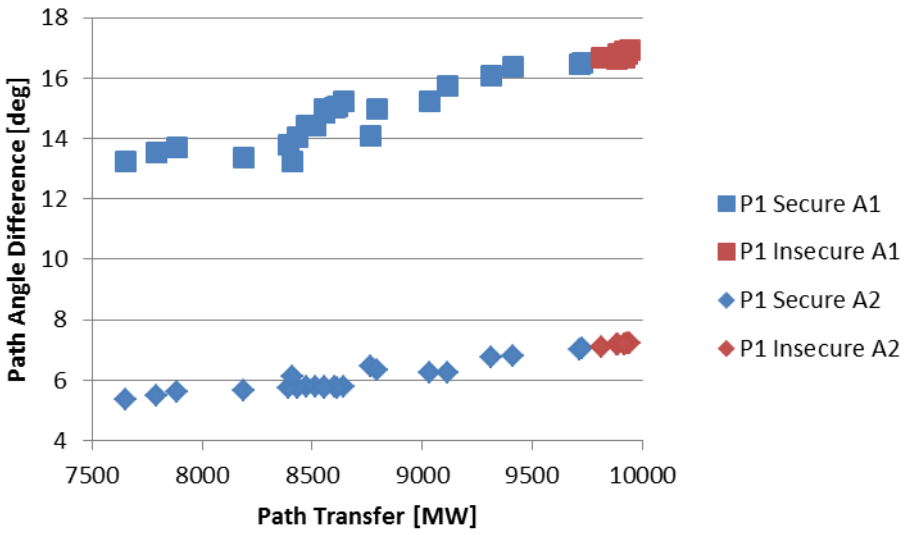

Figure 34. Upper Columbia-Seattle Corridor Classification

Based on these results, phase angle limits as defined in TABLE VII can be set. Note the significant difference in angle across the same path for the two lines. This is due to the impedance of the connecting lines and the lower voltage transmission reinforcements in the corridor.

TABLE VII. UPPER C-SEA ANGLE LIMITS

Path	Node 1	Node 2	Limit [deg]
Path 1	C	A	16.5
Path 1	D	B	7.1

3.5.2. Upper C-Seattle Seasonal Study Comparison

Flow across the Upper Columbia-Seattle Path varies drastically based on time of day, generation pattern, and most importantly season. During the summer months where imports from Canadian hydro are high, generation moves across the Path to serve Seattle load, southward to serve Portland load, and further south for export to California. With a path that is geographically and electrically more expansive, flows can differ between the two angle measurements across the path. During these summer months, the more southern paths are utilized more than the northern paths due to the transfers and stress patterns. Conversely, during the winter season power may be exported to Canada and Northwest hydro may be high so the northern elements of the Path will experience greater amounts of

stress. This changing stress pattern can affect the security boundary, as shown in Figure 35. While Angle 1, A1, increases in magnitude from Heavy Summer conditions to Heavy Winter conditions, Angle 2, A2, decreases slightly.

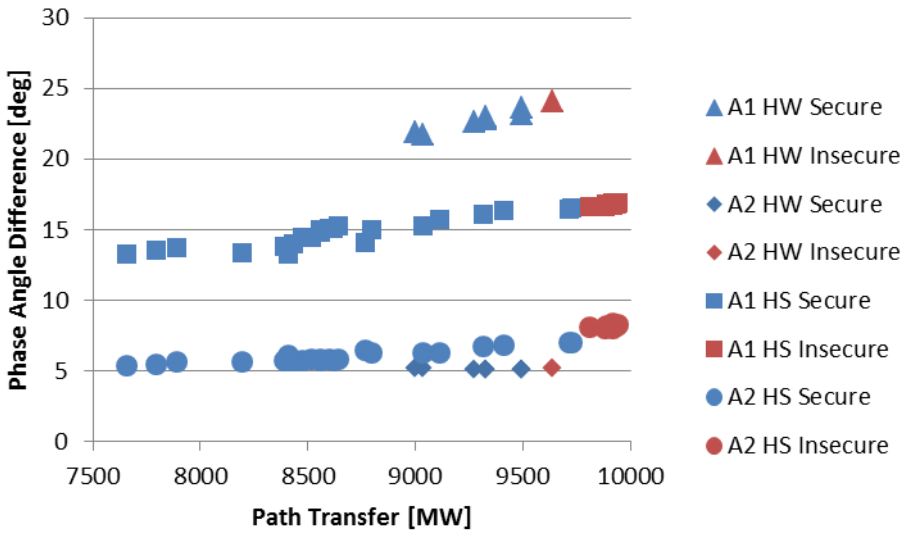

Figure 35. Upper Columbia-Seattle Seasonal Classification

3.6. Application Implementation Considerations

As mentioned previously, the phase angle alarming methodology has been performed manually as an explorative and research-oriented effort to better understand and quantify how phase angle limits can be implemented. However, the methodology is designed for both offline operations planning studies as well as potential online tools such as s state estimator application. These options are discussed briefly below.

Operations planning studies are used to set System Operating Limits for dispatchers to follow during real-time operation of the system. These SOLs are continuously studied and updated based on planned outages such as maintenance. Similarly, if an unforeseen operating point is expected, Operations Study Engineers may run quick studies to determine if this operating point is acceptable and update the limits accordingly. SOL studies are innately similar to the study methodology proposed in this research, except the SOL limits obtained are generally based on Path or line real power flows. These limits are "MW-based" rather than "angle-based". Integration of angle limits into the SOL studies would be straightforward.

State estimator cases can be used to obtain a recent state estimate of the system for creating a root base case to study from. This case is modified to test the expected future operating points, and sensitivities and scenarios are studies around this point. When an insecure operating point is determined, and remedial action is unable to return the system to within acceptable limits, the MW limits are obtained. Critical outages are also studied in the event that an outage occurs; these elements are generally adjacent EHV lines such as 230-500kV lines and transformers, breaker failure events, and specific lower voltage outages. Results are stored in lookup tables used by operators in the case of unexpected outages.

Implementing supplementary angle limits into the SOL studies would be a simple and effective safety net measure. When the Study Engineers extract the Path limits based on varying operating conditions, whether in day-ahead or on-the-fly studies, phase angle differences between PMU locations can be extracted as well. Entering these limits into a lookup table could be streamlined such that the entered values provide alarms or visual interpretation of stress. Figure 36 shows a conceptual angle alarming implementation using PI ProcessBook [84]. The angle database updated by the SOL studies and the angle alarming logic run continuously in the background. The front end application is used as a situational awareness tool in the case of unexpected conditions or a visual indication of system stress across the system. The focal point of the display is the wide-area map. The PMU group nodes are color-coded based on their frequency measurements, one color indicating reduced frequency and another indicating increased frequency. If sufficient PMUs are available within each of the groups, the nodes may be linked to inter-group angle measurements. For example, PMUs in the Portland or Seattle load areas may be used to calculate angle differences across the PMU groups. Changes in color could signify a problem in that area, and the node could be selectable by the operator to explore in greater depth the individual angles or real power flows in the area causing the problem. The branches are also color-coded based on the uploaded angle limits. The study results provide one degree of limits based on the security boundary. This limit can be classified by a yellow color on the display. Since there is inaccuracy in the studies due to constantly changing system conditions, alarms can be withheld for these limits. However, a small buffer may be added (e.g. 105-110% of studied limit) for alarming and red color on the

displays. It is highly likely that the system is in an insecure operating condition if these limits are exceeded. Alarms can be activated at this point to notify the operators of problematic areas of the system that may need attention. Blue links indicate that bad data is detected, and alarming has been disabled. Dispatcher Standing Orders (DSOs) can aid the operators in mechanisms for reducing phase angle differences across the system such as generation redispatch or schedule reduction.

Real-time phase angles are relatively new technology to system operators. Therefore, time series plots of angle accompany real power plots to allow operators capability to intuitively understand the relationship between angle and real power. Similarly, wide-area angles are also shown in the time series plots to unclutter the geographic display but also show the overall relative stress. Time interval selection options at the top allow operators to select the observation resolution. This allows trends to be observed for 15-minute, 2-hour, 24-hr, and 7-day intervals. Lastly, a 'Change Tag' option allows the operator to select other measurements of interest to add or remove to the display.

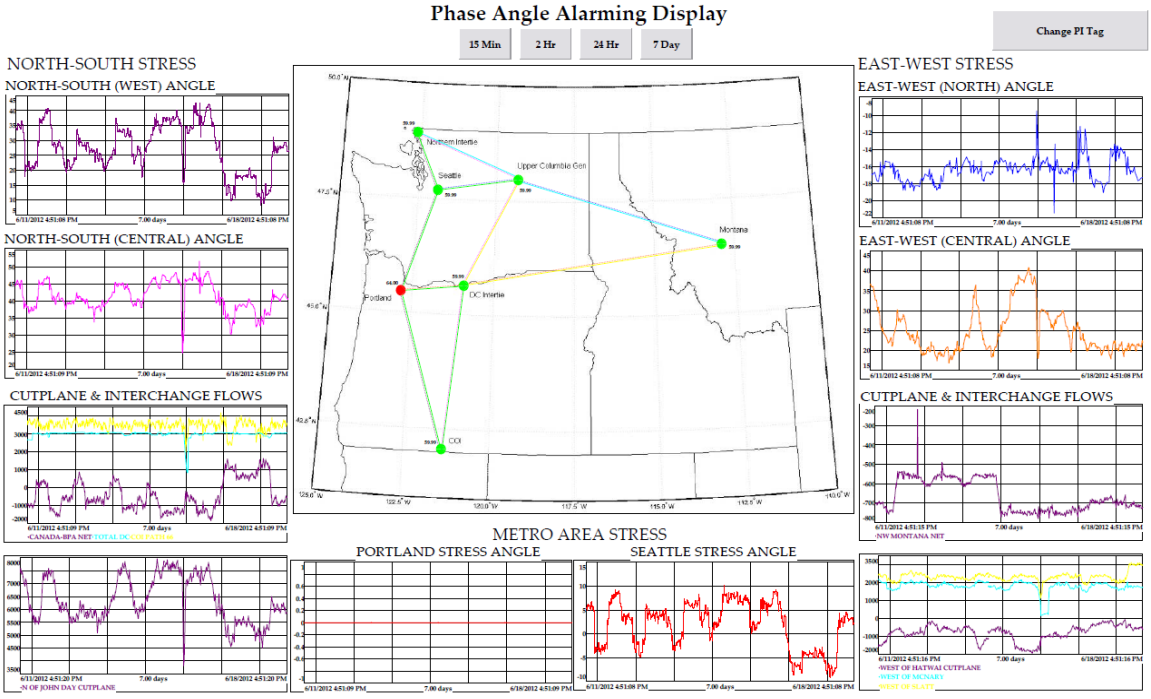

Figure 36. Conceptual Angle Alarm Display

3.7. Wide Area Angle Limits Based on Damping

Proposed thus far in this research is a methodology for determining phase angle limits based on static security assessment. The goal is to inform the operators of stressed system conditions by correlating phase angles with system security. Results provided have shown effective classification of acceptable vs. unacceptable operating points based on angular limits. However, the additional tier to this methodology is the application of wider-area angular limits to detect instability or risk of instability. This issue has raised a number of questions at recent WECC JSIS and NASPI meetings. "Can phase angles from PMUs provide a good indication of system stability if a contingency were to occur? Moreover, can the angle classify conditions in which oscillation damping is low following a major contingency?" The goal is therefore to explore correlation between pre-contingency system conditions and oscillation damping, and provide a methodology or tool for detecting low damping conditions [4, 85].

Before exploring analysis techniques and results obtained, let us identify the study methodology and breadth of operating conditions explored. Approximately 150 credible operating base cases are created with the assistance of Dr. Dmitry Kosterev, reflecting expected path flows and generation dispatch across the WECC. A list of Category B and C contingencies are simulated for each case; these contingencies have been identified as the most severe for WECC instability or low damping [39]. Prony analysis is used to estimate the major modes of oscillation based on ringdown of selected response signals, and identify the oscillation frequency and percentage damping of each mode [48]. There are two major modes in the WECC that affect system stability, including what are known as the North-South A 0.25Hz mode and the North-South B 0.35Hz mode (also known as the "Alberta mode"). A base case report tool is used to extract a database of pre-contingency variables including path flows and angles across the WECC. Path flows and angle are used as variables because these are the primary measurements received from real-time PMUs most indicative of system stress levels.

Each base case is assigned a post-contingency oscillation frequency, which is the most poorly damped mode of oscillation in the inter-area frequency range of interest 0.1-0.5Hz, and then classified as 'acceptable' or 'unacceptable' based on a classification threshold.

The analyses presented here use a 1.5% threshold for post-contingency ringdown damping. In addition, the Chief Joseph 1400MW Brake resistor simulation is used as a baseline of pre-contingency damping [86]. Pre-contingency damping can be used as an additional input variable to the decision tree application, assuming that tools such as the 'Mode Meter' can determine steady-state damping through eigenvalue analysis [87, 88].

To illustrate the database of operating conditions generated, Figure 37 shows various phase angles across WECC and the % damping assigned to the operating point. The original hypothesis was that a distinct classification of damping could be determined based on either angles or real power flows across the system. However, the variance of % damping for a given phase angle makes classification using visual inspection difficult; basic linear thresholds would be set overly secure or dependable. For example, *Angle 4* in Figure 37 can have a % damping between 0-3.5% for an angle measurement of 20 degrees. Conversely, *Angle 3* can vary between 65-95 degrees for a damping of 1.5% according to the study results.

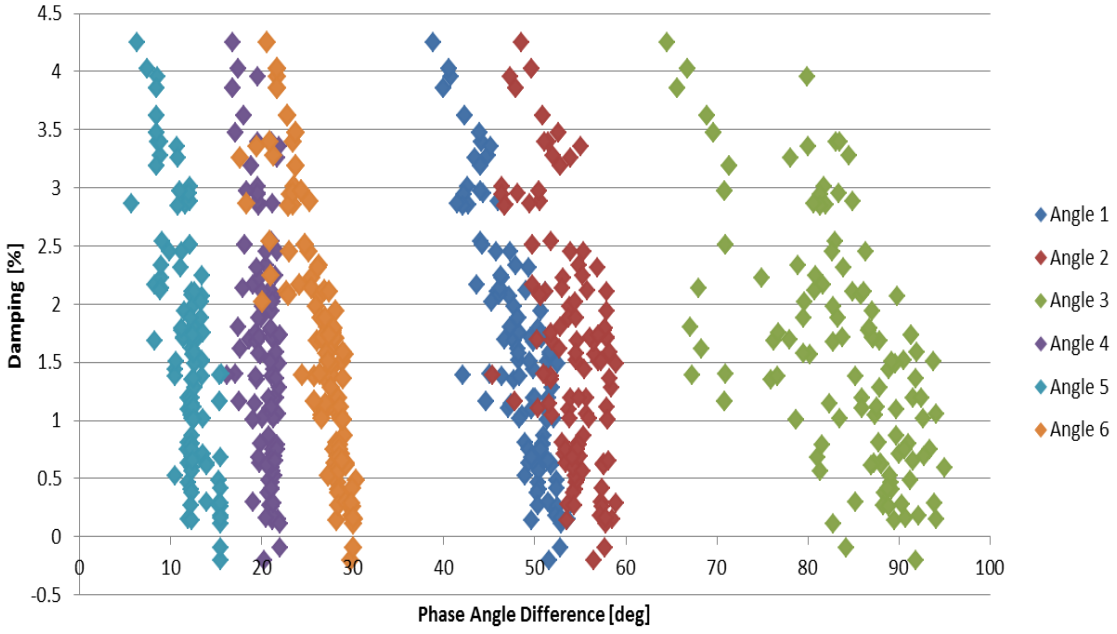

Figure 37. Phase Angle Difference vs. % Damping

Based on these observations, more sophisticated data mining tools were explored. These tools help:

1. Determine indicators of low damping conditions based on pre-contingency PMU measurements.
2. Estimate threshold values associated with the key indicators selected.
3. Understand system attributes with the greatest influence on post-contingency damping.
4. Describe changes in measurement selection based on varying operating conditions (i.e. element statuses, generation consistency, etc.).

System damping is a factor of numerous variables, some of which are not measureable by a single entity and would require a comprehensive view of the system. For example, it is well known that the amount of inertia on the system has an impact on system damping; light loading conditions often result in poor damping of inter-area oscillations because a substantial amount of generation is offline, resulting in decreased spinning inertia on the system [24]. Similarly, power system stabilizer settings and statuses, advanced remedial action schemes, governor response, and load characteristics can all influence the level of damping on the system. Therefore, pre-contingency operating characteristics have not, and most likely will not, be the universal indicator of low damping. However, they may provide *expected* levels of damping for given operating conditions and improve operator awareness of these risks.

Therefore, the goal of this project and the scope of its contribution must be defined explicitly. Simply understanding that low damping can occur during both heavy and light loading conditions illustrates that using pre-contingency measurements will not work in all situations. Such a vast operating range is both challenging to study and difficult to attain classification accuracy. However, if specific operating regions are known to be problematic for a particular system, using these tools on a subset of cases may prove effective for classifying conditions with poorly damped oscillation ringdown following a large disturbance. To explain the range of operating conditions explored in this study, refer to Figure 38. While the studied operating region is shown in the red box, the actual expected operating region based on historical data is encompassed in the green box. Note that this study explores operating conditions at the current operating limits in case of very high stress levels on the system. Based on engineering judgment and past experience, this

region is known to cause low damping conditions, i.e. risk of damping is known to be low during these conditions based on previous events.

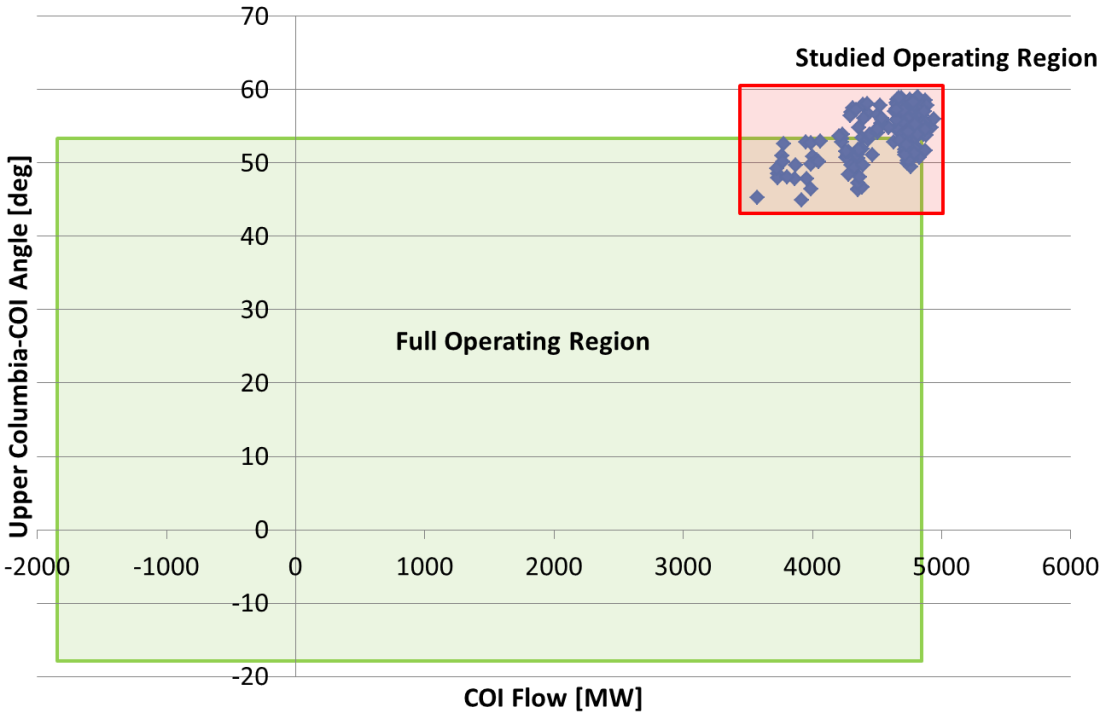

Figure 38. Damping Study Operating Region

A significant constraint in this project is the ability to use data mining tools for offline analysis, but any potential online application should not utilize these tools. This is due to the likelihood of control center operators adopting tools that are extremely unfamiliar and relatively unexplored in the industry. Therefore, these data mining tools are utilized in the offline study phase but are not considered for any potential online application.

3.7.1. Data Mining using Decision Trees

Decision trees are a form of machine learning used in statistics and data mining that can be applied to myriad topics including power systems. This form of machine learning has advantages for power system applications due to the complexity and size of information available to an operator or engineer. Decision tree learning generates a model based on the information provided that predicts the value of a *target variable* based on a set of input *attributes*. In addition, the tree created through this process provides a simple and effective answer for understanding the target variable in terms of potential attributes and their

respective thresholds. Decision trees have been used in the past for applications such as adaptive protection schemes, transient and voltage security assessment, high impedance fault detection, and controlled islanding [89, 90, 91, 92, 93, 94, 95]. The commonality between these applications is that a large database of offline studies are performed to generate a decision tree that provides useful information for classifying system conditions for effective real-time decision making and controls.

The analysis is based on a learning sample *L*, which is derived from the expected operating range of concern. Larger classification problems may tend to include all possible conditions while more detailed analyses may use a smaller subspace of the entire operating space. Regardless, it is critical to define the sample *L* of the decision tree so that the breadth of analysis is well-defined. Decision trees recursively split or partition the learning sample *L* such that the homogeneity of each group is improved with each decision split or until homogeneity cannot be further improved. Methods and mathematic derivation of building, pruning, and validating decision trees used in machine learning can be found in [96, 90].

This research utilizes decision trees as an analysis tool for understanding power system operating conditions. Therefore, it is important to describe the application of decision trees. Refer to Figure 39, which demonstrates an example decision tree and its components.

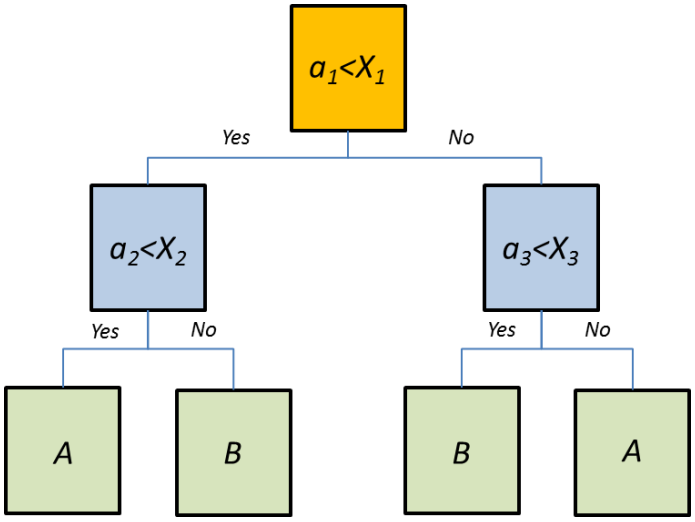

Figure 39. Example Decision Tree

A sample data set of interest can take the form

$$(x, Y) = (x_{1,}, x_2, x_3, \ldots, x_k, Y) \tag{3.10}$$

where Y is the target variable that is trying to be understood through machine learning. Input vector $\boldsymbol{x}$ is composed of attributes $x_{1,\ldots,}x_k$ that are used to classify or explain the target variable Y. The tree consists of three types of nodes: the root node, splitting nodes, and terminal nodes. Every tree has one root node, which makes the initial split in the data. This node encompasses the entire learning set L. Below the root node are either splitting nodes or terminal nodes. At each splitting node, the data set is split based on an attribute a_i and its threshold value $X_{t,i}$. The split creates two subsets t_L and t_R, which are the left and right child nodes of the splitting node, respectively. This process is continued down the splitting nodes until a terminal node is reached. For classification trees, the terminal nodes make the actual classification of the data point after traversing the tree. Specifically for binary classification trees, the classification will be of either group A or B. These groupings can be related to any classification problem that utilizes a large amount of variables to classify a given point.

3.7.2. Applying Decision Trees to Oscillation Damping Analysis

Key transmission flows and phase angle differences are extracted from the cases using a base case reporting tool. Two measurement data sets are used in the following analyses: the full list of measurements extracted ("Full WECC Dataset") and a restricted list of measurements ("BPA Dataset"), shown in TABLE VIII. The full list consists of major Path flows and angle differences across the WECC. The restricted list is defined as those measurements that are measurable within the BPA Control Area from potential BPA WISP PMUs.

TABLE VIII. DAMPING INPUT VARIABLE DATASETS

MW PATH FLOWS				ANGLE DIFFERENCES						MW PATH FLOWS		ANGLE DIFFERENCES	
#	Label	#	Label	#	Label	#	Label	#		#	Label	#	Label
1	BC-ALB	14	P-26	19	GMS-ING	32	MONR-MLN	45	TES-MIRA	1	BC-NW	11	MONR-JDA
2	MATL	15	EoR	20	KMO-ING	33	GCL-MLN	46	MIDW-MIRA	2	MT-NW	12	GCL-JDA
3	BC-NW	16	WoR	21	NIC-ING	34	JDA-MLN	47	PV-MIRA	3	NOH+SoNV	13	MONR-GRIZ
4	MT-NW	17	BorahW	22	ING-MONR	35	ING-TES	48	NAVA-MIRA	4	NOH+RP	14	GCL-GRIZ
5	NOH+SoNV	18	TOT2	23	ING-JDA	36	MONR-TES	49	FOURC-MIRA	5	NJD	15	MONR-MLN
6	NOH+RP			24	MONR-JDA	37	GCL-TES			6	PDCI	16	GCL-MLN
7	NJD			25	GCL-JDA	38	JDA-TES			7	COI	17	JDA-MLN
8	PDCI			26	COLS-JDA	39	MLN-TES			8	RATS		
9	COI			27	ING-GRIZ	40	ING-MIRA			9	MP-HW		
10	RATS			28	MONR-GRIZ	41	MONR-MIRA			10	SOG		
11	MP-HW			29	GCL-GRIZ	42	GCL-MIRA						
12	SOG			30	COLS-GRIZ	43	JDA-MIRA						
13	P-15			31	ING-MLN	44	MLN-MIRA						
FULL WECC DATASET										**BPA DATASET**			

It is well understood that the connection of Alberta to British Columbia and the rest of WECC significantly impacts the inter-area modes of oscillation. Therefore, the cases are separated into the following categories: all cases ("combined"), Alberta in service ("ALB In"), and Alberta disconnected ("ALB Out"). Each of the cases and their respective variables are processed through a decision tree algorithm. Full analysis is provided in Appendix B; let us explore the more enlightening results here.

The full WECC dataset is analyzed first, in three distinct forms: {MW & Angle}, {MW Only}, and {Angle Only}, as shown in Figure 40, Figure 41, and Figure 42, respectively. This utilizes the "Combined" set of base cases, with both Alberta In and Alberta Out.

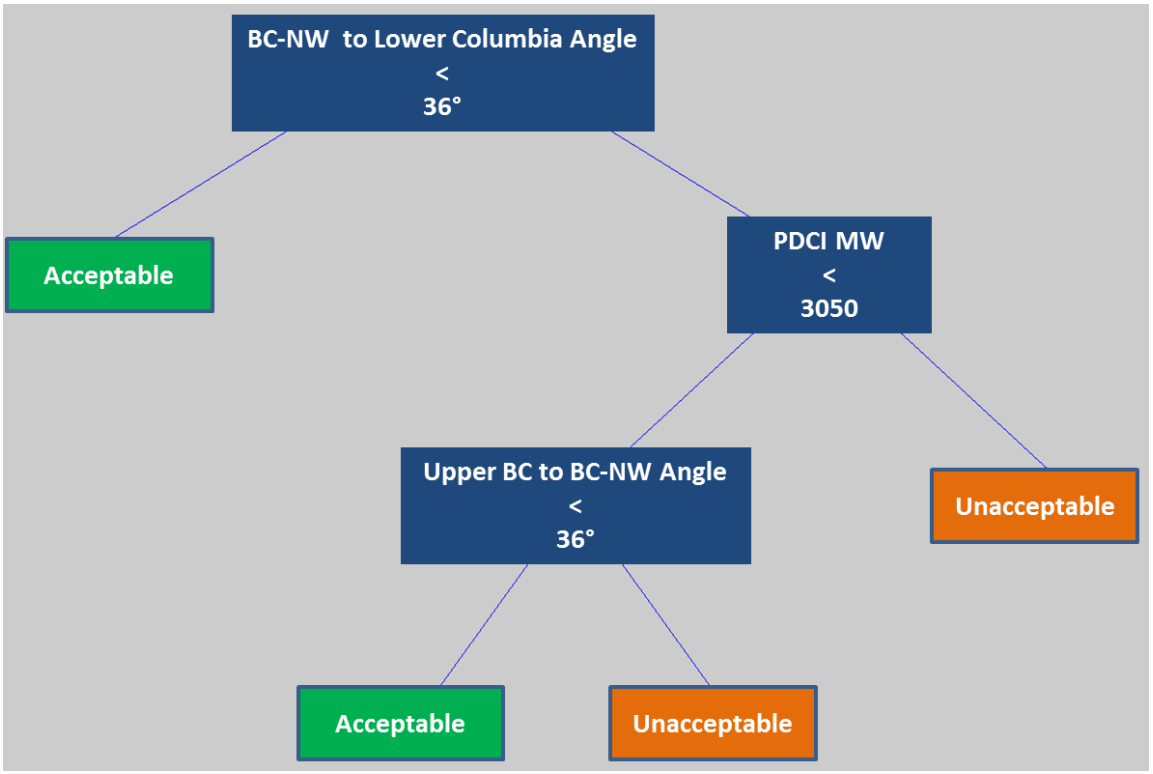

Figure 40. Damping Decision Tree: WECC, Combined, MW and Angle, Best Fit

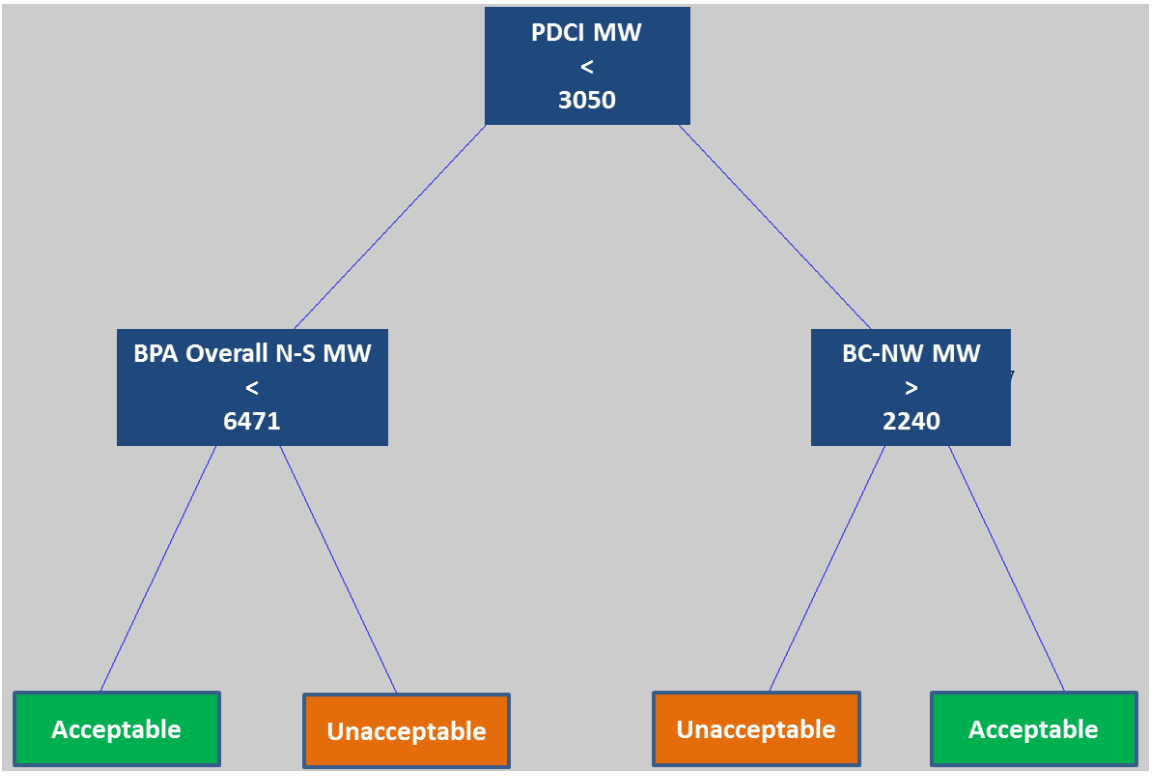

Figure 41. Damping Decision Tree: WECC, Combined, MW Only, Best Fit

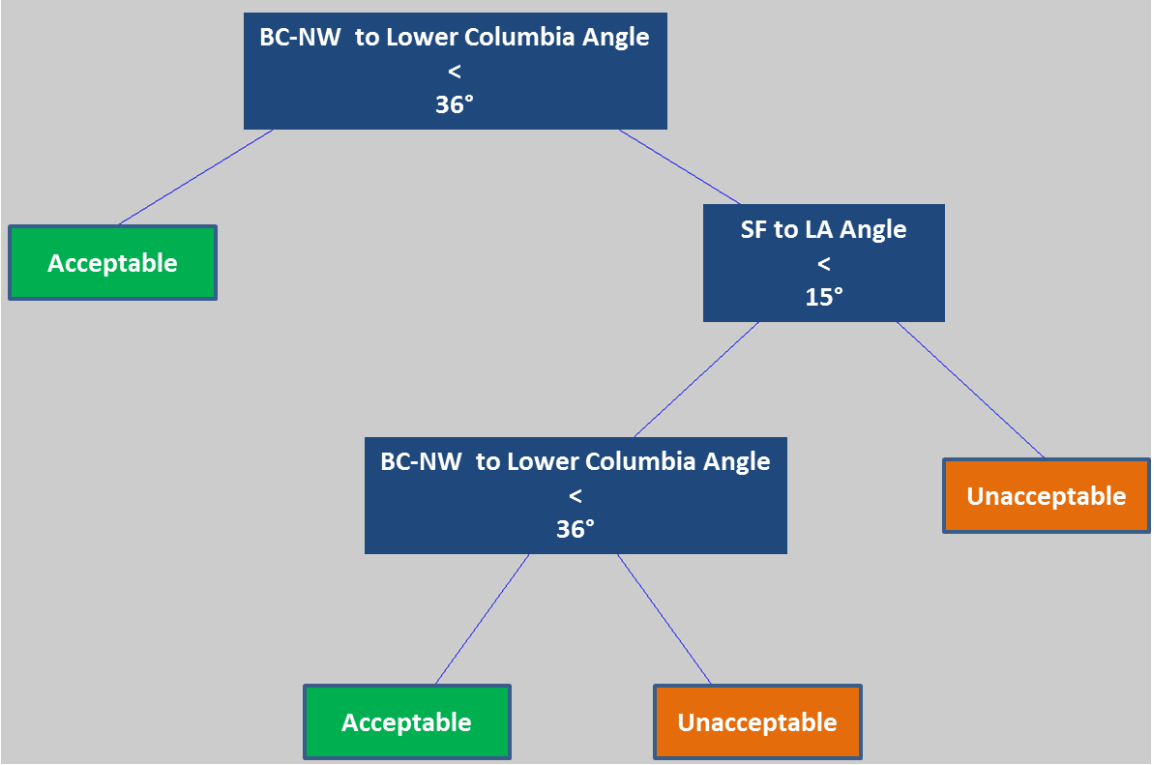

Figure 42. Damping Decision Tree: WECC, Combined, Angle Only, Best Fit

The results obtained from these decision tree models are highly informative for determining what measurements impact oscillation damping. All attributes used (MW and angle measurements) are in the North-South direction, i.e. damping is most impacted by North-South system stress. Additionally, the primary indicator of low damping is the angle difference between the north bus of the British Columbia-Northwest intertie and a substation in the Lower Columbia region. The PDCI has a threshold value of 3050MW, or essentially its operating limit (may be an anomaly of input data). Primarily, the flows from BC, across BPA, and down the COI to California can be used to indicate low damping.

Let us explore the BPA data set using the combination of cases. Figure 43, Figure 44, and Figure 45 show decision tree results for the {MW and Angle}, {MW Only}, and {Angle Only}, respectively.

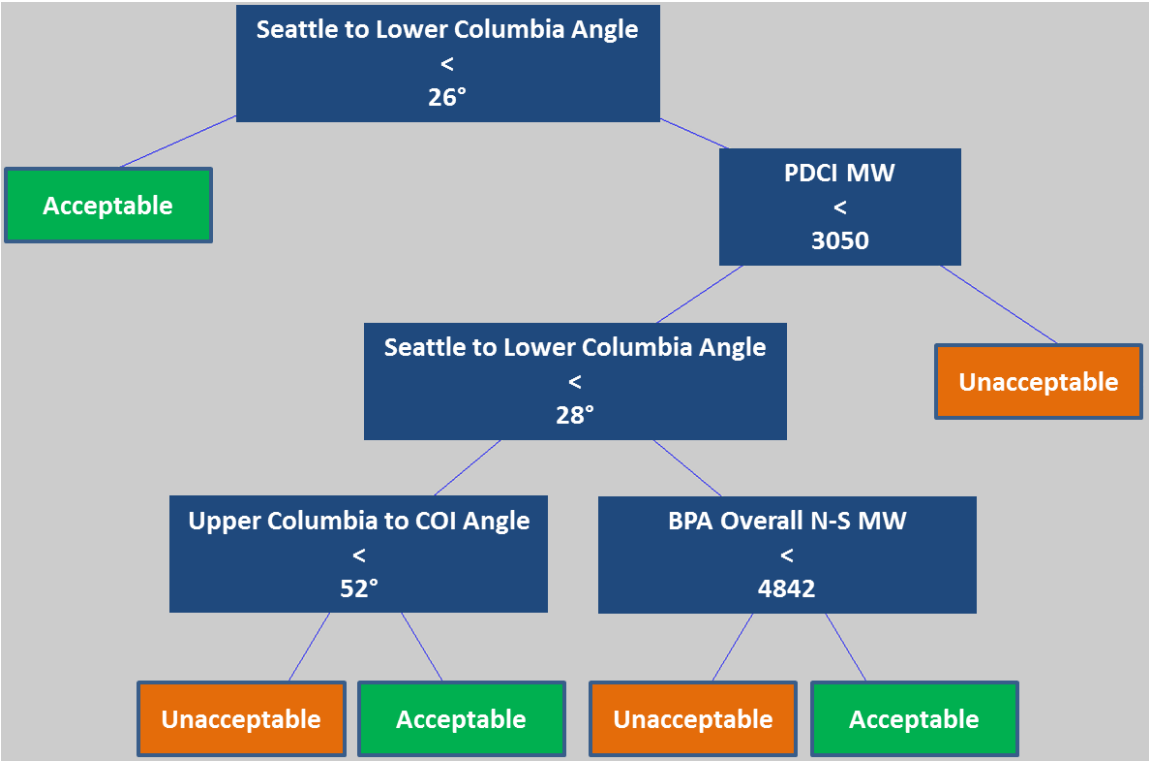

Figure 43. Damping Decision Tree: BPA, Combined, MW and Angle, Best Fit

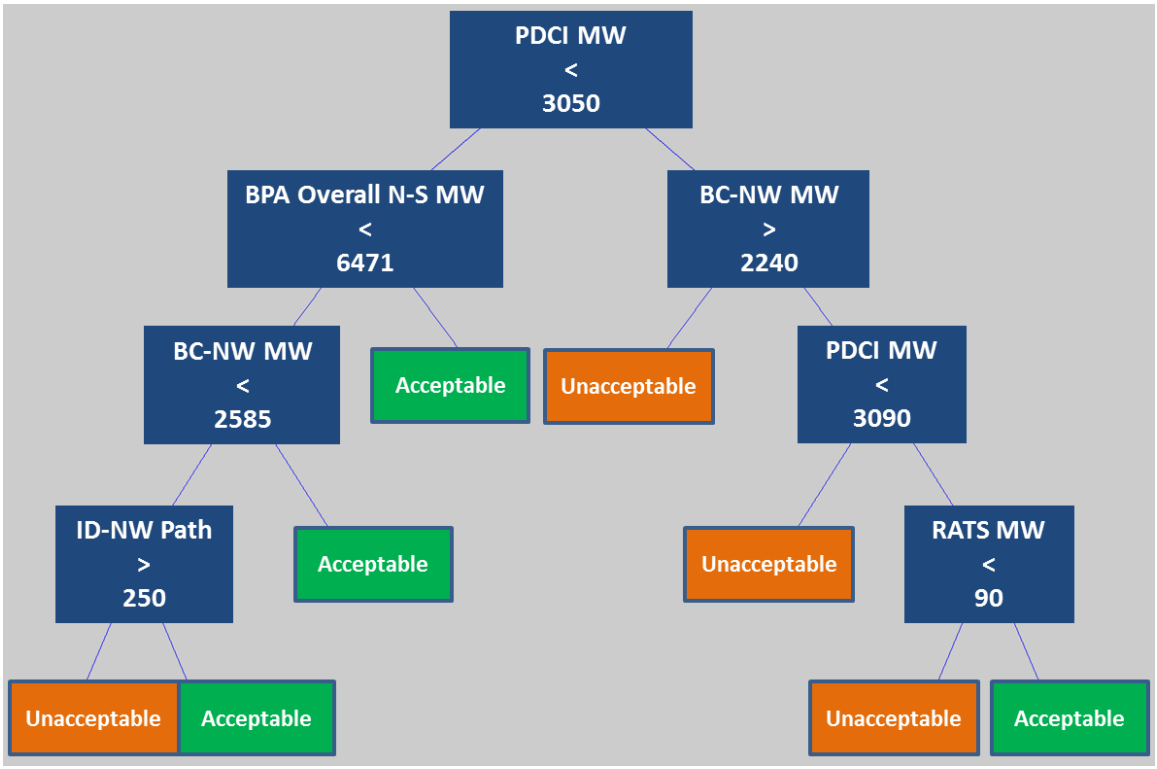

Figure 44. Damping Decision Tree: BPA, Combined, MW Only, Best Fit

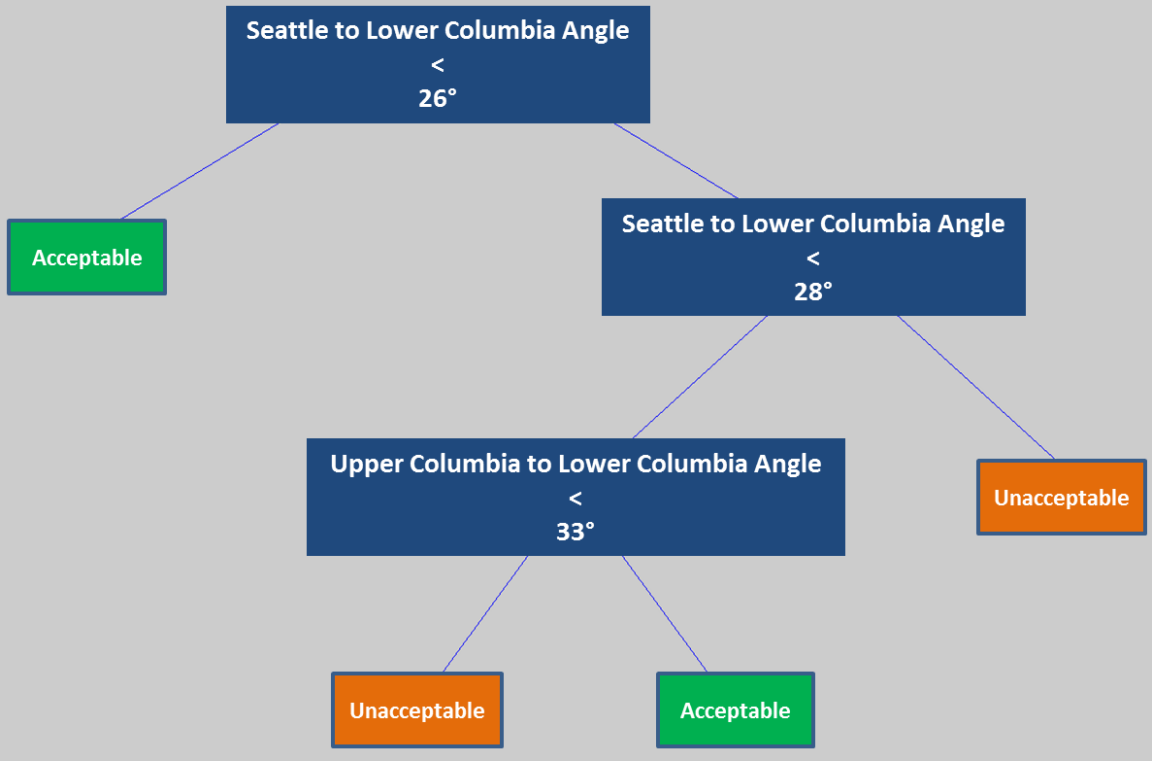

Figure 45. Damping Decision Tree: BPA, Combined, Angle Only, Best Fit

When the measurement set is reduced to the subset directly measurable by BPA PMUs, the results are relatively unchanged. Similar to the full WECC dataset, North-South flows from the Northern Intertie, across BPA, and down to the COI to California provide the best indication of low damping. Since the northern component of the BC-NW intertie is unavailable, that measurement pair is replaced by the angle difference between the Seattle area and Lower Columbia region. In addition, the angle difference from Upper Columbia and Lower Columbia (which is similar in characteristic to the overall BPA N-S stress) is also a critical indicator. The 'ID-NW Path' and 'RATS' MW flows are indicative of the sensitivity to COI as a backup indicator of damping since they reside towards the bottom of the tree structure.

To describe the effectiveness of classification for each tree, classification rate [%] of is measured, as shown in TABLE IX. This measure describes how well the decision tree can predict the expected target variable based on the input parameters for the given study space described. Note that even with a relatively small sample space, the decision trees are generally able to classify the operating conditions with over 90% accuracy for the full trees.

For the WECC dataset, classification changes with respect to selected measurement set and whether Alberta is in service or not. While MW combined with angle or MW solely provides the highest classification with Alberta in, angle or a combination of MW and angle provides the highest classification when Alberta is out. Therefore, the claim can be made that both MW and angle can be utilized for classifying low damping conditions. Another important concept to note is that classification of low damping conditions minimally changes when the dataset is reduced from the full WECC set to the BPA set.

TABLE IX. DECISION TREE CLASSIFICATION RATES

		WECC Data Set			BPA Data Set		
		C	AI	AO	C	AI	AO
MW & Angle	Full Tree	96.43	96.50	100.00	95.54	96.50	100.00
	Best Fit	92.41	95.00	95.83	92.86	92.00	95.83
MW Only	Full Tree	95.98	96.50	95.83	96.43	96.50	95.83
	Best Fit	86.16	96.50	62.50	92.41	89.00	87.50
Angle Only	Full Tree	94.64	98.0	100.00	95.54	96.00	95.83
	Best Fit	91.07	92.0	95.83	88.39	94.50	95.83

*C: Combined Cases, AI: Alberta In Cases, AO: Alberta Out Cases

The 'Mode Meter' pre-contingency system damping is integrated into the input measurement variables and the decision trees are reformulated. As mentioned, the pre-contingency damping is estimated by the oscillation damping following a Chief Joseph braking resistor insertion of 500ms. The combined MW and Angle decision tree does not change from the decision tree created in Figure 43. With both angle and power flows available from the PMUs, the addition of the Mode Meter application does not improve classification and is therefore not used. The updated decision trees for the MW Only and Angle Only datasets are shown in Figure 46 and Figure 47.

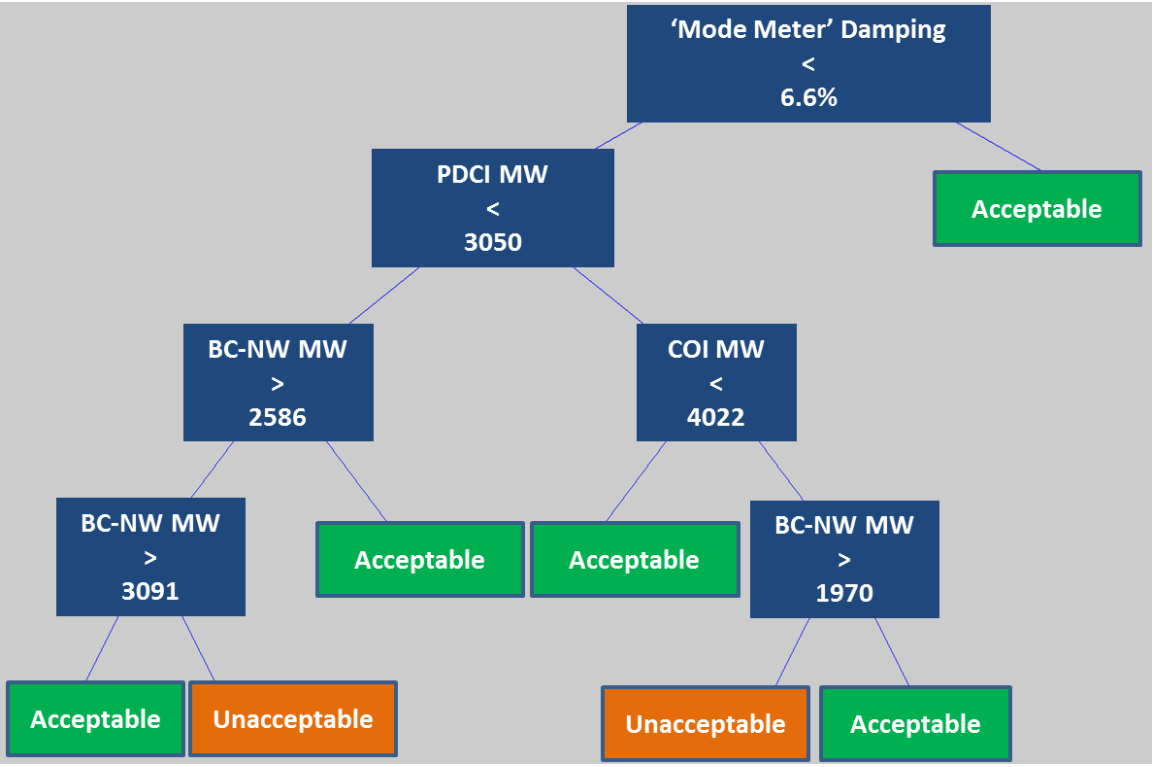

Figure 46. Damping Decision Tree: BPA w/ MM, Combined, MW Only, Best Fit

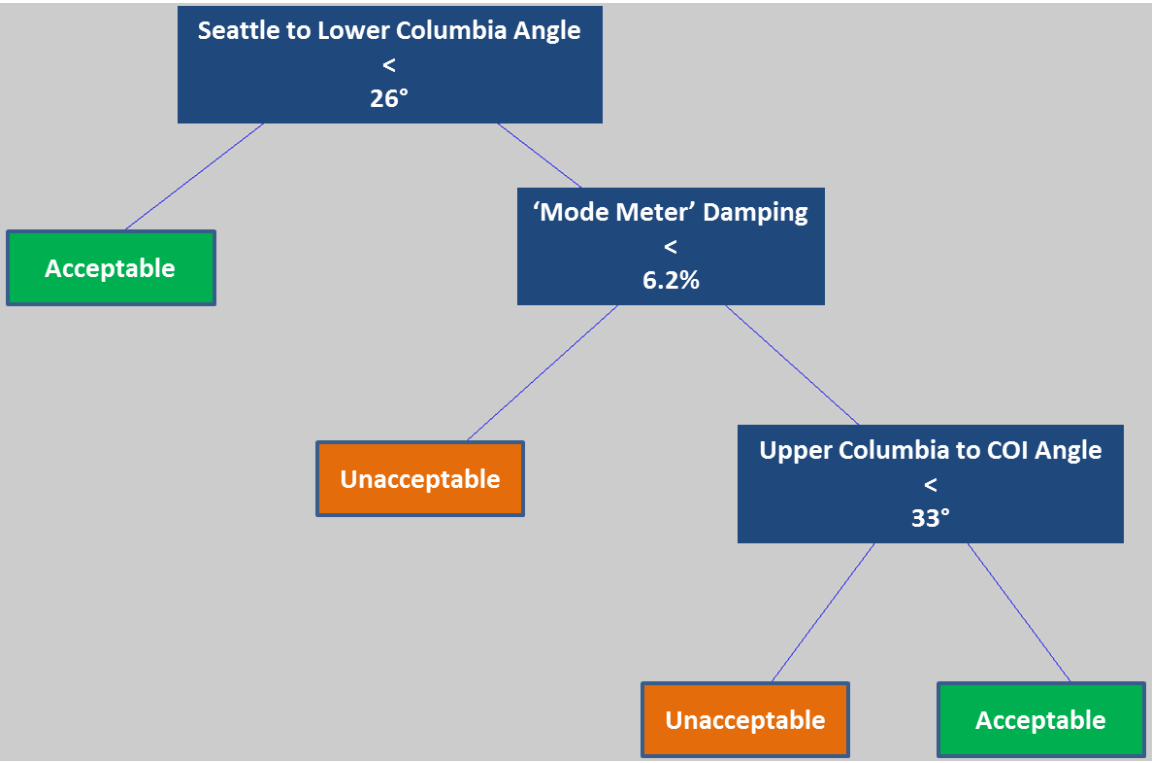

Figure 47. Damping Decision Tree: BPA w/ MM, Combined, Angle Only, Best Fit

When real power quantities are the only available measurements, the 'Mode Meter' steady-state damping is the best indicator of low damping conditions. Steady state damping greater than 6.6% results in acceptable oscillation ringdown for severe contingencies. If steady state damping is less than 6.6%, then the decision tree takes structure similar to the previous tree with no mode meter included. BC-NW and COI flows are the best indicators of low damping when the Mode Meter indicates steady state damping less than 6.6%. For Angle Only measurements, the critical indicator of low damping is still the Seattle-Lower Columbia phase angle difference. Above an angle difference of 26°, the 'Mode Meter' steady state damping and angle difference leading to the COI are the key indicators.

These results indicate that while the mode meter can identify steady-state damping, additional information based on system conditions (MW or angle) may be useful for supplementing this information. Pre-contingency operating conditions used in conjunction with the 'Mode Meter' damping can provide operators with real-time situational awareness of low damping risk. However, the use of decision trees for operator situational awareness is a challenge. Operators and control center engineers are conservative to adopt new technologies due to the high consequence of failure. Therefore, the decision tree results are used to derive potential applications or visualization tools for operators in the control center. Adaptations are discussed in the following section.

3.7.3. Adaptation of Results for Development of Online Tools

The decision tree approach to studying oscillation damping has provided extremely useful information on the key indicators and their respective thresholds for poor damping conditions. In addition, the tree identifies and prioritizes those key indicators. Therefore, converting the decision tree results into more widely accepted tools is fairly straightforward. Although classification rate will decrease, utilities may be accepting of this consequence if the tool is known to be effective in past experience. Examples of tools that are widely adopted and implemented today include basic logic diagrams and online nomograms. Therefore, the goal of this work is to devise a nomogram or logic diagram that fits the results and conclusions obtained thus far.

To explore the individual threshold values for any application, a single split (SS) decision tree is used with a single input variable. This simply gives the optimal threshold for highest classification rate using that one variable. In addition, a visual "best fit" threshold is selected by observing the data w.r.t. its classification and input variable values. TABLE X shows the outcome for a 2.0% damping threshold.

TABLE X. SUMMARY OF DAMPING THRESHOLD RESULTS

Variable	0.5% Limit		1.0% Limit		1.5% Limit		2.0% Limit	
	SS	BF	SS	BF	SS	BF	SS	BF
BC-NW	2962	2600	2586	2600	2241	2500	2241	2200
NOH+SoNV	6493	6100	6143	6100	5769	6100	5769	6000
NOH+RP	4808	4500	4529	4600	4207	4600	4207	4500
NJD	6992	6500	7045	6600	6304	6500	6304	6500
PDCI	3050	3070	3050	3070	3050	3070	3050	3070
COI	4507	4700	4504	4600	4615	4700	4227	4600
SOG	5237	4800	4824	4800	4824	4800	4812	4800

SS: Single Split, BF: Visual Best Fit

Three of the top splitting attributes are chosen for a possible nomogram and plotted in the 3-D plane as shown in Figure 48, Figure 49, and Figure 50. Although the PDCI MW shows up as a good indicator of low damping in the studies, the striated study results make application of this intertie value a challenge. Additionally, the PDCI MW is set based on a schedule and is not expected to correlate well in a broader study space due to its flexibility. The BC-NW MW flows show little capability for linear or piecewise linear classification for a nomogram; the use of BC-NW is also removed from the potential attributes. Although the overall BPA MW flow does not show a strong correlation, it provides the geographic diversity to the measurement set. Figure 50 shows a reasonably good fit to three dimensions of splitting variables. This consists of:

- Angle difference between Seattle area and Lower Columbia
- Overall BPA North-South real power flows
- Flows leading down to California and over to Idaho

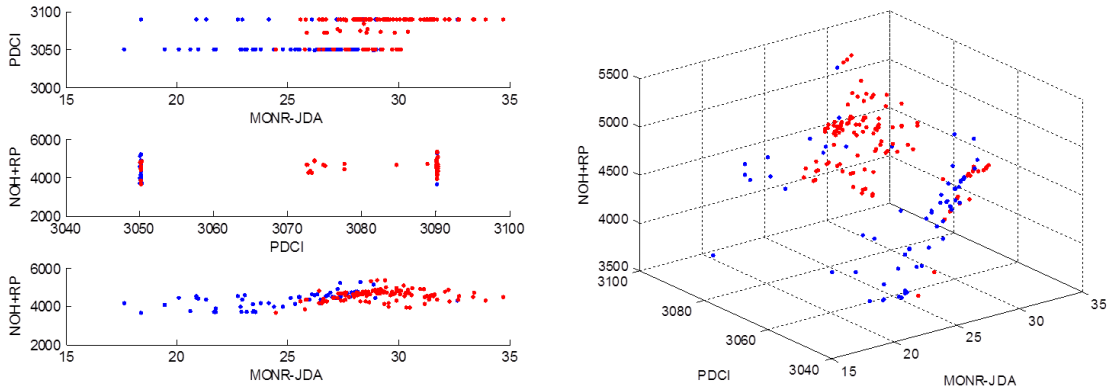

Figure 48. Damping Plots - Option 1

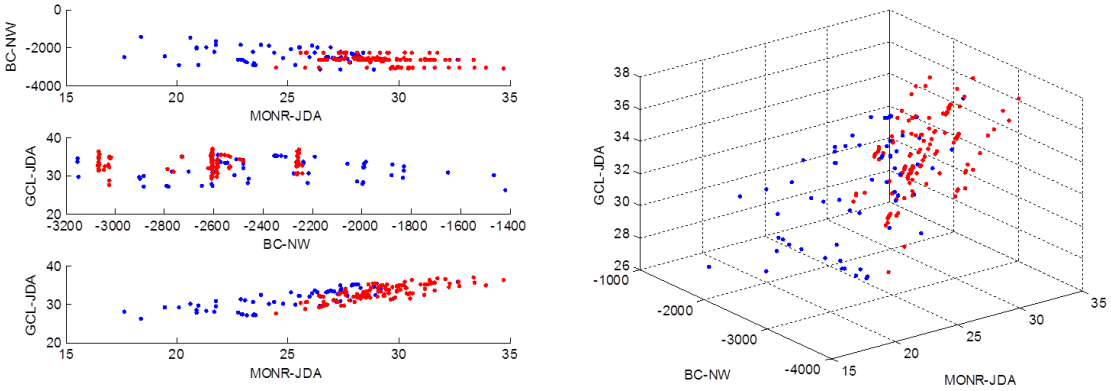

Figure 49. Damping Plots - Option 2

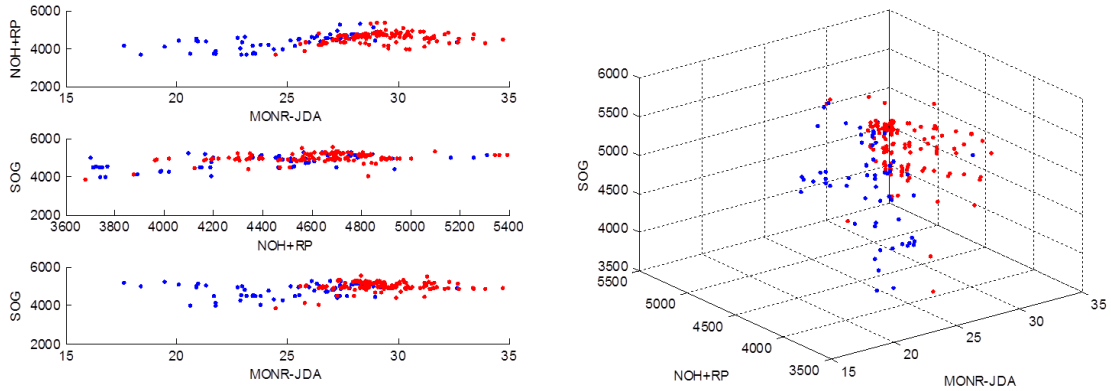

Figure 50. Damping Plots - Option 3

The ‘Mode Meter’ damping input has not been included in the nomograms thus far. If the ‘Mode Meter’ is a required input, the plots in Figure 51 are obtained for the ‘Mode Meter’ plus high priority splitting attributes.

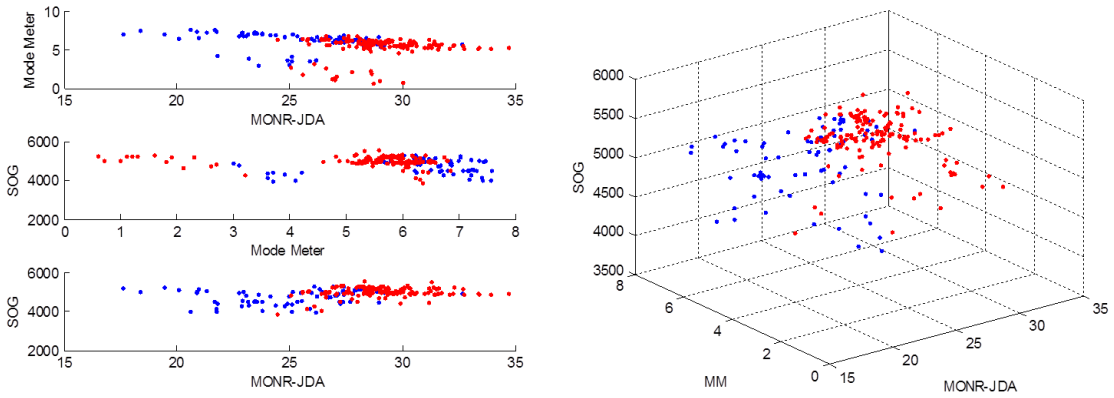

Figure 51. Damping Plots - Option 4

Based on these observations, the nomogram shown in Figure 52 is devised. It provides the operators with a three-dimensional snapshot of critical attributes that impact low damping for severe contingencies. This display could be trended over time in either three-dimensional or multiple two-dimensional spaces to give the operator a historical view of how power system stress is impacting damping. Baselining efforts could improve operator awareness by providing expected damping levels for a given operating condition.

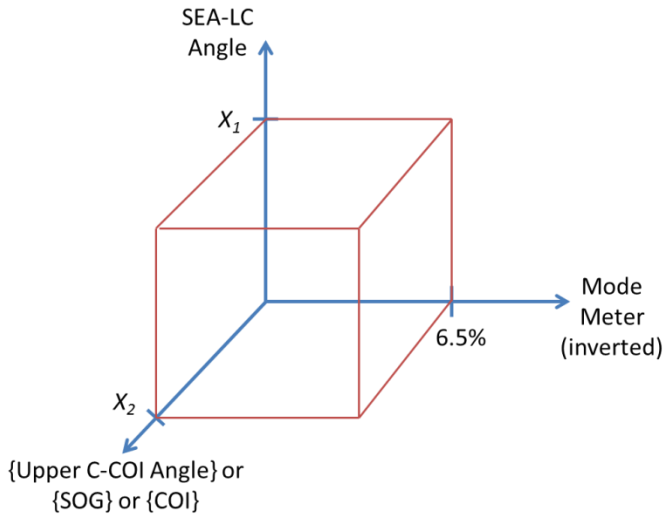

Figure 52. Three-Dimensional Damping Nomogram

An alternative to a nomogram is the application of a logic diagram to alarm or visually display low damping conditions to operators. Based on the information provided and the geographic diversity in the measurements, TABLE XI provides specifications that can be selected based on the offline studies.

TABLE XI. DAMPING LOGIC DIAGRAM SPECIFICATIONS

Input Parameters	Primary Measurement	Secondary Measurement
BPA North Attribute	BC-NW Flow	Seattle-Lower Columbia Angle
BPA Mid Attribute	BPA Overall North-South Flows	Upper C-Lower C Angle
BPA South Attribute	COI or South of Grizzly Flows	Upper C-COI Angle
Mode Meter	Mode Meter Application	
Alberta In Service?	Direct Measurement from SCADA	Oscillation Frequency on COI

The selected attributes shown above provide a fairly robust indication of damping risk in real time. To alarm the operator when damping becomes a concern, the logic diagram shown in Figure 53 may be used.

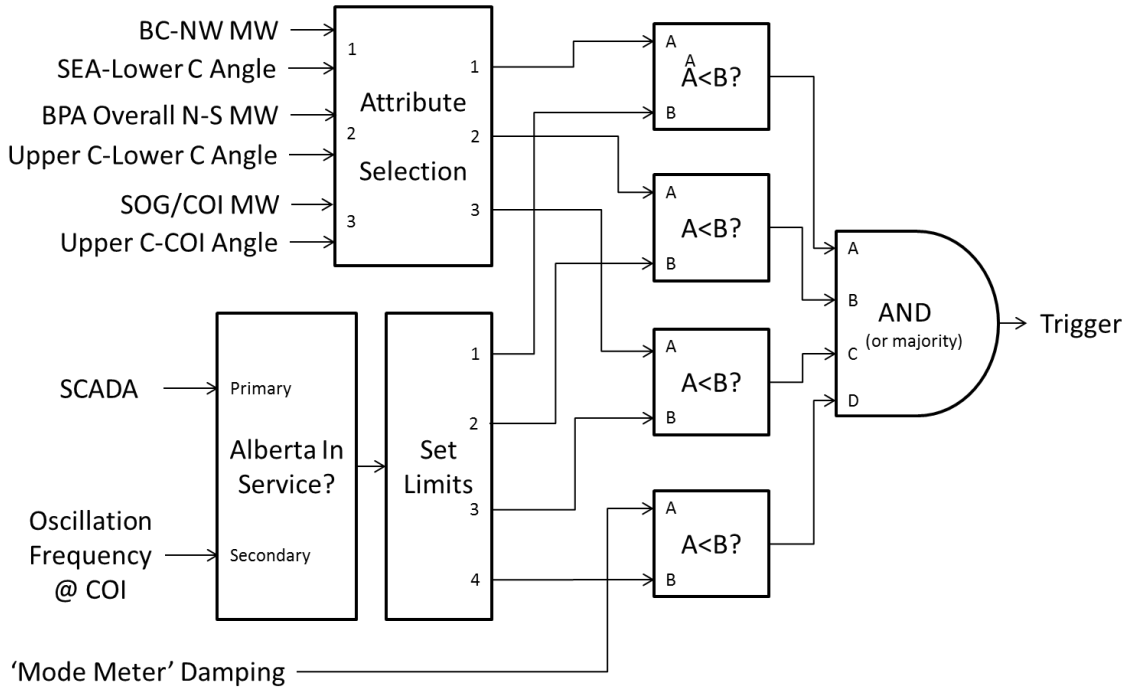

Figure 53. Damping Alarm Logic Diagram

3.7.3. The Need for Responsive Controls

Post-contingency damping is affected by a number of factors other than pre-contingency operating conditions. To illustrate one of the factors influencing system damping to large disturbances, a large disturbance is simulated with varying levels of control action. Special Protection Schemes (SPSs) or Remedial Action Schemes (RAS) are event- or response-driven controls to maintain acceptable transient and post-transient performance. However, actual operation of these controls may vary, misoperate, or fail to operate. An illustrative example of variation in automated controls is shown in Figure 54. A moderately stressed base case with COI flow just below 4400MW is used to show a fairly common operating point; the Pacific Northwest is an exporter of power to California. This example uses a PDCI bipole outage with remedial action schemes. Reactive switching of the FACRI is modeled, along with generation dropping in the Pacific Northwest. The amount of generation dropped is reduced from 2750MW to 0MW. As the figure shows, damping decreases and the amplitude of oscillation increases as the amount of generation dropped is reduced. The system is unable to maintain stability at 200MW generation dropped and below.

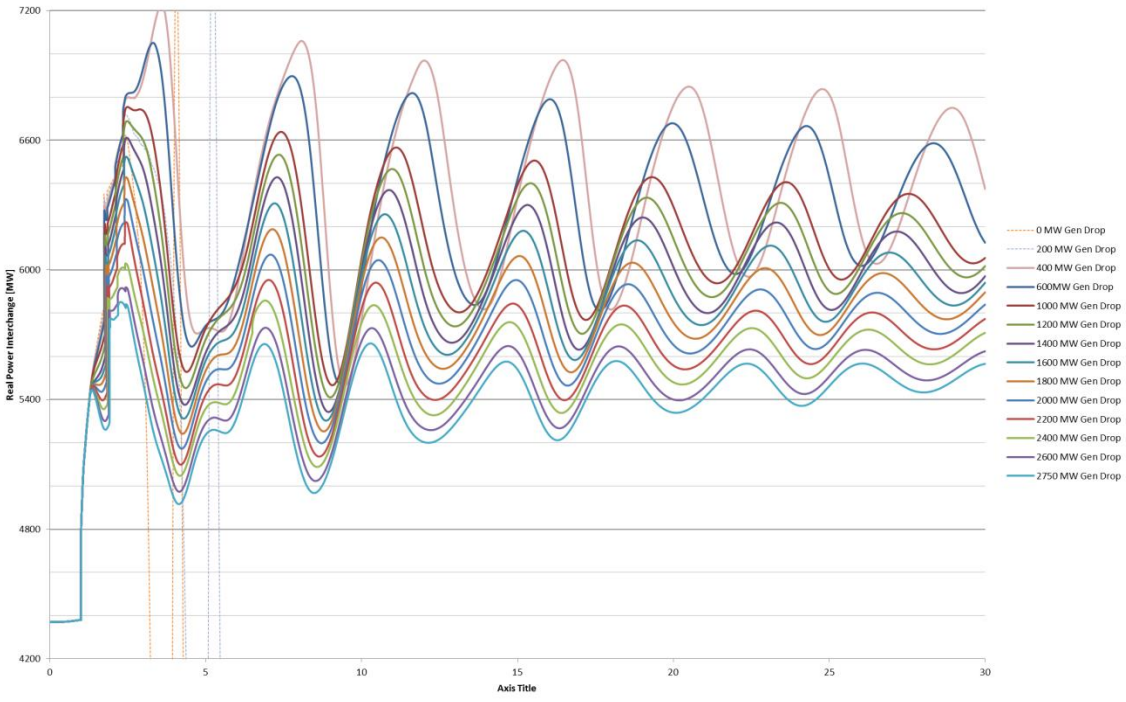

Figure 54. Post-Contingency Control Effects on System Performance

Stability is significantly impacted by post-contingency controls in addition to pre-contingency operating point. The operating point is held consistent in all the cases shown in Figure 54 while the stability of the contingency is changed dramatically. Therefore, in addition to pre-contingency monitoring of system conditions, industry must also focus on "safety net" schemes to mitigate the possibility of failed or insufficient controls. Response-based controls using synchrophasors are discussed in the next chapter.

3.8. Summary of Findings and Conclusions

Adaptation of the disturbance-based probabilistic rms-coherency algorithm has a number of significant benefits for application at the utility level:

1. The disturbance-based probabilistic rms-coherency algorithm is adapted for *selective PMU configuration* into clusters of coherent measurements.
2. The clustering adaptation is *easily implementable into a Transmission Planning* transient stability analysis application.
3. The PMU measurement clusters appear to *match a priori hypotheses* of measurement clustering, and the algorithm provides a technical justification behind these clusters.
4. Classification based on separation of coherency indices allows for *expert opinion* and *engineering judgment* to be applied, making the algorithm more robust and applicable for large power systems.
5. The clusters selected for the BPA WAMS network *overlay with large generation and load hubs*, connected through links or corridors that *align with major paths, flowgates, and interties* with neighboring utilities.
6. The clustering adaptation *can be performed on a large scale*, including Interconnection-wide studies of coherency.
7. The clustering algorithm provides a *technical basis for surrogate measurements* that are coherent to a given degree, when one measurement is unavailable.

The PMU clustering is applied to a methodology for determining phase angle alarming limits or thresholds. The following conclusions regarding phase angles and their respective limits are drawn from the technical work performed:

1. Representative phase angles between each cluster pose a problem of misclassification due to the complexity and uncertainty of operating conditions between the clusters. This method was deemed unacceptable for alarming.
2. Phase angle limits are highly dependent on topology changes within the study corridor. Changes in topology must be reflected in updated limits, similar to updated SOLs.
3. Phase angle limits are not affected significantly for topology changes outside the study corridor. Updated limits are not required for these outages, simplifying the number of outages that must be studied for each corridor.
4. Phase angle limits may be affected by lower voltage line outages in the study corridor. The extent to their impact on phase angle limits depends on transfer direction and utilization. Selection of which lines to include could be based on power transfer distribution factors (PTDFs) or those lines used in the SOL studies.
5. Season has a significant impact on phase angle limits due to the change in overload limits on the transmission lines. When overload limits are changed phase angle limits may also need to be updated to reflect this change. If voltage stability or reactive reserve margin are the limiting elements for security assessment, then altered overload limits may not affect angle limits.

With respect to wide-area angle limits based on damping studies, the following conclusions are drawn:

1. Classification based on damping of system response to studied contingencies is a challenge and may not provide the highest degrees of classification accuracy. However, data mining techniques such as decision trees can identify the critical indicators of low damping conditions in terms of pre-contingency operating conditions and their respective thresholds.
2. The utility industry may be less receptive to data mining solutions in real-time due to their slight obscurity, and may be willing to settle with simplified solutions that utilize less measurements and provide lower classification accuracy. However, the offline studies and results obtained from the data mining techniques can be used for measurement selection and threshold determination of abbreviated solutions.

3. For high stress conditions, power flows from British Columbia through BPA and down to California (North-South flows in the northern parts of WECC) and their respective angles are the strongest indicators of low damping conditions.
4. Damping studies that determine key attributes of low damping and their thresholds can be married with steady-state stability tools for a more comprehensive insight into poorly damped conditions in real-time.

In addition to the conclusions regarding the study methodology, additional benefits of this approach include:

1. A phase angle display and alarming application can serve two purposes: visualize stress at a system-wide level, and provide indication of problematic areas and conditions.
2. A two-pronged approach that incorporates both security limits at a regional basis and stability limits on a large area-based or system-based level is more beneficial.
3. Classification based on security assessment at Path flow levels provides a high degree of classification accuracy, but requires continuous updating and high resolution due to continuously changing conditions and outages.
4. Classification based on damping may have lower classification accuracy, but still provides the operator or engineer with a "last resort" indication of high degrees of stress.
5. Phase angle alarming and indication is not a replacement of real power thresholds or limits, but rather a complement to known operating procedures. Angle may provide levels of "safety" that do not show up solely with MWs. Unexpected outage conditions where real power limits are not studied, failed convergence of a state estimator solution, lack of measurement data for real power flows, and failed SCADA data are all examples where phase angle measurements from a PMU may provide qualitative and quantitative measurement of system conditions in case backup is desired or needed.

Chapter 4. Response-Based Synchrophasor Remedial Action Scheme

The power system is operated and controlled in real-time by system operators of various Control Areas. These operators follow predefined operating procedures such that their internal system conditions are maintained within acceptable limits. The assumption is that each Control Area studies expected conditions, accounting for the effects of contingencies on other areas, to minimize the potential for cascading outages [39]. The Southern California-Arizona outage of 2011 recommended that Control Areas share more data between themselves so that operational studies could better reflect expected system conditions and the effects outages can have on neighboring systems. The blackout report highlighted this issue as a potential cause of the outage [33]. Data sharing may provide increased reliability across an Interconnection, because the studies provide more accurate representation of approaching conditions. Although system operation adheres to standards and operating procedures to mitigate the potential for large-scale outages, real-time automated controls can further improve reliability and integrity of the system for major contingencies.

These types of controls generally fall under the category of a Special Protection Scheme (SPS), or Remedial Action Scheme (RAS) as they are referred to in the west. RAS is defined by NERC as "*an automatic protection system designed to detect abnormal or predetermined system conditions, and take corrective actions other than and/or in addition to the isolation of faulted components to maintain system reliability* [97]." SPS or RAS overlay conventional protection systems to provide wide-area controls for adverse conditions or large disturbances. RAS actions often take major actions such as "changes in demand, generation (MW and MVAr), or system configuration to maintain system stability, acceptable voltage, or power flows [97]." These schemes are differentiated from conventional protection systems that isolate faulted equipment such as distance protection, overcurrent protection, and out-of-step relaying. In addition, an SPS is differentiated from System Integrity Protection Schemes (SIPS), which defined as "*a category of protection schemes designed to protect the integrity of the power system from system instability, to maintain overall system connectivity, and/or avoid serious equipment damage during major events* [98]." SPS or RAS are included within the definition of SIPS, but SIPS may also include other schemes such as overvoltage or underfrequency load shedding. SIPS may also be referred to as "safety nets", which provide "countermeasures to slow and/or

stop cascading outages caused by extreme contingencies [98]." The most significant differentiation between safety nets and RAS is the necessity for RAS to operate when expected. RAS may be used in a number of situations such as permanent RAS to alleviate system conditions following significant studied outages or as a bridge solution to delay the necessity for more transmission infrastructure. During certain operating conditions, RAS may be "armed" by the operator so that the current operating point meets the reliability criteria for normal and emergency conditions. Without the RAS, disturbances could cause overload conditions that would violate the standards, and the system operating point must be changed by reducing schedules or redispatching generation. Safety nets, on the other hand, are generally used to remediate system conditions following extreme events such as loss of two or more Bulk Electric System (BES) elements [39]. In other words, the safety nets may try to provide additional support for unexpected extreme events, in an attempt to provide additional reliability support and help maintain system stability.

RAS may generally be considered as either event-driven or response-based. Event-driven RAS is based on predetermined events including line or generation outages that cause corrective actions to be taken. An example of this type of RAS is conventional Line Loss Logic (LLL), where detection of generation dropping during heavy export conditions. The benefit of this RAS is its independence with other protection schemes; events or protection schemes that are not directly affecting the LLL-enabled line will not cause the RAS to falsely operate. The drawback of event-driven RAS is the incapability of taking corrective action in response to disturbances. This type of RAS is "inward-looking" and focuses primarily on outages or events within the observable system boundaries. Response-based RAS is the converse of event-driven RAS in that it detects system conditions that may cause unacceptable operation. The responsive thresholds for these algorithms are based on offline system studies of expected operation. Unlike the event-driven RAS, response-based RAS is more reactive to changing system conditions but also more susceptive for false operations. The 2011 Southwest California-Arizona blackout was exacerbated by response-based RAS operated when it should not have, leading to the final response-based SONGS Separation Scheme operating and severing the system from the rest of WECC [2].

A consequent recommendation from the outage is the need to coordinate remedial action schemes to ensure that misoperations are minimized by determining the effects that RAS have on each other. Studying the effects of RAS on each other is not a trivial task. It requires a large database of operating cases and expected contingencies, but also a contributory RAS algorithm that can compare operations of each scheme. However, this analysis can be simplified by focusing solely on the response-based schemes rather than the independent event-driven schemes. The Bonneville Power Administration (BPA) RAS schemes are predominantly event-driven LLL that do not interact with other schemes. The reason for this explanation is that this research focuses on converting an event-driven existing RAS scheme into a response-based RAS using wide-area synchrophasor measurements. It is imperative that the responsive algorithm is configured to only operate for severe conditions, and that (mis)operation has no negative consequences.

The response-based schemes focus on prevailing system conditions. Many research efforts assume that all data is available, as a gross oversimplification. In reality, each Balancing Authority Area has observability of its own measurements and possibly critical measurement of neighboring utilities and generating stations. Synchrophasors allows for greater visibility through sharing of high resolution, fast data. However, inter-utility sharing of the data is vastly immature in terms of implementation and application, and data security and trusting the incoming measurements is a justified concern that could prohibit real-time decision making using the data. To clarify, this work assumes that the measurements observable by a BAA are “internal” while those that cannot are “external”. For example, breaker status of a major 500kV line within the BAA footprint is directly measurable and therefore internal. Voltage profile, equipment status, reactive reserve margin, generating unit statuses, etc., can be internal if they fall within the measureable boundary of the BAA. However, voltage and current measurements, equipment statuses, etc., outside the BAA footprint are not directly measurable and therefore external.

Real-time detection of severe events within an Interconnection provides a number of benefits, including:

1. Proactive remedial response to minimize negative impacts such as depressed system voltages or increased reactive power flows.
2. Minimization of real and reactive losses.
3. Mitigation of cascading events due to reduced likelihood of overloading.
4. Alleviation of dynamic voltage support devices by increased static support.

The concern that arises is how to detect disturbances external to a BAA footprint without requiring additional measurement information. In addition, setting thresholds for changing system conditions must account for the interaction between dependability and security. A response-based remedial action should be dependable, meaning it operates for conditions in which it is designed to operate for. Its design should also be secure, meaning it does not operate falsely for conditions it is not designed to operate for [99].

The following sections describe a response-based algorithm utilizing synchrophasor measurements that detects large disturbances. In addition, a reactive switching control action is studied for alleviating transient and post-transient performance following a disturbance.

4.1. Impacts of External Events on Internal System Conditions

Chapter 2 addresses the issue of Frequency Response of an Interconnection, and the phenomena behind real power mismatch between generation and load. Following a large loss of generation or load, frequency will deviate due to the real power imbalance. Generation will respond according to the direction of frequency movement in an attempt to rebalance the system. Depending on the location and composition of that generation, the Frequency Response can have very different effects on system conditions. The Frequency Response imbalance in the WECC between the north and south generators causes significant surges in power through major WECC transmission paths. Similarly, relatively large transmission outages such as N-2 common corridor or common tower contingencies can cause voltage collapse or transient stability problems throughout an Interconnection. This section demonstrates the need for detecting external events using an illustrative example of actual PMU data from the BPA WAMS.

This example is the same event used in Section 2.3. Figure 13 from that section shows the frequency deviation for a loss of generation in the southern part of WECC. During that time of year, the Pacific Northwest and Canada is rich in generation due to spring runoff from the myriad hydroelectric projects throughout the Columbia River basin. A relatively large portion of WECC generation exists in the north during this time, especially when the high water conditions are matched with high wind penetration in Washington and Oregon. Exports from the BPA control area into California through the California-Oregon Intertie (COI) are only about 3300MW prior to the event, as shown in Figure 55. Although the system is not heavily stressed in terms of real power transfer to California, the impact of a loss of generation causes fairly substantial pickup on the COI. Figure 56 shows the same event with better resolution at the time of the disturbance. As the figure shows, the first swing pickup and the longer timeframe governor response are approximately 700MW. This increase in power transfer accounts for about half the lost generation, meaning that half the Frequency Response for this event comes from north of the COI.

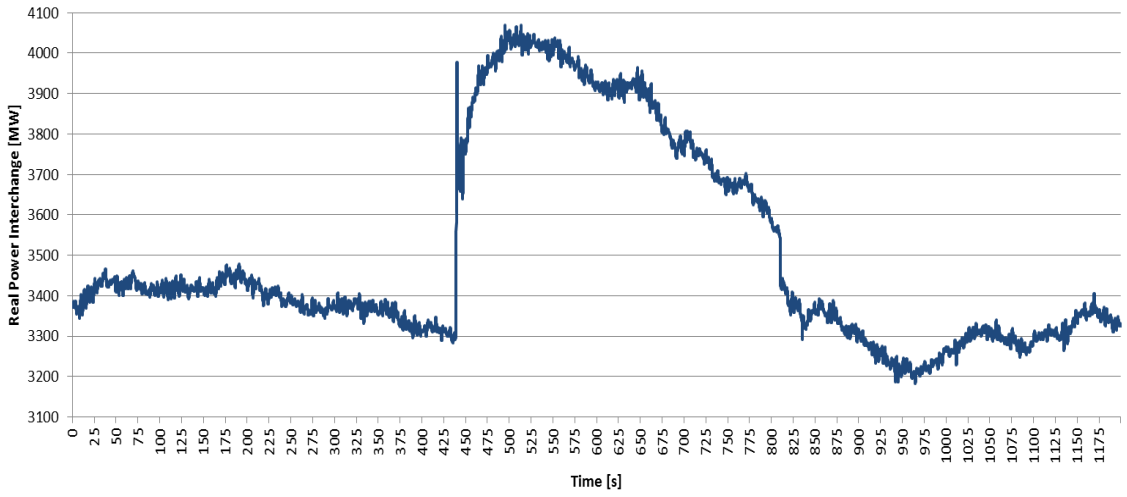

Figure 55. COI Pickup for Loss of Generation in South (Full Event)

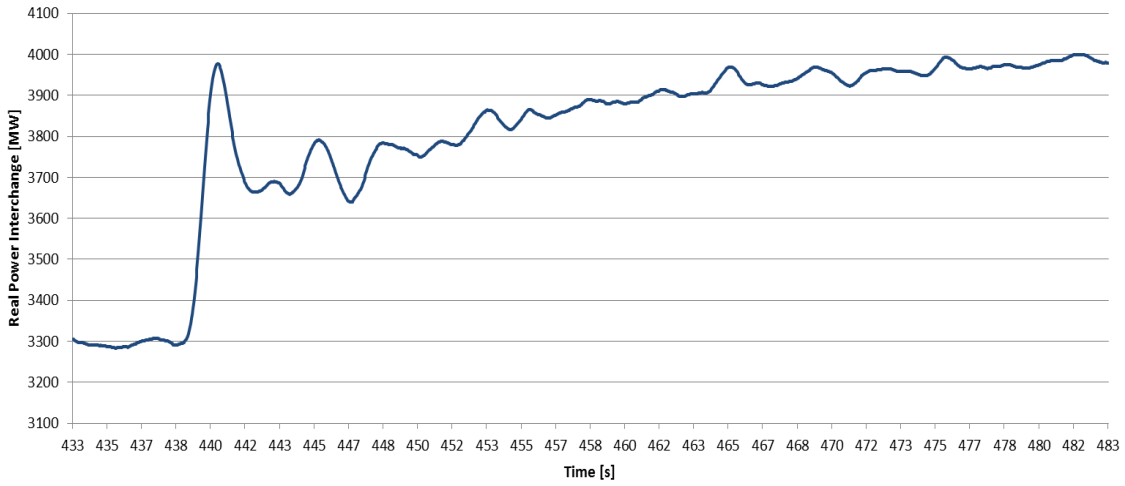

Figure 56. COI Pickup at Disturbance Time

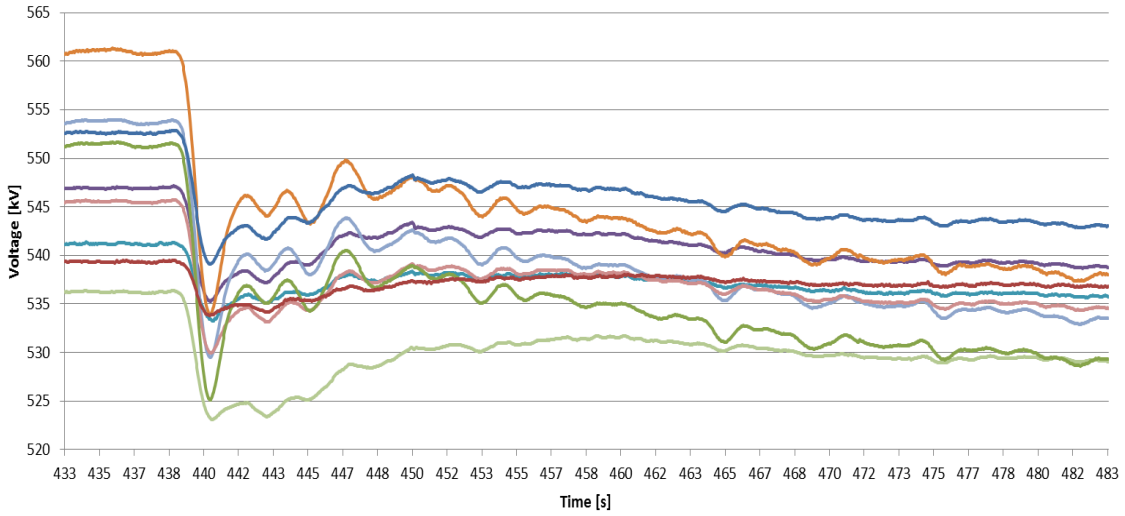

Figure 57. Voltage Depression for Loss of Generation in South

Frequency Response for an Interconnection improves stability because the available generation is able to account for a loss of load or generation and reinstate nominal frequency. The drawback of Frequency Response for this scenario is the possibility for degraded system conditions at the locations of greatest response. Figure 57 shows voltage levels for major 500kV substations across the BPA footprint. The figure illustrates how the response of generation and increase of path transfers from across the BPA BAA puts a noticeable stress on the system. Voltages drop from their scheduled levels down to levels outside the acceptable scheduled ranges. Although the decline falls within acceptable standards as defined by NERC and WECC for this type of contingency, corrective action

can provide the benefits discussed above such as increased capability of dynamic reactive support, reduced losses, and reduced likelihood of cascading outages due to voltage collapse.

This illustrative example uses a severe N-1 contingency, which is about one-half the size of the most severe credible contingency. There is always the rather likely possibility that system conditions will be more stressed and the contingency could be substantially worse. This is highlighted in detail later in this chapter, using PMU data for an extreme N-3 event that occurred in WECC. Regardless, this less severe example provides conceptual understanding of what the response-based synchrophasor RAS can prevent. Let us explore some of the existing control actions for BPA that impact WECC-wide system stability and security.

4.2. Reactive Insert Control Actions

As discussed in Section 2.6, there are a number of benefits and also a necessity for having static reactive support capability on high voltage transmission systems. BPA currently utilizes two major RAS schemes for reactive support, including shunt capacitor and reactor switching and series capacitor switching for post-contingency action. This section describes the concepts behind these reactive support schemes.

One of the most critical control actions in terms of system stability and increased transfers on the COI is the Fast AC Reactive Insert (FACRI). This scheme provides reactive support on the northern terminals of the COI through shunt and series compensation. When voltage drops below predefined thresholds, a timer is initiated. If the timer exceeds a delay limit, then the FACRI scheme is triggered. The voltage bands set for this scheme are substantially lower than acceptable steady state operating voltages, and therefore will only trigger for depressed voltages caused by a disturbance. Usually this is instigated by loss of generation or transmission line outage. A shunt switching algorithm intelligently trips shunt reactors and inserts shunt capacitors based on a priority order. As expected, shunt reactors are removed from service prior to capacitor insertion. The magnitude of the voltage drop determines the time delay before reactive elements are switched. Moderate Undervoltage Level 1 (FACRI-UVL1) conditions have a longer delay

than more severe Undervoltage Level 2 (FACRI-UVL2) conditions. In addition, series capacitors are inserted upon acknowledgement of the trigger signal to reduce the impedance between the generation hubs in the Pacific Northwest and the terminals of the COI such that power transfer can be increased rapidly. The series component improves angular stability by reducing impedance, while the shunt component provides the necessary voltage support to accommodate the increased transfers. FACRI is a novel RAS scheme that has attested to the benefits of coordinated and controlled response-based RAS.

Another important post-contingency RAS scheme used by BPA is the Voltage Stability Reactive Insert (VSRI), which is triggered by independent Line Loss Logic (LLL) signals across the system. Line Loss Logic is a common BPA RAS, in which detection of a line outage condition keys transfer trip signals to be sent to a centralized RAS controller, commonly over digital microwave communications. The LLL signal is not sent until the line is determined to be out of service at the remote location; most internal 500kV transmission lines are capable of triggering the VSRI. Once the AC RAS controller picks up a transfer trip signal, the logic determines if 1) the VSRI is armed by the operator, and 2) the LLL input has the capability of triggering the algorithm. If the VSRI output is enabled, a control signal is sent to shunt reactive support devices across the system; a handful of substations are equipped with VSRI-controllable shunt devices.

Enabling the VSRI output signal to the remote locations does not ensure that reactive devices will be switched. The concept of the VSRI is to provide static reactive support following a contingency only if the support is warranted. Each location is equipped with local voltage sensors that determine if the voltage is low enough such that the VSRI-enabled capacitors and reactors should be switched. The locations are controlled with either a control relay or programmable logic controller (PLC) for local voltage monitoring and switching selection. Both types of control schemes have the capability of simultaneous or sequential switching based on the magnitude of the voltage. Severely low voltage levels enable the Undervoltage Level 2 (VSRI-UVL2) to insert or remove multiple reactive devices simultaneously. Moderate voltage depression enables the Undervoltage Level 1 (UVL1) to insert or remove devices with time-delayed sequential priority.

Automatic Voltage Control (AVC) schemes are local voltage supervision controls for shunt capacitors and reactors, which operate as a last resort for control when voltages exceed uncharacteristic levels. AVCs across the system act as local voltage controllers to help the operator maintain acceptable voltage profile system-wide. The voltage settings for each local shunt device differ slightly based on the expected voltage schedule at that location; however, the settings are generally ± 30kV from the scheduled voltage, with time delays between 5-10 seconds of sustained high or low voltage. This is the simplest form of voltage control and provides reactive support for problems such as extremely heavy or light loading, or delayed voltage recovery after a fault is cleared. The time durations associated with these controls are not meant to help during or immediately after a severe disturbance.

The FACRI and VSRI schemes are designed to work interactively with each other and the Automatic Voltage Controls (AVCs) such that their operation does not conflict with each other. For example, the AVC limits are set well above and below the other voltage control limits and require sustained voltage levels. The FACRI voltage limits are set at the lowest levels such that they are only triggered for severe events. Similarly, the time delays associated with the FACRI are the shortest, so it generally will operate before the other schemes. In addition, the VSRI is event-driven so the set points are set closest to the scheduled voltage because an event has already been detected by LLL. Each scheme is configured such that it will not operate prior to a fault being cleared; the system has sufficient time for natural voltage recovery following a fault before control action is taken. Figure 58 shows a diagram of the voltage control level interaction.

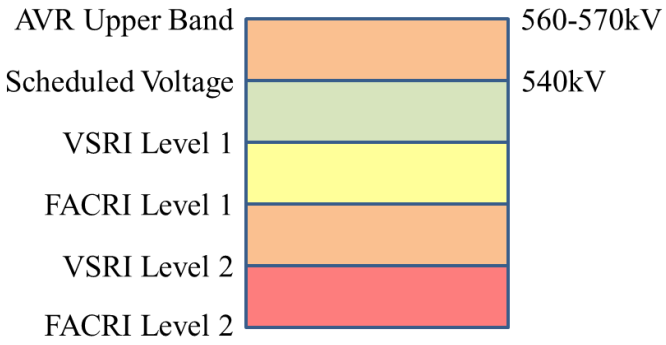

Figure 58. Voltage Control Scheme Interaction

As mentioned, the VSRI scheme is event-driven, and triggered by internal LLL signals from monitored major 500kV transmission lines. The goal is to expand this concept using a response-based scheme such that it can be triggered for external events as well. Therefore, a simple yet effective solution for detecting events external to the BPA system is required. A set of algorithms for RAS logic are presented in the following section to address this problem.

4.3. Response-Based Remedial Action Scheme

Large contingencies throughout the Western Interconnection are noticeable through many venues: nodal measurements such as frequency and voltage, or branch measurements such as line flows. Generation or load loss results in frequency deviation from nominal. Forced transmission outages may result in voltage depression or increased loading. However, system operating conditions may be degraded without the need for control actions taken. This research presents a set of remedial action scheme algorithms that monitor critical variables for rapidly changing system conditions. Unlike conventional event-driven RAS, these schemes use synchrophasor data to responsively take action when detected.

4.3.1. Intertie Rate-of-Change Algorithm

System operators are generally concerned with maintaining scheduled interchanges, maintaining voltage profile, and monitoring system frequency [76]. Therefore, it intuitively makes sense that response-based control schemes could also take advantage of these quantities. The algorithm presented in this section focuses on monitoring a critical intertie for drastic changes in power flow. Interties flows between BAAs are generally scheduled hourly, and operators attempt to maintain these flows at the scheduled quantity. A new schedule is set each hour and the system gradually adjusts to the new schedules being entered, starting 15 minutes prior to the top of the hour. Movement of the system to these changes is relatively slow compared to disturbances, and should not cause any response-based control scheme to operate. However, operator error is possible and could cause the system to begin moving in a direction towards insecurity without immediate notification. For example, an “INC” command on the power order of a DC intertie to

increase the real power transfer could be entered incorrectly and cause the path flows to increase substantially. This is a rather slow-moving problem that should also be considered. Therefore, it is important to consider not only the magnitude of quantities, but also their rate-of-change over time.

Let us consider an intertie, *I*, consisting of *n* number of transmission lines. The real power flow, P_I, of the intertie is

$$P_I = \sum_{i=1}^{n} P_i \tag{4.1}$$

In a simplified situation, system state will be static, meaning

$$\frac{dP_I}{dt_{ss}} = 0\,, \tag{4.2}$$

because the system is stationary and frequency is held constant. Unfortunately, the system is never in an ideal steady state so (4.2) can be generalized to

$$\frac{dP_I}{dt_{ss}} \approx 0 \tag{4.3}$$

for pseudo-steady state conditions. When intertie real power transfer reduces, area generation exceeds load on one or the other end of the intertie. From the exporting area's perspective, this occurrence is due to loss of load in the neighboring area or loss of generation in its own area, and results in

$$\frac{dP_I}{dt} < 0 \tag{4.4}$$

Conversely, intertie real power pickup generally refers to an increase of external load or internal generation, causing

$$\frac{dP_I}{dt} > 0\,. \tag{4.5}$$

The magnitude of this rate-of-change is dependent on the severity of the event, the topology of the system, and the path transfers or system stress patterns. Although the concept presented above is almost trivial, study and application of this concept is not a simple task. Comprehensive transient studies must be performed to understand system response to disturbances under an array of expected system conditions and contingencies.

Line outages cause a substantial instantaneous derivative in real power flow due to their impact on power transfer. Figure 59 shows response for a line outage compared with a generation outage. In terms of magnitude, the line outage has a more significant effect on transfers because the outage occurs on the intertie being measured. Also, the generation loss is electrically and geographically far from the intertie measurements. Regardless, notice the rate-of-change of the responses upon their respective contingencies occurring. The real power drops very quickly for the line outage compared with the relatively slow increase in transfers from the generation outage. A detection algorithm is not intended to trigger during fault conditions or during the event that causes the line outage, but is intended to operate immediately after to provide transient and post-transient support. Therefore, a time delay or duration must be included to restrain action during faults to allow for natural system recovery.

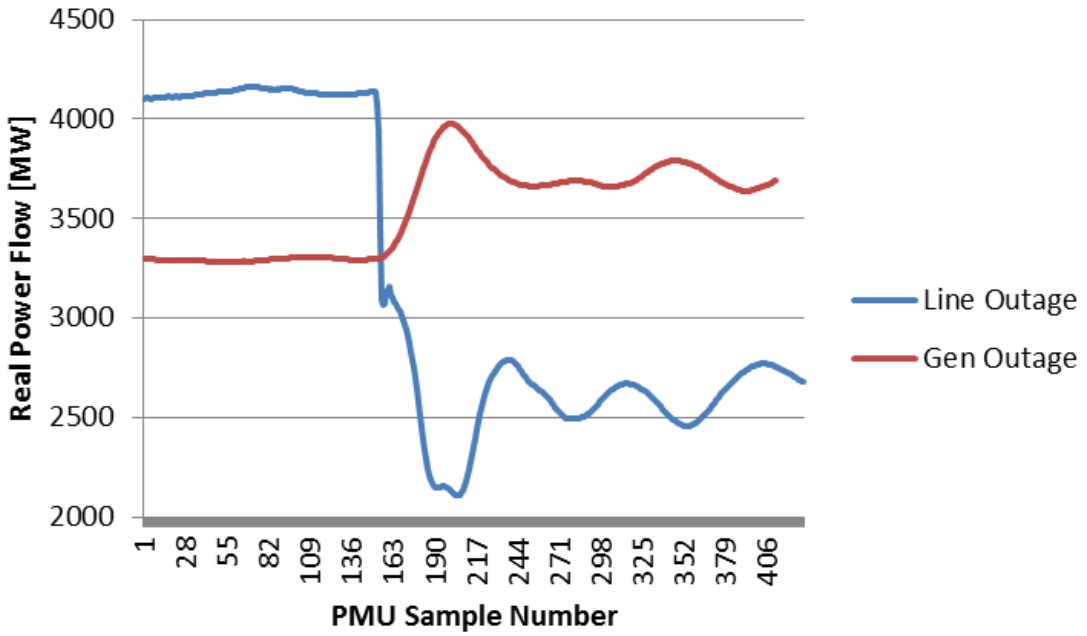

Figure 59. Intertie Response for Generation Outage vs. Line Outage

There are two design variables for the rate-of-change algorithm for intertie real power: rate-of-change magnitude and time duration. Let T be the rate-of-change magnitude threshold for real power across an intertie I, P_I be the total real power transfer across n transmission lines that compose the intertie, m be the number of synchrophasor data frames at reporting rate R corresponding to designed time delay D, and i be the most recent synchrophasor measurement. The rate-of-change calculation can be formulated as

$$\frac{dP_I}{dt} = \frac{d}{dt}\left(\sum_{i=1}^{n} P_i\right) \tag{4.6}$$

$$S := \frac{dP_I}{dt} > T \tag{4.7}$$

$$V := \sum_{i-m}^{i} S > \frac{D}{R} \tag{4.8}$$

S is a Boolean value representing the instantaneous rate-of-change of real power exceeding the magnitude threshold T. Trigger variable V operates when the threshold has been exceeded for a sufficient number of data points, defined by a duration D/R. As the equations show, this form of algorithm requires consecutive samples exceeding the threshold for a given time duration. However, it is advantageous to operate on the side of dependability by allowing variability in the samples. For example, higher frequency oscillations could cause $dP(t)/dt$ to oscillate around the threshold value, resulting in the algorithm resetting numerous times. To account for variability, a sliding window effect could be implemented such that a given number of samples within the window must exceed the threshold. If n_w is the sliding window length in terms of samples and X_p is the required percentage of positive triggers, then the algorithm can be formulated as

$$V := \frac{\sum_{i-m}^{i} S}{n_w} > X_p \tag{4.9}$$

Let us first explore some historical events using PMU data from the BPA WAMS. In 2010, an unexpected outage forced 1300MW of generation offline in the southern part of WECC. As described above, real power transfer on the COI accounts for approximately

half the generation loss. The increased COI real power transfer, or positive rate-of-change, corresponds to higher levels of stress on the BPA system. Figure 60 shows real power flow on the COI (blue) and its instantaneous rate-of-change (red) following the large N-1 contingency. As Figure 60 shows, there are two major events where a significant rate-of-change of intertie real power flow occurs. From the real power response, it is obvious that the first event is due to the loss of generation and consequent oscillation ringdown. The rate-of-change response experiences an oscillating behavior over the course of 10-15 seconds. The second event is slightly less expected, and can be classified as a "glitch" because it does not appear to be related to a large disturbance. It may, however, be due to switching on the transmission system or tripping of generation and/or load from the large contingency. As the real power response shows, the "glitches" have essentially no noticeable effect on the magnitude of flows, indicating that these switching events are most likely far from the intertie. Both the large N-1 contingency and the lesser switching events must be analyzed with greater resolution to explore their effects on the intertie rate-of-change algorithm.

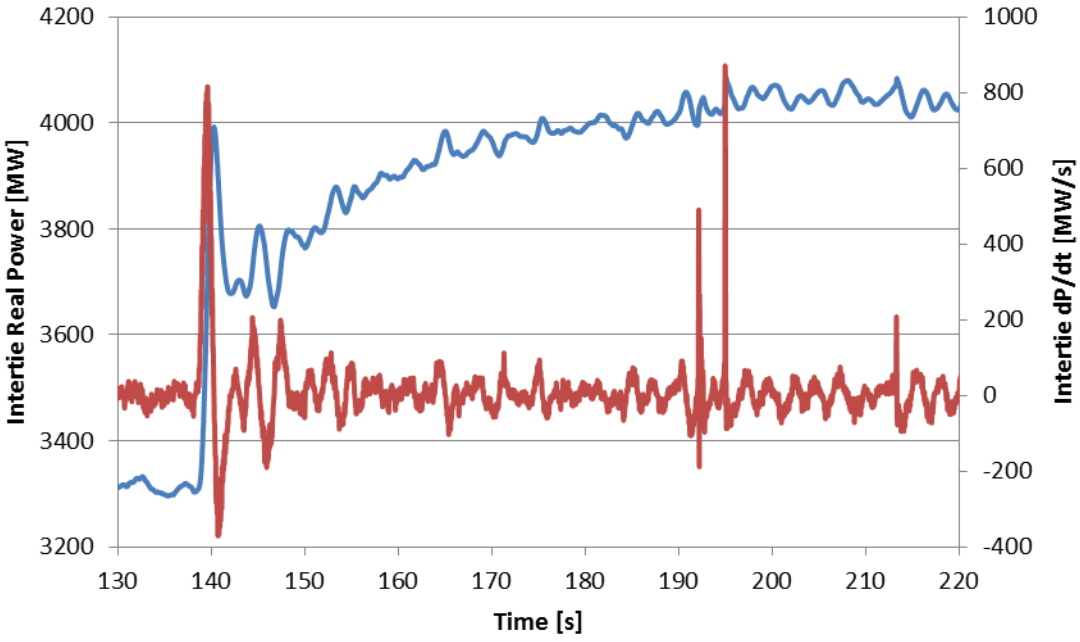

Figure 60. COI Real Power Response to N-1 Contingency and Switching

Figure 61 and Figure 62 show the two distinct events in greater resolution; COI real power and its rate-of-change are shown in blue and red, respectively. The rate-of-change

response in the first event due to the loss of generation exhibits oscillatory behavior with relatively extended duration. The second event has a similar magnitude but significantly less duration. In Figure 61, the rate-of-change first swing reaches approximately 800MW/s and decreases to oscillations with peaks of about 200MW/s. Table XII shows the range of *dP/dt* values and the longest duration each is exceeded. These results can aid in setting baseline the magnitude and time duration thresholds. Although there are myriad thresholds that can be selected, the 500MW/s magnitude threshold with a 0.50 second duration threshold are selected based on this contingency. Analyzing Figure 62 and Table XII in more detail, it is noted that the duration of exceeding any noticeable rate-of-change amplitude is relatively short. "Glitches" of this nature due to switching or tripping of system elements do not have a sustained effect on real power transfer on the COI. Comparing these observations with the threshold values selected, the algorithm would not trigger for these events due to the duration requirement of 0.50 seconds.

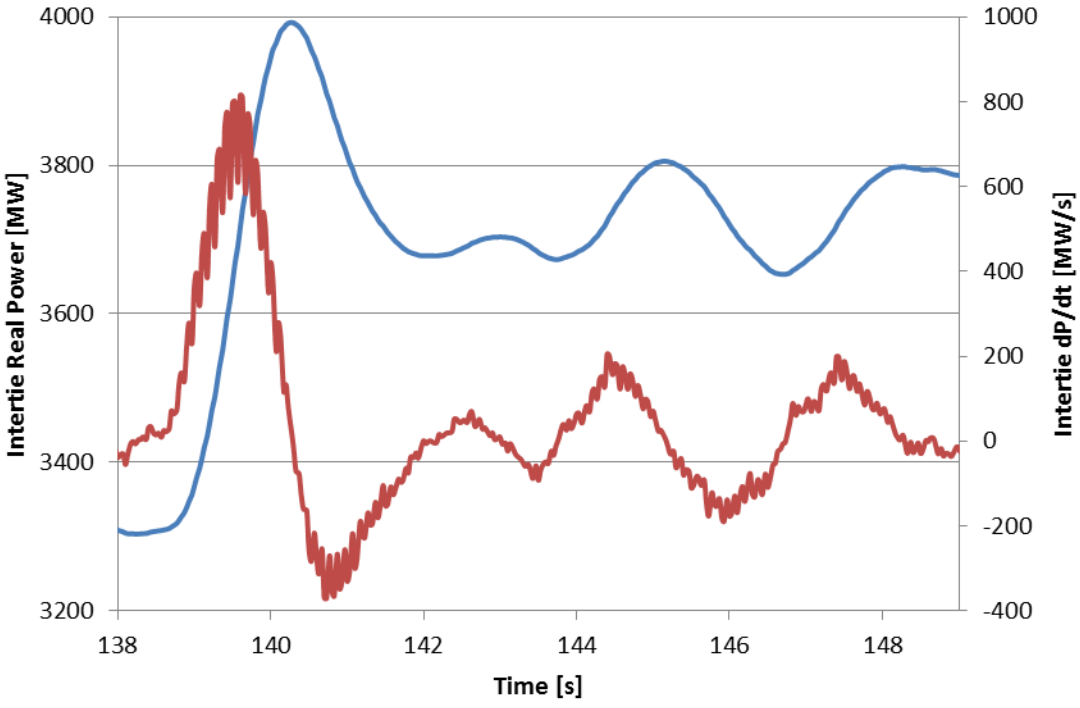

Figure 61. COI Real Power Response to Generation Loss

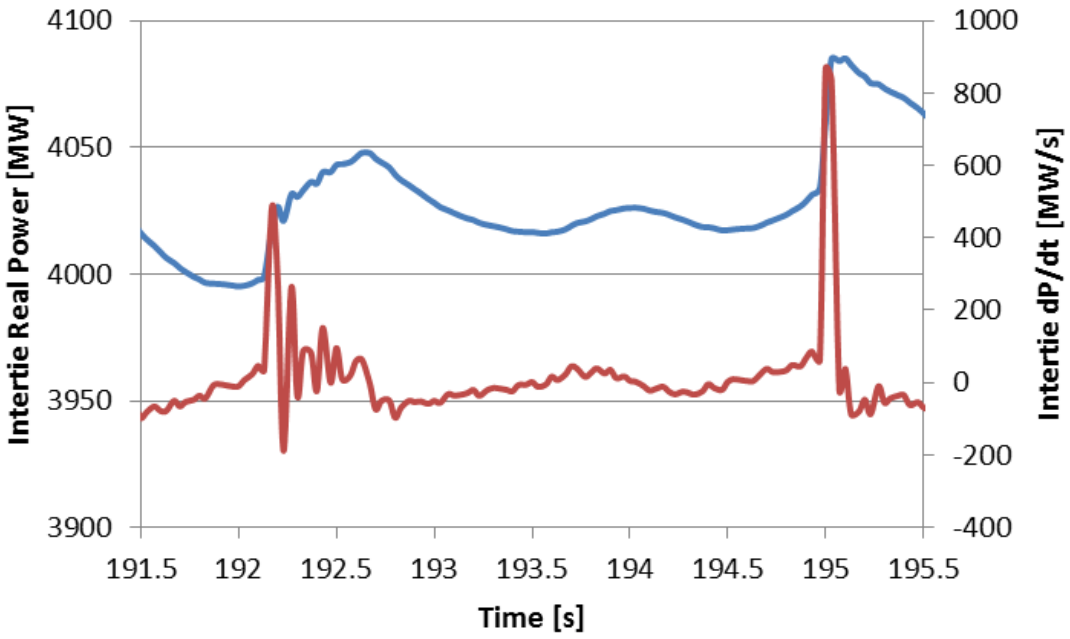

Figure 62. COI Real Power Response to Switching

TABLE XII. MAGNITUDE AND DURATION EXCEEDED FOR N-1 GENERATION LOSS

Magnitude [MW/s]	Event 1 Duration Exceeded [s]	Event 2 Duration Exceeded [s]
1000	0.0	0.0
800	0.066	0.066
600	0.170	0.066
500	0.570	0.066
400	0.770	0.066
300	1.070	0.066
250	1.070	0.066
200	1.270	0.066

As mentioned above, a major concern is preemptive operation of a response-based control schemes due to faults or line outage conditions. During a fault, voltages decline and fault currents increase substantially. Likewise, high voltage transmission line outages may reduce flows on the backbone system but increase stress on the underlying voltage level systems. In addition, the immediate change in flows can impact reactive power demand or production, and cause bus voltages to change significantly and the sending and/or receiving ends of the line. A response-based algorithm that utilizes reactive support devices should not trigger due to instantaneous voltage levels below predefined set points.

If a line is removed from service and the voltages return to acceptable levels after the event, a control action does not need to be taken otherwise overvoltage conditions can occur post-contingency. Let us analyze the response of the rate-of-change algorithm using a contingency from 2008 where one of the three COI lines tripped offline. Figure 63 shows the COI real power flow (blue) and its rate-of-change (red). Although the COI response is significantly different than the generation loss contingency, both exhibit major oscillations in COI real power flow. Since the detection algorithm is triggered for positive rate-of-change on the COI real power flow, Figure 64 shows only the positive values for *dP/dt*.

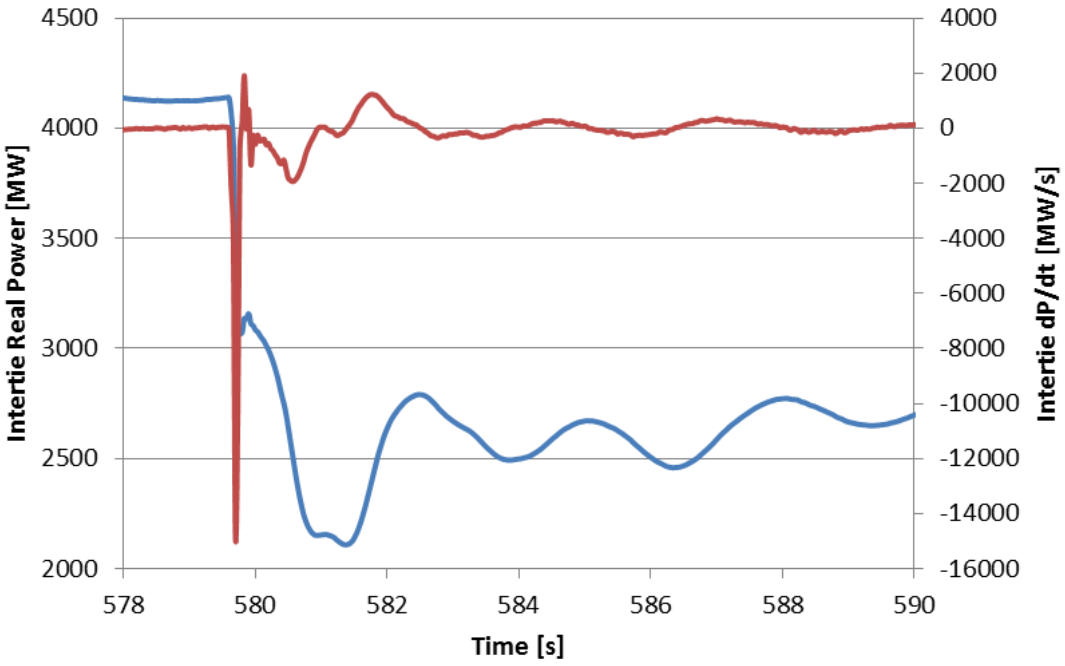

Figure 63. COI Real Power Response to Line Outage

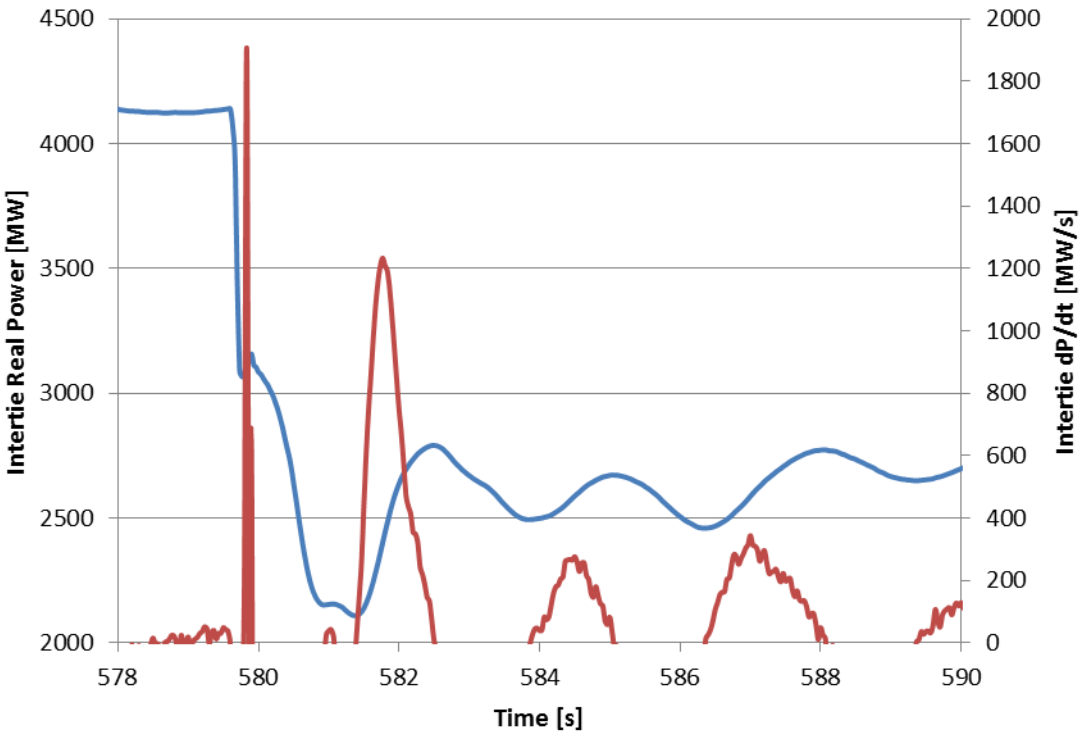

Figure 64. Higher Resolution Response to Line Outage

Note the significant negative rate-of-change due to the step change in COI flow from the line outage, followed by a small increase in COI transfers. This is due to the FAST AC Reactive Insert (FACRI) scheme within the BPA footprint, which inserts series and shunt capacitors north of the COI based on low voltage on the COI. Insertion of the series capacitors decreases the series reactance of the lines north of the COI, causing increased real power flows. In addition, note the characteristics of the rate-of-change for the initial disturbance as well as the consequent swings. The initial event is relatively fast and therefore will not trigger the algorithm due to the time duration requirement; however, the consequent swings may trigger the algorithm since they experience a slower, more sustained rate-of-change similar to the generator outages. This results in operation of the scheme as expected and designed for, where the initial event does not trigger the scheme, but the consequent response does if severe enough. Magnitude thresholds and their respective times exceeded are shown in TABLE XIII.

TABLE XIII. MAGNITUDE AND DURATION EXCEEDED FOR N-1 LINE OUTAGE

Magnitude	Event Duration Exceeded

[MW/s]	[s]
1000	0.260
800	0.400
600	0.540
500	0.570
400	0.700
300	0.800
250	0.833
200	0.900

Since the contingency occurs on the COI itself, the real power response to the contingency is more severe. The rate-of-change exceeds 1000MW/s for more than 260ms, while also exceeding 500MW/s for 570ms. This event could be triggered using higher magnitude and shorter duration settings; however, using these settings would not trigger the generator outage event, which would definitely be of concern. Therefore, it is proposed that multiple algorithm settings are used in parallel with each other to capture different types of phenomena, from fast moving and extremely severe events to slower moving but sustained events.

The following implementation strategy mirrors the effects of an inverse time characteristic overcurrent relay, where the pickup setting is inversely proportional to the time duration required to trip the relay. The concept of applying this to the rate-of-change algorithm is shown in Figure 65. Below the Level 1, *L1*, *dP/dt* magnitude setting the system responds naturally to changes in load, generation, switching events, and schedules. These events are considered normal steady-state operation or minor events where RAS action is unnecessary. Above the Level 1 threshold a sustained change for duration *T1* in real power flow on the COI is required to initiate the RAS action. Similarly, *dP/dt* above duration *T2* can also trigger the algorithm, which is configured for events such as large generator outages. Lastly, extreme rates-of-changes in real power above *L3* only require a short durations of *T3* for severe events such as line outages.

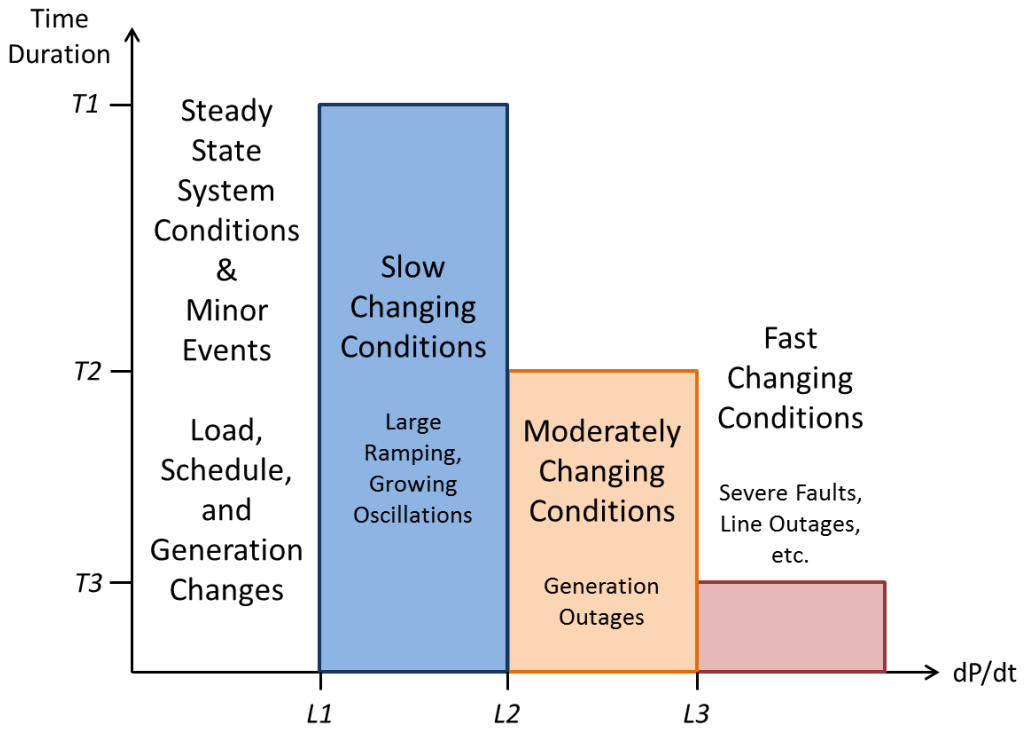

Figure 65. Inverse Time Characteristic Concept for Rate-of-Change Algorithm

To set rate-of-change magnitude and duration threshold values, a large number of disturbances and operating conditions must be considered. Thus far, analysis has focused on historical outages since they provide the most insight into how the system actually responds. Due to the relative lack of historical data for large outages, these contingencies must be simulated using transient simulations. System operators and planners are well aware of the probable and credible contingencies that have the largest risk to system reliability. Based on planning practices, these contingencies can range from a handful of severe disturbances to a database of hundreds of viable disturbances. Therefore, GE PSLF is used to simulate major N-1, N-2, and N-3 outages of concern throughout the WECC to create a database of potential contingencies [36]. A MATLAB script is used to determine the subset of contingencies that cause algorithm triggering based on the threshold values selected [100]. This MATLAB script is provided in Appendix D. Based on the simulated contingencies in conjunction with the historical disturbance analysis, TABLE XIV provides a set of three magnitude-duration threshold pairs for the rate-of-change algorithm. The table shows threshold values and the respective number of samples required using a 60

sample per second synchrophasor reporting rate. In addition, the sliding window algorithm fraction of samples is also provided for a higher level of dependability.

TABLE XIV. PROPOSED COI REAL POWER RATE-OF-CHANGE ALGORITHM SETTINGS

Magnitude [MW/s]	Duration [s]	60sps Samples	Sliding Window
1000	0.1	6	6/8
500	0.5	30	30/35
250	1.2	71	72/80

Figure 66 shows a logic diagram for implementation of a rate-of-change algorithm for the COI. The necessary real power quantities are either measured and recorded as analog values in the PMU or calculated in the controller application; the instantaneous total real power flow, *COI(t)*, is calculated from these values. The instantaneous rate-of-change, *dP/dt*, is calculated by taking the first derivative of the most recent measurement with respect to the previously recorded sample, using the time stamps included in the synchrophasor data frames. Three algorithms execute independently in parallel with each other, where the *dP/dt* is compared to the threshold values 1, 2, and 3. A Boolean *TRUE/FALSE* value is sent to the timer algorithm where consecutive or sliding window algorithm is implemented. Either algorithm compares the number of Boolean values obtained with the timer threshold values to determine if enough samples exceeding the threshold have been collected. If any one of the algorithms triggers, then the trigger signal is enabled from the COI real power rate-of-change algorithm.

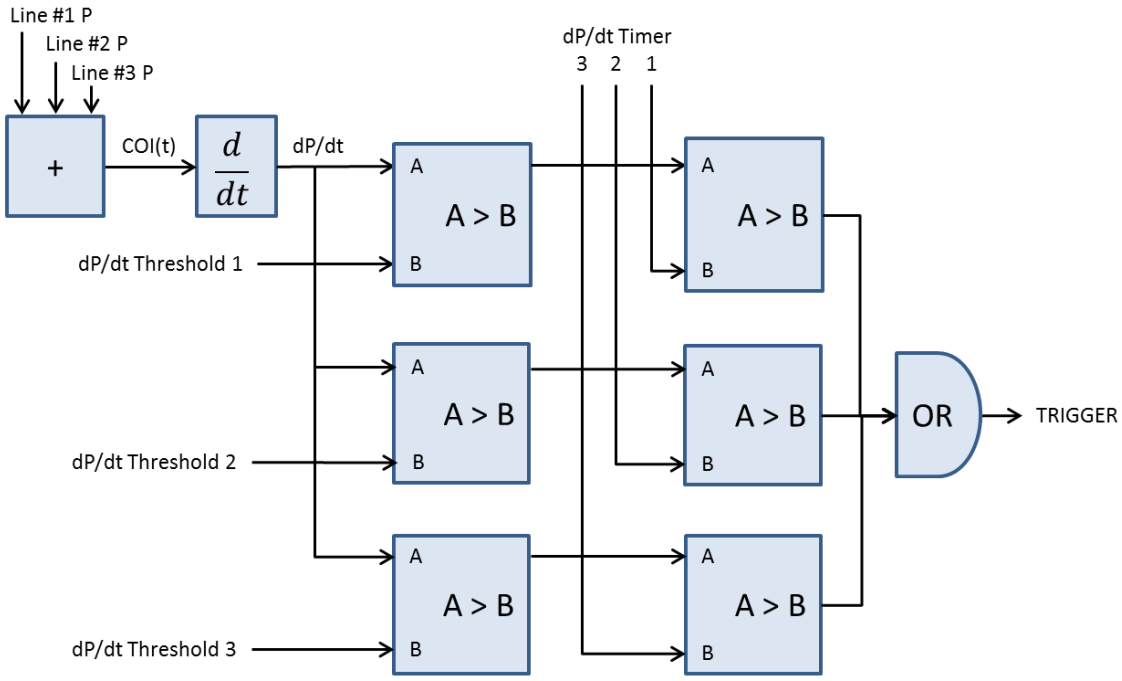

Figure 66. COI Real Power Rate-of-Change Algorithm Logic Diagram

4.3.2. Wide Area Phase Angle Rate-of-Change Algorithm

Section 2.1 describes the relationship between real power and phase angle, and provides the equations governing this connection. Since phase angle can be derived from power flow, and vice versa, it is expected that an algorithm utilizing phase angle differences can provide similar performance as an algorithm using real power measurements. In addition, wide area synchronized phasor measurement systems have the capability to measure relative phase angles at each instant in time. Therefore, a wide area phase angle algorithm can take advantage of the geographic diversity of WAMS measurements whereas the real power algorithm requires relatively localized measurements. Diversifying the measurement portfolio improves the reliability of the algorithms and overall control scheme. This section describes an algorithm similar to the real power rate-of-change algorithm that uses voltage phase angle measurements to detect significant events. As Chapter 3 highlights, phase angle difference can be an indicator of system stress, and play a useful role in situational awareness. However, it can also be used for automated controls where operator action is unavailable or inadequate.

Figure 67 is a reproduction from Section 3.1 for clarity to illustrate the BPA system and its overall WAMS configuration. The operating condition of most concern includes heavy exports to California through the California-Oregon Intertie (COI), with high generation output internally to BPA and high transfers from Montana (MT) and the Northern Intertie (NI). It is therefore intuitive to use phase angle quantities from these various locations, and reference them to the COI since it will generally have the smallest phase angle value for export conditions.

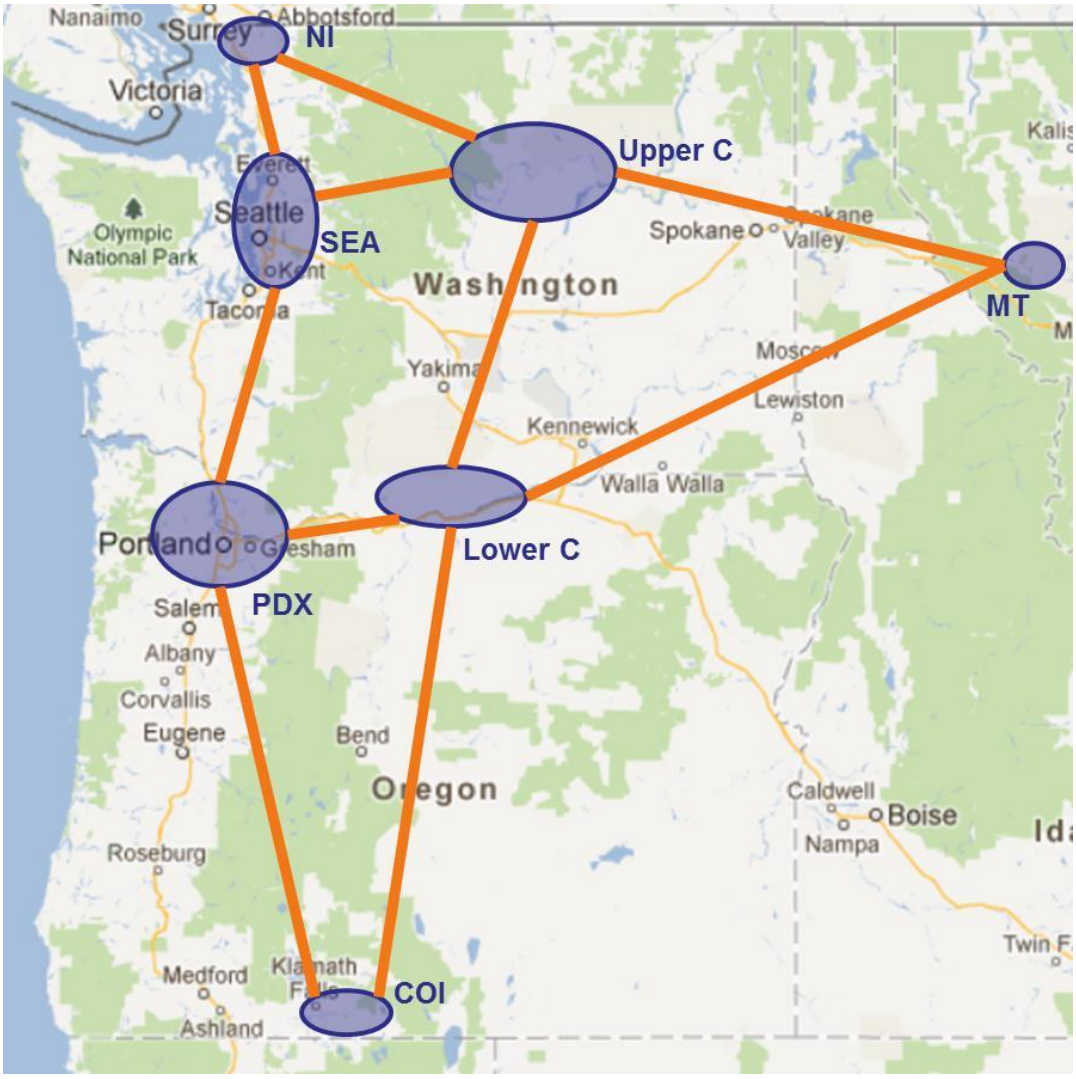

Figure 67. BPA Regional PMU Clustering

Based on the concept of wide area phase angle measurement for conditions of greatest concern, the following angle pairs are used:

- Northern Intertie (NI) – California-Oregon Intertie (COI)
- Upper Columbia (UC) – California-Oregon Intertie (COI)
- Montana (MT) – California-Oregon Intertie (COI)
- Lower Columbia (LC) – California-Oregon Intertie (COI)

The NI-COI, UC-COI, and MT-COI angle pairs act as primary measures while the LC-COI can act as a surrogate measurement if one of the pairs is unavailable. This is because the Lower Columbia is situated essentially at the midpoint of the BPA system and is encompassed in the other angle pairs.

Furthering the illustrative example of 1300MW generation loss in the southern parts of WECC, Figure 68 shows the phase angle differences overlaid with the COI real power flow. As expected the characteristics of these two types of waveforms are similar, with a large deviation from 'steady state' due to the inertial response of the system followed by oscillatory behavior and steady increase due to the governor response.

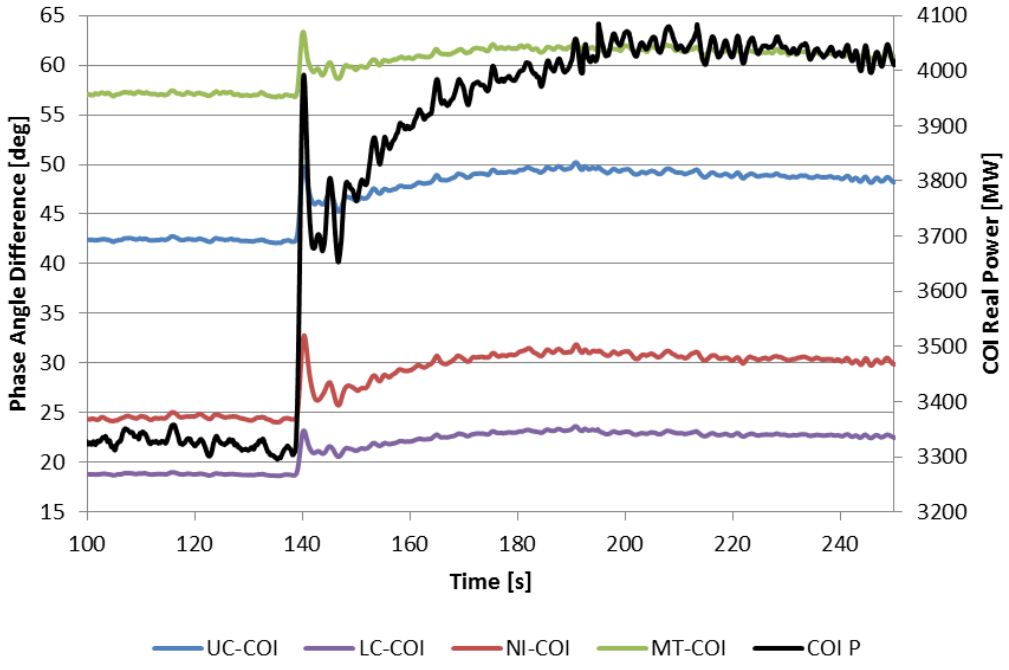

Figure 68. Phase Angle and COI Real Power Response to Generator Outage

Let us explore the phase angle rate-of-change overlaid by the COI real power rate-of-change, as shown in Figure 69 and Figure 70. The derivatives follow a similar behavior and

almost overlay each other exactly. Looking closer, you can visually see that the NI-COI angle difference oscillations with a fairly different frequency than the other angle differences. This may be due to the modes of oscillation excited for this disturbance. The NI-COI angle oscillates with the N-S B mode (formerly "Alberta mode") and the other angles oscillate closer to the N-S A mode (formerly "North-South" mode) [101].

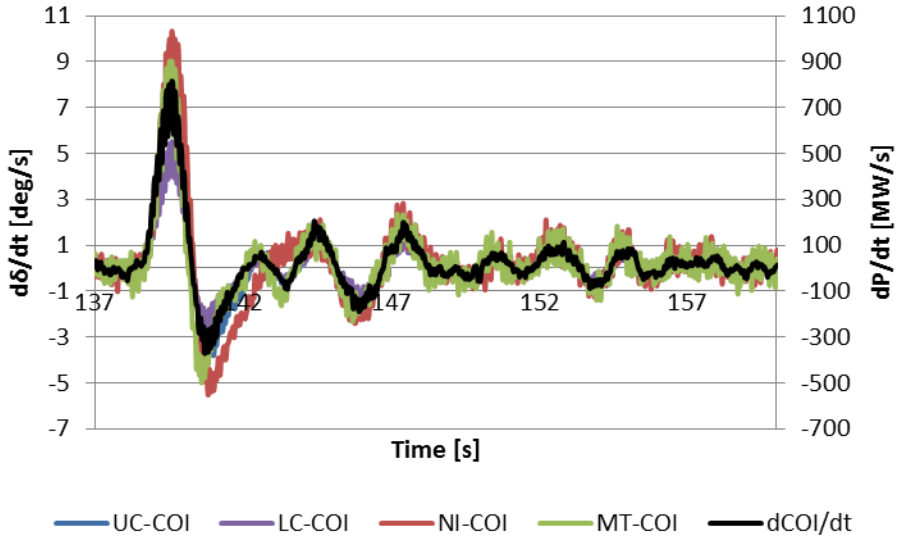

Figure 69. Phase Angle and COI Real Power Rate-of-Change

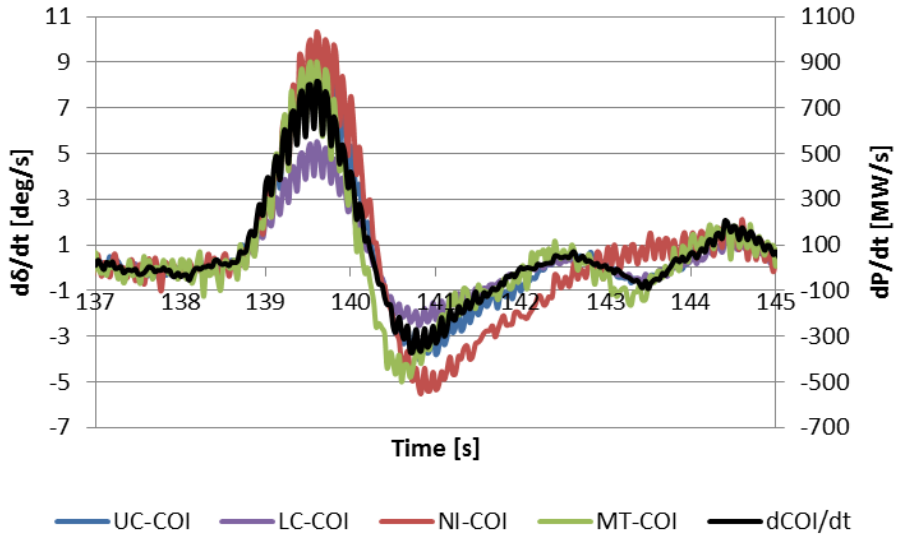

Figure 70. Higher Resolution Angle Rate-of-Change

The angular rate-of-change algorithm is also tested using other historical outages similar to the real power rate-of-change algorithm. In addition, simulated contingencies are also

tested against various thresholds to determine an effective set of thresholds. The MATLAB script used for testing is provided in Appendix D. As a simplification to the algorithm, the three primary angle pairs are given the same magnitude and duration thresholds (see TABLE XV). Note the similarity between the phase angle and real power rate-of-change algorithm threshold values. Since the two types of variables follow the same characteristic response, similar thresholds can be applied to both. This helps simplify the concept and implementation of the algorithms. Figure 71 shows a simplified logic diagram for the algorithm.

TABLE XV. PROPOSED PHASE ANGLE RATE-OF-CHANGE ALGORITHM SETTINGS

Magnitude [deg/s]	Duration [s]	60sps Samples	Sliding Window
10.0	0.1	6	6/8
5.0	0.5	30	30/35
2.5	1.2	71	72/80

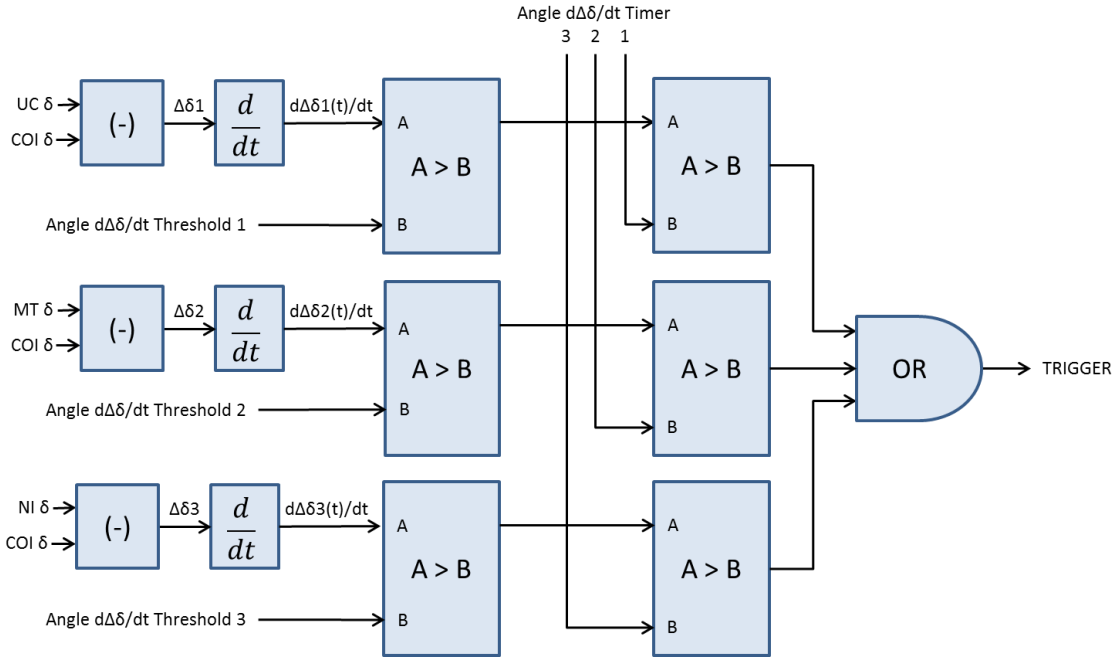

Figure 71. Phase Angle Rate-of-Change Algorithm Logic Diagram

4.3.3. Summary of Detection Algorithms

Both algorithm formulations are based on the BPA transmission system, but the concepts hold for any Balancing Authority Area or Control Area concerned with detecting events such as large generation or line outages. Two algorithms are presented, one based on the rate-of-change of real power transfer across a major intertie and an expansion of that algorithm using the rate-of-change of phase angle differences across the power system. Both algorithms have been tested using historical and simulated outages. Historical analysis uses wide area PMU data collected from the BPA labs while simulated data uses a database of modified 2013 WECC operations cases.

The algorithms are designed with consideration for control logic reliability. Both schemes require consistent measurement of 'triggerable' conditions before the algorithm is enabled. This can either be in the form of consecutive samples of synchrophasor data or a sliding window with a predefined percentage of positive triggers. Three magnitude-duration threshold pairs are selected with the intent to operate in parallel; the concept is to mirror the idea behind the inverse time overcurrent relay, where more severe operating conditions require shorter time duration to operate. The minimal observation time of either scheme is set to exceed the expected time for fault clearing. Shorter duration with larger magnitude threshold is intended to operate following fault conditions near the BPA BAA. Middle magnitude-duration settings are based on observations made for large generation N-1 and N-2 events. Longer duration with low magnitude is expected to catch swings or excessive ramps in power across the system.

With an algorithm in place for detecting external events that would otherwise be unobservable using conventional SCADA, a control scheme can be formulated to take corrective action when grid conditions may be degraded.

4.4. Response-Based Voltage Stability Reactive Insert (VSRI)

The research for SP RAS has outlined the concern for large contingencies causing adverse effects within the BPA system and an event detection algorithm to acknowledge when an event is occurring. The last element is to devise and demonstrate an effective control action for improving grid reliability and security. As discussed above, existing BPA reactive controls include the FACRI and VSRI. FACRI is a highly effective response-based controller that has significant benefits for the WECC dynamic response. VSRI is event-driven and provides post-transient voltage support following outages internal to BPA. The goal is to expand the VSRI using the synchrophasor-based RAS controller for improved responsiveness and diversification of controls. It is not 'good practice' to depend upon a single control strategy, even when designed fully redundantly. The VSRI can provide complimentary benefits if given the capability to operate when needed. The following subsections describe application of the VSRI through three approaches. First, historical PMU data is collected and analyzed to determine when the detection algorithm would trigger. Transient simulations are then performed for myriad operating cases and contingencies to test the effects and robustness of response-based VSRI. Furthermore, a large outage on June 14 2004 in the WECC is used as a platform for validating the VSRI [7]. A validated baseline case has been created by WECC for this disturbance, and this case is used here to test the controls. Lastly, the baseline case is stressed to higher levels to reflect different operating conditions that may have occurred that day. The VSRI is again tested for this severe event with a more stressed pre-contingency operating point.

4.4.1. Diversifying Reactive Controls with Response-Based VSRI

For any "safety net" scheme, it is critical to assess the impact of the scheme operating stand-alone as well as in conjunction with other protection and RAS schemes. Most important for the response-based VSRI RAS is its interaction with the FACRI, and the benefits and drawbacks this interaction may invoke. This section uses a 146GW load level modified WECC base case (fairly light load conditions) with moderate stress within the BPA system to illustrate the interaction of these schemes. The contingency chosen for the illustration is a simultaneous loss of three large generating units totaling 5200MW.

Although an N-3 contingency is considered a Category D contingency in terms of WECC reliability criteria, the event has occurred before on the WECC system (as discussed later in this chapter) and provides an excellent illustration of the effects of "safety net" schemes on system reliability.

Four scenarios are presented that show the various situations of interaction between the FACRI and VSRI:

- *FACRI, no VSRI*: This is the current configuration of the RAS schemes since the VSRI does not operate responsively for a contingency outside the BPA footprint, i.e. this is the status quo control.
- *No FACRI, No VSR*I: This is the situation in which the FACRI would fail to operate and no "safety net" scheme is implemented to protect against this failure. The FACRI is designed following NERC reliability standards for RAS schemes and failure to operate is improbable, but there is always a small probability of occurrence and planners should assess the risk associated with this failure.
- *No FACRI, VSRI*: This is the situation where FACRI has failed to operate, is out of service, etc., and the VSRI scheme is waiting in the background as a "safety net" to take action.
- *FACRI, VSRI*: Both schemes, if not restrained, may operate together for a severely large contingency on the system.

For this example, the FACRI when available will operate based on its local voltage measurement and time delays. The VSRI is set to have the capability of triggering after the event has been detected by the COI rate-of-change detection algorithm. Therefore, the VSRI control signal sent to the local voltage relays is not enabled until 2.625 seconds into this simulation since the contingency occurs at 1 second. The assumptions are that there is a 25 ms delay for PMU data to communicate the C37.118 data frames to the control center over fiber optic communications. 25 ms delay for controller processing, 50 ms delay for communication of the control signal to the remote, controllable reactive support sites, and 1 second delay for processing and capacitor insertion through breaker operation.

A contingency of this size will have a significant impact on the real power flow across the COI, as shown in Figure 72. As expected, operation of the FACRI provides system stability following the generation loss. When the FACRI is not applied and VSRI does not operate, the system becomes unstable. This is well known by power system planners across WECC; FACRI is of utmost importance for stable operation at fairly high transfers. Therefore, the blue and red responses in Figure 72 are expected. Incorporating the VSRI with the FACRI presents a number of benefits and drawbacks, as the figure shows. The most obvious benefit of the VSRI acting as a "safety net" scheme is that system stability can be maintained even without the FACRI operating. Although the response has relatively poor damping, the system is able to recover and hold on throughout the simulation. This embodies the definition of a "safety net" scheme, by allowing ancillary controls to take secondary response when needed for severe events. A concern arises for the situation where the VSRI and the FACRI both operate; the damping of the COI real power reduces for this situation. This may be due to much more activity occurring on the system during the disturbance, or may be due to the wide-area increase in voltage which could affect voltage-sensitive loads. Regardless, it is noted that operation of both FACRI and VSRI may decrease damping of system response.

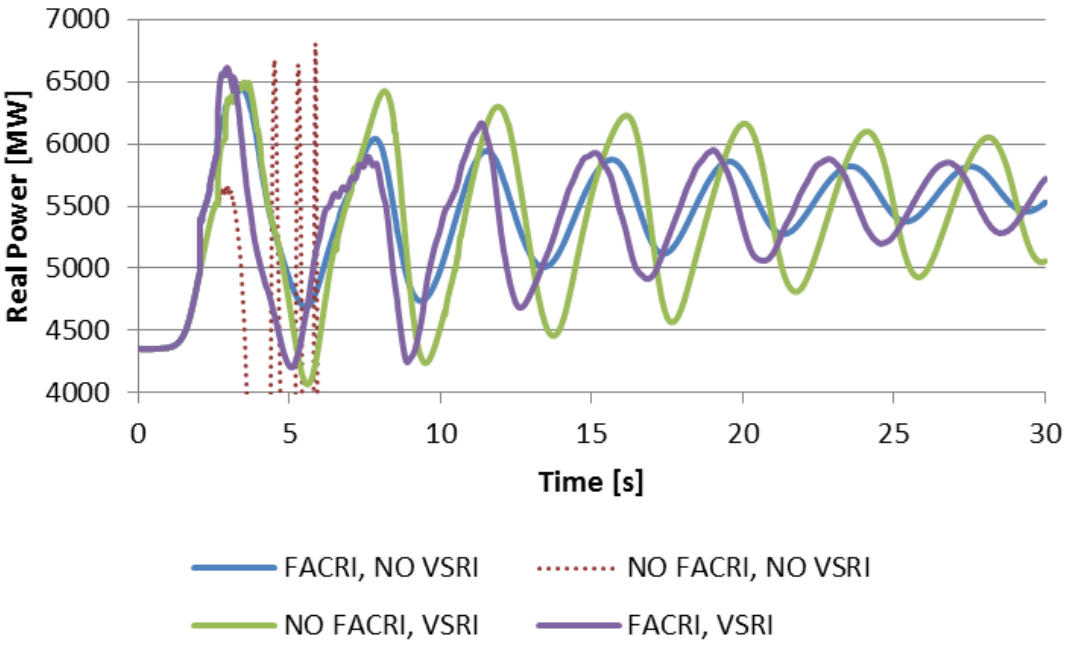

Figure 72. 146GW Case COI Real Power Transfer

Both RAS actions are reactive support schemes and will inevitably have a major impact on system voltage levels. Figure 73 shows the voltage magnitude at a critical 500kV bus in the southern part of the BPA footprint. As the figure shows, immediate voltage recovery is best when both the FACRI and VSRI operate. When the FACRI fails to operate and the VSRI does operate, the voltage plummets almost 400kV but is able to recover back to an rms value near scheduled voltage. With both the VSRI and FACRI operating, post contingency voltage levels appear to settle around 550kV, still within acceptable ranges. A valid concern for utilizing both VSRI and FACRI is the situation of overvoltage; however, this disturbance shows that both FACRI and VSRI may result in oscillations upwards near 575kV, but the post-contingency steady state settles within acceptable ranges near scheduled voltage.

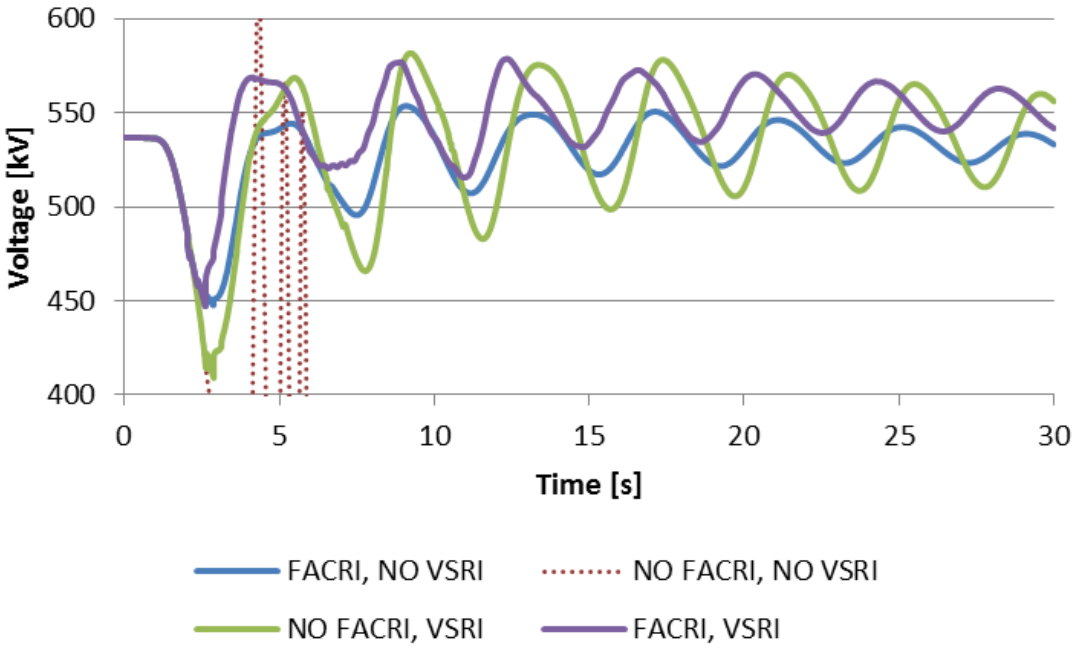

Figure 73. 146GW Case 500kV Bus Voltage

Figure 74 shows the same voltage profile, but with improved resolution near the points of operation for the FACRI and VSRI. When the FACRI operates at about 2 seconds, the voltage is able to recover; without the FACRI, the voltage continues to plummet until the VSRI scheme is initiated at about 2.625 seconds. The argument can be made based on this

observation that the VSRI must be switched in a timely manner after the FACRI has had time to operate for it to be an effective "safety net" scheme.

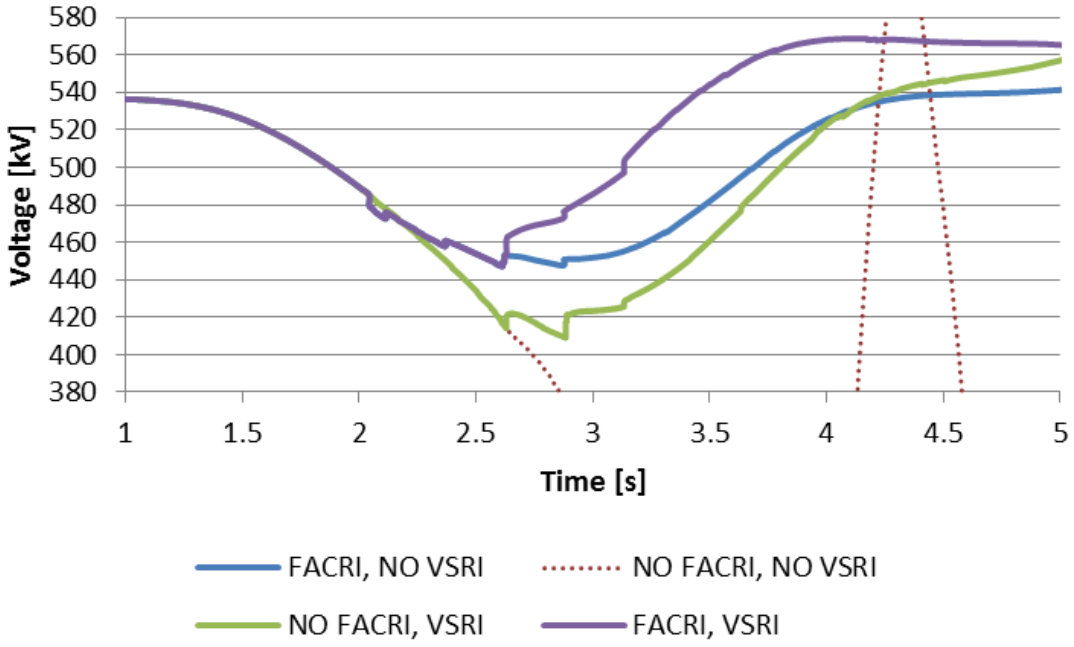

Figure 74. 146GW Case 500kV Bus Voltage Response to VSRI/FACRI

Frequency and phase angle difference are also monitored to determine how they are impacted by the FACRI and VSRI. Figure 75 shows frequency and how the VSRI may decrease damping of frequency oscillations. Comparing the FACRI-only and FACRI+VSRI scenarios, it appears that the increased voltage profile across the system due to the wide-area voltage support from the VSRI causes the voltage dependent loads to increase real power demand. This increases the real power imbalance and slightly suppresses the frequency further. Phase angle difference is also monitored, as shown in Figure 76 and Figure 77. The increased reactive support reduces the phase angle difference between voltages at a major generation source and the COI tie lines. Figure 77 shows this phenomenon in more detail, with the large step change in angle occurring due to the FACRI at about 2 seconds, and subsequent smaller changes from the VSRI actions. Damping is reduced for the cases where VSRI action occurs. However, the magnitude of phase angle difference between two key locations decreases when both the VSRI and FACRI operate.

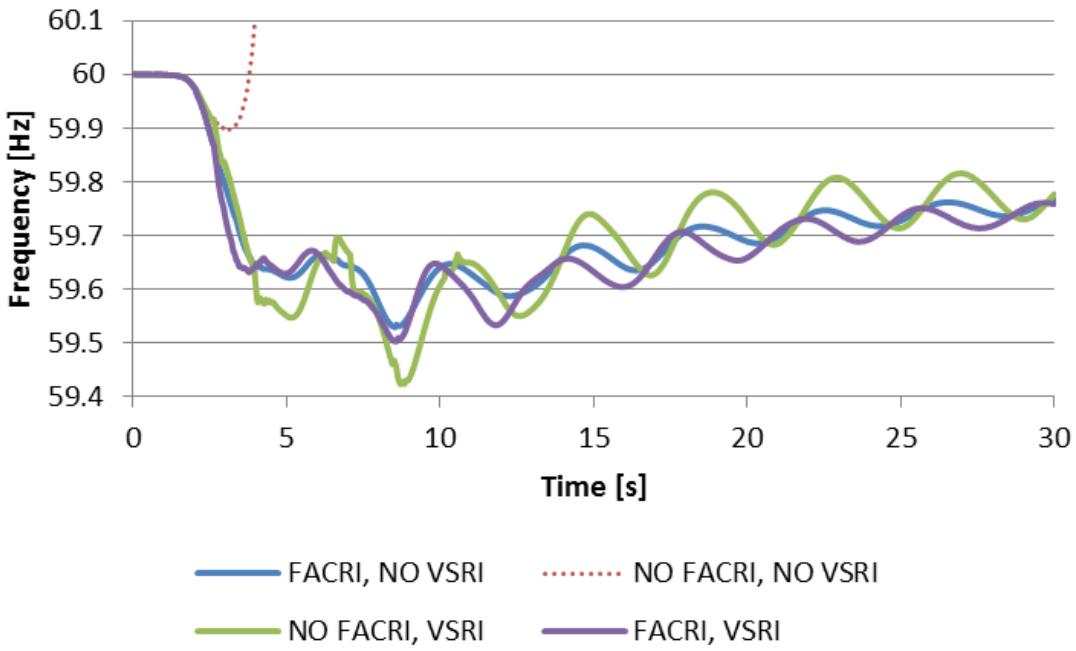

Figure 75. 146GW Case Bus Frequency

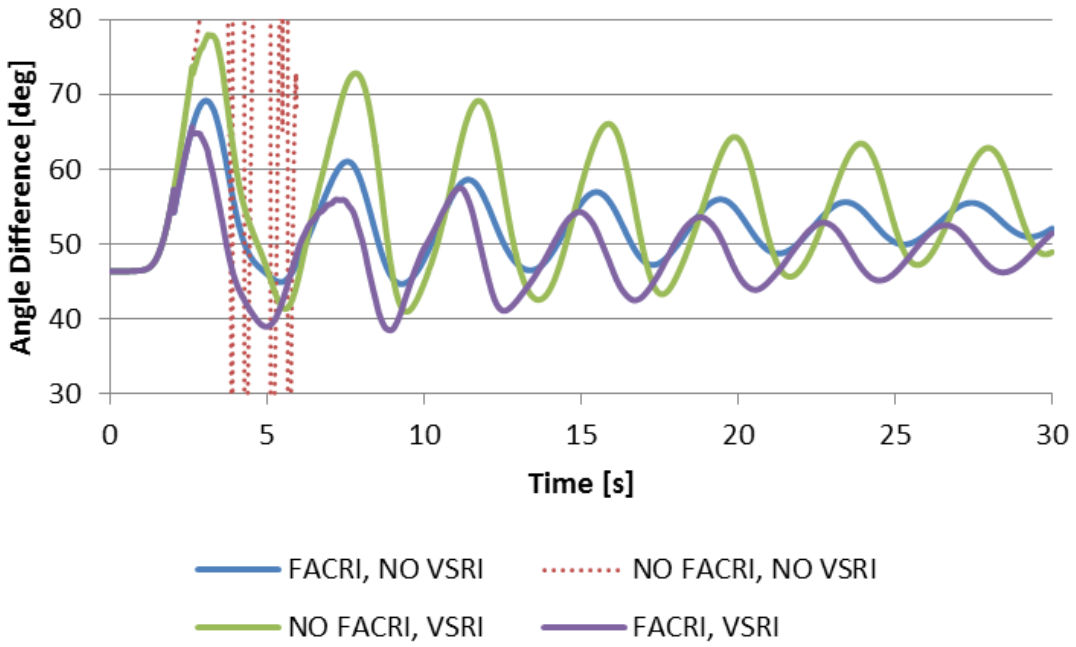

Figure 76. 146GW Case Phase Angle Difference

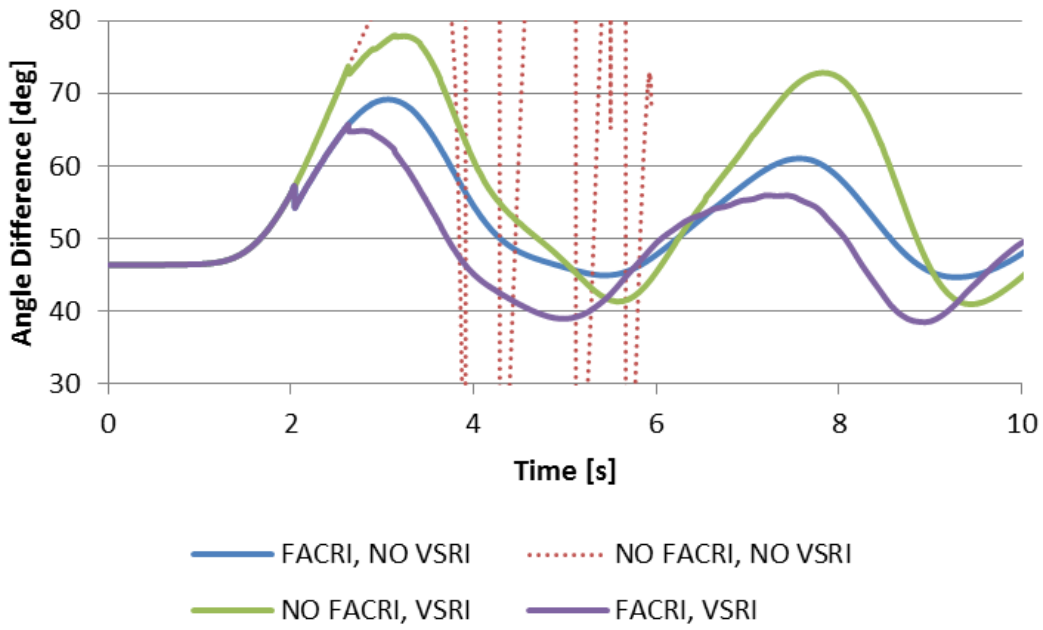

Figure 77. 146GW Case Phase Angle Difference Response to FACRI/VSRI

VSRI and FACRI interaction is tested using cases between 105GW (light load) and 179GW (heavy load). Appendix E provides results for these studies using voltage, frequency, COI MW, and angle difference as performance metrics. Figure 78 shows that the system is unstable for the N-3 contingency with no control taken. VSRI maintains stability for the N-3 event, except for the 105GW light load with high transfers case.

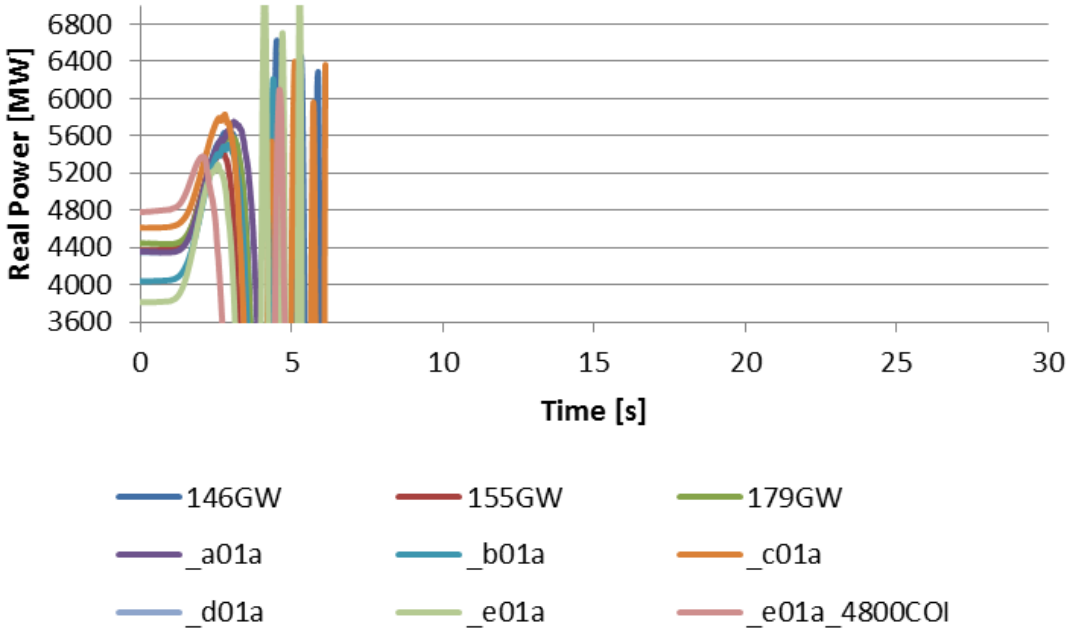

Figure 78. System Instability for Large N-3 Contingency

Bus voltage at a 500kV substation on the COI is shown in the following three plots to demonstrate the differences in system response to the VSRI and FACRI. Figure 79 is the response to FACRI operation as currently exists today for the range of operating conditions. The oscillation is damped and able to maintain stability for all cases except a severely stressed, light load situation. However, the contingency causes the voltage to drop to dangerously low levels of about 360kV at the nadir. All stable simulations settle relatively close to pre-contingency operating voltages. Looking at Figure 80, system response is substantially different. Since the FACRI does not operate for this scenario, damping of the oscillations is reduced. A major benefit of the VSRI operation, however, is that post-contingency voltage only drops to about 410kV, which is a 50kV improvement. Similar to the FACRI operation scenario, voltages settle near their pre-contingency levels. Lastly, Figure 81 shows a scenario where both the VSRI and FACRI operate. The voltage response achieve both benefits of the series and shunt capacitor operations by alleviating the post-contingency voltage dip to above 430kV and providing oscillation damping. Voltages settle only slightly higher than pre-contingency levels.

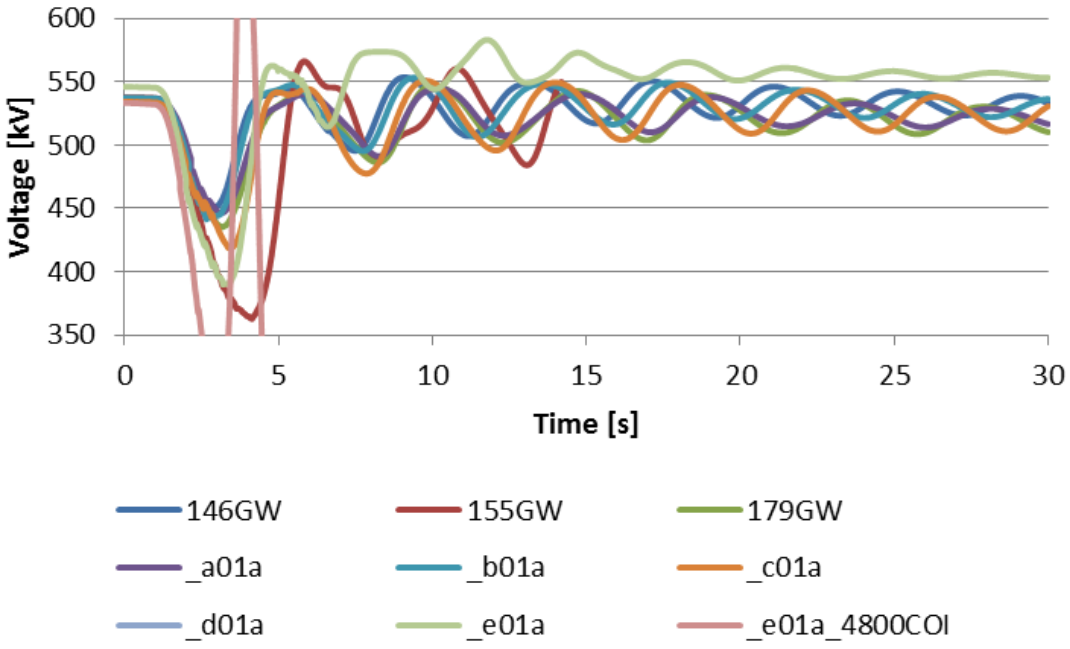

Figure 79. FACRI with No VSRI Operating Scenario

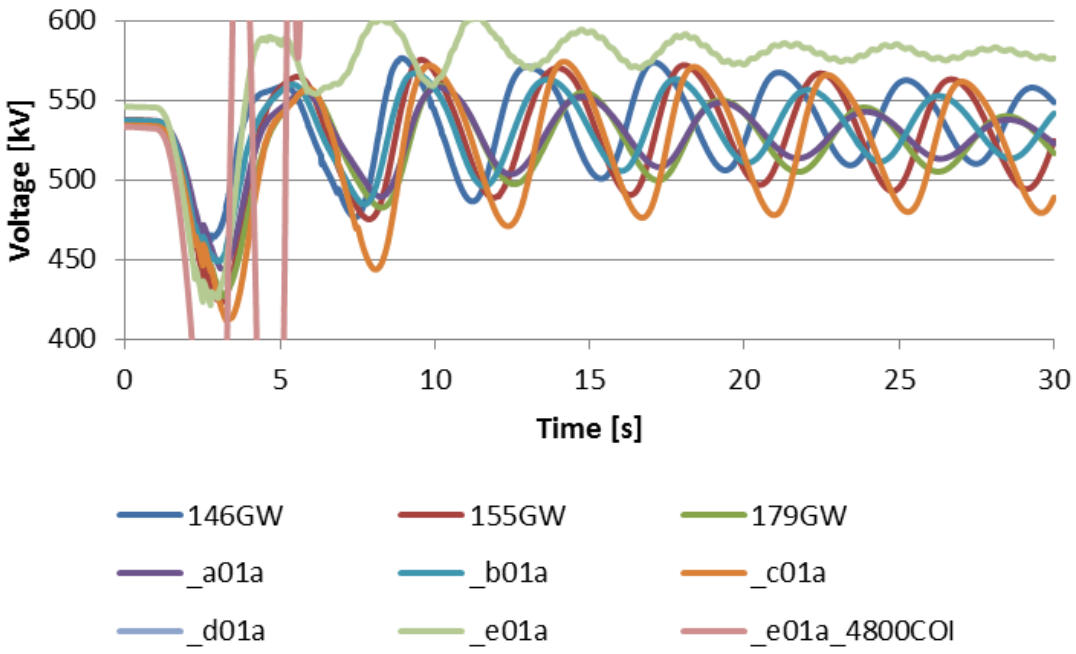

Figure 80. No FACRI with VSRI Operating Scenario

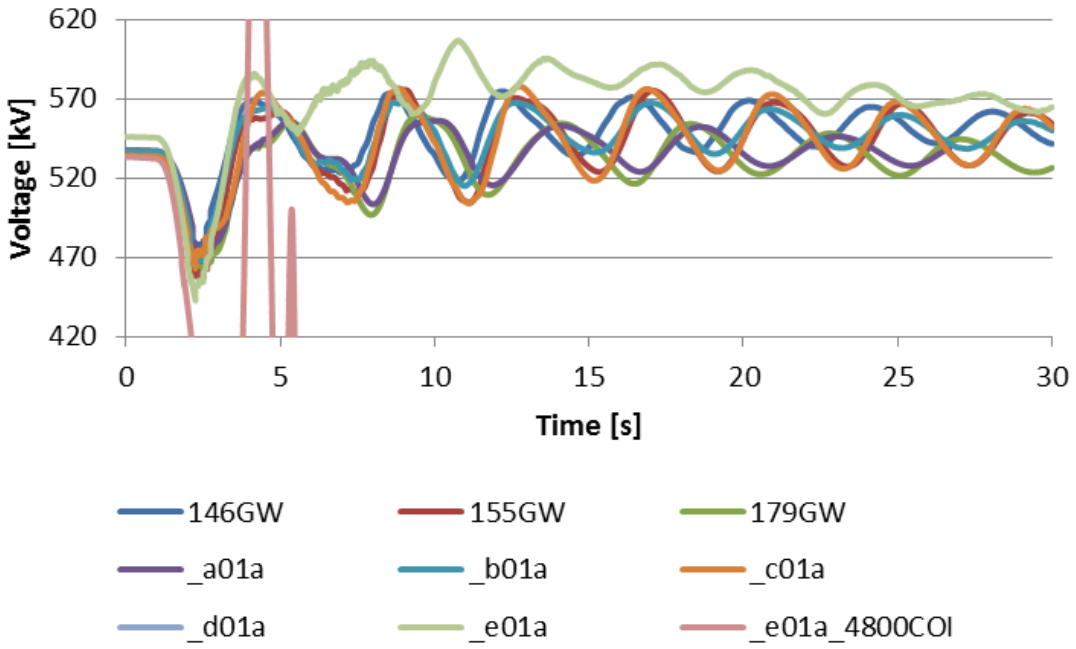

Figure 81. FACRI with VSRI Operating Scenario

Similar results are shown in Appendix E for the other signal responses. These results demonstrate the effectiveness and application of the VSRI as a "safety net" scheme for reliable operation of the power system.

4.4.2. VSRI Operation for June 14, 2004 Baseline Case

The VSRI is also tested on a baseline case created by WECC for the June 14, 2004 event [7]. On this day, a large, complex set of contingencies occurred resulting in seven 500kV lines and all 3 Palo Verde nuclear units tripping offline at the 500kV Palo Verde bus. The fault type changed many times during the event, from a phase-to-ground fault to a three-phase fault within 12 seconds. A total of 4800MW of generation, including 3900MW of Palo Verde units, was lost from this event, resulting in power surges across the WECC, and severe transient and post-transient voltages [7]. In addition, a number of lines were out of service that day for maintenance, which resulted in relatively lower flows than expected. The lines were reinserted in the model, stress levels were increased on the California-Oregon Intertie (COI), and the simulations were re-run using the higher stress case. Historical PMU data collected from the BPA wide area measurement system, simulation results of the baseline case, and simulation results of the stressed case are all used to test the algorithm response and VSRI impacts.

Following the loss of the three nuclear generating units in Arizona, system frequency dropped to 59.55Hz within the BPA BAA and remained suppressed following the outage (Figure 82). Real power on the COI increased to 5500MW during the first swing, and the unbalanced frequency response in the WECC caused sustained intertie pickup to 4500MW (Figure 83). Measured voltage on the COI shows transient dip to less than 440kV, with recovered voltage levels, but continuing decline during the primary governor response (Figure 84). Phase angle difference across the BPA system, referenced to the COI angle measurement, peaked at 60 degrees, damping out but continuing to increase during the governor response (Figure 85). These measures of system conditions indicate a severe contingency near the edge of cascading outages and instability.

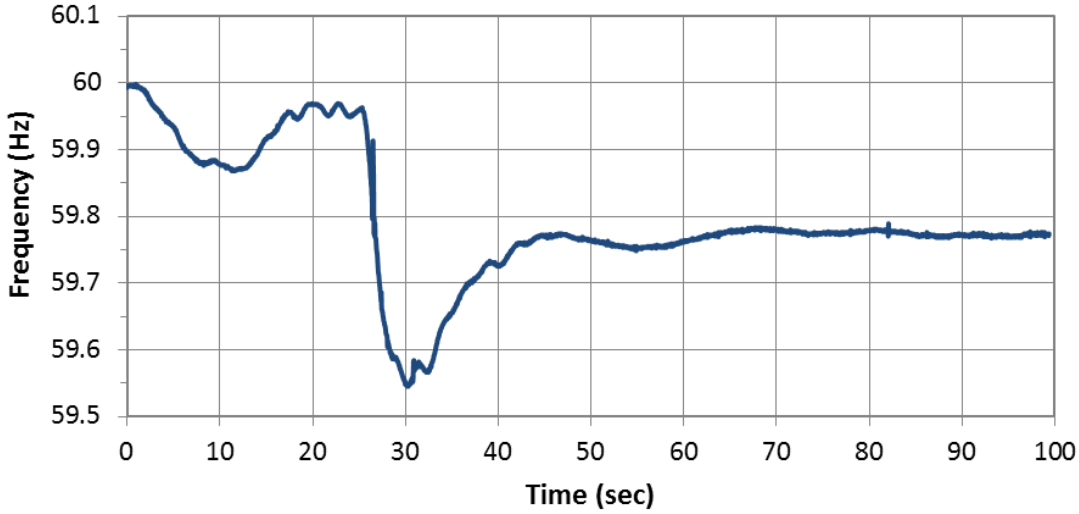

Figure 82. System Frequency for June 14 2004 Event (BPA PMU Data)

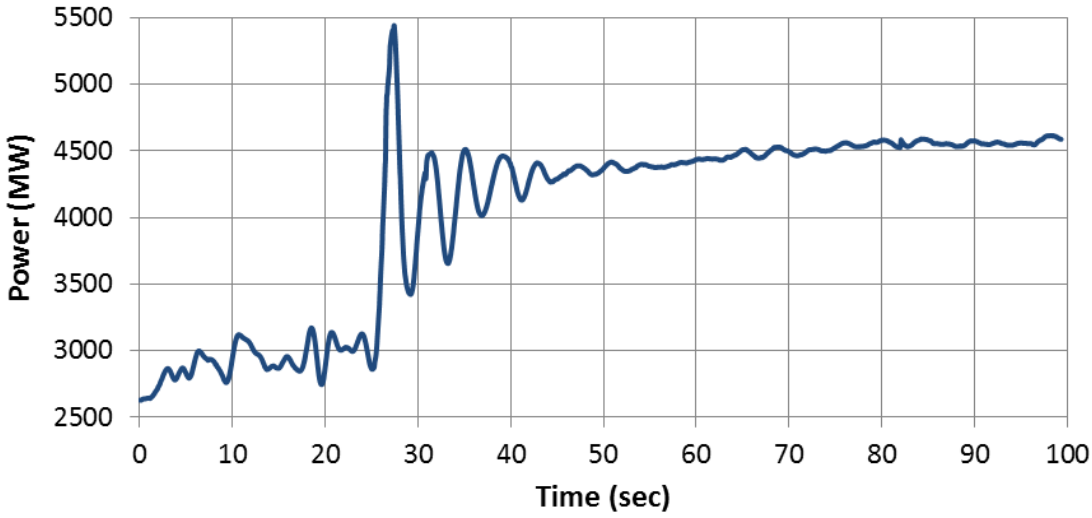

Figure 83. COI Real Power Flow for June 14 2004 Event (BPA PMU Data)

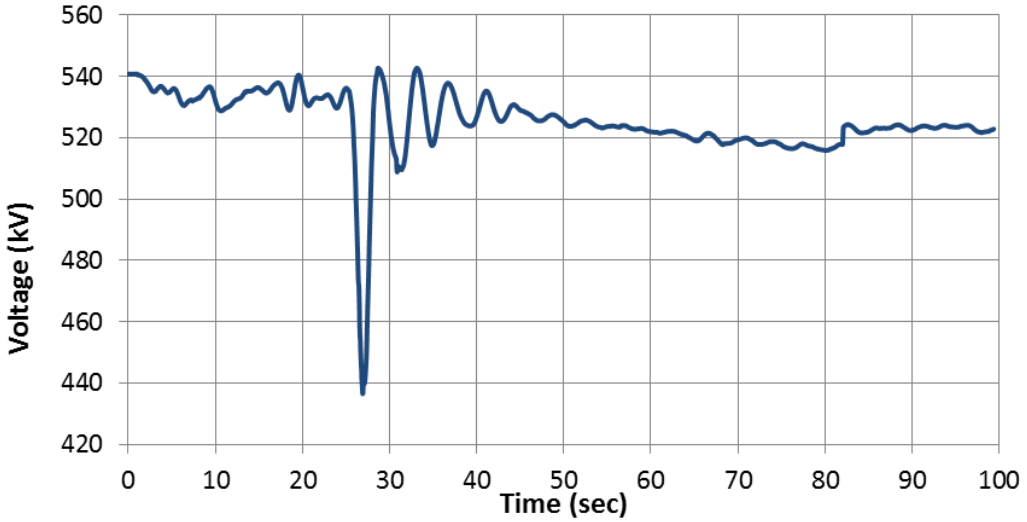

Figure 84. Voltage on COI for June 14 2004 Event (BPA PMU Data)

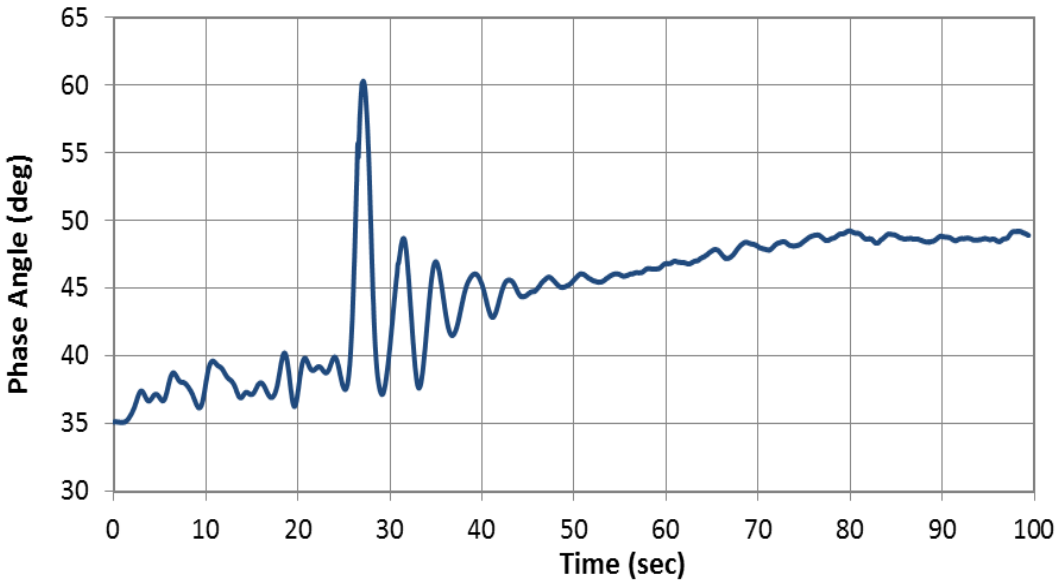

Figure 85. BPA Phase Angle for June 14 2004 Event (BPA PMU Data)

Historical PMU data for this event is first analyzed to determine timing of the event detection algorithm. Based on real power rate-of-change, 500MW/s magnitude threshold exceeds 500ms at recording time 26.0 seconds. The 1000MW/s magnitude threshold exceeds 100ms at recording time 25.7 seconds. Therefore, the algorithm would trigger between 25.7 and 26.0 seconds. Regardless, the VSRI is tested for enabling at: 0.0s, 20.0s, 25.0s, 25.2s, 25.5s, 25.6s, 26.0s, and 30.0s. Key variables are compared for 'no VSRI

action' and '26.0s VSRI action' scenarios to determine how the integrated control strategy would likely perform.

Transient and post-transient voltage is drastically affected by the VSRI timing. Figure 86 shows COI voltage response to VSRI switching for the various timing scenarios. The 'No VSRI' serves as the baseline simulation for no control action taken. VSRI triggered prior to approximately 25 seconds causes the VSRI to trigger as quickly as possible and mitigates the impact of the first swing voltage decline. The VSRI is able to arrest voltage drop at the COI from below 440kV to approximately 505kV, a 65kV improvement. The preemptive reactive controls result in the highest post-transient voltage as well. Voltages settle around 550kV for these simulations, which is well within acceptable post-contingency levels. For the 30.0 second insertion, the delay in control action improves post-transient voltages but does not mitigate the transient voltage dip concern. This illustrates the criticality of fast detection and responsive control action.

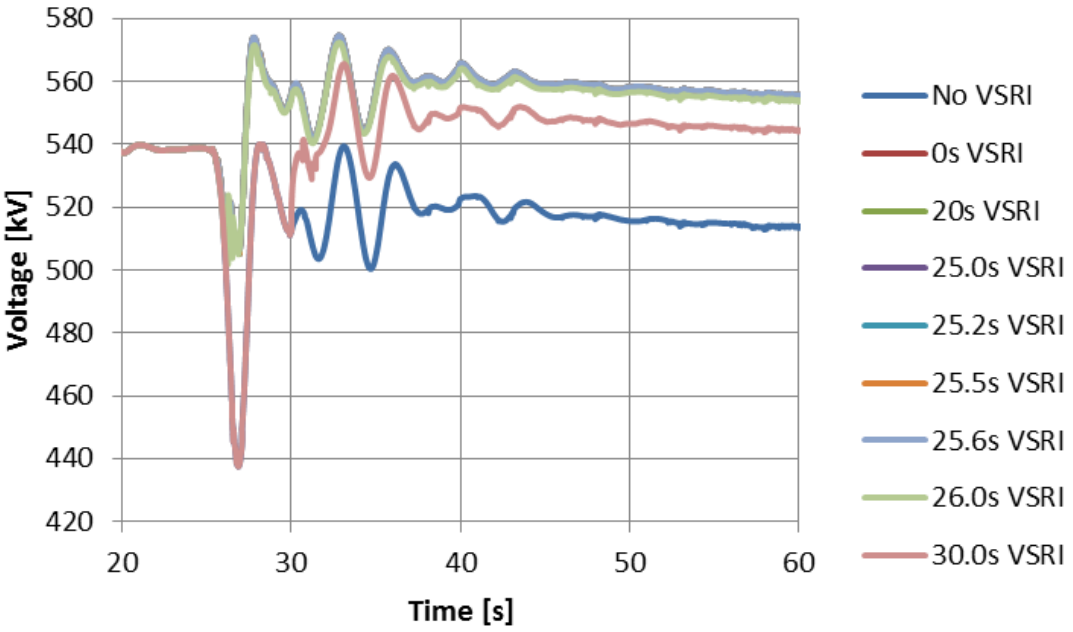

Figure 86. COI Voltage for VSRI Insertion for June 14 2004 Event (Baseline Case)

Phase angle across the BPA system experiences a similar response to voltage (Figure 87). Timely insertion of the VSRI shunt reactive elements results in lower transient angle during the first swing as well as post-transient angle by approximately 5 degrees. The 30.0

second insertion is able to reduce angle difference in the post transient timeframe but fails to limit the angle difference during the first swing. This timing option would not benefit the transient stability in terms of phase angle. Figure 88 shows the first swing phase angle response. Note how the 'No VSRI' and '30.0s' scenarios experience a large step change in angle prior to the other schemes. This is because the FACRI operates faster for the 'No VSRI' cases since the voltage is able to decline faster and with worsened magnitude. However, regardless of FACRI timing, the VSRI causes a response that is reduced in magnitude from 61 degrees to about 56 degrees.

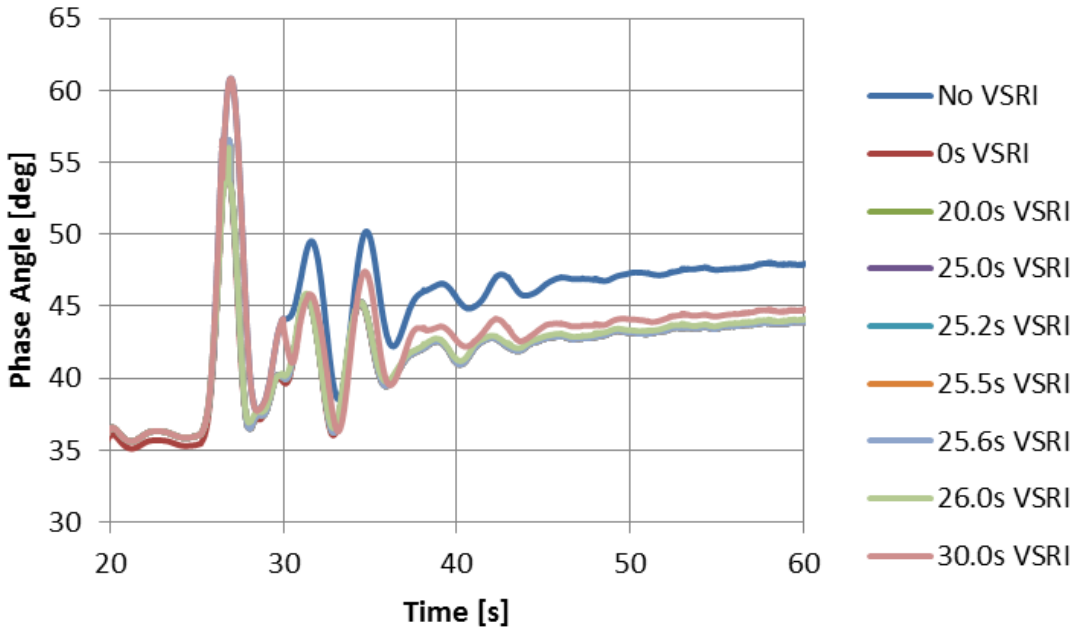

Figure 87. BPA Angle for VSRI Insertion for June 14 2004 Event (Baseline Case)

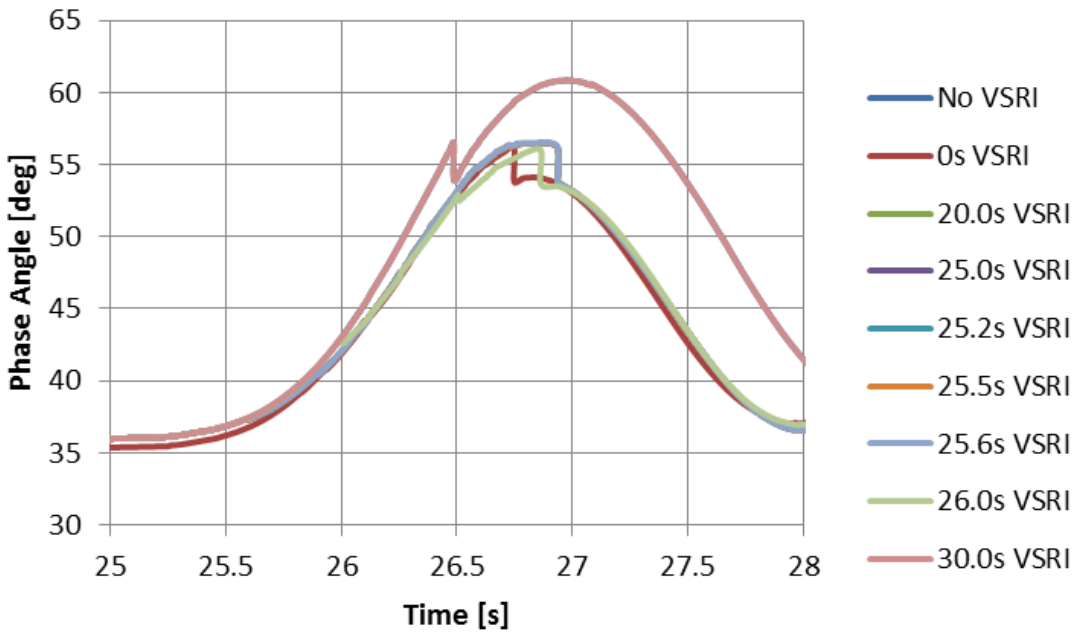

Figure 88. Angle Swing for VSRI Insertion for June 14 2004 Event (Baseline Case)

The COI real power transfer and the frequency are minimally affected by the VSRI action. Real power (Figure 89) and frequency (Figure 90) decrease slightly following the shunt element insertions. This is attributed to the voltage sensitive load increasing slightly for higher voltage following the capacitor insertions across BPA. This will add to the real power imbalance following the loss of generation.

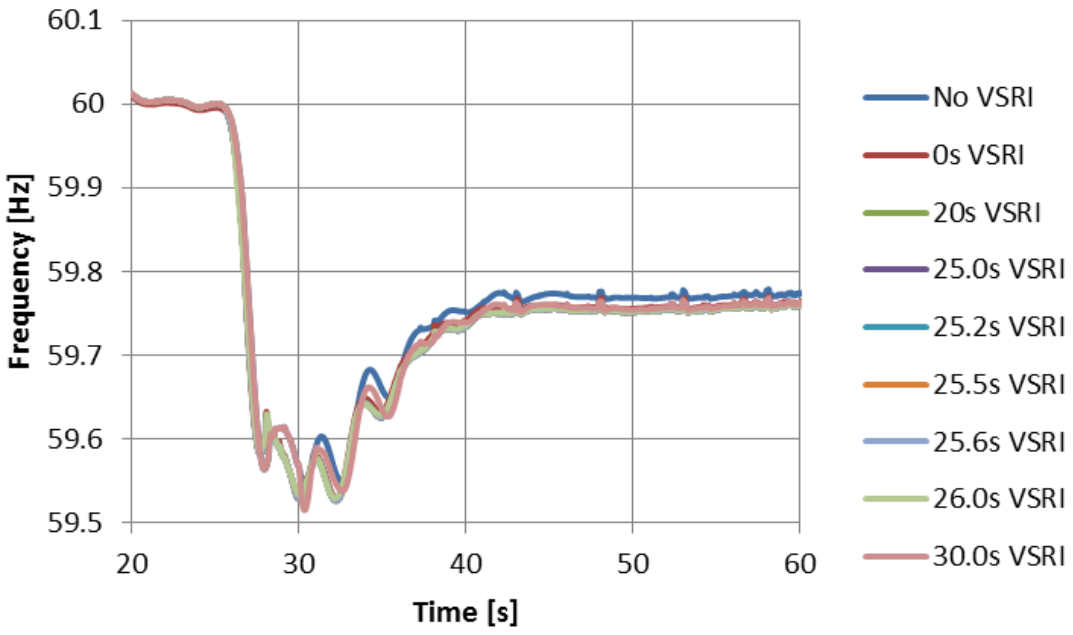

Figure 89. Frequency for VSRI Insertion for June 14 2004 Event (Baseline Case)

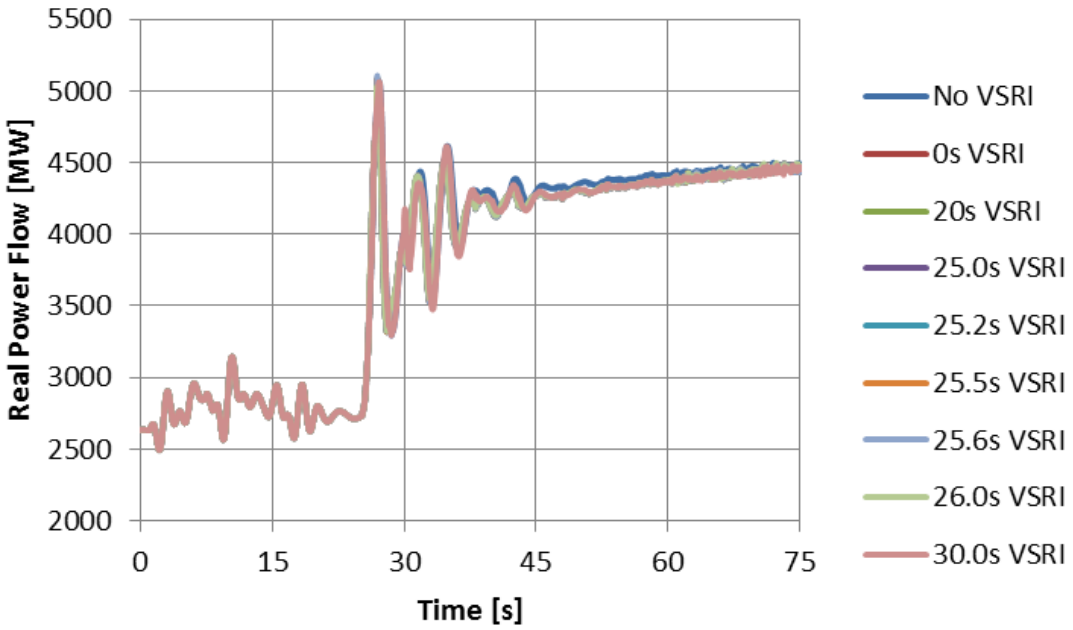

Figure 90. COI Power for VSRI Insertion for June 14 2004 Event (Baseline Case)

The ’26.0s VSRI’ simulation is compared against the ‘No VSRI’ simulation to clearly demonstrate how the control scheme operates for this event if it was placed in service. The historical data shows that the trigger would occur around 25.7 seconds, but 300 ms are

added to this time as an assumption for time delays due to measurement, communications both to the control center and back to the field, and controller delays. Transient voltage is maintained above 1.0 per unit (500kV) and improved about 40kV in the post-transient timeframe (Figure 91). Phase angle experiences a step change reduction during the first swing, which improves the amplitude of phase angle throughout the simulation and improves transient stability (Figure 92). Minimal effect is experienced on system frequency (Figure 93) and COI real power (Figure 94).

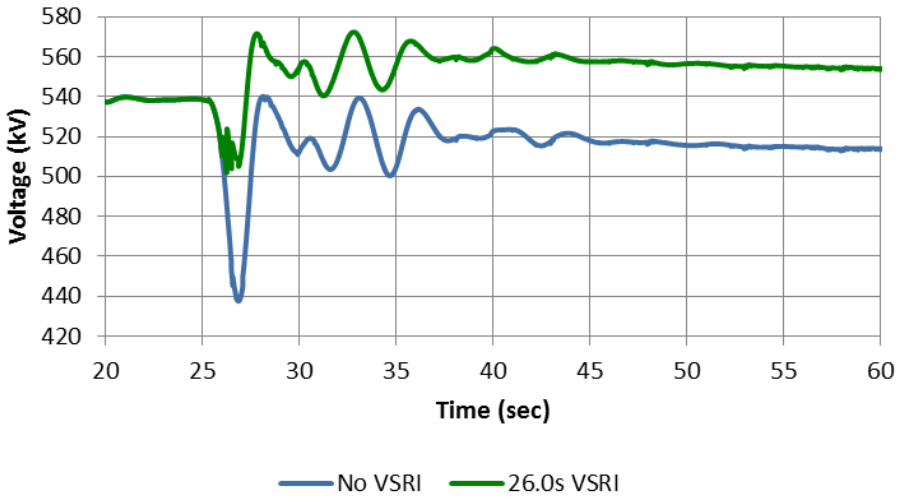

Figure 91. Voltage for June 14 2004 Event Expected VSRI (Baseline Case)

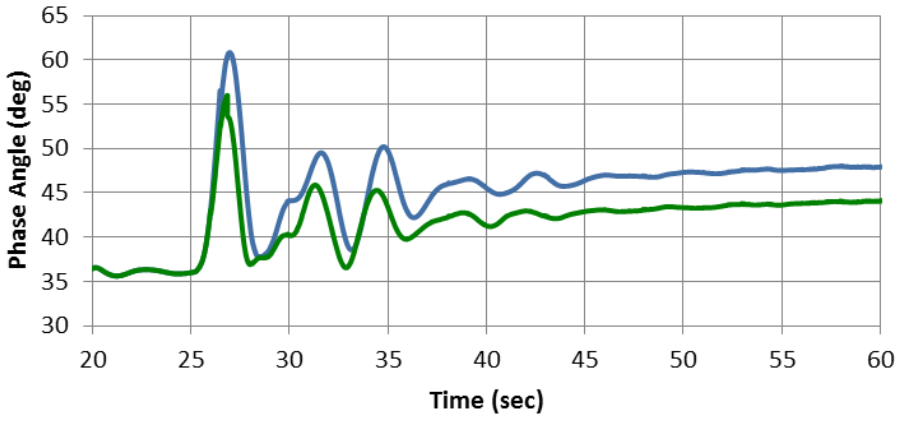

Figure 92. Angle for June 14 2004 Event Expected VSRI (Baseline Case)

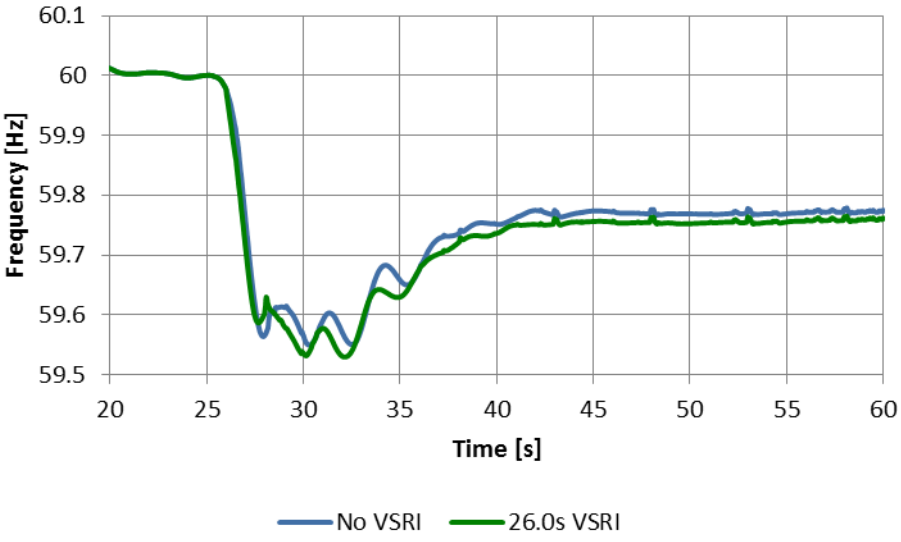

Figure 93. Frequency for June 14 2004 Event Expected VSRI (Baseline Case)

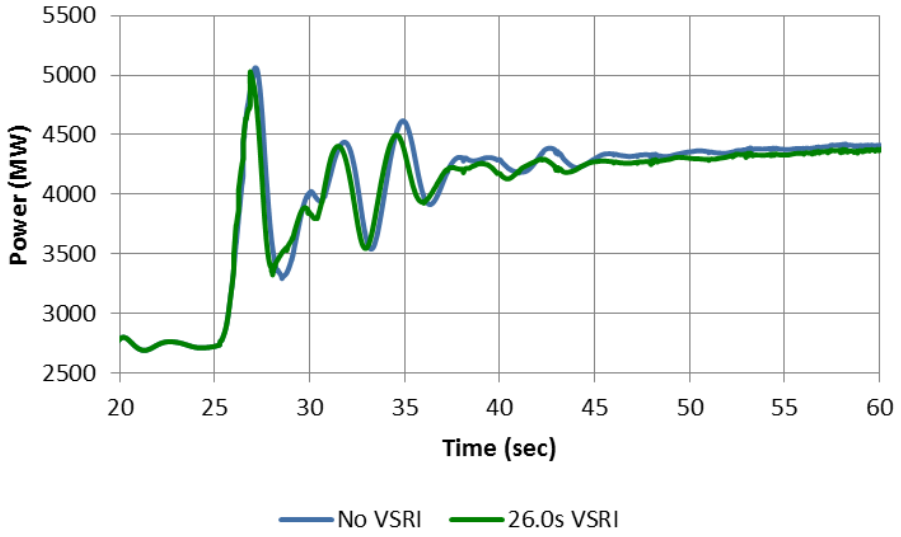

Figure 94. COI Real Power for June 14 2004 Event Expected VSRI (Baseline Case)

The original baseline case is augmented to reflect higher levels of stress across WECC by redispatching generation, returning outaged lines to service, and increasing flows on major paths such as the COI. The conditions created reflect a potential operating condition for that day that could have likely occurred. For example, change in temperature in California could cause higher imports from the north, high river runoff conditions could result in high Canada and Pacific Northwest exports, or fuel and/or market price could change the economic dispatch of thermal generation which could rearrange regional flows.

The updated model is tested against the same contingency definition, with varying VSRI timing. Note that the remaining figures in this section show numerical instability for one of the cases, which results in bad simulated data. However, the numerical results from that simulation are included to show instability.

Voltage magnitude demonstrates the arresting capability of the VSRI against eminent collapse. It is determined that any VSRI control action after 26.3 seconds cannot maintain stability following the N-3 Palo Verde nuclear unit outage. Reducing the trigger time from 26.4 seconds to 25.5 seconds, Figure 95 shows the improvement in response. Furthermore, Figure 96 shows the first swing voltage magnitude. The minute step changes in voltage magnitude are due to the reactive switching events across the BPA system. Note how the faster timing of the VSRI trigger results in improved damping and voltage dip. Comparing the 26.3s action with 25.5 seconds action, transient voltage dip is improved by approximately 70kV. Phase angle (Figure 97), frequency (Figure 98), and COI real power (Figure 99) experience similar improvement.

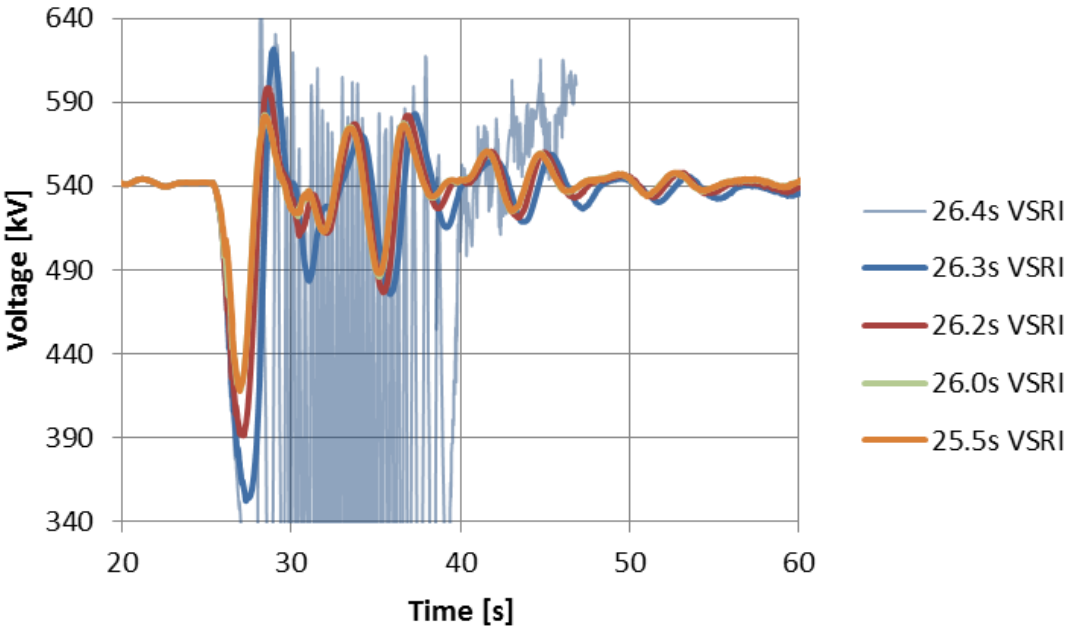

Figure 95. Voltage for June 14 2004 Event Expected VSRI (Stressed Case)

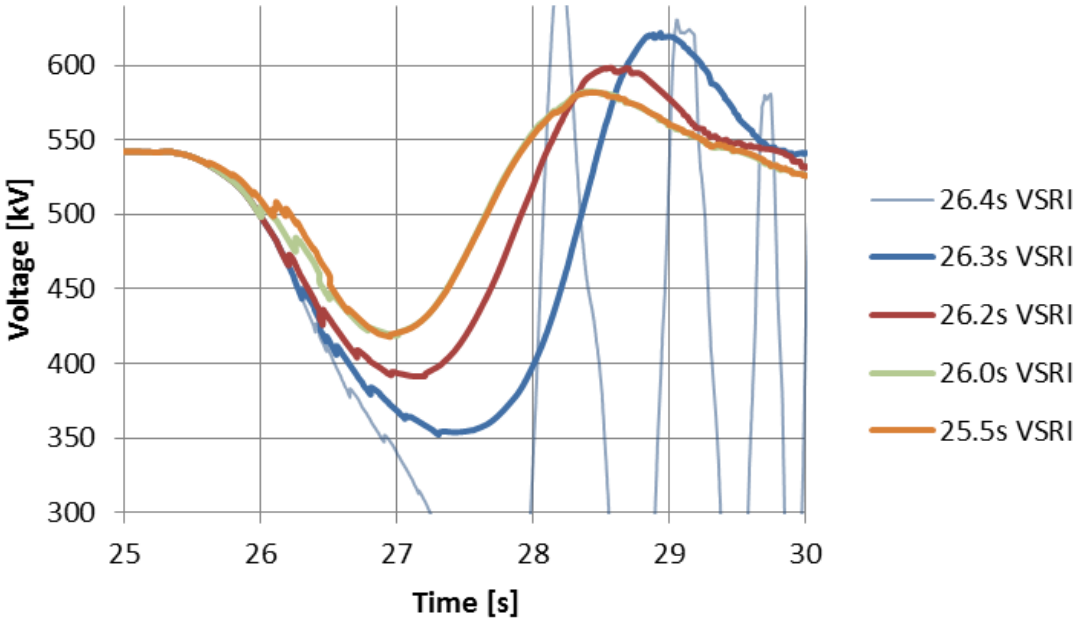

Figure 96. Voltage Swing for June 14 2004 Event Expected VSRI (Stressed Case)

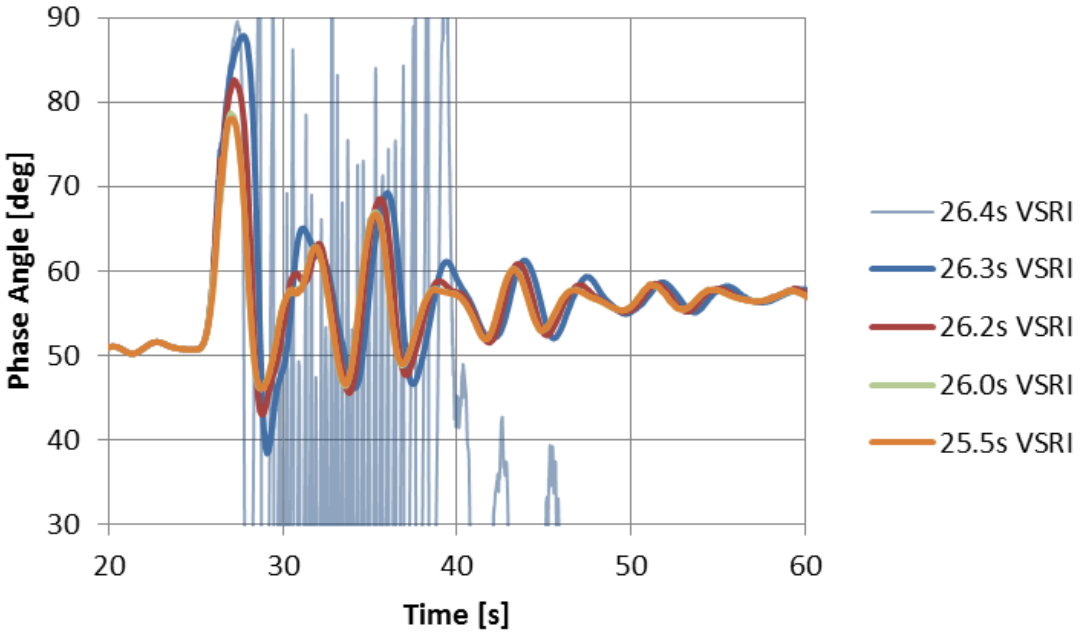

Figure 97. Phase Angle for June 14 2004 Event Expected VSRI (Stressed Case)

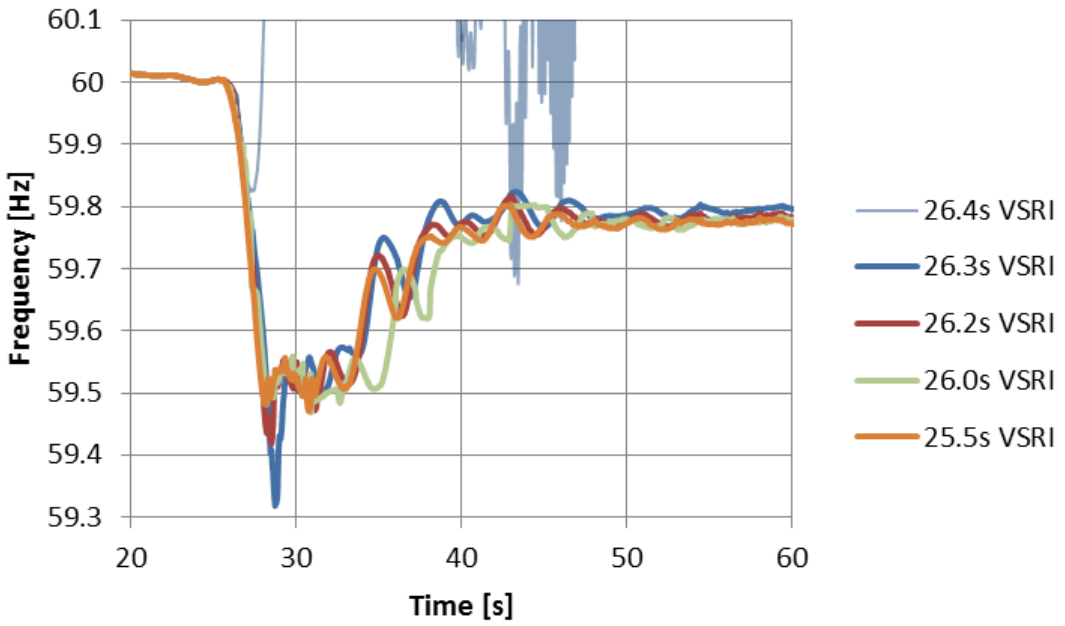

Figure 98. Frequency for June 14 2004 Event Expected VSRI (Stressed Case)

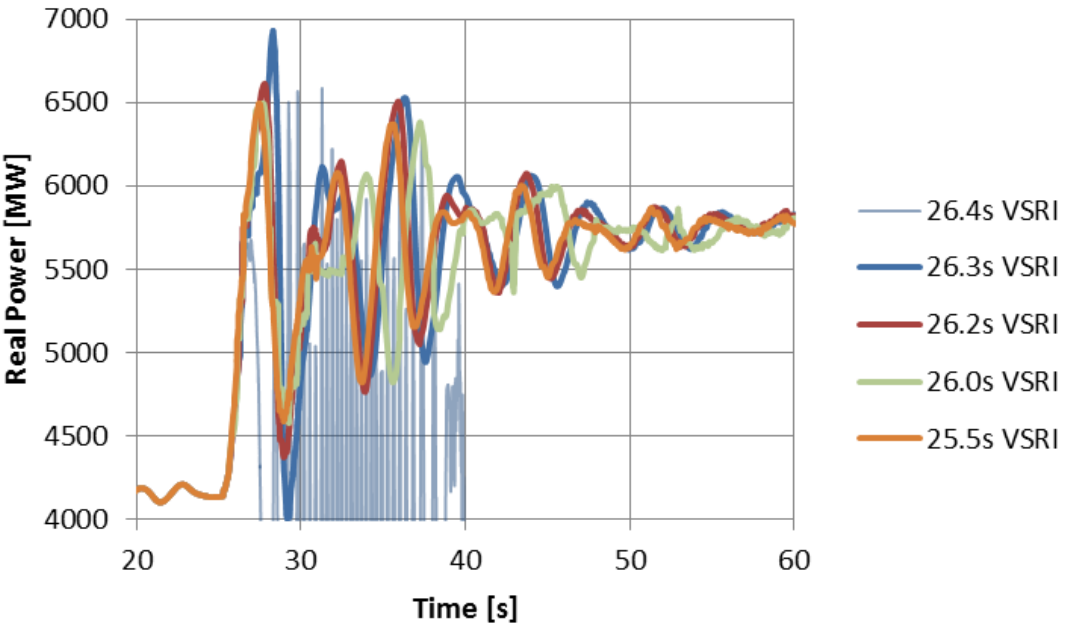

Figure 99. COI Real Power for June 14 2004 Event Expected VSRI (Stressed Case)

As with the baseline case, the ’26.0s VSRI’ action is compared with the ‘No VSRI’ action; however, note that the ‘No VSRI’ contingency is unstable for this operating point. The VSRI control action is able to maintain stability for a Category D contingency in the WECC, and acts as a highly effective ‘safety net’ scheme for BPA and the WECC [39].

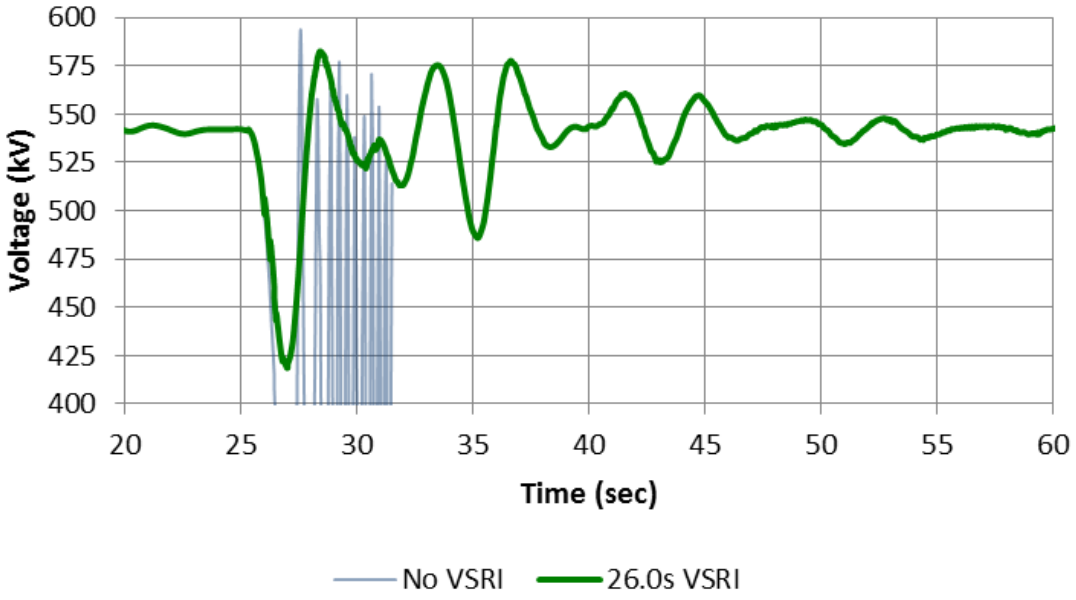

Figure 100. Voltage for June 14 2004 Event Expected VSRI (Stressed Case)

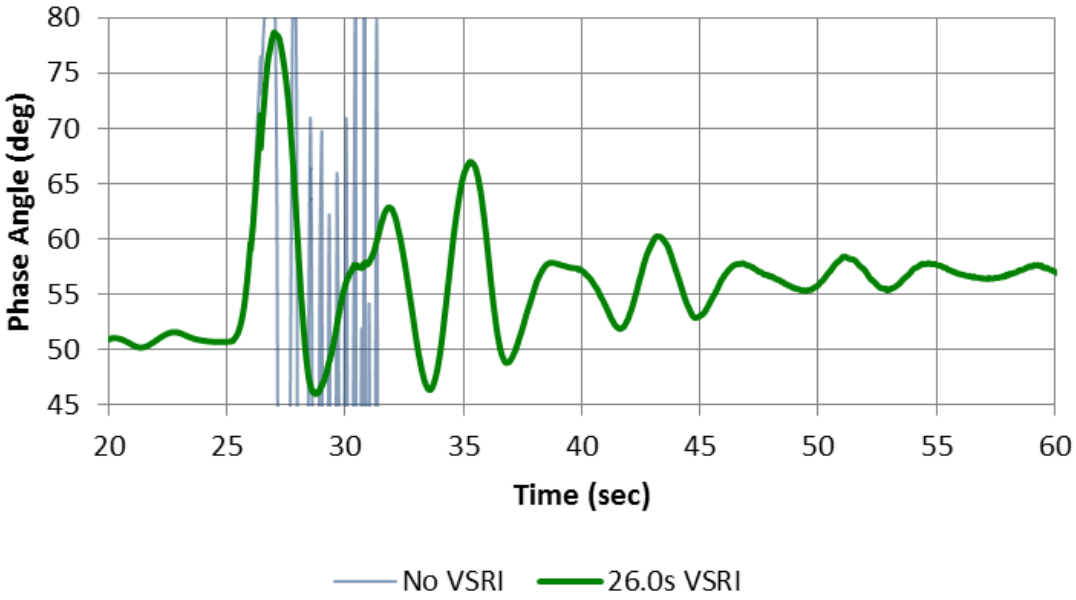

Figure 101. Angle for June 14 2004 Event Expected VSRI (Stressed Case)

4.5. Summary of Findings and Conclusions

Response-based controls using real-time synchronized phasor measurements have a number of significant benefits for improved reliability and "safety net" schemes:

1. Existing event-driven remedial action schemes do not capture changing system conditions outside the BPA-observable region. The major advantage is the independence of RAS schemes, but the major drawback is unresponsiveness to degrading conditions where action is needed.
2. Existing event-driven Line Loss Logic RAS can be efficiently supplemented with response-based schemes using the existing infrastructure. Additional inputs from a new synchrophasor-based control system can be integrated into existing controllers.
3. Unbalanced frequency response in the WECC creates large power swings across the Interconnection for major line and generation outages.
4. PMU measurements provide fast, geographically diverse, time-synchronized measurement for real-time control of power systems.
5. In particular, real power and angle measurements from PMUs can detect large changes in system conditions in a relatively short amount of time. The rate-of-change of these quantities have proved to be effective measures of large disturbances.
6. Timers for varying threshold levels, similar to inverse time characteristic relaying, are used to capture different system responses.
7. Fast detection of changing system conditions can occur with sufficient time for remedial action to be taken, including PMU measurement, algorithm detection, communication delays, and breaker action.

The response-based control strategy, using existing wide-area controls based on PMU measurements, also have key benefits:

1. Voltage Stability Reactive Insert (VSRI) provides wide-area voltage support following major outages on the BPA system.

2. Inclusion of external events detected using the PMU response-based RAS scheme to the VSRI trigger expands the breadth and capability of control for large disturbances.
3. The VSRI is tested and proved effective for alleviating and mitigating transient voltage dip violations and post-contingency low voltage violations.
4. Wide-area controls of VSRI are shown to improve responses for real power flow on the California-Oregon Intertie (COI), wide area BPA voltages, and phase angle differences across BPA and the WECC, with minimal degradation of system frequency across the Interconnection.
5. Most importantly, the response-based VSRI is proved to maintain stability for severely large disturbances in the WECC. This includes the potential N-3 Palo Verde outage, which occurred in 2004.

The conjunction of synchrophasor response-based control algorithms with wide-area response-based reactive switching provides major benefits to system reliability for large-scale outages within an Interconnection.

Chapter 5. Conclusions and Future Work

The research performed in this dissertation is multifaceted, but aims at expanding the understanding, tools, and applications for synchrophasor technology in the electric power industry. Although wide area synchronized phasor measurement was first developed and deployed over 25 years ago, the technology is relatively adolescent with respect to its implementation and integration into existing measurement and control applications. Utilities across the world, including the Bonneville Power Administration and WECC, are making remarkable investments in this technology with the goal of providing faster, higher resolution, time stamped data. This information can hopefully unlock new and innovative solutions for offline tools as well as online applications.

5.1. Conclusions

Power system reliability is a comprehensive subject; it includes adequately planning for expected conditions and disturbances, operating the grid within acceptable limits, and implementing tools and control schemes to mitigate the potential for cascading outages when events inevitably occur. The research presented here focuses on utilizing synchrophasor data to improve operation and automated control of the grid.

As production-grade PMUs become available, grid operators can take advantage of synchronized phase angle measurements. As an indicator of system stress, and a potential precursor to large-scale outages, utilizing phase angle in real-time applications such as visualization and alarming can provide operators with improved situational awareness [1, 33]. At the time of writing, setting limits on wide area phase angles is a relatively unexplored aspect of synchrophasor applications. This work illustrates the concepts related to any phase angle alarming tool or application, and demonstrates these findings through study of the BPA transmission system. A methodology for clustering PMUs and determining phase angle limits is presented for offline studies; recommendations are also made for utilizing these concepts in a real-time application.

The initial hypothesis of setting limits on wide area representative angles is prone to misclassification because of the variability of generation, load, and transmission between the clusters. Within a transmission corridor, topology plays a major role in both the phase

angle and its limits, and these limits must be updated to reflect the topology at a given instant. Lower voltage systems such as 230kV or 115kV may have a noticeable impact on phase angle limits if they lie within the corridor. Studies can be performed to determine which lines have significant impact on angle limits. A real-time application should be adaptive to changing system topology to provide more accurate representation of system conditions. On the other hand, topology changes outside the corridor have minimal effect on the corridor angle limits when dealing with security assessment. Transient stability limits can be captured through wider area limits, but are highly dependent on factors that cannot be captured solely through phase angle. Therefore, misclassification may also be greater for these limits.

Pre-contingency operating conditions can be a supplemental input to operator situational awareness for low damping conditions. A specific high-risk operating region is tested through transient stability and offline study classification trees. The decision trees provide the pre-contingency measurements and their respective thresholds that indicate poorly damped conditions based on the study results. Strongest indicators include North-South real power flows and angle differences in or adjacent to the BPA network. The full WECC dataset and the BPA restricted dataset of measurements perform similarly; low damping can be captured through BPA synchrophasor measurements. Classification of the decision trees is greater than 90%; this may not be acceptable for online tools, but provides useful offline study information. The decision tree results are used create possible online tools using logic diagrams and multi-dimensional nomograms. Although classification accuracy may be reduced, operators are more likely to accept these existing tools and integrate them with current operating procedures.

Offline planning and real-time monitoring of security and system state are not always sufficient for reliable operation. Use of automated remedial action schemes (RAS) is growing due to their ability to meet reliability criteria at a significantly lower cost than building transmission infrastructure. Most BPA RAS is event-driven based on predetermined system conditions from offline planning studies. The reporting rate and geographic synchronism of synchrophasors allows for response-based actions immediately following a disturbance. Large generation and transmission outages create significant

fluctuations in real power across the system due to generator frequency response and redistribution of flows. These changes can be picked up using intertie real power flow and phase angle difference. Specifically, the rate-of-change of these system variables provides an effective means of detecting large events. While minor events or sudden changes in response can endure a large rate-of-change magnitude, these events are usually not sustained. On the other hand, large outages can cause severe oscillations or large excursions from steady state, which are sustained over a given period of time. Simulated contingencies, validated simulation events, and historical PMU data are all used to select appropriate threshold values for the design parameters.

The focus of the research relating to response-based synchrophasor RAS is on diversifying the potential control schemes that can improve system reliability. A controllable shunt reactive support scheme, the Voltage Stability Reactive Insertion (VSRI), is triggered by the response-based algorithms discussed. The capability of responding to changing system conditions rather than triggering solely on event-driven outages can improve reliability of the grid by expanding the breadth of contingencies to protect against. As a complement to the Fast AC Reactive Insert (FACRI), the VSRI can improve transient and post-transient voltages as well as other forms of support such as decreased phase angle during the first transient swing. Response-based VSRI has proved effective through studies for maintaining stability in the case of failed RAS action and severe N-3 contingencies.

The grid is operated within strict reliability guidelines; however, recent outages have shown that improved operator situational awareness and special protection schemes can play a critical role. This work aims at providing insight into the concepts and implementation concerns of using phase angles for operator alarms. Additionally, existing event-driven RAS is expanded to consider large events undetectable with existing measurement techniques. This response-based RAS scheme takes advantage of the synchronism and geographic diversity of synchrophasors. Therefore, the presented work provides an improvement over present methods and implementation strategies.

5.2. Major Contributions

Chapter 1 explores the sequence of events and causes of the Southwest California-Arizona blackout in 2011. The outage report highlights the need for improved operator situational awareness and the implications of response-based remedial action schemes. Bonneville Power Administration is developing a control-quality synchrophasor wide area situational awareness and control infrastructure. Proposed applications include Phase Angle Alarming and response-based Synchrophasor RAS.

In terms of the phase angle alarming application, the following contributions of this dissertation include:

- Adaptation of probabilistic rms-coherency clustering of a defined set of PMUs for a full power system model.
- Determination of PMU clustering based on coherency for the BPA WAMS.
- Analysis and determination that wide area phase angle limits based on static security are not accurately classifiable or recommended.
- A study methodology using inter-cluster PMUs for setting limits on phase angles based on static security assessment.
- Implementation strategy recommendations for offline study or real-time tools.
- Analysis and initial selection of phase angle limits for the BPA phase angle alarming application.
- Study of WECC risk to low damping conditions through data mining tools, specifically application of decision trees for offline studies.
- Identification of key indicators of poorly damped system conditions in the event of a severe outage.
- Development of potential online tools based on the offline study results, including a multi-dimensional nomogram and logic diagram.
- Study of the interaction between steady state damping tools such as the ‘Mode Meter’ and studied post-contingency oscillation damping levels.

For the Synchrophasor RAS system, the contributions include:

- Analysis of past disturbances in the WECC and their effects on the BPA footprint during transient and post-transient timeframes.
- A response-based event detection algorithm based on the California-Oregon Intertie (COI) real power rate-of-change that detects relatively large generation and transmission outages.
- A complementary response-based event detection algorithm based on BPA control area wide area phase angle differences and their rate-of-change.
- Synchrophasor-based RAS controller algorithm design and implementation strategy.
- Expansion of the Voltage Stability Reactive Insert (VSRI) RAS based on synchrophasor measurement initiation.
- Demonstration of the SP RAS-controlled VSRI as a safety net scheme for existing RAS to maintain stability for severe outages including an N-3 Palo Verde outage.

5.3. Future Work

The phase angle alarming work provides BPA and the industry with a better understanding of the implications of setting limits on phase angles. The study method provides a highly classifiable dynamic limit; however, there is room for improvement in terms of application. The study is performed on a few root cases that explore the impacts of various operating conditions. The limits extracted provide initial values for an alarming application. These limits cannot be maintained for an extended amount of time. A utility must decide how it plans on implementing a phase angle limit algorithm based on the capabilities of existing resources. For example, a utility highly dependent on its state estimator and real-time contingency analysis tools would expect to have a tool capable of integration with these applications. Therefore, implementation of an alarming tool would be embedded in the energy management system (EMS) or other synchrophasor wide area measurement system (WAMS). On the other hand, if the state estimator is not used for real-time operation and control decisions, offline studies may be more desirable. Integration of safety net phase angle limits with real power-based System Operating Limits (SOLs) is an alternative solution.

The complexity of relating phase angles with system damping is significant. Around a specific operating point, angle may be able to help provide indication of acceptable operating limits. However, expanding this operating space creates gross misclassification of the operating point based on angle measurements. More work needs to be done to better understand the relationship between angle difference and damping, and identify a simple method for informing operators of potentially poorly damped conditions based on PMU measurements such as phase angle. Furthermore, an effective damping analysis tool would provide the industry with more confident and efficient means of measuring oscillation damping following disturbances in both real and simulated data.

Next steps of the synchrophasor response-based remedial action scheme include prototyping the RAS controller, testing its design offline, and monitoring the algorithm performance during online 'test mode'. Online analysis of algorithm response to ambient data and disturbances helps build confidence in the algorithms as well as further refines the threshold values set in the controller. The goal of these schemes is to detect severe events on the system, and past disturbance history points to only a handful of applicable events each year. Monitoring the RAS response for operations (correct, false positives, and "fail to operate") quantifies the RAS controller responsiveness to expected events. "Fail to operate" may include expert opinion regarding which contingencies or events the controller should and should not operate for. To test this, the algorithms are being implemented in a MATLAB-based online testing environment which reads in real-time PMU data from a PDC.

In terms of algorithm development, there is room for further expansion and elaboration. The opportunities with wide area measurement and response-based control are endless, but careful selection of effective algorithms is necessary. The algorithms should be simple yet effective to minimize the maintenance and updating of algorithms, and minimize unnecessary redundancy. For example, a restraint option could be implemented within the algorithms to detect events that will not result in overvoltage conditions, such as lost generation in Canada for export conditions to California. This could increase security of the algorithms but reduce dependability.

Further work on the controllable VSRI scheme could include analyzing additional historical PMU data, simulated data, and validated simulated disturbances. Expanding the scope of analysis by running sensitivity cases and scenario cases increases the confidence in applying the VSRI as a safety net scheme. In particular, a more recent validated N-2 disturbance could be used to test the VSRI for a wide array of operating points around the base case. Moreover, changes in system topology and pre-contingency status of the shunt reactive devices could change the benefit of the VSRI following the contingencies.

References

[1] U.S-Canada Power System Outage Task Force, "Final Report on the August 14, 2003 Blackout in the United States and Canada: Causes and Recommendations," US/Canada, 2004.

[2] Staffs of FERC and NERC, "Arizona-Southern California Outages on September 8, 2011: Causes and Recommendations," FERC/NERC, 2012.

[3] NERC, "North American Electric Reliability Corporation," 2012. [Online]. Available: http://www.nerc.com/.

[4] NASPI, "NASPI - North American Synchrophasor Initiative," 2012. [Online]. Available: https://www.naspi.org/.

[5] A. Phadke, "Synchronized phasor measurements in power systems," *IEEE Computer Applications in Power* , vol. 6, pp. 10-15, 1993.

[6] J. Thorp, A. Phadke and K. Karimi, "Real Time Voltage Phasor Measurement for Static State Estimation," *IEEE Transactions on Power Apparatus and Systems,* Vols. PAS-104, pp. 3098-3106, 1985.

[7] B. Agrawal and D. Kosterev, "Model Validation Studies for a Disturbance Event That Occurred on June 14 2004 in the Western Interconnection," in *2007 IEEE Power Engineering Society General Meeting*, 2007.

[8] D. Kosterev, C. Taylor and W. Mittelstadt, "Model Validation for the August 10, 1996 WSCC System Outage," *IEEE Transactions on Power Systems,* vol. 14, no. 3, pp. 967-979, 1999.

[9] D. Kosterev, "Hydro turbine-governor model validation in pacific northwest," *IEEE Transactions on Power Systems,* vol. 19, no. 2, pp. 1144-1149, 2004.

[10] C. Taylor, D. Erickson, K. Martin, R. Wilson and V. Venkatasubramanian, "WACS-Wide-Area Stability and Voltage Control System: R&D and Online Demonstration," *Proceedings of the IEEE,* vol. 93, no. 5, pp. 892-906, 2005.

[11] R. Wilson and C. Taylor, "Using dynamic simulations to design the wide-area stability and voltage control system (WACS)," *IEEE PES Power Systems Conference and Exposition, 2004,* pp. 100-107, 2004.

[12] C. Taylor, "BPA's wide-area stability and voltage control system (WACS) for blackout prevention," *Power Systems Conference and Exposition, 2004,* pp. 10-13, 2004.

[13] Bonneville Power Administration, "BPA - Bonneville Power Administration," 2012. [Online]. Available: http://www.bpa.gov/.

[14] Western Electricity Coordinating Council, "WECC -Western Electricity Coordinating Council," 2012. [Online]. Available: http://www.wecc.biz/.

[15] WECC, "The Western Interconnection Synchrophasor Program (WISP)," 2012. [Online]. Available: http://www.wecc.biz/awareness/pages/wisp.aspx.

[16] J. De La Ree, V. Centeno, J. Thorp and A. Phadke, "Synchronized Phasor Measurement Applications in Power Systems," *IEEE Transactions on Smart Grid,* vol. 1, pp. 20-27, 2010.

[17] D. Novosel, V. Madani, B. Bhargava, K. Vu and J. Cole, "Dawn of the Grid Synchronization," *IEEE Power and Energy Magazine*, pp. 49-60, January/February 2008.

[18] V. Terzija, G. Valverde, D. Cai, P. Regulski, V. Madani, J. Fitch, S. Skok, M. Begovic and A. Phadke, "Wide-Area Monitoring, Protection, and Control of Future Electric Power Networks," *Proceedings of the IEEE*, vol. 99, no. 1, pp. 80-93, 2011.

[19] E. Schweitzer, D. Whitehead, G. Zweigle and K. Ravikumar, "Synchrophasor-based power system protection and control applications," *2010 63rd Annual Conference for Protective Relay Engineers*, pp. 1-10, 2010.

[20] P. Kundur, J. Paserba, V. Ajjarapu, G. Andersson, A. Bose, C. Canizares and et al., "Definition and classificaiton of power system stability IEEE/CIGRE joint task force on stability terms and definitions," *IEEE Transactions on Power Systems*, vol. 19, pp. 1387-1401, 2004.

[21] NERC, "Glossary of Terms Used in NERC Reliability Standards," North American Reliability Corporation, 2012.

[22] NERC, "Definition of 'Adequate Level of Reliability'," North American Electric Reliability Corporation, 2012.

[23] L. Fink and K. Carlsen, "Operating Under Stress and Strain," *IEEE Spectrum*, pp. 48-53, 1978.

[24] P. Kundur, Power System Stability and Control, New York: McGraw-Hill, Inc., 1994.

[25] K. Tomsovic, D. Bakken, V. Venkatasubramanian and A. Bose, "Designing the Next Generation of Real-Time Control, Communication, and Computations for Large Power Systems," *Proceedings of the IEEE*, vol. 93, no. 5, pp. 965-979, 2005.

[26] Z. Ming, V. Centeno, J. Thorp and A. Phadke, "An Alternative for Including Phasor Measurements in State Estimators," *IEEE Transactions on Power Systems*, vol. 21, pp. 1930-1937, 2006.

[27] "IEEE Standard for Synchrophasor Measurements for Power Systems," *IEEE Std C37.118.1-2011 (Revision of IEEE Std C37.118-2005)*, pp. 1-61, 2011.

[28] North American Electric Reliability Corporation, "Real-Time Application of Synchrophasors for Improving Reliability," NERC, Princeton, NJ, 2010.

[29] "IEEE Standard for Synchrophasor Data Transfer for Power Systems," *IEEE Std C37.118.2-2011 (Revision of IEEE Std C37.118-2005)*, pp. 1-53, 2011.

[30] K. Martin, "Phasor measurement systems in the WECC," *IEEE Power Engineering Society General Meeting, 2006*, pp. 1-7, 2006.

[31] Federal Energy Regulatory Commission, "FERC - Federal Energy Regulatory Commission," 2012. [Online]. Available: http://www.ferc.gov/.

[32] WECC, "WECC Fact Sheet," 2012. [Online]. Available: http://www.wecc.biz/About/Documents/WECC_FactSheet.pdf.

[33] Federal Energy Regulatory Commission, "Staff Report on the Arizona-Southern California Outages on September 8, 2011.," 2012.

[34] Western Electricity Coordinating Council, "NERC/WECC Planning Standards," WECC, 2003.

[35] P. Corporation, "PowerWorld Simulator," 1997. [Online]. Available: http://www.powerworld.com/products/simulator/overview. [Accessed 2013].

[36] General Electric, "Concorda PSLF Simulation Engine," GE, 2012. [Online]. Available: http://www.ge-energy.com/products_and_services/products/concorda_software_suite/concorda_pslf_simulation_engine.jsp.

[37] S. AG, "PSS Product Suite - PSS/E," 2002-2013. [Online]. Available: http://www.energy.siemens.com/us/en/services/power-transmission-distribution/power-technologies-international/software-solutions/pss-e.htm. [Accessed 2013].

[38] M. Glavic, D. Novosel, E. Heredia, D. Kosterev, A. Salazar, F. Habibi-Ashrafi and M. Donnelly, "See It Fast to Keep Calm: Real-Time Voltage COntrol Under Stressed Conditions," *IEEE Power and Energy Magazine,* vol. 10, no. 4, pp. 43-55, July 2012.

[39] NERC, "TPL-001 - TPL-004," NERC Transmission Planning (TPL) Standards, 2011.

[40] C. Martinez, S. Xue and M. Martinez, "Review of the Recent Frequency Performance of the Eastern, Western, and ERCOT Interconnections," Lawrence Berkeley National Laboratory, 2010.

[41] Frequency Task Force of the NERC Resource Subcommittee, "Frequency Response White Paper," NERC, 2004.

[42] R. Cummings, "Overview of Frequency Response Initiative," NERC, 2010.

[43] North American Electric Reliability Corporation, "Frequency Response Standard Background Document," NERC, 2012.

[44] G. Prony, "Essai experimental et analytique ...," *J. l'Ecole Polytech. (Paris),* vol. 1, pp. 24-76, 1795.

[45] J. Hauer, "Initial Results in the Use of Prony Methods to Determine the Damping and Modal Composition of Power System Dynamic Response Signals," Bonneville Power Administration, Portland OR, 1988.

[46] J. Hauer, *Fast Damping Estimators for Use with the Transient Stability Program,* Communicated to WSCC 0.7Hz Ad Hoc Work Group on October 22, 1987, BPA Memorandum, Feb 20, 1987.

[47] F. Hildebrand, Introduction to Numerical Analysis, New York: McGraw-Hill, 1956.

[48] J. Hauer, C. Demeure and L. Scharf, "Initial Results in Prony Analysis of Power System Response Signals," *IEEE Transactions on Power Systems,* vol. 5, pp. 80-89, 1990.

[49] J. Hauer, "Application of Prony Analysis to the Determination of Modal Content and Equivalent Models for Measured Power System Response," *IEEE Transactions on Power Systems,* vol. 6, no. 3, pp. 1062-1068, 1991.

[50] D. Trudnowski, J. Johnson and J. Hauer, "Making Prony Analysis More Accurate using Multiple Signals," *IEEE Transactions on Power Systems,* vol. 14, no. 1, pp. 226-231, 1999.

[51] National Institue of Standards and Technology, "Pseudo Inverse," NIST, 21 1 2009. [Online]. Available: http://www.itl.nist.gov/div898/software/dataplot/refman2/auxillar/pseudinv.htm.

[Accessed 2013].

[52] R. Kumaresan, D. Tufts and L. Scharf, "A Prony Method for Noisy Data: Choosing the Signal Components and Selecting the Order in Exponential Signal Models," *Proceedings of the IEEE,* vol. 72, no. 2, pp. 230-233, 1984.

[53] C. Taylor, Power System Voltage Stability, New York: McGraw-Hill, 1994.

[54] North American Electric Reliability Corporation, "Reactive Support and Control Whitepaper," TIS - Reactive Support and Control Subteam, Princeton, NJ, 2009.

[55] L. Pereira, "Cascade to black," *IEEE Power and Energy Magazine,* vol. 2, no. 3, pp. 54-57, 2004.

[56] C. Taylor and D. Erickson, "Recording and analyzing the July 2 cascading outage [Western USA power system]," *IEEE Computer Applications in Power,* vol. 10, no. 1, pp. 26-30, 1997.

[57] C. Taylor, "Improving grid behaviour," *IEEE Spectrum,* vol. 36, no. 6, pp. 40-45, 1999.

[58] Federal Energy Regulatory Commission, "Principles for Efficient and Reliabile Reactive Power Supply and Consumption," Washington DC, 2005.

[59] F. Kiessling, P. Nefzger, J. Nolasco and U. Kaintzyk, Overhead Power Lines: Planning, Design, Construction, Berlin: Springer-Verlag, 2003.

[60] B. Weedy, B. Cory, N. Jenkins, J. Ekanayake and G. Strbac, Electric Power Systems, 5th ed., Chichester, United Kingdom: Wiley, 2012.

[61] M. El-Hawary, Electrical Power Systems: Design and Analysis, Piscataway, NJ: IEEE Press, 1995.

[62] A. Guile and W. Paterson, Electrical Power Systems, Pergamon Press, 1977.

[63] IEEE Power & Energy Society Transmission and Distribution Committee, "IEEE Guide for Application of Shunt Power Capacitors," *IEEE Std 1036-2010 (Revision of IEEE Std 1036-1992),* pp. 1-85, 2011.

[64] Bonneville Power Administration, "System Electrical Data - Shunt Capacitors," BPA, Vancouver, WA, 2012.

[65] Bonneville Power Administration, "Voltage Schedules," BPA, Vancouver, WA, 2012.

[66] B. Ray, "Enhancing power system dynamic and steady-state performance with past-switched shunt compensation to postpone major bulk transmission capital investments," in *1998 IEEE 8th International Conference on Transmission & Distribution Construction, Operation & Live-Line Maintenance,* 1998.

[67] E. Kimbark, "Improvement of System Stability by Switched Series Capacitors," *IEEE Transactions on Power Apparatus and Systems,* Vols. PAS-85, no. 2, pp. 180-188, 1966.

[68] North American Electric Reliability Corporation, "PRC-023 Reference: Determination and Application of Practical Relaying Loadability Ratings," System Protection and Control Task Force of the NERC Planning Committee, Princeton, NJ, 2007.

[69] "IEEE Standard for Series Capacitor Banks in Power Systems," *IEEE Std 824-2004 (Revision of IEEE Std 824-1994),* pp. 1-53, 2005.

[70] W. Mittelstadt, "Four Methods of Power System Damping," *IEEE Transactions on*

Power Apparatus and Systems, Vols. PAS-87, no. 5, pp. 1323-1329, 1968.

[71] D. Kosterev and W. Kolodziej, "Bang-Bang Series Capacitor Transient Stability Control," *IEEE Transactions on Power Systems,* vol. 10, no. 2, pp. 915-924, 1995.

[72] M. El-Sharkawi, Fundamentals of Electric Drives, Toronto: Cengage Learning, 2000.

[73] A. Fitzgerald, C. Kingsley, Jr. and S. D. Umans, Electric Machinery, Sixth ed., New York: McGraw-Hill, 2003.

[74] D. Kosterev, "Design, installation, and initial operating experience with line drop compensation at John Day powerhouse," *IEEE Transactions on Power Systems,* vol. 16, no. 2, pp. 261-265, 2001.

[75] G. Heydt, S. Kalsi and E. Kyriakides, "A Short Course on Synchronous Machines and Synchronous Condensers," PSERC, 2003.

[76] NASPI, "NASPI Visualization Workshop," Orlando, FL, 2012.

[77] S. Sastry and P. Varaiya, "Coherency for Interconnected Power Systems," *IEEE Transactions on Automatic Control,* Vols. AC-26, pp. 218-226, 1981.

[78] R. Podmore, "Identification of Coherent Generators for Dynamic Equivalents," *IEEE Transactions on Power Apparatus and Systems,* Vols. PAS-97, no. 4, pp. 1344-1354, 1978.

[79] S. Lee and F. Schweppe, "Distance Measures and Coherency Recognition for Transient Stability Equivalents," *IEEE Transactions on Power Apparatus and Systems,* Vols. PAS-92, no. 5, pp. 1550-1557, 1973.

[80] I. Kamwa, A. Pradhan and G. Joos, "Automatic Segmentation of Large Power Systems into Fuzzy Coherent Areas for Dynamic Vulnerability Assessment," *IEEE Transactions on Power Systems,* vol. 22, pp. 1974-1985, 2007.

[81] I. Kamwa and R. Grondin, "PMU Configuration for System Dynamic Performance Measurement in Large Multiarea Power Systems," *IEEE Transactions on Power Systems,* vol. 22, pp. 385-394, 2002.

[82] I. Kamwa, R. Grondin and L. Loud, "Time-varying contingency screening for dynamic security assessment using intelligent-systems techniques," *IEEE Transactions on Power Systems,* vol. 16, pp. 526-536, 2001.

[83] G. Maps, "Map of Pacific Northwest," Google, 2012.

[84] OSIsoft, "The PI System - the industry standard in enterprise infrastructure for management of real-time data and events," 2012. [Online]. Available: http://www.osisoft.com/software-support/what-is-pi/What_Is_PI.aspx. [Accessed 2013].

[85] WECC, "WECC Joint Synchronized Information Subcommittee (JSIS)," 2012. [Online]. Available: http://www.wecc.biz/committees/JSWG/default.aspx.

[86] M. Shelton, P. Winkelman, W. Mittelstadt and W. Bellerby, "Bonneville power administration 1400-MW braking resistor," *IEEE Transactions on Power Apparatus and Systems,* vol. 94, no. 2, pp. 602-611, 1975.

[87] J. Pierre, D. Trudnowski and M. Donnelly, "Initial Results in Electromechanical Mode Identification from Ambient Data," *IEEE Transactions on Power Systems,* vol. 12, no. 3, pp. 1245-1251, 1997.

[88] D. Trudnowski, J. Pierre, N. Zhou, J. Hauer and M. Parashar, "Performance of Three Mode-Meter Block-Processing Algorithms for Automated Dynamic Stability Assessment," *IEEE Transactions on Power Systems,* vol. 23, no. 2, pp. 680-690, 2008.

[89] R. Quint, *Practical Implementation of a Security-Dependability Adaptive Voting Scheme Using Decision Trees,* M.S. Thesis, Dept. Elect. & Comp. Eng., Virginia Polytechnic Inst. & State Univ., Blacksburg, VA, 2011.

[90] E. Bernabeu, *Methodology for a Security-Dependability Adaptive Protection Scheme based on Data Mining,* PhD Dissertation, Dept. Elect. & Comp. Eng., Virginia Polytechnic Ins. & State Univ., Blacksburg, VA, 2009.

[91] E. Bernabeu, J. Thorp and V. Centeno, "Methodology for a Security/Dependability Adaptive Protection Scheme Based on Data Mining," *IEEE Transactions on Power Delivery,* vol. 27, no. 1, pp. 104-111, 2012.

[92] L. Wehenkel, M. Pavella, E. Euxibie and B. Heilbronn, "Decision Tree Based Transient Stability Method: A Case Study," *IEEE Transactions on Power Systems,* vol. 9, no. 1, pp. 459-469, 1994.

[93] K. Sun, S. Likhate, V. Vittal, V. Kolluri and S. Mandal, "An Online Dynamic Security Assessment Scheme Using Phasor Measurements and Decision Trees," *IEEE Transactions on Power Systems,* vol. 22, no. 4, pp. 1935-1943, 2007.

[94] N. Senroy, G. Heydt and V. Vittal, "Decision Tree Assisted Controlled Islanding," *IEEE Transactions on Power Systems,* vol. 21, no. 4, pp. 1790-1797, 2006.

[95] Y. Sheng and S. Rovnyak, "Decision Tree-Based Methodology for High Impedance Fault Detection," *IEEE Transactions on Power Delivery,* vol. 19, no. 2, pp. 533-536, 2004.

[96] Classification and regression trees, Belmont, CA: Wadsworth International Group, 1984.

[97] North American Electric Reliability Corporation, "Special Protection Systems (SPS)/Remedial Action Schemes (RAS): Assessment of Definition, Regional Practices, and Applicaiton of Related Standards," NERC, Atlanta, GA, 2012.

[98] IEEE PSRC Working Group C4, "Global Industry Experiences with System Integrity Protection Schemes (SIPS)," IEEE PSRC, 2009.

[99] S. Horowitz and A. Phadke, Power System Relaying, 3rd ed., Chichester, England: Wiley/Research Studies, 2008.

[100] MathWorks, "MATLAB - The Language of Technical Computing," MathWorks, 2012. [Online]. Available: http://www.mathworks.com/products/matlab/.

[101] J. Hauer, W. Mittelstadt, K. Martin, J. Burns, H. Lee, J. Pierre and D. Trudnowski, "Use of the WECC WAMS in Wide-Area Probing Tests for Validation of System Performance and Modeling," *IEEE Transaction on Power Systems,* vol. 24, no. 1, pp. 250-257, 2009.

Appendix A: Security Analysis Study Results

The following table shows the study results as extracted from the power flow program for classifying and organizing the security assessment.

Seattle-Portland

Case	_01	_02	_03	_04	_05	_06	_07	_08	_09	_10
Node 1 230 Ang	70.59	14.12	62.19	61.15	60.03	57.93	49.23	71.46	71.78	69.26
Node 2 230 Ang	66.08	12.57	58.02	57.50	56.89	55.35	47.25	66.80	67.06	64.28
Node 3 230 Ang	70.12	13.71	61.67	60.68	59.62	57.58	48.93	71.00	71.33	68.83
Node 4 500 Ang	69.18	15.69	61.04	60.55	59.99	58.47	50.37	69.96	70.20	67.55
Node 5 500 Ang	68.18	15.73	60.19	59.85	59.44	58.10	50.20	68.89	69.08	66.23
Node 6 500 Ang	60.12	13.41	53.95	53.74	53.46	52.71	45.47	59.83	59.11	52.26
Node 7 500 Ang	58.78	12.89	53.10	52.90	52.6	51.94	44.76	58.40	57.68	51.33
Node 8 500 Ang	50.44	5.54	43.99	43.85	43.65	43.29	36.46	49.23	48.36	45.13
Node 9 500 Ang	46.37	3.35	39.78	39.70	39.57	39.43	32.95	45.62	45.15	43.15
Node 9 230 Ang	43.56	0.52	36.80	36.73	36.61	36.57	30.12	42.47	41.94	40.58
Node 10 500 Ang	43.93	1.84	37.21	37.17	37.07	37.04	30.76	43.32	42.98	41.86
Node 11 230 Ang	42.82	0.06	35.87	35.84	35.75	36.04	29.71	41.97	41.60	41.72
Node 12 500 Ang	44.41	2.23	37.53	37.51	37.43	37.51	31.24	43.88	43.61	43.13
Path 1	1021	304	798	783	765	692	610	1135	1258	1749
Path 2	2153	1729	2271	2253	2235	2144	2046	2287	2282	1482
Path 3	2629	2066	2734	2712	2686	2579	2460	2613	2483	1784
Path 4	1553	1157	1639	1624	1607	1544	1463	1529	1483	994
Path 5	1097	694	1155	1142	1126	1079	1001	1023	968	582
Generation 1	1500	1500	1500	1500	1500	1500	1500	1500	1500	0
Generation 2	0	490	490	490	490	490	490	0	0	0
Generation 3	165.5	165.5	89.7	89.7	89.7	89.7	89.7	165.5	0	0
Generation 4	250	250	250	250	250	250	250	250	250	250
Generation 5	0	0	0	0	0	0	0	0	0	0
Generation 6	0	0	0	0	0	0	0	0	0	0
Generation 7	130	130	130	130	130	130	130	130	130	130
Generation 8	245	245	245	245	245	245	245	0	0	0
Generation 9	205	205	205	205	205	205	205	205	160	205
Generation 10	189.4	189.4	299.4	299.4	299.4	299.4	299.4	0	0	0
Generation 11	365.3	365.3	252.5	252.5	252.5	252.5	252.5	365.3	260.5	365.3
Angle Diff 1	9.06	2.28	7.09	6.81	6.53	5.75	4.90	10.13	11.08	15.29
Angle Diff 2	8.07	2.33	6.24	6.11	5.98	5.39	4.73	9.06	9.97	13.97
Angle Diff 3	9.68	7.86	9.97	9.89	9.82	9.42	9.02	10.61	10.76	7.13
Angle Diff 4	1.33	0.52	0.86	0.85	0.83	0.78	0.71	1.43	1.43	0.93
Angle Diff 5	8.35	7.35	9.11	9.05	8.98	8.65	8.30	9.17	9.33	6.21
Angle Diff 6	4.06	2.20	4.21	4.15	4.08	3.86	3.51	3.61	3.21	1.98
Angle Diff 7	2.44	1.51	2.57	2.53	2.50	2.38	2.19	2.30	2.17	1.29
Overall Diff	24.01	11.68	22.82	22.52	22.19	20.31	17.93	25.29	25.79	23.73
Class (1:secure)	1	1	1	1	1	1	1	1	1	0
Violating Path										1

Case	_11	_12	_13	_14	_15	_16	_17	_18	_19	_20
Node 1 230 Ang	68.81	71.98	69.06	68.81	69.07	61.87	62.14	63.32	70.75	71.67
Node 2 230 Ang	64.15	67.21	64.20	64.08	64.25	57.84	58.10	59.20	66.85	67.51
Node 3 230 Ang	68.38	71.54	68.63	68.38	68.64	61.34	61.61	62.80	70.22	71.15
Node 4 500 Ang	67.26	70.36	67.42	67.22	67.43	60.81	61.06	62.18	69.71	70.52
Node 5 500 Ang	66.12	69.22	66.15	66.04	66.21	60.04	60.28	61.37	69.01	69.66
Node 6 500 Ang	55.15	58.90	53.13	54.29	53.87	55.07	55.01	55.72	65.14	63.19
Node 7 500 Ang	54.06	57.43	52.42	53.87	53.41	54.27	54.16	54.66	64.32	62.24
Node 8 500 Ang	46.93	47.83	45.76	46.60	45.64	45.14	44.63	42.95	55.60	51.87
Node 9 500 Ang	44.36	44.89	43.58	44.14	43.73	40.44	40.18	39.35	49.17	48.12
Node 9 230 Ang	41.69	41.63	40.99	41.49	41.05	37.47	37.13	35.79	46.09	45.03
Node 10 500 Ang	42.70	42.78	42.16	42.54	42.24	37.68	37.49	36.76	46.02	45.64
Node 11 230 Ang	42.43	41.41	41.98	42.30	42.01	36.29	36.09	35.02	44.08	44.50
Node 12 500 Ang	43.75	43.46	43.36	43.63	43.39	37.88	37.73	37.08	45.94	46.20
Path 1	1396	1299	1643	1491	1559	640	678	719	500	827
Path 2	1758	2330	1584	1718	1792	2300	2387	2782	2350	2571
Path 3	2054	2416	1880	2009	1907	2891	2818	2751	3537	2765
Path 4	1182	1460	1062	1152	1105	1721	1709	1726	1970	1674
Path 5	752	939	643	724	673	1240	1214	1138	1455	1157
Generation 1	750	1500	0	0	0	1500	1500	1500	1500	1500
Generation 2	0	0	245	580	580	560	560	600	560	580
Generation 3	0	0	0	0	0	255.2	255.2	255.2	255.2	255.2
Generation 4	250	250	250	250	250	250	250	250	250	250
Generation 5	0	0	0	0	0	0	195	195	195	120
Generation 6	0	0	0	0	0	0	0	33	40	33
Generation 7	130	0	130	130	130	280	0	0	360	130
Generation 8	0	0	0	0	0	245	245	0	0	0
Generation 9	205	160	205	205	0	205	205	0	205	0
Generation 10	0	0	0	0	0	299.4	299.4	0	464.4	0
Generation 11	365.3	260.5	365.3	365.3	365.3	252.5	252.5	147.8	468.3	365.3
Angle Diff 1	12.11	11.46	14.29	12.93	13.56	5.74	6.05	6.47	4.56	7.34
Angle Diff 2	10.98	10.32	13.02	11.75	12.33	4.97	5.27	5.65	3.87	6.48
Angle Diff 3	8.22	11.07	7.37	7.70	8.24	9.93	10.37	12.77	9.54	11.32
Angle Diff 4	1.09	1.47	0.71	0.42	0.47	0.80	0.85	1.06	0.83	0.94
Angle Diff 5	7.13	9.61	6.66	7.28	7.77	9.14	9.52	11.71	8.72	10.38
Angle Diff 6	2.57	2.94	2.18	2.45	1.91	4.70	4.45	3.59	6.43	3.74
Angle Diff 7	1.66	2.11	1.42	1.60	1.49	2.76	2.70	2.59	3.15	2.48
Overall Diff	22.90	26.10	23.39	22.95	23.39	22.26	22.67	24.45	22.96	23.74
Class (1:secure)	1	1	0	1	0	1	1	0	0	1
Violating Path			1		1			2	3	

Case	_21	_22	_23	_24	_25	_26	_27
Node 1 230 Ang	71.58	71.92	71.63	71.61	71.27	71.22	71.86
Node 2 230 Ang	67.48	67.77	67.55	67.60	67.36	67.25	67.77
Node 3 230 Ang	71.05	71.40	71.10	71.08	70.73	70.68	71.33
Node 4 500 Ang	70.46	70.77	70.52	70.53	70.24	70.19	70.74
Node 5 500 Ang	69.63	69.91	69.70	69.75	69.52	69.46	69.93
Node 6 500 Ang	63.59	63.47	63.84	64.66	65.21	65.06	64.11
Node 7 500 Ang	62.64	62.48	62.90	63.79	64.41	64.26	63.09
Node 8 500 Ang	52.25	51.67	52.55	53.95	55.26	55.15	52.08
Node 9 500 Ang	48.34	48.06	48.50	49.06	49.61	49.54	48.35
Node 9 230 Ang	45.26	44.85	45.36	45.89	46.48	46.42	45.11
Node 10 500 Ang	45.80	45.58	45.90	46.23	46.63	46.58	45.78
Node 11 230 Ang	44.66	44.33	44.65	44.39	44.78	44.74	44.50
Node 12 500 Ang	46.32	46.13	46.38	46.48	46.78	46.75	46.28
Path 1	772	821	750	654	556	567	743
Path 2	2588	2644	2562	2453	2345	2332	2704
Path 3	2820	2714	2827	3132	3270	3255	2771
Path 4	1699	1694	1732	1842	1904	1894	1734
Path 5	1185	1158	1208	1313	1382	1372	1194
Generation 1	1500	1500	1500	1500	1500	1500	1500
Generation 2	580	580	580	580	580	580	580
Generation 3	89.7	89.7	89.7	89.7	89.7	89.7	255.2
Generation 4	250	250	250	250	250	250	250
Generation 5	120	120	120	120	120	120	120
Generation 6	33	33	33	33	33	33	33
Generation 7	130	130	350	350	350	350	130
Generation 8	0	0	0	0	0	0	0
Generation 9	0	0	0	0	290	290	0
Generation 10	0	0	0	464.4	464.4	464.4	0
Generation 11	395.3	212.8	212.8	212.8	212.8	212.8	212.8
Angle Diff 1	6.86	7.30	6.68	5.87	5.03	5.13	6.63
Angle Diff 2	6.04	6.44	5.86	5.09	4.31	4.40	5.81
Angle Diff 3	11.34	11.80	11.29	10.71	9.95	9.90	12.04
Angle Diff 4	0.95	0.99	0.94	0.87	0.80	0.79	1.03
Angle Diff 5	10.39	10.81	10.35	9.84	9.15	9.11	11.01
Angle Diff 6	3.91	3.61	4.05	4.89	5.65	5.61	3.73
Angle Diff 7	2.54	2.49	2.59	2.83	2.98	2.96	2.57
Overall Diff	23.57	24.06	23.56	23.40	22.81	22.79	23.89
Class (1:secure)	1	1	1	1	0	0	1
Violating Path					4,5	4,5	

Appendix B: Damping Study Results

The following script is an example of the MATLAB code used for damping analysis using decision trees. This code was adapted for the various studies (damping threshold, input parameters, etc.) described in this work.

```
% ------------------------------------------------------------------------ %
% ------------------------------------------------------------------------ %
% This code reads in operating case information and runs the results
% through a decision tree analysis script to determine the various trees
% and their performance.
% ------------------------------------------------------------------------ %

clc; clear all; close all hidden;
dampingThresh = 1.5;

[data headers] = xlsread('Damping Results - Combined.xlsx');

damping = [data(:,64) data(:,66) data(:,68)];
minDamping = min(damping,[],2);

name = []; count = 0;
for i = 1:size(damping,1)
   if minDamping(i) <= dampingThresh
       name = char(name,'Unacceptable');
   else
       name = char(name,'Acceptable'); count = count + 1;
   end
end
name = name(2:end,:);
sprintf('%d cases acceptable out of %d total cases', count, size(damping,1))

MW = data(:,1:18);
MW = MW(:,3:12);

angles = data(:,20:50);
angles = [angles(:,6:7) angles(:,10:11) angles(:,14:16)];

allMeas  = [MW angles];

% ------------------------------------------------------------------------ %
% ------------------------------------------------------------------------ %

% TREE WITH ALL MEASUREMENTS
s = sprintf('\n DT with BPA Angle and MW Measurements'); disp(s);
t=classregtree(allMeas,name);
view(t);
sfit=eval(t,allMeas);
rw=strcmp(sfit,name);
pct=mean(strcmp(sfit,name))% %right

bad = [];
for i = 1:size(rw,1)
    if rw(i) == 0
        if minDamping(i) > dampingThresh
            s = sprintf('# %d has damping greater than threshold, but is
classified as unacceptable.  False Positive.',i); disp(s)
            bad = [bad; i 1];
        else
```

```
            s = sprintf('# %d has damping less than threshold, but is classified
as acceptable.  Failed.',i); disp(s)
            bad = [bad; i 2];
        end
    else
        bad = [bad; i 0];
    end
end

% BEST FIT TREE BASED ON CROSS VALIDATION - ALL MEASUREMENTS
t=classregtree(allMeas,name);
[c,s,n,best] = test(t,'cross',allMeas,name);
tmin = prune(t,'level',best)
view(tmin);
sfit=eval(tmin,allMeas);
rw=strcmp(sfit,name);
pct=mean(strcmp(sfit,name))% %right

for i = 1:size(rw,1)
    if rw(i) == 0
        if minDamping(i) > dampingThresh
            s = sprintf('# %d has damping greater than threshold, but is
classified as unacceptable.  False Positive.',i); disp(s)
        else
            s = sprintf('# %d has damping less than threshold, but is classified
as acceptable.  Failed.',i); disp(s)
        end
    end
end

% ------------------------------------------------------------------------ %

% TREE WITH MW ONLY
s = sprintf('\n DT with BPA MW Measurements Only'); disp(s);
t=classregtree(MW,name);
view(t);
sfit=eval(t,MW);
rw = strcmp(sfit,name);
pct=mean(strcmp(sfit,name)) % %right

for i = 1:size(rw,1)
    if rw(i) == 0
        if minDamping(i) > dampingThresh
            s = sprintf('# %d has damping greater than threshold, but is
classified as unacceptable.  False Positive.',i); disp(s)
        else
            s = sprintf('# %d has damping less than threshold, but is classified
as acceptable.  Failed.',i); disp(s)
        end
    end
end

% BEST FIT TREE BASED ON CROSS VALIDATION - MW MEASUREMENTS
t=classregtree(MW,name);
[c,s,n,best] = test(t,'cross',MW,name);
tmin = prune(t,'level',best)
view(tmin);
sfit=eval(tmin,MW);
rw=strcmp(sfit,name);
pct=mean(strcmp(sfit,name))% %right

for i = 1:size(rw,1)
    if rw(i) == 0
```

```
        if minDamping(i) > dampingThresh
            s = sprintf('# %d has damping greater than threshold, but is
classified as unacceptable.  False Positive.',i); disp(s)
        else
            s = sprintf('# %d has damping less than threshold, but is classified
as acceptable.  Failed.',i); disp(s)
        end
    end
end

% ------------------------------------------------------------------------ %

% TREE WITH ANGLE ONLY
s = sprintf('\n DT with BPA Angle Measurements Only'); disp(s);
t=classregtree(angles,name);
view(t);
sfit=eval(t,angles);
rw = strcmp(sfit,name);
pct=mean(strcmp(sfit,name)) % %right

for i = 1:size(rw,1)
    if rw(i) == 0
        if minDamping(i) > dampingThresh
            s = sprintf('# %d has damping greater than threshold, but is
classified as unacceptable.  False Positive.',i); disp(s)
        else
            s = sprintf('# %d has damping less than threshold, but is classified
as acceptable.  Failed.',i); disp(s)
        end
    end
end

% BEST FIT TREE BASED ON CROSS VALIDATION - ANGLE MEASUREMENTS
t=classregtree(angles,name);
[c,s,n,best] = test(t,'cross',angles,name);
tmin = prune(t,'level',best)
view(tmin);
sfit=eval(tmin,angles);
rw=strcmp(sfit,name);
pct=mean(strcmp(sfit,name))% %right

for i = 1:size(rw,1)
    if rw(i) == 0
        if minDamping(i) > dampingThresh
            s = sprintf('# %d has damping greater than threshold, but is
classified as unacceptable.  False Positive.',i); disp(s)
        else
            s = sprintf('# %d has damping less than threshold, but is classified
as acceptable.  Failed.',i); disp(s)
        end
    end
end

% ------------------------------------------------------------------------ %


disp('Done');
```

The results below refer to the damping studies and decision tree analyses performed.

WECC Data Set

MW PATH FLOWS

#	Label	#	Label
1	BC-ALB	14	P-26
2	MATL	15	EoR
3	BC-NW	16	WoR
4	MT-NW	17	BorahW
5	NOH+SoNV	18	TOT2
6	NOH+RP		
7	NJD		
8	PDCI		
9	COI		
10	RATS		
11	MP-HW		
12	SOG		
13	P-15		

ANGLE DIFFERENCES

#	Label	#	Label	#	
19	GMS-ING	32	MONR-MLN	45	TES-MIRA
20	KMO-ING	33	GCL-MLN	46	MIDW-MIRA
21	NIC-ING	34	JDA-MLN	47	PV-MIRA
22	ING-MONR	35	ING-TES	48	NAVA-MIRA
23	ING-JDA	36	MONR-TES	49	FOURC-MIRA
24	MONR-JDA	37	GCL-TES		
25	GCL-JDA	38	JDA-TES		
26	COLS-JDA	39	MLN-TES		
27	ING-GRIZ	40	ING-MIRA		
28	MONR-GRIZ	41	MONR-MIRA		
29	GCL-GRIZ	42	GCL-MIRA		
30	COLS-GRIZ	43	JDA-MIRA		
31	ING-MLN	44	MLN-MIRA		

MW PATH FLOWS ONLY

#	Label	#	Label
1	BC-ALB	14	P-26
2	MATL	15	EoR
3	BC-NW	16	WoR
4	MT-NW	17	BorahW
5	NOH+SoNV	18	TOT2
6	NOH+RP		
7	NJD		
8	PDCI		
9	COI		
10	RATS		
11	MP-HW		
12	SOG		
13	P-15		

ANGLE DIFFERENCES ONLY

#	Label	#	Label	#	
1	GMS-ING	14	MONR-MLN	27	TES-MIRA
2	KMO-ING	15	GCL-MLN	28	MIDW-MIRA
3	NIC-ING	16	JDA-MLN	29	PV-MIRA
4	ING-MONR	17	ING-TES	30	NAVA-MIRA
5	ING-JDA	18	MONR-TES	31	FOURC-MIRA
6	MONR-JDA	19	GCL-TES		
7	GCL-JDA	20	JDA-TES		
8	COLS-JDA	21	MLN-TES		
9	ING-GRIZ	22	ING-MIRA		
10	MONR-GRIZ	23	MONR-MIRA		
11	GCL-GRIZ	24	GCL-MIRA		
12	COLS-GRIZ	25	JDA-MIRA		
13	ING-MLN	26	MLN-MIRA		

Combined Cases, MW and Angle, Full Tree

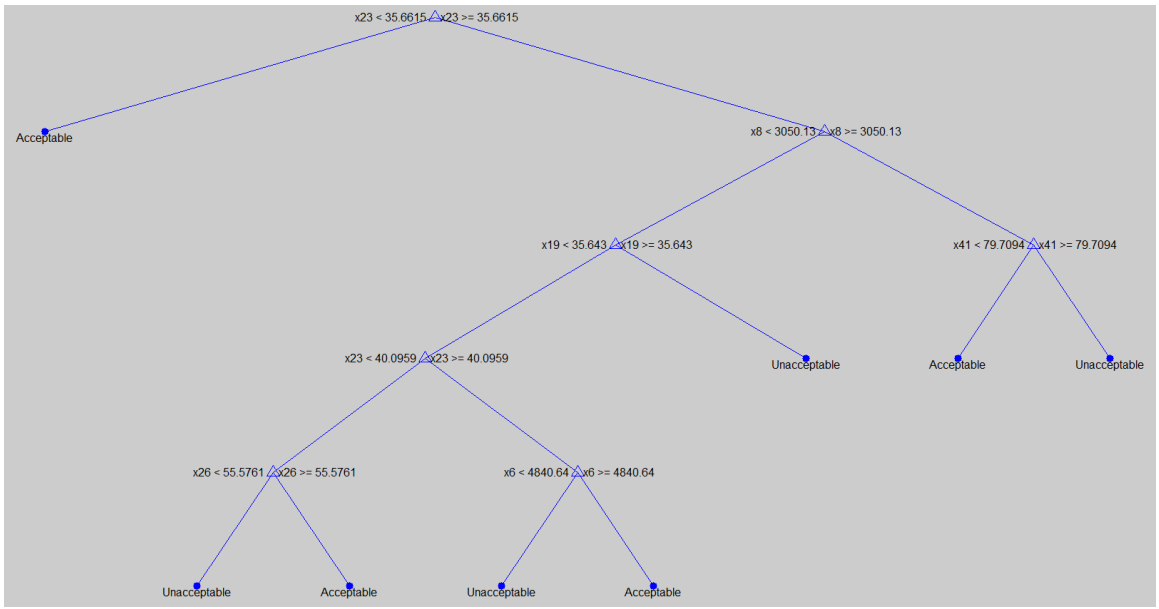

Combined Cases, MW Only, Full Tree

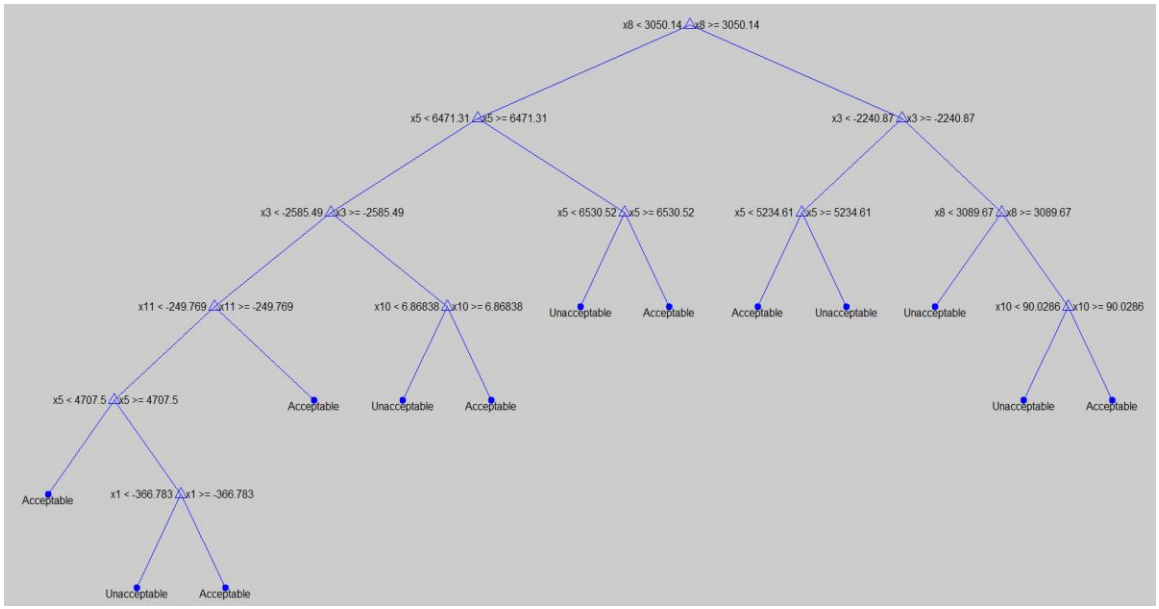

Combined Cases, Angle Only, Full Tree

Alberta In, MW and Angle, Full Tree

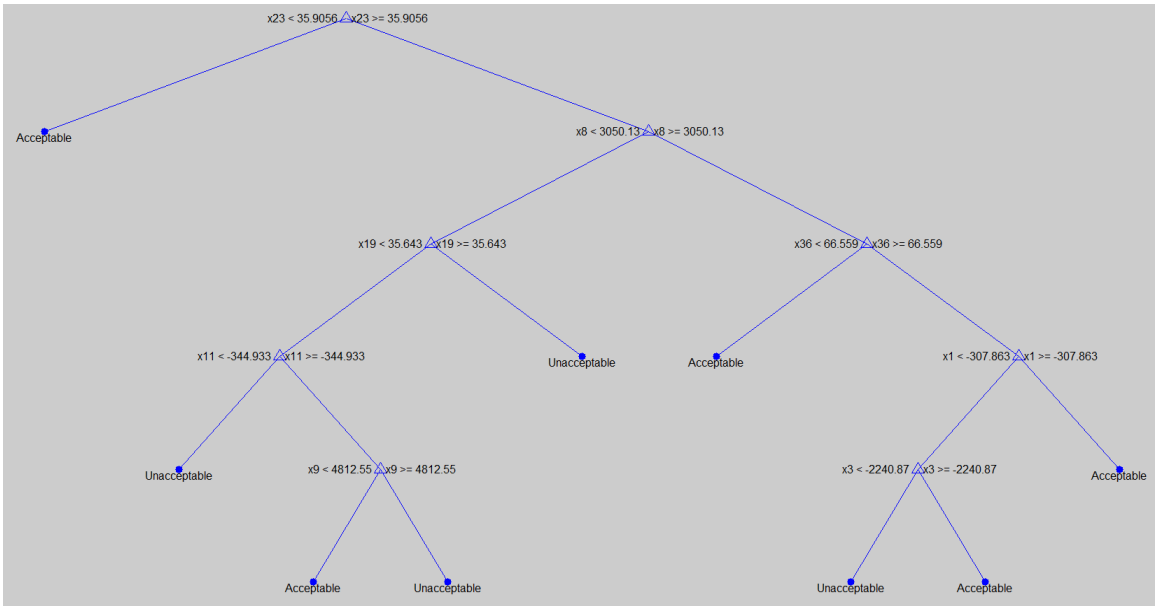

Alberta In, MW Only, Full Tree

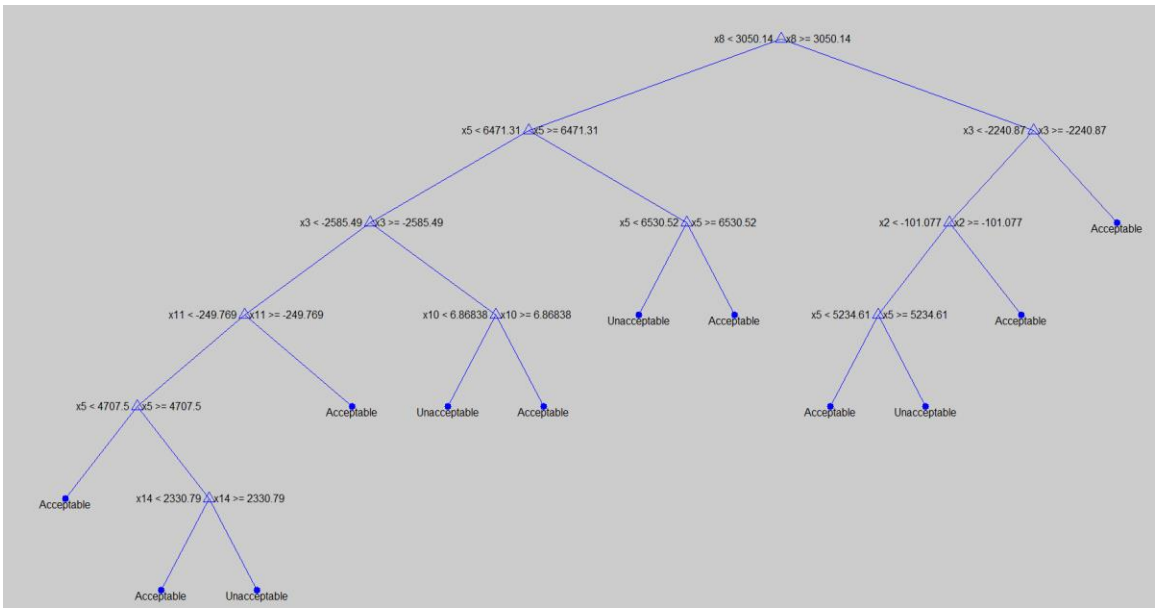

Alberta In, Angle Only Full Tree

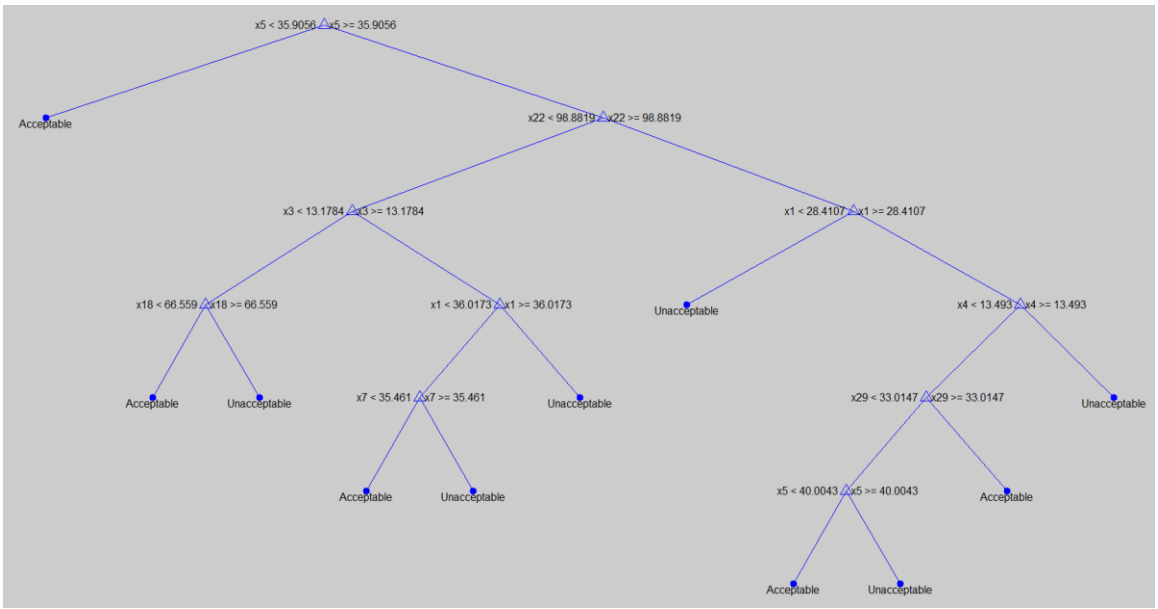

Alberta Out, MW and Angle, Full Tree

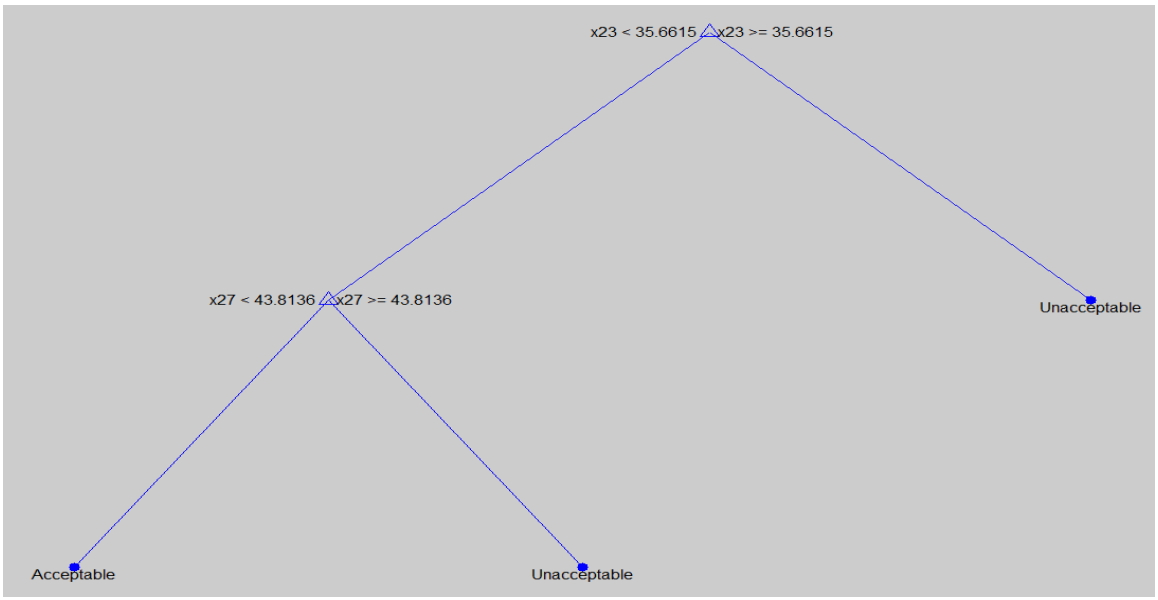

Alberta Out, MW Only, Full Tree

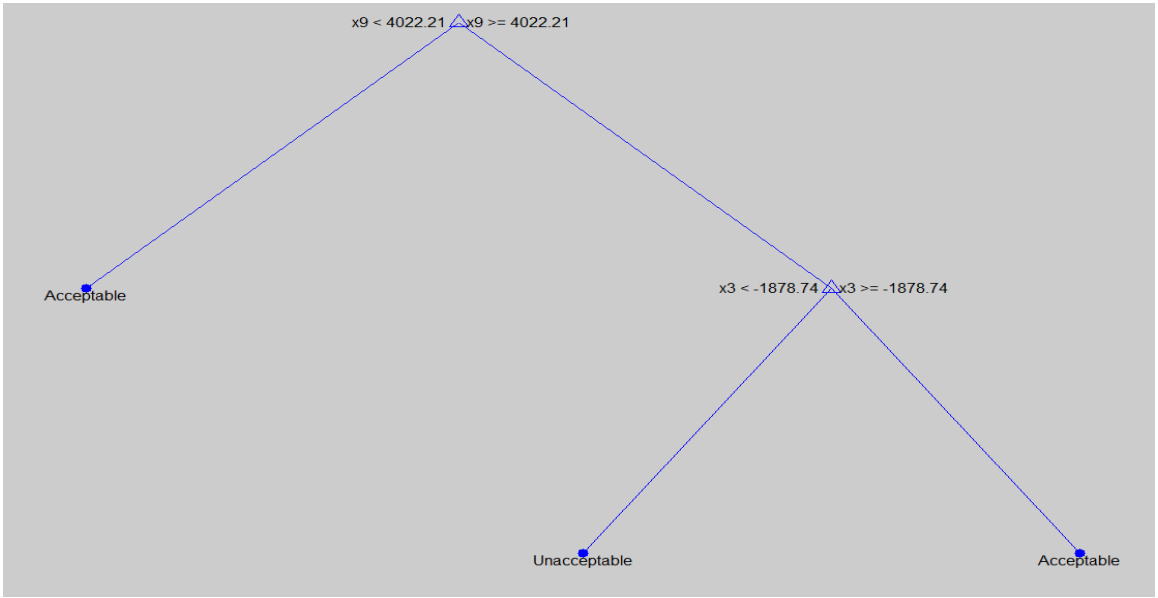

Alberta Out, Angle Only, Full Tree

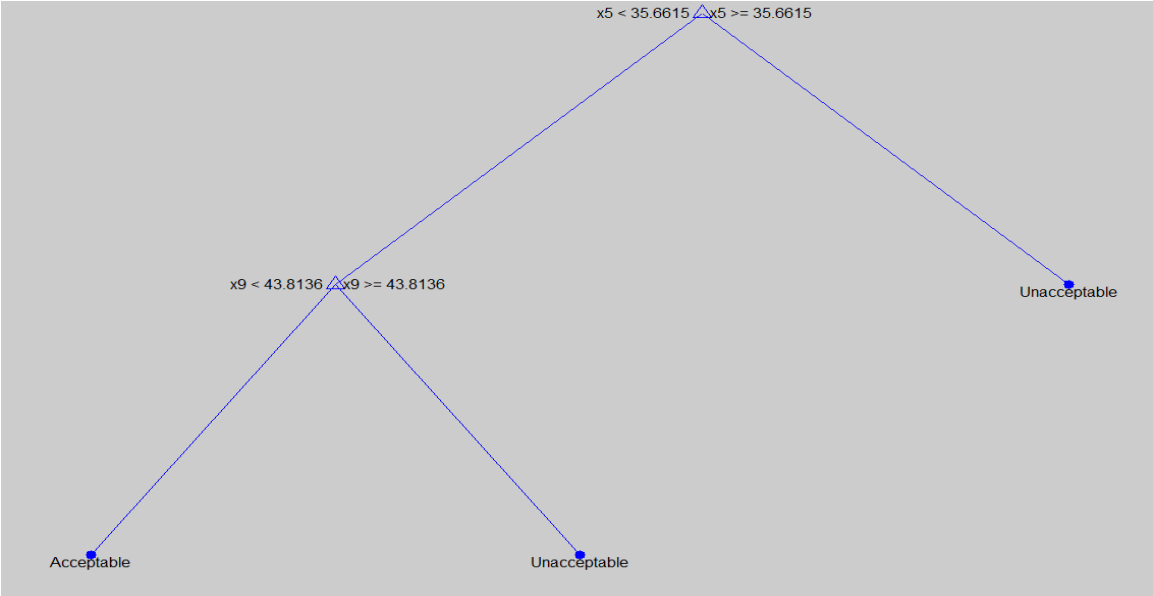

BPA Data Set

MW PATH FLOWS

#	Label
1	BC-NW
2	MT-NW
3	NOH+SoNV
4	NOH+RP
5	NJD
6	PDCI
7	COI
8	RATS
9	MP-HW
10	SOG

ANGLE DIFFERENCES

#	Label
11	MONR-JDA
12	GCL-JDA
13	MONR-GRIZ
14	GCL-GRIZ
15	MONR-MLN
16	GCL-MLN
17	JDA-MLN

MW PATH FLOWS ONLY

#	Label
1	BC-NW
2	MT-NW
3	NOH+SoNV
4	NOH+RP
5	NJD
6	PDCI
7	COI
8	RATS
9	MP-HW
10	SOG

ANGLE DIFFERENCES ONLY

#	Label
1	MONR-JDA
2	GCL-JDA
3	MONR-GRIZ
4	GCL-GRIZ
5	MONR-MLN
6	GCL-MLN
7	JDA-MLN

Combined Cases, MW and Angle, Full Tree

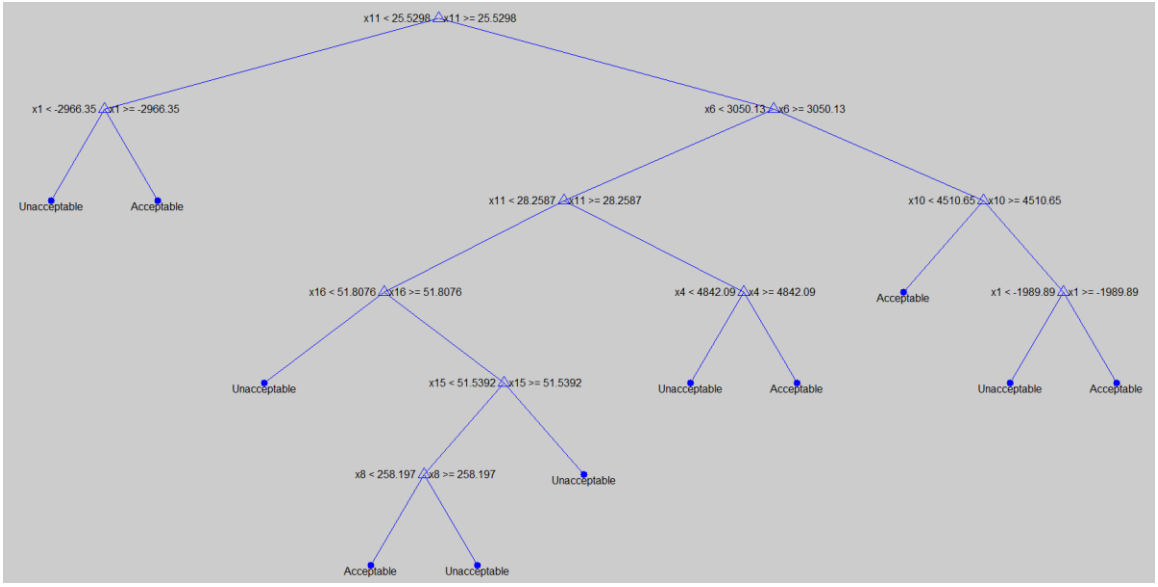

Combined Cases, MW Only, Full Tree

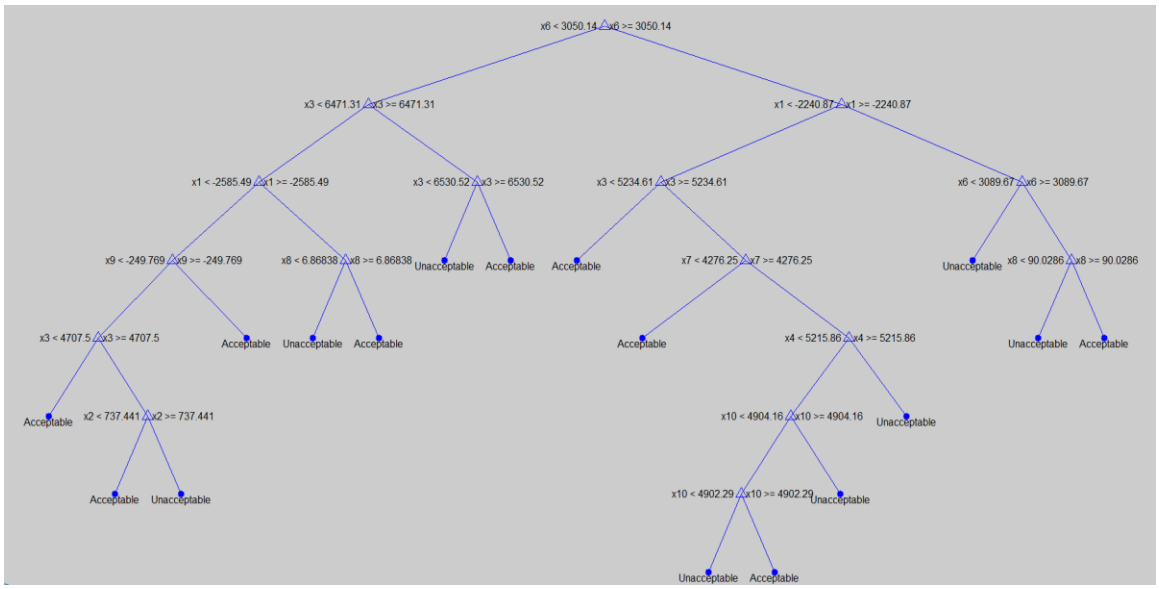

Combined Cases, Angle Only, Full Tree

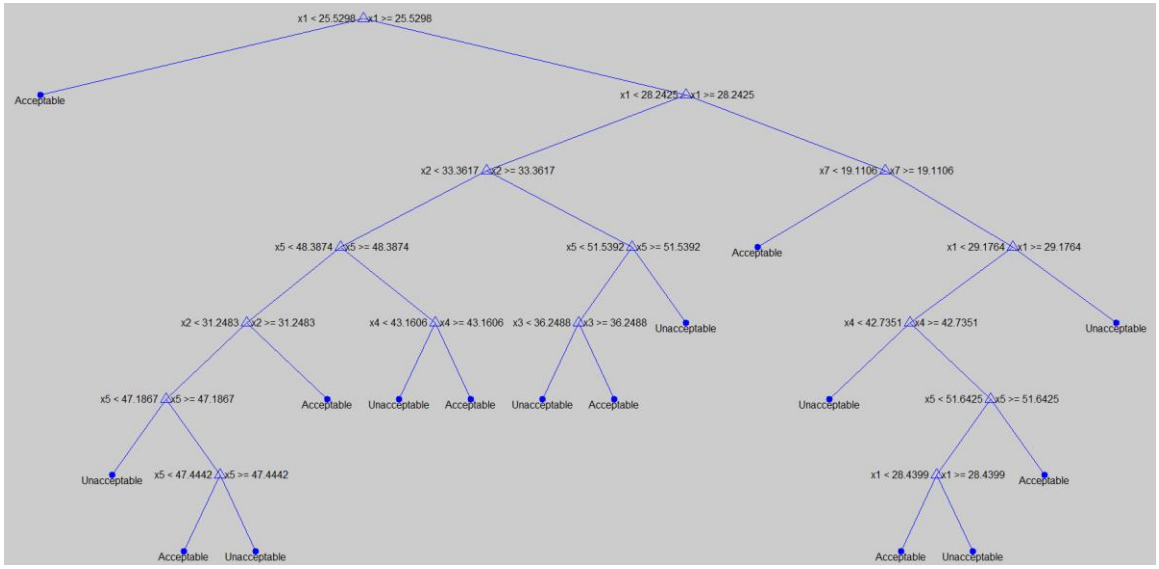

Alberta In, MW and Angle, Full Tree

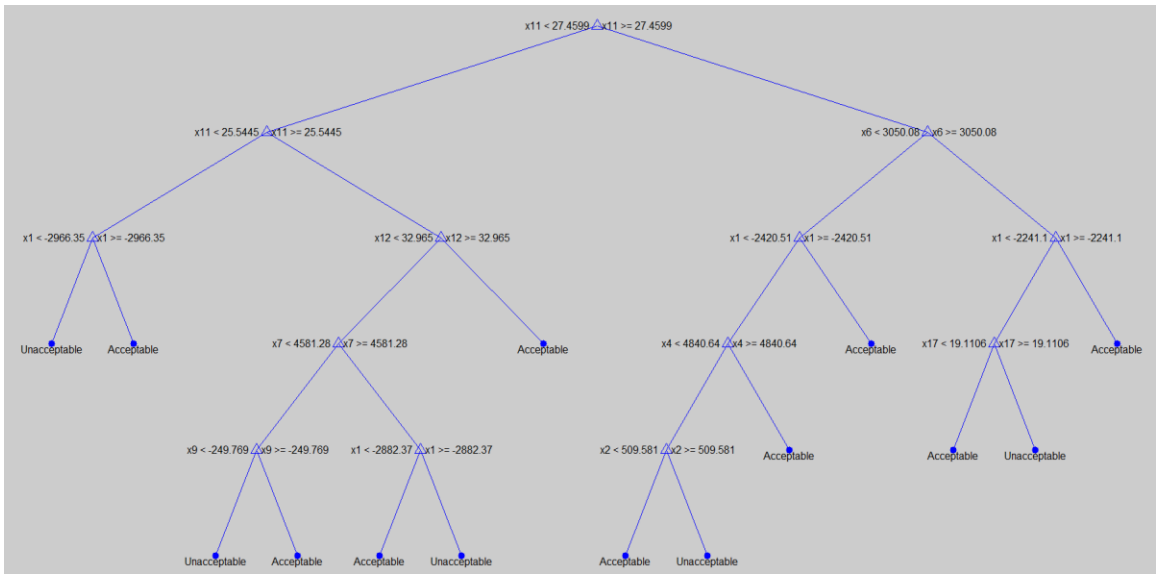

Alberta In, MW Only, Full Tree

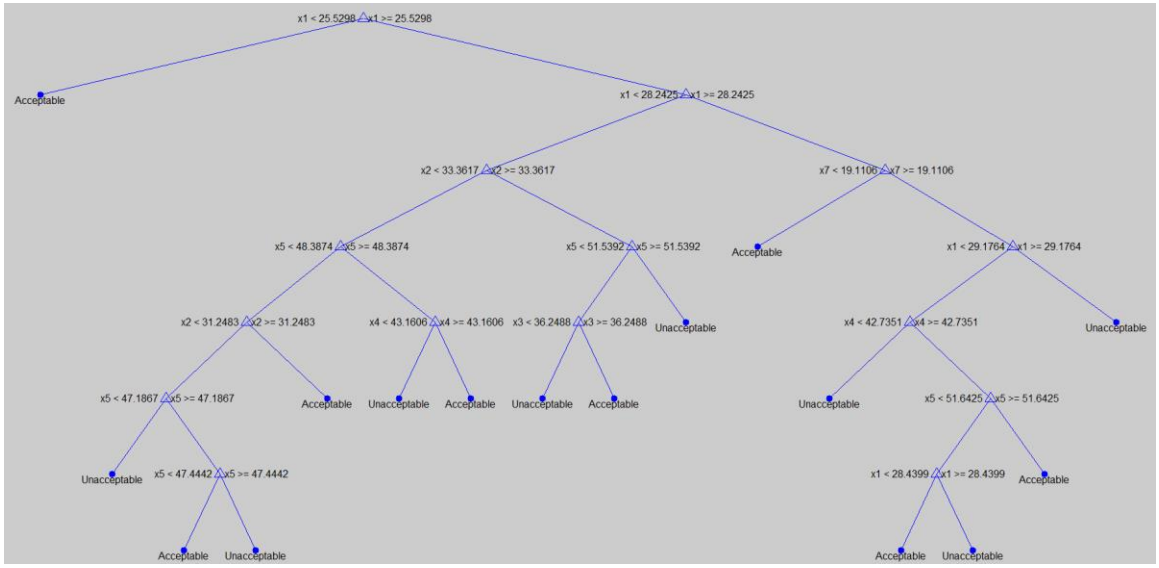

Alberta In, Angle Only, Full Tree

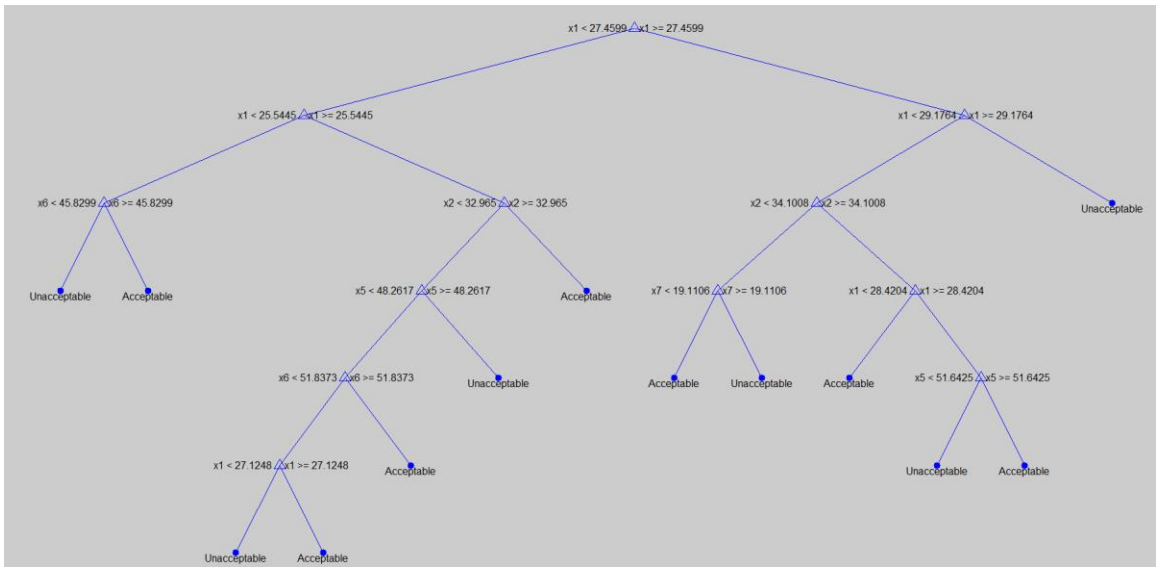

<u>BPA Data Set w/ Mode Meter Included</u>

MM Included, Combined Cases, MW and Angle, Full Tree

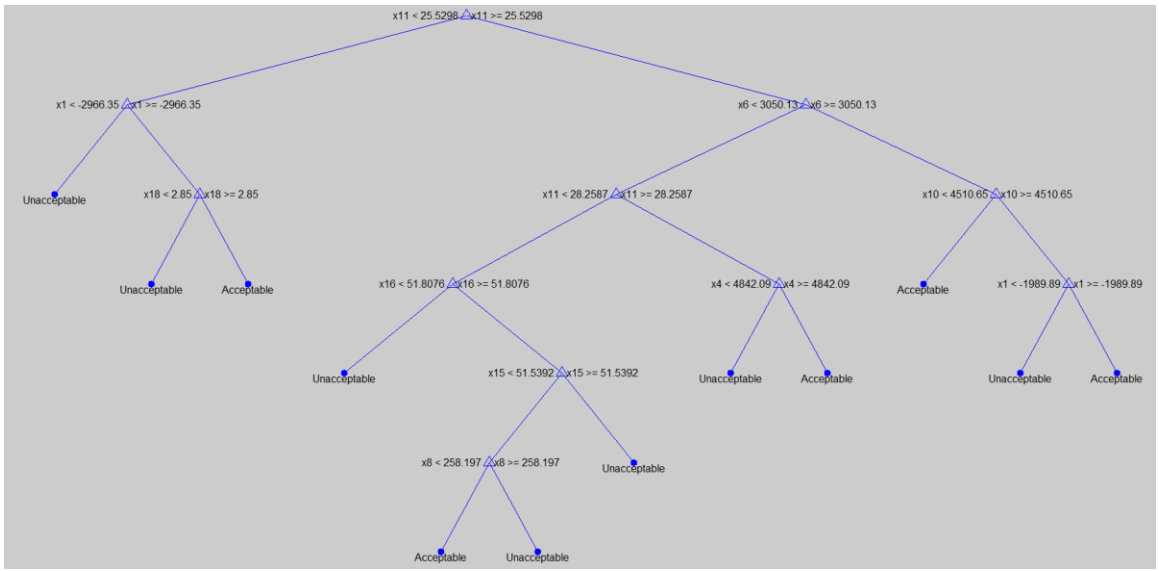

MM Included, Combined Cases, MW Only, Full Tree

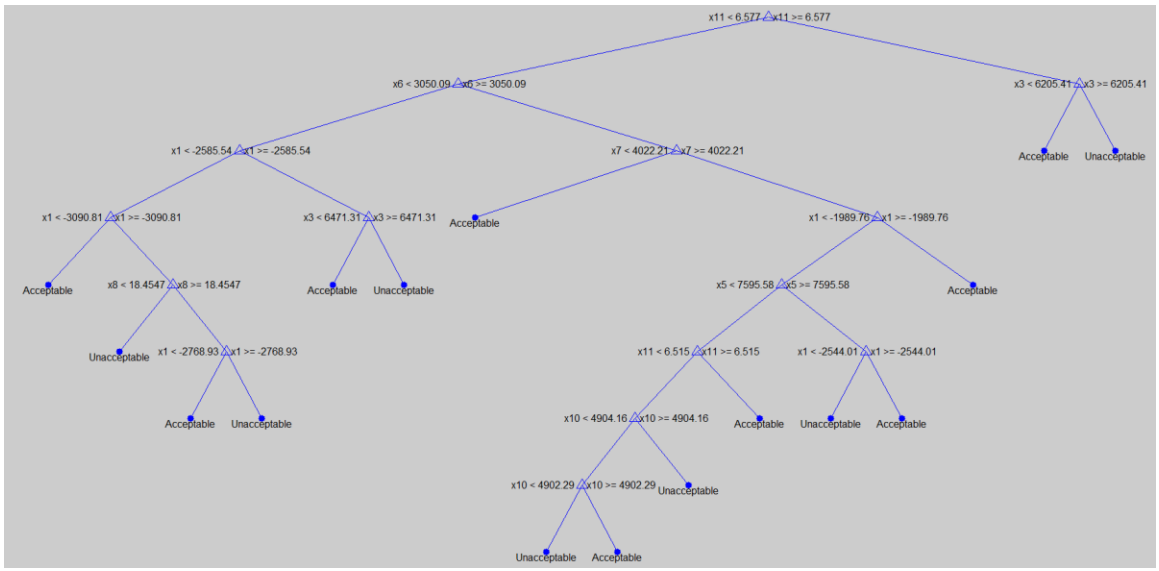

MM Included, Combined Cases, Angle Only, Full Tree

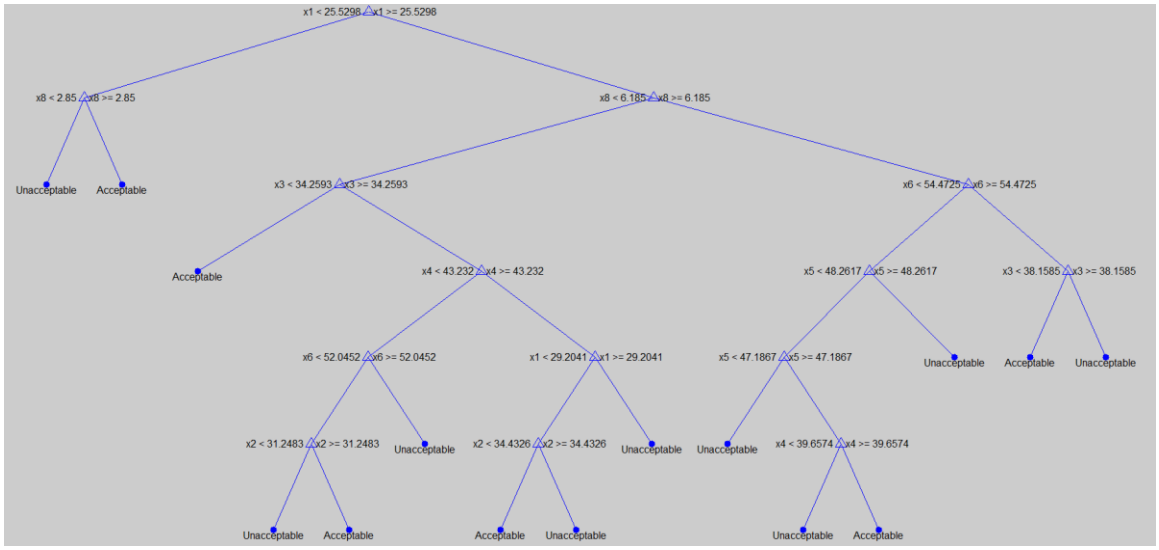

Appendix C: Contingency Simulation Code Framework

This section provides a framework for running large sets of contingencies in PSLF EPCL.

"SIMULATECONTINGENCIES.P"

```
dim *filelist[1][120], *filename[1][120], *savfile[1][120]
dim *dydfile[7][120], *pltfile0[1][120], *pltfile[1][120], *temp[1][256]

/*****************************************************************************/

/* OUTAGE SELECTION                                                          */

@genOutage1             = 0     /* N-1 Gen Outage:  X MW                    */
@genOutage2             = 0     /* N-2 Gen Outage:  X MW                    */
@genOutage3             = 0     /* N-3 Gen Outage:  X MW                    */

@transOutage1           = 0     /* N-1 Trans Outage                         */
@transOutage2           = 0     /* N-2 Trans Outage                         */

/*****************************************************************************/

@tstart    = 1.0
@tstop     = 30.0

/*****************************************************************************/

*filelist[0] = "SimulateDynamics.txt"

@ret = setinput(*filelist[0])
if (@ret < 0 )
        logterm("Base Case List ", *filelist[0], " cannot be opened. <")
        end
endif

for @k = 0 to 100

        @ret = inline(*filelist[0], *temp[0])
        if (@ret < 0 )  /* end of file */
                @ret = close(*filelist[0])
                end
        endif

        if(format(toupper(*temp[0]),1,0) = "#")
                /* comment, skip the record */
        elseif(*temp[0] = "")
                /* blank record */
        else
                @ret = inbuf(*temp[0], @sim_flag, *filename[0], *dydfile[0],*dydfile[2] )
                if (@sim_flag > 0.5 )
                        /* Run Simulation */

                        *savfile[0]   = "___" + *filename[0] + ".sav"
                        *pltfile0[0]  = "___" + *filename[0] + "-" + *dydfile[0] + "-" + *dydfile[2]

                        *dydfile[0]   = "___" + *dydfile[0] + ".dyd"
                        *dydfile[1]   = "___" + "facri.dyd"
                        *dydfile[2]   = "___" + *dydfile[2] + ".dyd"
                        *dydfile[3]   = "___" + "meters.dyd"
                        *dydfile[4]   = "___" + "vsri.dyd"
```

```
                                @nplot  = 15
                                @nprint = 50

                                $repfile   = "temp.rep"

                                gosub disturbance

                        endif
                endif
next

@ret = close(*filelist[0])

end


/*****************************************************************************/
/*****************************************************************************/

subroutine disturbance

/*****************************************************************************/
/*  Gen Drop Selection                                                       */
/*****************************************************************************/

@ret = getf(*savfile[0])
@ret = soln();

@ret   = flowcalc(1)
@i3a   = flow_index(#####,#####,"1")
@i3b   = flow_index(#####,#####,"2")
@path3 = flox[@i3a].p +  flox[@i3b].p
@hgd = 0          /* entire gen drop in PNW only */
if (@path3 > ____)
        @hgd = 1    /* ___ MW of gen drop in __ */
        endif
if (@path3 > ____)
        @hgd = 2    /* ___ MW of gen drop in __ */
        endif


/*****************************************************************************/
/* N-1 Gen Outage:  X MW                                                     */
/*****************************************************************************/

if ( @genOutage1 > 0.5 )

*pltfile[0] = *pltfile0[0] + "-genOutage1.chf"

@ret = getf(*savfile[0])
@ret = soln();
@ret = psds();
@ret = rdyd(*dydfile[0], 0, 1, 0, 1)
@ret = rdyd(*dydfile[2], 0, 0, 0, 1)
@ret = epcl("setrecordlvls.p")
@ret = rdyd(*dydfile[3], 0, 0, 0, 1)
@ret = init(*pltfile[0], $repfile, "1","1")

dypar[0].nplot =  @nplot
dypar[0].nprint = @nprint
```

```
dypar[0].tpause    = @tstart
@ret = run()
/* N-1 GEN OUTAGE */
@ret  =  rec_index( 2, 3, "NAME KV", -1, "ID", 0, 0)
dypar[0].new_fact  =  1

/* RAS Actions */
dypar[0].tpause    = @tstart + ##/60
@ret = run()
gosub ras_action
dypar[0].new_fact  =  1

dypar[0].tpause    = @tstop
@ret = run()

@ret = dsst()

endif


/*****************************************************************************/
/* N-2 Gen Outage:  X MW                                                     */
/*****************************************************************************/

if ( @genOutage2 > 0.5 )

*pltfile[0] = *pltfile0[0] + "-genOutage2.chf"

@ret = getf(*savfile[0])
@ret = soln();
@ret = psds();
@ret = rdyd(*dydfile[0], 0, 1, 0, 1)
@ret = rdyd(*dydfile[1], 0, 0, 0, 1)
@ret = rdyd(*dydfile[2], 0, 0, 0, 1)
@ret = epcl("setrecordlvls.p")
@ret = rdyd(*dydfile[3], 0, 0, 0, 1)
@ret = init(*pltfile[0], $repfile, "1","1")

dypar[0].nplot =  @nplot
dypar[0].nprint = @nprint

dypar[0].tpause    = @tstart
@ret = run()
/* N-2 GEN OUTAGE */
@ret  =  rec_index( 2, 3, "NAME KV", -1, "ID", 0, 0)
@ret  =  rec_index( 2, 3, "NAME KV", -1, "ID", 0, 0)
dypar[0].new_fact  =  1

/* RAS Actions */
dypar[0].tpause    = @tstart + ##/60
@ret = run()
gosub ras_action
dypar[0].new_fact  =  1

dypar[0].tpause    = @tstop
@ret = run()

@ret = dsst()

endif
```

```
/*****************************************************************************/
/* N-3 Gen Outage:  X MW                                                     */
/*****************************************************************************/

if ( @genOutage3 > 0.5 )

*pltfile[0] = *pltfile0[0] + "-genOutage3.chf"

@ret = getf(*savfile[0])
@ret = soln();
@ret = psds();
@ret = rdyd(*dydfile[0], 0, 1, 0, 1)
@ret = rdyd(*dydfile[1], 0, 0, 0, 1)
@ret = rdyd(*dydfile[2], 0, 0, 0, 1)
@ret = epcl("setrecordlvls.p")
@ret = rdyd(*dydfile[3], 0, 0, 0, 1)
@ret = init(*pltfile[0], $repfile, "1","1")

dypar[0].nplot =  @nplot
dypar[0].nprint = @nprint

dypar[0].tpause    = @tstart
@ret = run()
/* N-3 GEN OUTAGE */
@ret  =  rec_index( 2, 3, "NAME KV", -1, "ID", 0, 0)
@ret  =  rec_index( 2, 3, "NAME KV", -1, "ID", 0, 0)
@ret  =  rec_index( 2, 3, "NAME KV", -1, "ID", 0, 0)
dypar[0].new_fact  =  1

/* RAS Actions */
dypar[0].tpause    = @tstart + ##/60
@ret = run()
gosub ras_action
dypar[0].new_fact  =  1

dypar[0].tpause    = @tstop
@ret = run()

@ret = dsst()

endif


/*****************************************************************************/
/* N-1 Transmission Outage                                                   */
/*****************************************************************************/

if ( @transOutage1 > 0.5 )

*pltfile[0] = *pltfile0[0] + "-transOutage1.chf"

@ret = getf(*savfile[0])
@ret = soln();
@ret = psds();
@ret = rdyd(*dydfile[0], 0, 1, 0, 1)
@ret = rdyd(*dydfile[1], 0, 0, 0, 1)
@ret = rdyd(*dydfile[2], 0, 0, 0, 1)
@ret = epcl("setrecordlvls.p")
@ret = rdyd(*dydfile[3], 0, 0, 0, 1)
@ret = rdyd(*dydfile[4], 0, 0, 0, 1)
@ret = init(*pltfile[0], $repfile, "1","1")
```

```
dypar[0].nplot =  @nplot
dypar[0].nprint = @nprint

dypar[0].fault_from     = "FROMBUS#"
dypar[0].fault_to       = "TOBUS#"
dypar[0].fault_ck       = "ID1"
dypar[0].fault_sec      = 1
dypar[0].fault_position = 0.0
dypar[0].t_fault_on     = @tstart
dypar[0].t_from_clear   = @tstart + 3/60
dypar[0].t_to_clear     = @tstart + 4/60
dypar[0].faultr         = 0.0
dypar[0].faultx         = 0.001

/* By-Pass Series Capacitors - On Faulted Line If Necessary */
dypar[0].tpause    = @tstart
@ret = run()
@ret = rec_index( 1, 1, FROMBUS#, TOBUS#, "ID1", SECT1, 2 )
dypar[0].new_fact  =  1

dypar[0].tpause    = @tstart + 4/60
@ret = run()
@ret = rec_index( 1, 1, FROMBUS#, TOBUS#, "ID1", SECT2, 0 )
@ret = rec_index( 1, 1, FROMBUS#, TOBUS#, "ID1", SECT3, 0 )
dypar[0].new_fact  =  1

/* RAS Actions */
dypar[0].tpause    = @tstart + ##/60
@ret = run()
gosub ras_action
dypar[0].new_fact  =  1

dypar[0].tpause    = @tstop
@ret = run()

@ret = dsst()

endif


/*****************************************************************************/
/* N-2 Transmission Outage                                                   */
/*****************************************************************************/

if ( @transOutage2 > 0.5 )

*pltfile[0] = *pltfile0[0] + "-transOutage2.chf"

@ret = getf(*savfile[0])
@ret = soln();
@ret = psds();
@ret = rdyd(*dydfile[0], 0, 1, 0, 1)
@ret = rdyd(*dydfile[1], 0, 0, 0, 1)
@ret = rdyd(*dydfile[2], 0, 0, 0, 1)
@ret = epcl("setrecordlvls.p")
@ret = rdyd(*dydfile[3], 0, 0, 0, 1)
@ret = rdyd(*dydfile[4], 0, 0, 0, 1)
@ret = init(*pltfile[0], $repfile, "1","1")

dypar[0].nplot =  @nplot
dypar[0].nprint = @nprint
```

```
dypar[0].fault_from     = "FROMBUS#"
dypar[0].fault_to       = "TOBUS#"
dypar[0].fault_ck       = "ID1"
dypar[0].fault_sec      = 1
dypar[0].fault_position = 0.0
dypar[0].t_fault_on     = @tstart
dypar[0].t_from_clear   = @tstart + 3/60
dypar[0].t_to_clear     = @tstart + 4/60
dypar[0].faultr         = 0.0
dypar[0].faultx         = 0.001

/* By-Pass Series Capacitors - On Faulted Line If Necessary */
dypar[0].tpause    = @tstart
@ret = run()
@ret = rec_index( 1, 1, #####, #####, "ID1", SECT#, 2 )
dypar[0].new_fact  =  1

dypar[0].tpause    = @tstart + 4/60
@ret = run()
@ret = rec_index( 1, 1, FROMBUS#, TOBUS#, "ID1", SECT2, 0 )
@ret = rec_index( 1, 1, FROMBUS#, TOBUS#, "ID2", SECT1, 0 )
@ret = rec_index( 1, 1, FROMBUS#, TOBUS#, "ID2", SECT2, 0 )
dypar[0].new_fact  =  1

/* RAS Actions */
dypar[0].tpause    = @tstart + ##/60
@ret = run()
gosub ras_action
dypar[0].new_fact  =  1

dypar[0].tpause    = @tstop
@ret = run()

@ret = dsst()

endif

return


/*************************************************************************/
/*************************************************************************/

/*************************************************************************/
/*  RAS Action                                                           */
/*************************************************************************/

/* Generation Drop RAS Action */

subroutine ras_action

@pdrop = 0.0

/* Generator 1 - X MW*/
@ret  =  rec_index( 2, 3, "NAME KV", -1, "ID1", 0, 0)
            @pdrop = @pdrop + gens[@ret].pgen
@ret  =  rec_index( 2, 3, "NAME KV", -1, "ID2", 0, 0)
            @pdrop = @pdrop + gens[@ret].pgen
@ret  =  rec_index( 2, 3, "NAME KV", -1, "ID3", 0, 0)
            @pdrop = @pdrop + gens[@ret].pgen

/* Generator 2 - X MW*/
```

```
@ret  =  rec_index( 2, 3, "NAME KV", -1, "ID1", 0, 0)
            @pdrop = @pdrop + gens[@ret].pgen
@ret  =  rec_index( 2, 3, "NAME KV", -1, "ID2", 0, 0)
            @pdrop = @pdrop + gens[@ret].pgen

/* Generator 3 - X MW*/
@ret  =  rec_index( 2, 3, "NAME KV", -1, "ID1", 0, 0)
            @pdrop = @pdrop + gens[@ret].pgen
@ret  =  rec_index( 2, 3, "NAME KV", -1, "ID2", 0, 0)
            @pdrop = @pdrop + gens[@ret].pgen

logterm("RAS Gen Drop of ", @pdrop:10:2, " MW<")
logdy("RAS Gen Drop of ", @pdrop:10:2, " MW<")

return
```

“SIMULATEDYNAMICS.TXT”

```
0  "basecase_01"    "dyd_01"   "comploadmod_01"
0  "basecase_02"    "dyd_01"   "comploadmod_01"
0  "basecase_03"    "dyd_01"   "comploadmod_01"
1  "basecase_04"    "dyd_01"   "comploadmod_01"
1  "basecase_05"    "dyd_01"   "comploadmod_01"
```

Appendix D: MATLAB Algorithm Analysis Code

The following MATLAB code is used for determining the subset of contingencies resulting in algorithm triggering for the real power and angle rate-of-change algorithms.

Algorithm Testing Wrapper Function

```
% ------------------------------------------------------------------------
% This is a wrapper script for testing the online RAS algorithm functions.
% It reads in a .csv file and executes the code as it would in real-time.
% By Ryan Quint (rdquint@bpa.gov), Vancouver, WA - 08/25/2012

clear all; close all; clc;

% ------------------------------------------------------------------------
% -----ONLY VARIABLES REQUIRED TO SET-------------------------------------
coi_col = 33;
alg = 1; % 1: consecutive, 11: sliding window

% ------------------------------------------------------------------------
% ------------------------------------------------------------------------

% Parameters and Setup ---------------------------------------------------
Fs_ID = 60;                 % Input Data Sampling Rate [sps]

% Grab All *.csv Files in Interpolated Data Directory
csvFile = dir('*.csv');     csvName = {csvFile.name};
inf =
struct('cont',{{csvFile.name}},'freq',{zeros(size(csvFile,1),2)},'damping',{zeros
(size(csvFile,1),2)});

allcases = [];
triggercases = [];

numIter = length(csvFile);
for icase = 1:numIter
    disp('////////////////////////////////////////////////');
    s = sprintf('Analyzing case:  %s', strcat(csvName{icase})); disp(s);
    data = xlsread(strcat(csvName{icase}));  % Import Data
    allcases = char(allcases,strcat(csvName{icase}));

    time = data(:,1);

    % Interpolate for Equidistant Samples - 'pchip' --------------------------
    pc_data = []; meas_new = [];
    for r = coi_col
        x_data = data(:,r);
        [time,u_index] = unique(time);
        for r = 1:length(time)
            meas_new(r,:) = x_data(u_index(r),:);
        end
        samp_time = (time(1):(1/Fs_ID):time(end))';
        pc_data = [pc_data pchip(time,meas_new,samp_time)];
    end
    time = samp_time;
    data = pc_data;

    % ------------------------------------------------------------------------

    % ALGORITHM 1 (COI RATE OF CHANGE) TEST SECTION
```

```
    if alg == 1

        signals = data(:,1);
        status  = zeros(size(signals));
        for c = 1:size(signals,1)
            if c == 1
                trigger = SPRAS_Alg1Trigger_Consec(1, time(c,:), signals(c,:),
status(c,:));
            else
                trigger = SPRAS_Alg1Trigger_Consec(0, time(c,:), signals(c,:),
status(c,:));
            end

            if trigger == 1
                triggercases = char(triggercases,strcat(csvName{icase}));
                break
            end

        end

        % ALGORITHM 1 (COI RATE OF CHANGE) TEST SECTION - WINDOW
    elseif alg == 11
        signals = data(:,1);
        status  = zeros(size(signals));
        for c = 1:size(signals,1)
            if c == 1
                trigger = SPRAS_Alg1Trigger_Window(1, time(c,:), signals(c,:),
status(c,:));
            else
                trigger = SPRAS_Alg1Trigger_Window(0, time(c,:), signals(c,:),
status(c,:));
            end

            if trigger == 1
                triggercases = char(triggercases,strcat(csvName{icase}));
                break
            end

        end
    end
end

allcases
triggercases

disp('Done')
```

Real Power dP/dt Rate-of-Change – Consecutive

```
% ------------------------------------------------------------------------
% This script reads in the COI flows and determines if and when Algorithm
% 1 dP/dt would trigger.
%

function [trigger] = SPRAS_Alg1Trigger_Consec(init, time, signals, status)

persistent dPdT_thresh
persistent dPdT_timer

persistent COIprev
persistent tPrev
```

```
persistent tStart
persistent tDiff

persistent flag
persistent trig

% INITIALIZATION
if init == 1
    dPdT_thresh = [2000; 500; 250];
    dPdT_timer  = [0.25; 0.5; 1.2];
    tStart = [0; 0; 0];
    flag   = [0; 0; 0];
    tDiff  = [0; 0; 0];
    trig = [0; 0; 0];

    COIprev = 0;
    tPrev = 0;

    trigger = 0;
% ALGORITHM EXECUTION
else

    % PMU Data Quality Check
    if sum(status) == 0

        % Calculate Total COI Real Power Flow
        COI = sum(signals);
        dCOIdt = (COI-COIprev)/(time-tPrev);

        % First Threshold
        if (dCOIdt > dPdT_thresh(1)) && (flag(1) == 0)
            tStart(1) = time;
            flag(1) = 1;
            tDiff(1) = 0;
        elseif dCOIdt > dPdT_thresh(1)
            tDiff(1) = time - tStart(1);
        else
            flag(1) = 0;
            tDiff(1) = 0;
        end

        % Second Threshold
        if (dCOIdt > dPdT_thresh(2)) && (flag(2) == 0)
            tStart(2) = time;
            flag(2) = 1;
            tDiff(2) = 0;
        elseif dCOIdt > dPdT_thresh(2)
            tDiff(2) = time - tStart(2);
        else
            flag(2) = 0;
            tDiff(2) = 0;
        end

        %Third Threshold
        if (dCOIdt > dPdT_thresh(3)) && (flag(3) == 0)
            tStart(3) = time;
            flag(3) = 1;
            tDiff(3) = 0;
        elseif dCOIdt > dPdT_thresh(3)
            tDiff(3) = time - tStart(3);
        else
            flag(3) = 0;
```

```
            tDiff(3) = 0;
        end

        % Store current value and time
        COIprev = COI;
        tPrev = time;

        trig = [0; 0; 0]; algTrig = '';
        % EVENT TRIGGERED
        if tDiff(1) > dPdT_timer(1)
            flag(1) = 0; trig(1) = 1; algTrig = [algTrig '2000/0.25'];
        end

        if tDiff(2) > dPdT_timer(2)
            flag(2) = 0; trig(2) = 1; algTrig = [algTrig '500/0.5'];
        end

        if tDiff(3) > dPdT_timer(3)
            flag(3) = 0; trig(3) = 1; algTrig = [algTrig '250/1.2'];
        end

        trigger = sum(trig);

        % Algorithm Has Triggered
        if trigger > 0
            v = sprintf('      ALG 01 dP/dt (Consecutive) {%s} Triggered at %6.3f
sec', algTrig, time); disp(v);
        end
    end
end

end
```

Real Power dP/dt Rate-of-Change – Window

```
% ------------------------------------------------------------------------
% This script reads in the COI flows and determines if and when Algorithm
% 1 dP/dt would trigger.
%

function [trigger] = SPRAS_Alg1Trigger_Window(init, time, signals, status)


persistent dPdT_thresh
persistent dPdT_timer

persistent COIprev
persistent tPrev

persistent trig

persistent window1
persistent window2
persistent window3
persistent windowLimits
persistent windowLength
persistent sampRate

% INITIALIZATION
if init == 1
    dPdT_thresh = [5000; 500; 250];
```

```
    dPdT_timer  = [0.25; 0.5; 1.2];
    trig = [0; 0; 0];

    COIprev = 0;
    tPrev = 0;

    sampRate = 60;
    windowLimits = round(dPdT_timer/(1/sampRate));
    windowLength = round(windowLimits*1.1);

    window1 = zeros(windowLength(1),1);
    window2 = zeros(windowLength(2),1);
    window3 = zeros(windowLength(3),1);

    trigger = 0;

% ALGORITHM EXECUTION
else

    window1 = window1(1:end-1,1);
    window2 = window2(1:end-1,1);
    window3 = window3(1:end-1,1);

    % PMU Data Quality Check
    if sum(status) == 0

        % Calculate Total COI Real Power Flow
        COI = sum(signals);
        dCOIdt = (COI-COIprev)/(time-tPrev);

        % First Threshold
        if (dCOIdt > dPdT_thresh(1))
            window1 = [1; window1];
        else
            window1 = [0; window1];
        end

        % Second Threshold
        if (dCOIdt > dPdT_thresh(2))
            window2 = [1; window2];
        else
            window2 = [0; window2];
        end

        %Third Threshold
        if (dCOIdt > dPdT_thresh(3))
            window3 = [1; window3];
        else
            window3 = [0; window3];
        end


        % Store current value and time
        COIprev = COI;
        tPrev = time;

        trig = [0; 0; 0]; algTrig = '';
        % EVENT TRIGGERED
        if sum(window1) >= windowLimits(1)
            window1 = zeros(windowLength(1),1); trig(1) = 1; algTrig = [algTrig
'2000/0.25'];
        end
```

```
        if sum(window2) >= windowLimits(2)
            window2 = zeros(windowLength(2),1); trig(1) = 1; algTrig = [algTrig
'500/0.5'];
        end

        if sum(window3) >= windowLimits(3)
            window3 = zeros(windowLength(3),1); trig(1) = 1; algTrig = [algTrig
'250/1.2'];
        end

        trigger = sum(trig);

        % Algorithm Has Triggered
        if trigger > 0
            v = sprintf('      ALG 01 dP/dt (Window) {%s} Triggered at %6.3f
sec', algTrig, time); disp(v);
        end

    end
end

end
```

Phase Angle Difference Rate-of-Change

```
% ------------------------------------------------------------------------
% This script reads in all .csv files created from .chf files. If the
% required signal responses exceed the algorithm design thresholds, the
% contingency is included in a subset of contingencies which
% cause the algorithm to 'trigger'.
% ------------------------------------------------------------------------

clear all; close all; clc;

% Parameters and Setup
dAnglethresh = 5;
dAngletime   = 0.5;

% Grab All *.csv Files in Interpolated Data Directory
csvFile = dir('*.csv');     csvName = {csvFile.name};

allcases = [];
triggercases = [];
for icase = 1:length(csvFile)
    allcases = char(allcases,strcat(csvName{icase}));
    s = sprintf('#%d  Analyzing case:  %s', icase, strcat(csvName{icase}));
disp(s);
    [data, headers] = xlsread(strcat(csvName{icase}));  % Import Data

    a = [];    trigger = 0;    triggerTime = 0;
    time = data(:,1);
    voltages = data(:,3:12);

    COI = data(:,2);
    A_UC = data(:,36); PH_UC = 1.*cosd(A_GUC)+1i.*sind(A_GUC);
    A_LC = data(:,37); PH_LC = 1.*cosd(A_LC)+1i.*sind(A_LC);
    A_COI = data(:,39); PH_MLN = 1.*cosd(A_COI)+1i.*sind(A_COI);
    A_NI = data(:,33); PH_NI = 1.*cosd(A_NI)+1i.*sind(A_NI);
    A_MT = data(:,35); PH_GAR = 1.*cosd(A_MT)+1i.*sind(A_MT);

    A_UC_COI = angle((PH_UC).*conj(PH_MLN)).*180/pi;
    A_NI_COI = angle((PH_NI).*conj(PH_MLN)).*180/pi;
```

```
A_MT_COI = angle((PH_GAR).*conj(PH_MLN)).*180/pi;

dA_UC_COI = zeros(size(A_UC_COI,1),1);
dA_NI_COI = zeros(size(A_NI_COI,1),1);
dA_MT_COI = zeros(size(A_MT_COI,1),1);

for i = 2:size(A_UC_COI,1)
    dA_UC_COI(i) = (A_UC_COI(i)-A_UC_COI(i-1))/(time(i)-time(i-1));
    dA_NI_COI(i) = (A_NI_COI(i)-A_NI_COI(i-1))/(time(i)-time(i-1));
    dA_MT_COI(i) = (A_MT_COI(i)-A_MT_COI(i-1))/(time(i)-time(i-1));
end


flag1 = 0; flag2 = 0; flag3 = 0;
for i = 1:size(dA_UC_COI,1)

    %Upper Columbia-COI Angle Magnitude Check
    if dA_UC_COI(i) > dAnglethresh && flag1 == 0
        tStart1 = time(i); flag1 = 1;
    elseif dA_UC_COI(i) > dAnglethresh
        tDiff1 = time(i) - tStart1;
    else
        flag1 = 0; tDiff1 = 0;
    end

    %Northern Intertie-COI Angle Magnitude Check
    if dA_NI_COI(i) > dAnglethresh && flag2 == 0
        tStart2 = time(i); flag2 = 1;
    elseif dA_NI_COI(i) > dAnglethresh
        tDiff2 = time(i) - tStart2;
    else
        flag2 = 0; tDiff2 = 0;
    end

    %Montana-COI Angle Magnitude Check
    if dA_MT_COI(i) > dAnglethresh && flag3 == 0
        tStart3 = time(i); flag3 = 1;
    elseif dA_MT_COI(i) > dAnglethresh
        tDiff3 = time(i) - tStart3;
    else
        flag3 = 0; tDiff3 = 0;
    end

    %Upper Columbia-COI Duration Check
    if tDiff1 > dAngletime
        a = sprintf('      UC-COI dAngle/dt Trigger @ %6.3f sec', time(i));
        disp(a);
        trigger = 1;
        triggercases = char(triggercases,strcat(csvName{icase}));
        triggerTime = time(i);
        break
    end

    %Northern Intertie-COI Duration Check
    if tDiff2 > dAngletime
        a = sprintf('      NI-COI dAngle/dt Trigger @ %6.3f sec', time(i));
        disp(a);
        trigger = 1;
        triggercases = char(triggercases,strcat(csvName{icase}));
        triggerTime = time(i);
        break
    end
```

```
        %Montana-COI Angle Duration Check
        if tDiff3 > dAngletime
            a = sprintf('      MT-COI dAngle/dt Trigger @ %6.3f sec', time(i));
            disp(a);
            trigger = 1;
            triggercases = char(triggercases,strcat(csvName{icase}));
            triggerTime = time(i);
            break
        end

    end

    s = sprintf('#%d Case:  %s', icase, strcat(csvName{icase}));
    figure;
    subplot(3,1,1);
    plot(time,A_UC_COI,'k'); hold on;
    plot(time,A_NI_COI,'r'); hold on;
    plot(time,A_MT_COI,'b');
    title(s,'Interpreter','none');
    legend('UC-COI','NI-COI','MT-COI');
    xlabel('Time [s]'); ylabel('Angle Difference [deg]');

    subplot(3,1,2);
    plot(time,dA_UC_COI,'k'); hold on;
    plot(time,dA_NI_COI,'r'); hold on;
    plot(time,dA_MT_COI,'b');
    legend('UC-COI','NI-COI','GAR-COI');
    if isempty(a)
        a = sprintf('      Angle Rate of Change Does Not Trigger');
    else
        yL = get(gca,'YLim');
        line([triggerTime triggerTime],yL,'Color','r');
    end
    title(a,'Interpreter','none');
    xlabel('Time [s]'); ylabel('dAngle/dt [deg/sec]');

    subplot(3,1,3);
    plot(time,voltages);
    title('VSRI Voltages');
    xlabel('Time [s]'); ylabel('Voltage [kV]');
    ylim([500 560]);

end

allcases
triggercases

disp('Done')
```

Appendix E: N-3 Contingency Study Results

These figures show plots voltage, frequency, COI real power flow, and phase angle difference as measures of performance for the VSRI as a "safety net" scheme.

Voltage

FACRI, No VSRI

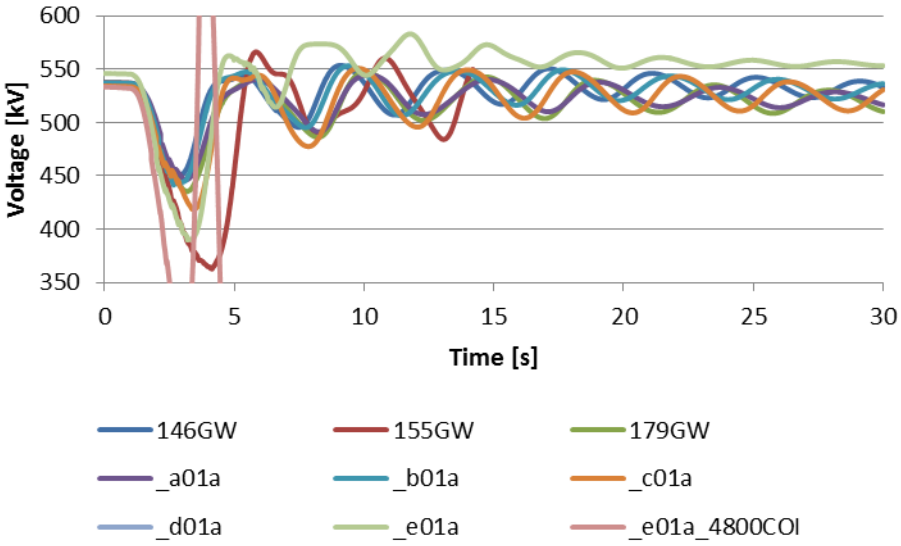

No FACRI, VSRI

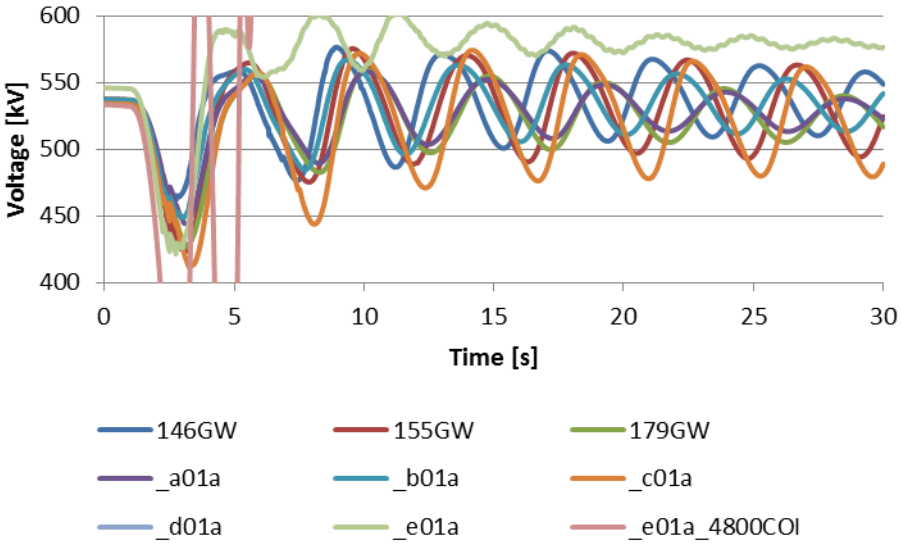

FACRI, VSRI

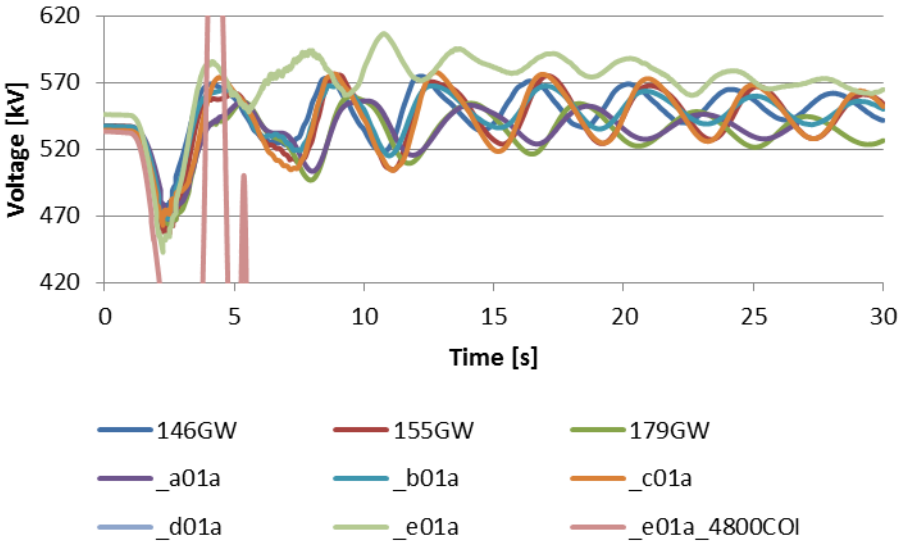

Frequency

FACRI, No VSRI

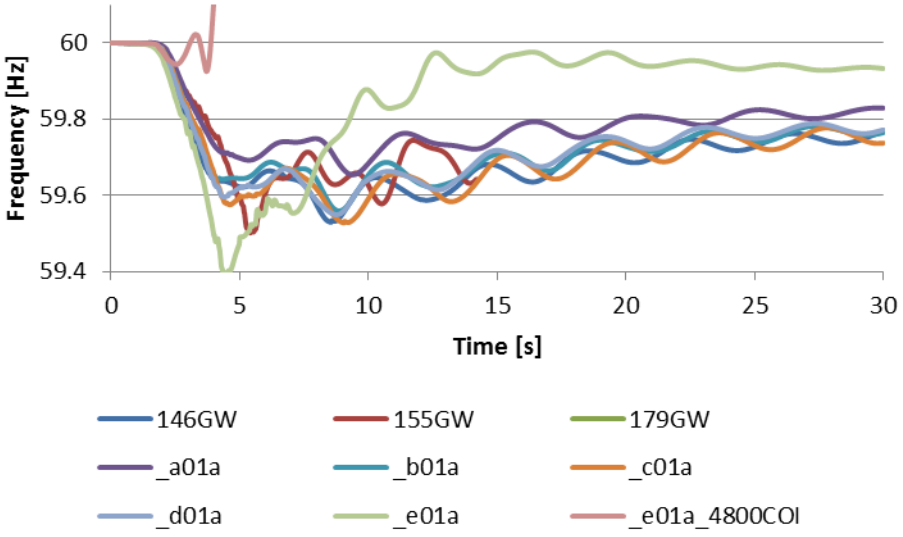

No FACRI, VSRI

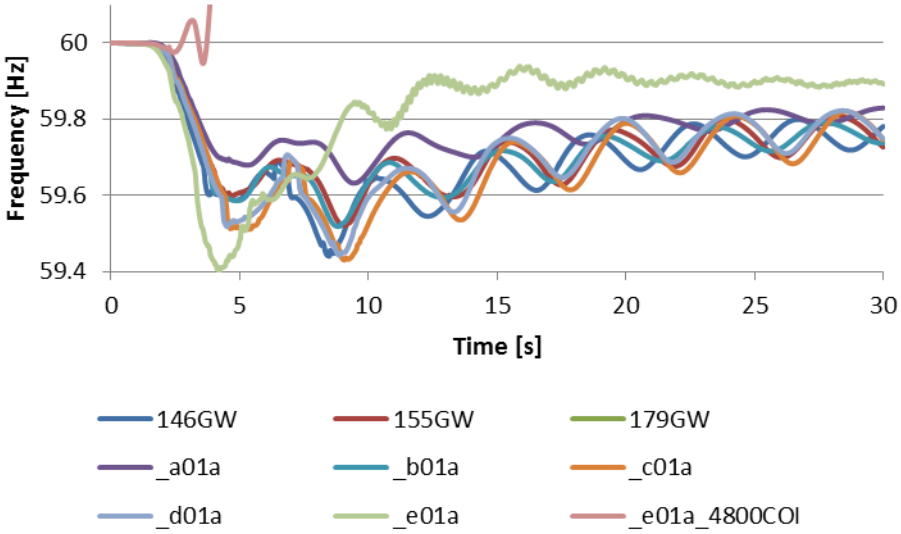

FACRI, VSRI

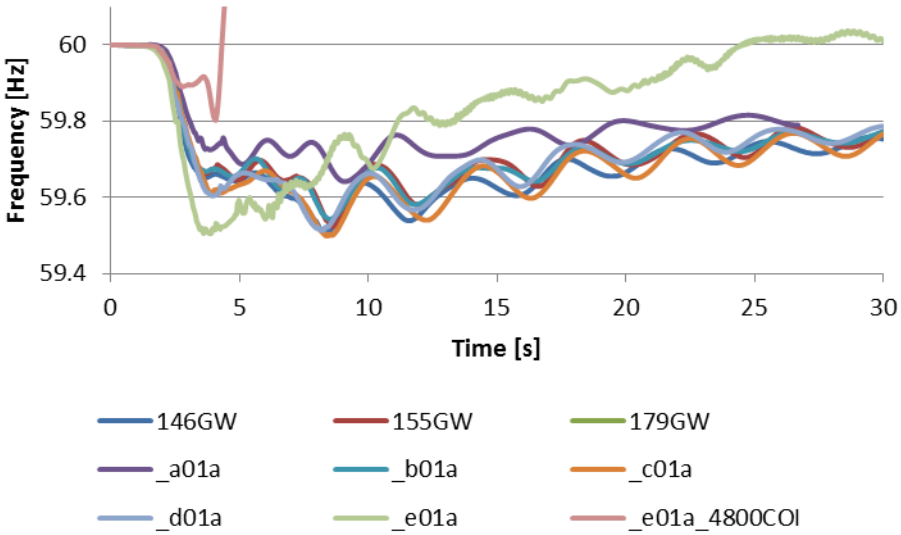

COI Real Power

FACRI, No VSRI

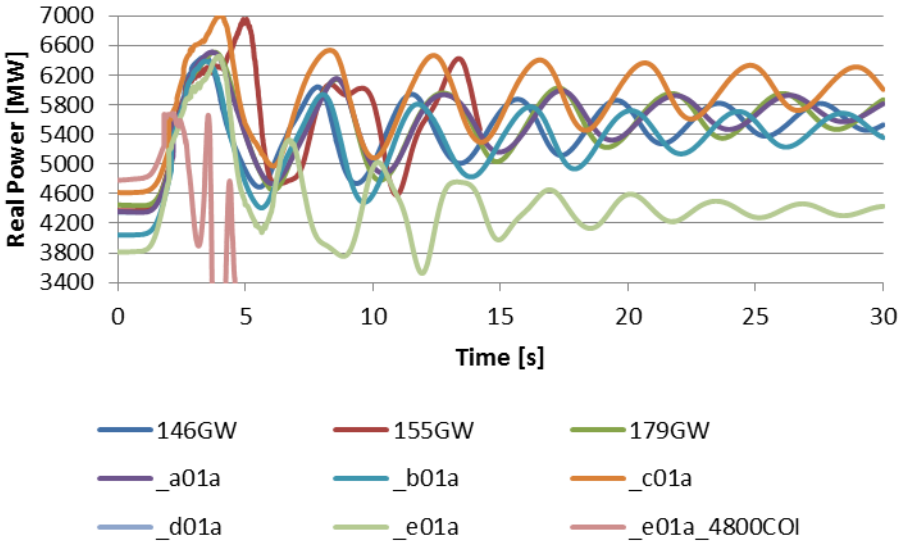

No FACRI, VSRI

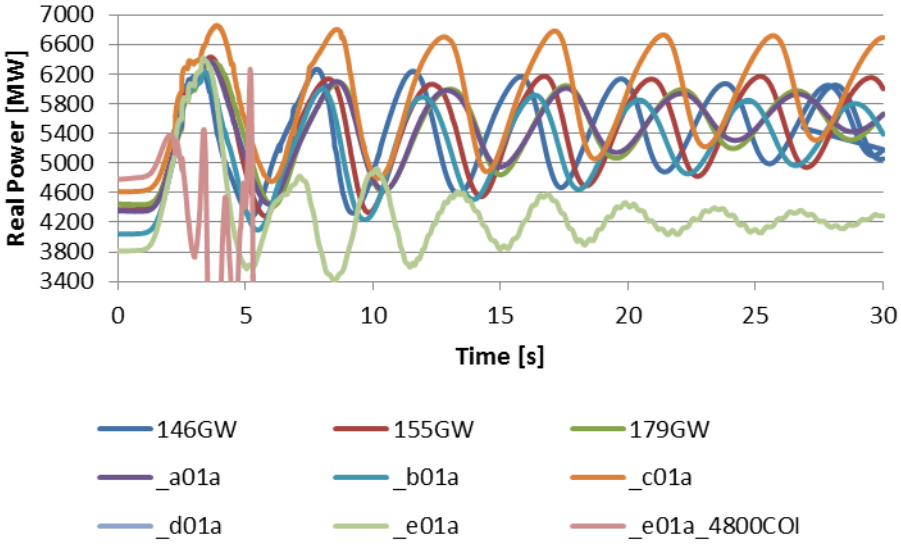

FACRI, VSRI

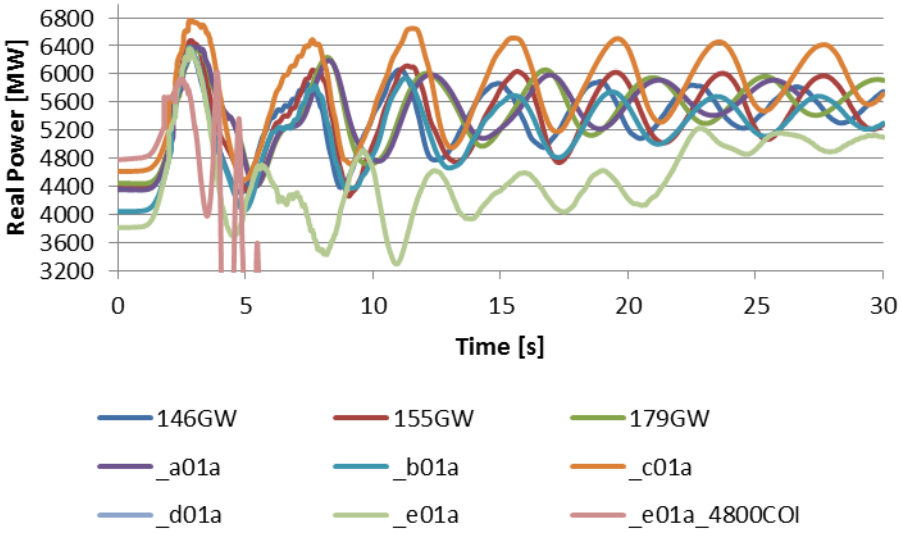

Phase Angle Difference

FACRI, No VSRI

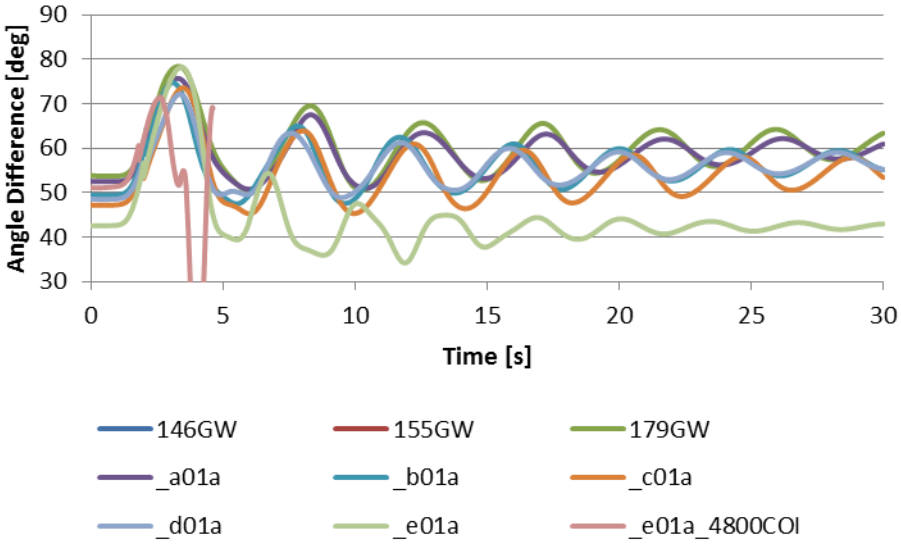

No FACRI, VSRI

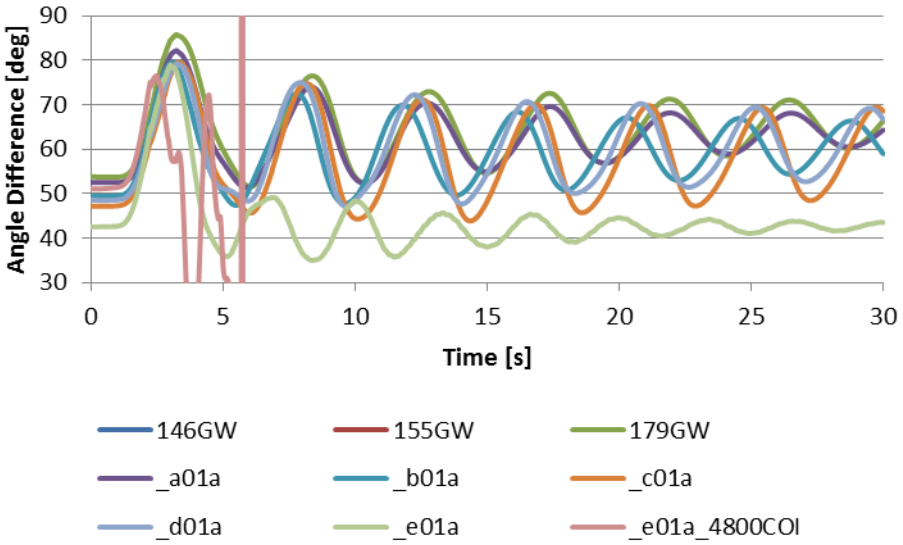

FACRI, VSRI